

SEISMICITY, EARTHQUAKE MECHANISMS, AND SEISMIC WAVE ATTENUATION
IN THE NORTHEASTERN UNITED STATES

by

Jay J. Pulli

B.S. Worcester Polytechnic Institute, Worcester, MA
(1975)

SUBMITTED IN PARTIAL FULFILLMENT
OF THE REQUIREMENTS FOR THE DEGREE OF
DOCTOR OF PHILOSOPHY

at the

© MASSACHUSETTS INSTITUTE OF TECHNOLOGY
June 10, 1983

Signature of Author.....
Department of Earth and Planetary Sciences

Certified by.....
M. Nafi Toksöz
Thesis Supervisor

Accepted by.....
Chairman, Departmental Committee on Graduate Students

MASSACHUSETTS INSTITUTE OF TECHNOLOGY
LIBRARIES
NOV 1 1983
LIBRARIES
Lindgren
Lindgren

*SEISMICITY, EARTHQUAKE MECHANISMS, AND SEISMIC WAVE ATTENUATION
IN THE NORTHEASTERN UNITED STATES*

by

Jay J. Pulli

*Submitted to the Department of Earth and Planetary Sciences
on June 10, 1983, in partial fulfillment of the requirements
for the degree of Doctor of Philosophy*

ABSTRACT

The northeastern United States and southeastern Canada (hereafter abbreviated as NEUS-SEC) is an intraplate region which includes two physiographic provinces. There is a stable continental platform to the west (the Grenville Province), an old mountain belt to the east (the Appalachians). Since the NEUS-SEC was one of the first areas of North America to be explored and settled, the history of earthquake activity is quite long and complete. The area is more seismically active than expected given the geologic setting. The vast majority of the earthquakes in the NEUS-SEC are small, but in a number of instances, moderate-to-large earthquakes have struck the area. For example, in 1755 an earthquake believed to have been located east of Cape Ann, MA produced intensity VII to VIII (M.M.) effects in Boston and surrounding areas. In 1925, an earthquake of magnitude 6.6 near La Malbaie, PQ produced intensity IX effects in the epicentral area. Why do destructive earthquakes occur in this geologically stable intraplate area, and if large events reoccur, what will be the resulting ground motions. Much can be learned from the historical record; however, instrumental network data are necessary in order to reduce the level of uncertainty in risk studies. In 1975, a consortium of NEUS-SEC universities and agencies was formed for the purpose of installing a dense short period seismic network in the area. This thesis consists of an examination of the data collected by this network during the past seven years, as well as an analysis of the historical record. The goal of this thesis is to provide a better understanding of fundamental seismicity parameters in the NEUS-SEC for use in the estimation of earthquake risk. The area of consideration in this study covers latitudes 40 to 50 degrees, and longitudes -80 to -66 degrees.

The historical seismicity, defined here as covering the time period 1534-1975, was examined using two regionalization algorithms for the purpose of defining seismic zones. The

frequency regionalization, which is a two-dimensional spatial filter applied to the earthquake catalog (with aftershocks removed), reveals three major seismic zones in the area. The first zone, termed the Western Quebec Seismic Zone, spans an area from Lake Champlain in VT to the PQ-ONT border. The mean return time for a magnitude 6.0 (mb) earthquake in this zone, using a least squares estimator, is 188 years with a 41% probability of occurrence in 100 years. For an mb 6.5 earthquake, the mean return time is 526 years with a 17% probability of occurrence in 100 years. The second zone, termed the Charlevoix Seismic Zone, is a concentrated area of activity which has experienced some of the largest earthquakes in the study area. Here, the mean return time for an mb 6.5 earthquake is 120 years with a 56% probability of occurrence in 100 years. For an mb 7.0 event, the mean return time is 231 years with a 35% probability of occurrence in 100 years. The third major zone is termed the Boston - NH Seismic Zone, a band of seismicity running from the Lakes Region of central NH to eastern MA. Here, the mean return time of an mb 6.0 earthquake is 408 years with a 39% probability of occurrence in 200 years. For a magnitude 6.5 event, the mean return time is 1060 years with a 17% probability of occurrence in 200 years. The energy regionalization of the area shows that most of the seismic energy release has taken place in four small areas: Timiskaming, ONT; Cornwall, ONT - Massena NY; Charlevoix, PQ; and Cape Ann, MA. These zones are not surrounded by regions of lower seismic energy release. This may mean that the physical processes responsible for the events may be very small in spatial extent.

The instrumental dataset, covering the time period October 1975 through September 1981, shows that in most (but not all) cases the distribution of seismicity is space stationary, i.e., instrumental epicenters cluster in areas of historically active seismicity. Earthquake locations computed from network data are in most cases accurate to within 5 km, and in areas of high station concentration, accurate to 2 km. In some areas, in particular the Cape Ann area, the occurrence of earthquakes is much lower than in the past. Focal depths are known for only a handful of events which have occurred near seismic stations or have been studied with aftershock surveys. West of the Appalachians, in the Grenville Province, earthquakes occur at depths ranging from the near surface to almost 20 km. In the Appalachian Province, earthquakes are confined to the upper 10 km of the crust.

Fault plane solutions were determined for ten earthquakes in the study area using P-wave first motion data and crustal models applicable to the source areas. In addition, a literature search was undertaken and a dataset compiled which includes 53 earthquake fault plane solutions and 18 non-seismic stress measurements (hydrofracturing, overcoring, fault slip and core offsets, and pop-ups). This dataset was used to produce a crustal stress map for the NEUS-SEC. The area is characterized by a horizontal compressive stress field; however, the direction of this stress field is not uniform across the entire study area.

In the Grenville Province, the compressive stress field is highly uniform and trends in an ENE-WSW direction. Earthquakes in this area show primarily thrust faulting on NW-SE trending fault planes. However, in the Appalachian Province, the compressive stress field is highly non-uniform. Earthquakes in this area show both thrust and strike-slip motions. If we interpret the dataset for the largest, best constrained events, the scatter remains. There may be an underlying compressive stress field in this area, but it may be modified by crustal inhomogeneities, such as the presence of crustal blocks, or by topographic loading stresses.

Seismic wave attenuation was measured in the study area from the time decay of coda wave amplitudes on narrow bandpass filtered seismograms. The frequency band of interest was 0.75 to 10 Hz. Q_c was found to increase with frequency across this band, but there was also a difference between this frequency dependence for short and long lapse times of coda wave propagation. For short lapse times, corresponding to wavepaths primarily in the upper crust, Q increases from 400 at 3 Hz to 1300 at 10 Hz. For long lapse times, corresponding to wavepaths in the lower crust and upper mantle, Q was found to vary from 660 at 1 Hz to 1500 at 10 Hz. If we interpret this dataset in terms of a model incorporating both scattering and anelastic attenuation, we find that the mean free path of seismic waves is 80 km in the crust, and 400 km in the mantle. If we assume that scattering is entirely responsible for the observed attenuation, we find that the minimum mean free path in the crust is about 75 km over all frequencies, whereas in the mantle, the minimum mean free path decreases from 400 km at 0.75 Hz to 90 km at 10 Hz.

These Q measurements were then used to develop and test a ground motion attenuation model for New England. We began by taking an intensity attenuation model and converting it to an equivalent particle velocity attenuation model using a velocity-intensity correlation. The resulting model successfully predicts the peak horizontal velocities observed for the 19 January 1982 Gaza, NH earthquake. The model also compares favorably with the theoretical seismic wave attenuation assuming L_g propagation and the Q values measured in this work. These models were then used to compute the ground motions for four hypothetical NEUS-SEC earthquakes.

In summary, the seismic characteristics of the Grenville and Appalachian Provinces were found to be quite different. In the Appalachian Province, earthquake epicenters scatter over broad areas, are shallower, and exhibit more varying focal mechanisms than in the Grenville. The attenuation and scattering of seismic waves is also greater in the Appalachians. Potential ground motions may be much less predictable in this province.

Thesis Advisor: M. Nafi Toksöz
Professor of Geophysics

ACKNOWLEDGEMENTS

In 99% of the theses which I have read, the acknowledgements begin by thanking the thesis advisor. One begins to wonder if this is merely an academic courtesy or a way of buttering-up the advisor just before the defense. However, in my case I can honestly say that the person who has had the greatest influence on my academic career has been my advisor, Prof. Nafi Toksöz. Most of what I have learned from Nafi has taken place during the so-called "off-hours", meaning nights, weekends, and over dinner, rather than scheduled course times. Consequently, it is not the details of science which Nafi has taught me but rather his approach and insights into scientific problems and how to solve them. Nafi's particular version of the Socratic method takes a little getting used to (loooong pauses between sentences, cleaning his glasses with his tie), but after the initial break-in period, one begins to appreciate his progression of thoughts from first concepts to final recommendations. So whether consciously or unconsciously, I will likely approach many of my future scientific projects by wondering "what would Nafi do in this case".

I would also like to thank Prof. Kei Aki who served as a general advisor to me and introduced me to the use of coda waves for the study of small earthquakes. Those of us who like to look ahead to the future areas of seismological research generally end up scrounging through Kei's preprint file. Kei has a tremendous influence on seismology and the seismological community, but I

still cannot figure out how he arranged for an earthquake to be felt during his lecture on the Boston earthquake of 1755.

The operation and analysis of data from a seismic network is never a one man project. I have been fortunate over the years to have worked with a dedicated group of undergraduates who assisted in the daily operation of the M.I.T. Seismic Network and developed much of the software and hardware which transformed the network from electronic antiquity into a modern seismic data processing facility. My present crew of ace scientists includes Carl Godkin, Mike Guenette, Jim MacArthur, Andy Osler, Seth Rubin, Kirk Chao, Trish Curtin (imported from Wellesley College), and Steve Gildea. Jeanne Sauber, our new grad student, has brought a fresh California perspective to our research in the past few months. Without this group, I could never have undertaken the scope of problems included in this work. Previous aces who have worked on this project include Andy Michael, Paul Cunningham, and Naomi Benaron. Andy Michael and Steve Gildea were the driving force behind the conversion of the network from analog to digital recording on the HP-1000 computer. The M.I.T. Seismic Network was originally planned and deployed by Dave Johnston, George Keough, and Al Taylor. Steve Taylor kept the network running during his tenure at M.I.T., and through his research provided us with much of what we know about the crust and upper mantle structure of the area.

Many of the results in this thesis would not have been possible without the free exchange of data among the various

network operators in northeastern North America. Our group had nearly weekly contact with Weston Observatory of Boston College, and we are particularly indebted to John Ebel, Vladimir Vudler, and Fr. James McCaffrey who provided us with arrival time data and original records for our examination. Our friends to the west at Lamont-Doherty Geological Observatory include Alan Kafka, Ellyn Schlessinger-Miller, and Noel Barstow. Although not officially part of the northeast network, the group at Woodward-Clyde Consultants in New Jersey kindly went out of their way to provide us with timely information from their shifting networks. Staff members at WCC who have been particularly helpful to us include Tom Statton, Mark Houlday, and Rich Quittmeyer. To the south, M.I.T. alumnus Cliff Thurber monitored the seismic activity in the Long Island area, which is no easy task when you're sitting on a sand bar. To the north, the Canadian network group, led by Bob Wetmiller, put up with our invasion of their country during the winter of 1982. Coordination of network operation and research has been skillfully provided by Paul Pomeroy of Rondout Associates, who since 1975 has represented the interests of northeast seismology to the funders of our research. And as a funder, or more specifically a monitor for the funders, Andy Murphy of the U.S. Nuclear Regulatory Commission saw that we all had the money to continue our research, despite a number of financial crises along the way.

Weston Geophysical Corporation kindly made available to me

its vast collection of seismicity data for the eastern US. I am particularly indebted to Dr. Gabriel Leblanc who spent many hours with me discussing what we really need to know about eastern US earthquakes. His advice and tremendous insight into earthquake problems will always be appreciated. I would also like to thank George Klimkiewicz of WEGE who made available his ground motion attenuation models prior to publication. George was always there to add a little "industrial criticism" to my work, which is an important perspective for us flighty academic types to consider.

Outside of thesis and network research, many of the folks at the Earth Resources Laboratory added to my education and enjoyment of M.I.T. . Roger Turpening was always there to satisfy my urge to talk about fast cars, capitalism, and conservative politics. Besides that, his barn was always warm for auto repairs and his winecellar was usually stocked with Cabs and Chardonnays. He's still trying to convince me to get out of the earthquake business, in spite of the present oil glut. Arthur Cheng found it necessary to hound me about giving more wine tastings. If not well logging, Arthur has taught me to be "critical". Sara Muffy Brydges always managed to find money around somewhere whenever I had to take a trip or hire another student. I expect to testify on her behalf someday in front of IRS attorneys. She also kindly read this thesis for me, fixing most of the grammar and deleting all of the "is thats" I picked up from Nafi. Judith Randolph built up her muscles by carrying

all of our quarterly reports to the Post Office, while Kelly Worrall kindly took phone messages from all those New Englanders who reported unusual pet behavior just before earthquakes on the other side of the globe. There are also my fellow grad students from whom I have learned more science than all of the faculty combined. (Should I have said that?) They include Ken Tubman, John Nabelek, Rob Stewart, Paul Huang, Rob Comer, Steve Roecker, Mark Willis, Eric Bergman, and Dale Sawyer. I am convinced that without graduate students, M.I.T. would grind to a halt.

Lest anyone think that I forgot to acknowledge some underpaid typist for producing this final document, I'll thank my fingers, the COMPOSE program on MULTICS, and the amazing laser printer at IPS. This research was supported by the U.S. Nuclear Regulatory Commission under contract NRC-04-76-209, by the U.S. Geological Survey under contract 14-08-0001-21284, and by gifts to M.I.T. by the late George R. Wallace, Jr. of Fitchburg, MA.

SEISMICITY, EARTHQUAKE MECHANISMS, AND SEISMIC WAVE ATTENUATION
IN THE NORTHEASTERN UNITED STATES

TABLE OF CONTENTS

		<i>Page</i>
	ABSTRACT	1
	ACKNOWLEDGEMENTS	4
	
CHAPTER 1	INTRODUCTION	14
	Figure Captions	23
	Figures	24
	
CHAPTER 2	THE HISTORICAL AND INSTRUMENTAL SEISMICITY OF THE NORTHEASTERN UNITED STATES AND SOUTHEASTERN CANADA	
2.1	Introduction	25
2.2	Historical Seismicity	28
	2.2.1 Distribution and Regionalization of Epicenters	29
	2.2.2 Return Times and Probabilities of Earthquake Occurrence	45
2.3	Instrumental Seismicity	60
	2.3.1 The N.E.U.S.S.N.	61
	2.3.2 Distribution and Regionalization of Epicenters	65
	2.3.3 Magnitudes of NEUS-SEC Earthquakes	67
	2.3.4 Focal Depths of NEUS-SEC Earthquakes	71
2.4	Comparison of Historical and Instrumental Seismicity	76
	Tables	80

	<i>Figure Captions</i>	89
	<i>Figures</i>	93
.....		
CHAPTER 3	FAULT PLANE SOLUTIONS AND CRUSTAL STRESSES IN THE NORTHEASTERN UNITED STATES	
3.1	<i>Introduction</i>	114
3.2	<i>Determination of Fault Plane Solutions</i>	117
3.2.1	<i>Data and Analysis</i>	117
3.2.2	<i>Fault Plane Solutions</i>	124
3.2.3	<i>Discussion and Error Analysis</i>	128
3.3	<i>Literature Review of Fault Plane Solutions and Geologic Stress Measurements</i>	131
3.3.1	<i>Fault Plane Solutions</i>	131
3.3.2	<i>Geologic Stress Measurements</i>	139
3.4	<i>Crustal Stresses in the NEUS-SEC</i>	142
	<i>Tables</i>	153
	<i>Figure Captions</i>	159
	<i>Figures</i>	162
.....		
CHAPTER 4	Q MEASUREMENTS AND STRONG MOTION ATTENUATION MODELS FOR NEW ENGLAND	
4.1	<i>Introduction</i>	175
4.2	<i>Q Measurements Using Coda Waves</i>	178
4.2.1	<i>Some Properties of Coda Waves</i>	179
4.2.2	<i>Data and Analysis</i>	186
4.2.3	<i>Results</i>	191
4.2.4	<i>Attenuation and Scattering of Seismic Waves</i>	196
4.2.5	<i>Discussion of Possible Errors</i>	198

4.3	<i>Ground Motion Attenuation Models for New England</i>	202
4.3.1	<i>Strong Motion Data</i>	206
4.3.2	<i>Seismic Intensity and Strong Ground Motion</i>	210
4.3.3	<i>Testing of the Ground Motion Attenuation Model</i>	219
	<i>Tables</i>	225
	<i>Figure Captions</i>	235
	<i>Figures</i>	239
.....		
CHAPTER 5	SEISMOTECTONICS OF NORTHEASTERN NORTH AMERICA	
5.1	<i>Introduction</i>	256
5.2	<i>Tectonic History and Crustal Structure</i>	256
5.2.1	<i>Tectonic History of the Northern Appalachians</i>	257
5.2.2	<i>Crustal Structure</i>	259
5.2.3	<i>Contrasts Between Grenville and Appalachian Provinces</i>	261
5.3	<i>Comparison with Other EUS Seismotectonic Settings</i>	264
5.3.1	<i>New Madrid, MO</i>	265
5.3.2	<i>Giles County, VA</i>	266
5.3.3	<i>Charleston, SC</i>	268
	<i>Tables</i>	270
	<i>Figure Captions</i>	271
	<i>Figures</i>	272
.....		
	REFERENCES	276
.....		

APPENDIX A	SIGNIFICANT EARTHQUAKES OF THE NORTHEASTERN UNITED STATES AND SOUTHEASTERN CANADA	
A.1	Introduction	290
A.2	Three Important Earthquakes	290
A.3	A Catalog of Significant Earthquakes in the NEUS-SEC	305
	Tables	308
	Figure Captions	310
	Figures	311
.....		
APPENDIX B	APPLICATION OF THE "WINDING-NUMBER ALGORITHM" TO CATALOGUED EARTHQUAKE DATA	316
	Figure Captions	318
	Figures	319
.....		
APPENDIX C	SEISMIC STATIONS IN THE NEUS-SEC	320
	Tables	320
	Figure Captions	324
	Figures	325
.....		
APPENDIX D	THE M.I.T. SEISMIC NETWORK	
D.1	Introduction	330
D.2	Network Configuration and Instrumentation	330
D.3	ASAP2 - A Digital Data Acquisition System	331
	Tables	343
	Figure Captions	344
	Figures	345
.....		

APPENDIX E	PUBLISHED FAULT PLANE SOLUTIONS IN THE NORTHEASTERN UNITED STATES AND SOUTHEASTERN CANADA	353
	Tables	354
	Figure Captions	356
	Figures	358
.....		
APPENDIX F	A CLOSER LOOK AT SOME RECENT EARTHQUAKES	
	F.1 Introduction	367
	F.2 18Apr1979 Bath, ME	367
	F.3 23Nov80 and 23Jun38 Chelmsford-Lowell, MA	371
	F.4 21Oct81 Long Island Sound, NY	376
	Tables	380
	Figure Captions	382
	Figures	383
.....		
	Biographical Note	390

CHAPTER 1
INTRODUCTION

The northeastern United States and southeastern Canada (hereafter referred to as the NEUS-SEC) has the longest history of reported earthquake activity on the North American continent. Descriptions of earthquakes in the NEUS-SEC can be found in the journals and diaries of the first explorers and settlers of the area. The majority of the earthquakes in the NEUS-SEC are small, as is expected in an intraplate setting; however moderate-to-large earthquakes have occasionally struck this area. The earliest catalogued event in this area occurred in 1534 near Les Eboulements, PQ and was of intensity IX (M.M.). Other important earthquakes include: Nov. 9, 1727, intensity VII and Nov. 18, 1755, intensity VII-VIII at Cape Ann, MA; Mar. 1, 1925, intensity IX (mb=6.7) at La Malbaie, PQ; Dec. 20 and 24, 1940, intensity VII (mb=5.4) at Ossipee, NH; and recently Jan. 9, 1982, magnitude 5.7 in central New Brunswick. Perhaps more than any other event, the Cape Ann, MA earthquake of 1755 has served to classify the NEUS as an area of "moderate earthquake hazard".

Even though the record of earthquake activity is quite long, the amount of quantitative information on the seismicity of the NEUS-SEC is low when compared to the western US. There are many reasons for this situation.

First, the largest earthquakes in the NEUS-SEC occurred

during historical times or before the installation of seismic networks. Thus the epicentral locations, magnitudes, and focal depths can only be estimated from intensity data. The mechanisms and other source properties of these large events remain in the realm of speculation.

Second, until 1975 the distribution of seismograph stations in the NEUS was quite sparse. Epicentral locations could only be determined for the larger events, and these locations were based on crude approximations to the velocity structure in the area. The focal depths of the events were unknown.

Third, the level of seismic activity is quite low when compared to the western US. Earthquakes with magnitudes greater than 3 1/2 (mb) generally occur only a few times each year. Thus the data collection process is a slow one, even with the area fully instrumented.

Fourth, the bedrock in the NEUS is covered with a thick layer of sediments and glacial till. Surface faulting has never been observed for an earthquake in this area. Thus it is difficult to correlate the seismic activity with the geologic structures which may be responsible for the events. At present, there is no causative mechanism known for the occurrence of NEUS-SEC earthquakes.

It should be clear that the estimation of the earthquake hazard in the NEUS (i.e., expected ground motion as a function of probability) is a difficult problem. However, it is a problem which must be addressed because of the large concentrations of

population and critical facilities within the area. These critical facilities, as well as residential and commercial buildings, must be properly designed to withstand the damaging ground motion generated by large earthquakes. However, economics dictates that structures be designed to survive the largest "expected" earthquake intensities, which in most cases is less than intensity XII (M.M.). The determination of these expected earthquake intensities or ground motions is a significant problem for modern seismology.

We can graphically illustrate the earthquake hazard problem in this area using four figures. In Figure 1.1a, we have plotted the locations of earthquake epicenters in the study area for the period 1534-1980. This figure illustrates the degree of earthquake activity which has been documented in this area. Although the vast majority of these events are small, some moderate-to-large events have occurred. In Figure 1.1b, we have plotted the locations of what we shall call "significant earthquakes". These events are of epicentral intensity at least VII, or magnitude at least 5.2 (mb). There are 41 known events which meet these requirements. In Figure 1.1c, the locations of major cities have been indicated. Finally, in Figure 1.1d, we have plotted the locations of nuclear power plants in the U.S. (operating and planned).

We may summarize the earthquake hazard problem in the NEUS-SEC by a single observation and four questions:

Observation - Moderate-to-large earthquakes have occurred in the NEUS-SEC during historical times.

Question - How large were these earthquakes?

Question - What are the geologic sources of these earthquakes?

Question - Will large events re-occur, and will they re-occur in the same places?

Question - If they re-occur, what will be the ground motions generated by these events?

The answers to these questions may seem remote; however, given enough reliable data, we should be able to answer them with some degree of certainty. The solution to the problem requires an interdisciplinary approach, transcending both seismology and geology.

One must begin with an examination of the historical record of seismicity in the area. This will reveal where the largest earthquakes have occurred and may delineate specific sites of earthquake concentrations. The historical record also provides the fundamental data necessary to estimate the probability of earthquake occurrence in the area. However in many cases, historical records of earthquakes often contain errors which tend to remain in modern catalogs. Examples of errors include the misinterpretation of intensity data, errors in epicentral

locations due to sparse population distributions, and the inclusion of meteorological and other non-tectonic phenomena such as frost heaves. The examination of original data sources, although time consuming and expensive, is often necessary, especially when the largest events are in the historical record. Fortunately, considerable effort has already taken place to re-examine the data for many of the historical earthquakes in this area.

The next step is to gather instrumental seismicity data. This includes the determination of the crust and upper mantle structure and its lateral variations. The instrumental data will allow the accurate determination of earthquake hypocenters, as well as magnitudes. Once the distribution of the present earthquakes has been established, a comparison of the present seismicity with the historical record is necessary in order to determine if the seismicity is space stationary. Of course, high quality instrumental data will allow the further study of the earthquake source parameters.

The mere distribution of earthquake hypocenters may not reveal the causes of the events, especially in an intraplate region such as the NEUS-SEC. The next relevant parameter which characterizes the earthquake source is its fault plane solution. From the fault plane solution we obtain the orientation of the two possible fault planes, and by inference, the state of stress at the earthquake focus. The distribution of the fault plane solutions may reveal linear trends of faults and areas of uniform

stress conditions. This is important in the determination of seismogenic zones. Other stress indicators should also be examined at this time, such as in-situ methods and geologic evidence, such as pop-up orientations.

Any further analysis of the earthquake sources requires a knowledge of the seismic wave attenuation in the crust and upper mantle, its lateral variations, and its frequency dependence. Information on attenuation actually serves two purposes. First, observed amplitudes must be corrected for attenuation if we are to properly derive source parameters, such as magnitude, seismic moment, and corner frequency. These source characteristics greatly influence the radiation of seismic energy from earthquake sources. And second, if we are to predict the ground motions at various sites generated by a model earthquake, we must apply an attenuation operator to the source.

At this point, an integration of the tectonics of the area with the seismicity data should come into play. The ultimate objective of any study such as this is to answer the question "Why do earthquakes occur in this area?". And since all earthquakes must have geologic sources, the identification of these sources is essential to the quantification of the earthquake hazard.

The purpose of this thesis is to provide basic seismological input into the problem of earthquake hazards estimation in the NEUS-SEC. The thesis draws primarily from data gathered during the past six years of northeast network operation.

Chapter 2 presents the examination of the historical and instrumental seismicity of the NEUS-SEC. For the historical dataset (1534-1975), we begin by reviewing the problems associated with the use of intensity data in earthquake hazards studies. Then we go on to apply two computer regionalization algorithms to the dataset in order to define seismic zones in the area. Next, we use four statistical methods to estimate the return times and probabilities of earthquake occurrence in each of the major seismic zones. For the instrumental dataset (October 1975 through September 1981), we start by describing the location procedures and magnitude calculations for NEUS-SEC earthquakes using the network data. Then we apply the same regionalization algorithms and compare the results with the historical dataset. Finally, we review focal depth information for NEUS-SEC earthquakes and calculate depths for some New England events.

Chapter 3 focuses on the determination of fault plane solutions and the state of stress in the NEUS. New fault plane solutions will be presented as well as a review of previously published mechanisms and geologic stress measurements. These data will be used to produce a map of crustal stresses in the NEUS-SEC. The distribution of crustal stresses will be compared with models of plate tectonic stresses.

Chapter 4 presents the measurement of Q in the NEUS. The method used to determine Q as a function of frequency and region is based on the analysis of coda waves generated by local

earthquakes and recorded digitally on stations of the M.I.T. Seismic Network. These measurements will then be interpreted in terms of a model which incorporates both anelastic attenuation and scattering. Then, we turn to the development of a strong ground motion attenuation model for New England. We begin with an intensity attenuation model and convert this to an equivalent particle velocity attenuation model using a velocity-intensity correlation. This model will then be compared with the available strong motion data in the area and the theoretical seismic wave attenuation from the measured Q values. Finally, we use these models to compute the theoretical ground motion for a number of large hypothetical NEUS-SEC earthquakes.

In Chapter 5 we review the tectonic history and crustal structure of the NEUS-SEC. The aim of this review will be to compare and contrast the seismotectonic settings of the Grenville and Appalachian Provinces. Then, we compare the seismotectonics of the study area with those of the central and southeastern US, two other intraplate areas which have experienced large earthquakes in the past. We will be concerned with whether or not the seismic studies conducted in these areas can be extrapolated to New England.

A number of appendices are also included at the end of this work. In Appendix A, we review the data for three important NEUS-SEC earthquakes and compile a table and map of "significant earthquakes" in this area. Appendix B describes the "Winding-Number Algorithm" which was applied to the selection of

events from the long epicentral datafiles in Chapter 2. Appendix C lists the locations of the seismic stations in this area and includes maps of the station distributions in various subareas of the network. Appendix D presents a detailed description of the M.I.T. seismic network. This includes a description of the digital data acquisition system and event detection algorithm installed during the course of this study. In Appendix E, fault plane solutions are shown for those events compiled from the literature in Chapter 3. Finally, in Appendix F we take a closer look at some of the earthquakes which have been studied in detail during the course of this research.

Figure Captions

Figure 1.1 a) Map of earthquake epicenters in the study area for the period 1534-1980. The epicenters plotted are from the catalog of Chiburis (1981). b) Map of significant earthquakes, i.e., those of epicentral intensity greater than or equal to VII or magnitude at least 5.2 (mb). c) Map of major cities in the study area. d) Map of U.S. nuclear power plant locations in the study area.

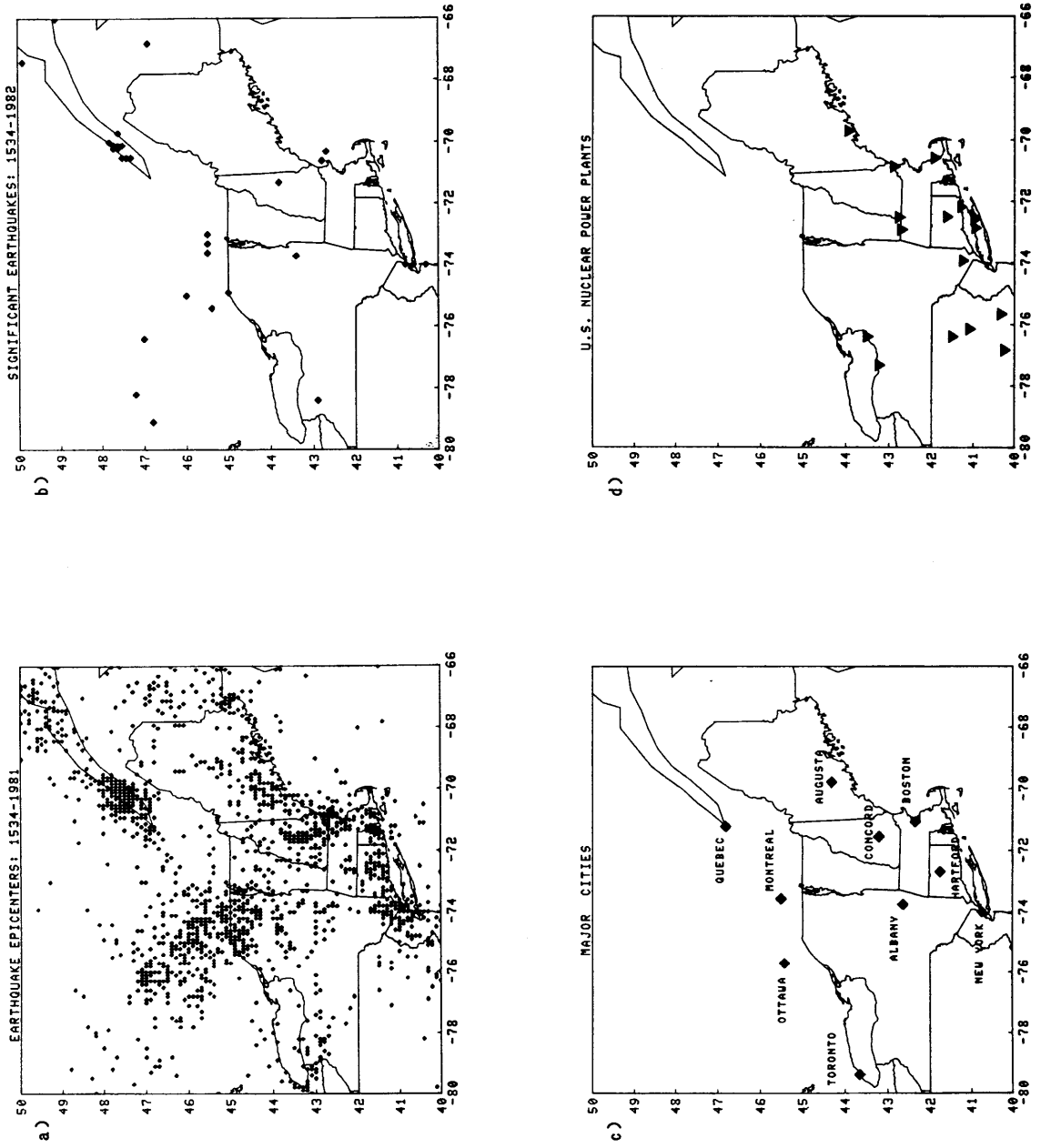


FIGURE 1.1

CHAPTER 2
THE HISTORICAL AND INSTRUMENTAL SEISMICITY
OF THE NORTHEASTERN UNITED STATES
AND SOUTHEASTERN CANADA

2.1 Introduction

The first documented occurrence of an earthquake in the northeastern United States and southeastern Canada (NEUS-SEC) was in 1534. This earthquake, which is believed to have occurred in the so-called Charlevoix Seismic Zone of the upper St. Lawrence River Valley, has a catalogued intensity of IX. (All intensities, unless otherwise specified, refer to the Modified Mercalli intensity scale of Wood and Neumann, 1931.) Thus, the earthquake history of the NEUS-SEC spans almost 450 years. During this time, over 3000 earthquakes have been documented or instrumentally detected. (This figure does not include the results of recent aftershock studies.) Of course, the number of earthquakes documented per year has gradually increased with time as the population spread and microearthquake networks were deployed. Nevertheless, the NEUS-SEC probably has the most complete earthquake history of any area on the North American continent. This fact, combined with the large population and number of critical facilities, has prompted a number of studies of the earthquake hazard in this area (e.g., Crosby, 1923).

In this chapter, a detailed examination is made of both the historical and instrumental seismicity of the NEUS-SEC. The historical seismicity forms the basic input dataset in any

earthquake hazards study. If the catalog of historical events is complete, it will reveal where the largest events have occurred, and may define important zones of seismicity. Knowledge of the statistical distribution of earthquake magnitudes (or intensities) with time will also allow us to calculate the return times of the largest events. However, historical earthquake catalogs often suffer from the limitations of inaccurate epicenter and source size estimations which must be determined from the distribution of seismic intensities. This sometimes leads to severe errors in interpretation. Thus, any detailed examination of the historical seismicity must include a re-examination of original data sources, especially for the largest events. Fortunately, considerable effort has already taken place to re-evaluate the data for many important NEUS-SEC earthquakes (e.g. Weston Geophysical Corp., 1977; Leblanc, 1981; Stevens, 1980a; Fox and Spiker, 1977).

Given the uncertainties inherent in historical earthquake data, it is often necessary to operate a multi-element seismic network in the study area so that earthquake locations and magnitudes can be accurately determined. Such a project began in this area in 1975, and the second half of this chapter is concerned with the analysis of the data accumulated by this network during the past six years of operation.

It is appropriate at this time to define the time periods covered in the interpretation of the historical and instrumental seismicity of the NEUS-SEC. The historical dataset begins with

the first documented event in 1534, and we define the end at the year 1975. This ending year was chosen since it marks the start of publication of the Northeastern United States Seismic Network (N.E.U.S.S.N.) Bulletins by Weston Observatory. These bulletins, which are published quarterly, are complete to September 1981 as of this writing. Thus, the instrumental dataset covers the time period from October 1975 through September 1981. (The catalog of instrumental seismicity for the area covered by the M.I.T. Seismic Network is now complete to January 1983. Since the data from five subnetworks are compiled into the N.E.U.S.S.N. Bulletins, delays in publication often occur.)

For the historical dataset, we begin by examining the distribution of seismicity in space and in time. Then, we apply two regionalization algorithms to delineate seismic zones in terms of the frequency of earthquake occurrence and the seismic energy release. For the major seismic zones, we then estimate the return times and probabilities of earthquake occurrence using four statistical methods. For the instrumental dataset, we present a discussion of the network, the data collected, and the calculation of earthquake epicenters and magnitudes. Then we apply the same two regionalization algorithms to the dataset, and compare the results with those of the historical record. We also review the available focal depth information in the area and compute focal depths for some New England earthquakes.

2.2 *Historical Seismicity*

In this section, a comprehensive examination of the historical seismicity of the NEUS-SEC is undertaken. We begin by examining the distribution of earthquake epicenters in the study area (both in space and in time), and will then apply two computer regionalization algorithms to define seismic zones in terms of the frequency of earthquake occurrence and the seismic energy release per unit area. We will also consider the problems of the completeness of the historical dataset, and the location and magnitude estimation of earthquakes from intensity data. Then, we compute the return times and probabilities of earthquake occurrence in each of the major zones using four statistical methods.

A number of earthquake catalogs are available for studying the historical seismicity of the NEUS-SEC, including Smith (1962, 1966), Coffman and von Hake (1973), Brooks (1960), Mather and Godfrey (1927), Chung and Ingersoll (1975), Weston Geophysical Corp. (1977), Chiburis (1981), Winkler (1979), and Nottis *et al.* (1981). Each of these catalogs suffers from a certain degree of inaccuracy and cross-referencing. Some of the more recent publications have been corrected for errors and have included the results of recent re-examinations of intensity data, meaning that some locations and magnitude estimates have changed. In this study, we have chosen to use the catalog of Chiburis (1981) for the study of the distribution and recurrence of epicenters since it is available in machine-readable form and has included many

revisions on source sizes and locations. However, Chiburis' (1981) catalog is not error free. For example, he has catalogued the magnitudes of the 1940 Ossipee, NH earthquakes as 5.7, while recent reexaminations of the seismograms by Street and Turcotte (1977) have shown the magnitudes to be 5.4 (mb). Another problem with the Chiburis (1981) catalog of events is that the epicentral locations are given to an accuracy of only 0.1 degree. Although this is a conservative margin of error for events prior to 1925, the locations of some historical events are known to a greater accuracy, which Chiburis does not take into account in his catalog.

In addition, numerous other papers and catalogs have been consulted for detailed information on a number of important earthquakes in this area, including Fox and Spiker (1977), Leblanc (1981), Street and Turcotte (1977), Street and Lacroix (1979), Stevens (1979), Weston Geophysical Corp. (1977), Meyer (1967), Rothman (1968), Devlin et al. (1942), Leet and Linehan (1942), Collins (1937a,b), Devane and Holt (1967), Hodgson (1925), Leet (1938), MacCarthy (1963), Perry (1941), Porter (1924), and Reid (1911). In Appendix A of this work, the effects of three large NEUS-SEC earthquakes are described in detail. This appendix, as well as the references just cited, should serve as a bibliography of the historical seismicity of the NEUS-SEC.

2.2.1 Distribution and Regionalization of Epicenters

One of the first epicentral maps available for the NEUS-SEC was that of the Canadian seismologist Smith (1962, 1966). The

1966 version of this map, which covers the time period 1534 - 1959, is reproduced in Figure 2.1. Although the map is more complete for Canadian earthquakes than for those in the NEUS, it serves to illustrate some of the general features of the seismicity of the study area. The most prominent feature on the map is the concentration of epicenters in the St. Lawrence River Valley near La Malbaie, PQ. This zone of events has come to be known as the Charlevoix Seismic Zone (Basham et al., 1979). (The term "seismic zone" will be frequently used in this work. This term is defined simply as a spatial association of epicenters. The term does not imply any physical or causal relationship between the earthquakes within a zone, although this may be the case for some zones.) Many of the largest earthquakes known to have occurred in the NEUS-SEC have been located in this zone. A review of the data for the 1925 La Malbaie, PQ earthquake, which was of magnitude 6.6 (mb) and intensity IX, is presented in Appendix A of this work. Early interpretations using this map led some investigators to propose the existence of a continuous zone of seismicity stretching northwest from the Boston area to western Quebec. This proposed zone became known as the Boston-Ottawa Seismic Belt (Leblanc et al., 1973; Sbar and Sykes, 1973). Sykes (1978) postulated that the Boston-Ottawa Seismic Zone was a continuation of the New England Seamount Chain, a northwesterly trend of volcanic seamounts located approximately 1000 km southeast of Boston. Upon further scrutiny of larger scaled versions of Smith's maps, it was later shown that the

Boston-Ottawa zone is not a continuous belt of seismicity, due to the lack of earthquake epicenters in western NH and northern VT. Recent interpretations, as well as compilations of instrumentally located events, favor the existence of two seismic zones in this area. The first is the Western Quebec Zone, extending from Lake Champlain, VT to the PQ-ONT border. The second zone covers the area from Boston to central NH near the Lakes Region. This is sometimes referred to as the Boston to NH Seismic Zone. Other areas of earthquake concentration shown in Smith's (1966) map include coastal ME, central CT, the Hudson River Valley, the New York City to NJ coastal area, and western NY state.

A map produced from the epicentral data in the Chiburis (1981) catalog of events is shown in Figure 2.2. This map covers the years 1534-1975. Many of the same features shown in Smith's map can also be seen in Figure 2.2, however, since the dataset has been completed for events in the NEUS, there is considerably more scatter in the pattern of seismicity. In fact, it can be seen that there are few areas of the NEUS-SEC which have not experienced some earthquake activity (however minor) during the historical record. Some areas with significant numbers of events not shown in Smith's (1966) map include the lower St. Lawrence River Valley, New Brunswick, Narraganset Bay, central NY, and eastern PA. There is even a conspicuous concentration of small earthquakes in central MA, although the presence of numerous quarries in this area casts some doubt on the natural origin of some of these events.

In order to evaluate the usefulness of an historical earthquake catalog, it is necessary to somehow establish the degree of completeness of the dataset. This evaluation can only be done qualitatively, based on the distribution of population and seismograph stations in the area. We now review these two aspects of the catalog, and will then examine the distribution of seismicity with time. We will also consider the problem of earthquake location and size specification from intensity data.

Distribution of Settlement and Seismic Stations: The early population distribution in New England was studied by Weston Geophysical Corp. (1977) for the purpose of evaluating the intensity data for the 1755 Cape Ann earthquake. They found that the Boston area and parts of Cape Cod were settled by 1625, while most of eastern MA, southern and central CT, southwest coastal ME, and the lower Hudson River Valley was settled by 1700. By 1780, the population had spread to central ME, NH, VT, and most of eastern NY. This of course means that the catalogs will only be accurate for the largest events before 1800. However, even in these cases, there may still be significant errors in epicentral locations and estimates of the total felt areas of events, which is useful in the determination of earthquake magnitudes.

An examination of the early settlements in eastern Canada was presented in Basham et al. (1979). The earliest settlement in eastern Canada was in Quebec City in 1608. The population moved up the St. Lawrence River to Kingston, ONT by 1673. The Maritime Provinces were settled in the 1700's. The population

spread significantly in Ontario, Quebec, and Newfoundland in the late 1800's, but permanent settlement in western Quebec and northern Ontario did not occur until the 1900's.

The history of seismic station deployment in the NEUS-SEC was compiled and reviewed by Stevens (1980b). The first continuously operating seismic station in North America was installed in Toronto in 1897. This was followed in Canada by stations in Ottawa (1906), Halifax (1915), and Kirkland Lake (1939). Most of these early stations used low gain, long period instruments installed for the purpose of recording large teleseisms and were not of use for the location of local events. Thus, they rarely recorded NEUS-SEC earthquakes of magnitude less than 5. After the occurrence of the 1925 La Malbaie, PQ earthquake (see Appendix A of this work), short period seismic stations were installed along the St. Lawrence River Valley for the purpose of recording and locating small events. In the NEUS, early stations included those at Cambridge (1908), Fordham (1910), Weston (1930), East Machias (1932), Harvard (1933), and Williamstown (1937). A telemetered seismic network was operated by Weston Observatory in the 1960's. Since the station separation was on the order of 200 km, the computed epicentral locations cannot be considered very accurate.

Given this distribution of population and seismic stations, it seems unlikely that the catalog of events is complete below magnitude 5 before 1800. The sparse population in some areas may also mean that some larger events may have their magnitudes

underestimated by the available intensity data.

Seismicity versus Time: The seismicity of the NEUS-SEC has been replotted for four time periods in Figures 2.3 a, b, c, and d, beginning in 1534. Again, the source of epicentral data for these plots is the Chiburis (1981) catalog. Mapping the events in this way allows us to make some qualitative judgements about the completeness of the historical dataset in various parts of the study area.

1534-1700: During this time period, there were 34 documented earthquakes in the study area. The first event occurred near Les Eboulments, PQ near La Malbaie. Little is known about this event, except that it probably occurred between the two voyages of Jacques Cartier (1534 to 1535). The event has a catalogued intensity of IX, although clearly there is little supporting evidence for such a high intensity. As indicated in Figure 2.3a, the event locations are coincident with those of the early settlements and trading centers. The known seismicity is confined to the upper St. Lawrence River Valley, eastern MA, and central CT. The events in central CT probably occurred near the town of Moodus, which derives its name from the Indian word "Morehemoodus" which means "the place where noises come from the ground" (Brigham, 1871). Other important events during this time period include three large events at La Malbaie, PQ, including an event in 1663 with a catalogued intensity of X.

1700-1800: Two of the most important events to affect earthquake hazards estimation in southern New England occurred

during this time period. Both events are assumed to have occurred near Cape Ann, MA. The first event, in 1727, has a catalogued intensity of VII. Street and Lacroix (1979) estimate that the magnitude of this event was 5.0 (mb). The second event, in 1755, has a catalogued intensity of VIII. An in-depth examination and review of the data for this event is presented in Appendix A of this work. There are 170 documented earthquakes in the study area during this time period. Figure 2.3b shows that again, the known seismicity is confined to the coastal regions which were the first to be settled. There are also some scattered events in NH, and a series of earthquakes in Moodus, CT beginning in 1791 with an intensity VI event. The event which is located off Cape Cod occurred in 1766 and is listed in Smith's (1966) catalog as having caused intensity VI effects on the Cape.

1800-1900: As the population grew and spread during this time period, we find significantly more events documented in the study area. There are approximately 500 events in the Chiburis (1981) catalog for this period, and as we see in Figure 2.3c, we begin to see the appearance of some definite trends in the seismicity. Many events are concentrated along coastal New England, with a prominent band of seismicity covering central NH to eastern MA. The seismicity also includes events in central CT, the New York City area, and along the NY - Canadian border. A number of moderate earthquakes affected the region during the 19th century, including intensity VII events at Wilmington, DE in 1871 and in New York City in 1884. Three intensity VII events were

documented in the Montreal, PQ area between 1893 and 1897.

1900-1975: The pattern of seismicity during this time period, shown in Figure 2.3d, shows little difference from that of the total pattern of seismicity (Figure 2.2). There are about 1700 documented events during this time period. Significant numbers of events are listed for the Canadian area, since the Canadians devoted considerable attention to earthquake hazards studies after the intensity IX earthquake at La Malbaie in 1925. A number of important events occurred during this time period, and since the population had spread to most areas and some instruments were in operation, they provide considerable information on earthquake hazards in the NEUS-SEC. These include an intensity VIII event at Attica, NY in 1929, an mb 6.2 earthquake at Timiskaming, ONT in 1935, two mb 5.4 (intensity VII) events at Ossipee, NH which are also discussed in Appendix A, and an mb 5.9 (intensity VIII) earthquake at Massena, NY in 1944. An event which is out of the study area yet deserves mention here is the Grand Banks, Newfoundland earthquake of Nov. 18, 1929 which was of mb 7.2 (Street and Turcotte, 1977). This event was felt throughout New England and eastern Canada. The turbidity current generated by this earthquake snapped twelve transatlantic communications cables, and caused a tsunami which struck Placentia Bay, Newfoundland, causing widespread destruction and some deaths.

Locations and Magnitudes from Intensity Data: Since many of the important earthquakes in the study area occurred prior to the

instrumental era, we must consider the problems of locating events and estimating their size (magnitude) from intensity data alone.

When locating an event with intensity data, there is little one can do besides place the event in the area of maximum intensity, or at the center of the isoseismal pattern. However, since many factors influence the site intensity, such as the local soil conditions or the quality of construction, locating an event in this way can sometimes lead to large errors. Two recent events illustrate this problem. The first is the July 1980 northern Kentucky earthquake. This event, which was of magnitude 5.2 (mb), caused the greatest damage (intensity VII) in an area 50 km northeast of the epicenter near Maysville, KY (Mauk et al., 1982). The cause of the high intensities far from the epicenter was the focusing of seismic waves in the valley sediments which constituted the Maysville area. Without instrumental data for this event, any seismotectonic interpretations based on the intensity derived location would be completely erroneous. The second event which illustrates this problem is the recent New Brunswick earthquake of January 9, 1982. Because of the very sparse population in the epicentral area (and also over a radius of 100 km from the epicenter), there was little damage caused by this mb 5.7 earthquake. Intensity data alone would suggest an epicenter 100 km to the west at the ME-NB border, where some intensity VI effects were observed.

One can envision a scenario where we have an isolated

population center (such as Boston in the 17th century) with few if any settlements in the surrounding area. If events occur in a large area surrounding the population center, then there is no way of telling the distance to the events (other than possibly by the duration of shaking). Consequently, any earthquake catalog for that time period would have recorded events only at the population center with the larger and distant events catalogued as low intensity local earthquakes.

Estimation of the earthquake magnitude from intensity data presents the same problem in that the intensity is a result of a number of factors which are not related to the earthquake source size. In general, the increase in intensity with magnitude has led many investigators to use a simple linear relationship of the form

$$M = A + B(I_0) \quad (2.1)$$

where I_0 is the epicentral intensity. A form of equation (2.1) which works well in New England is

$$m_b = 1.0 + 0.6(I_0) \quad (2.2)$$

Klimkiewicz (1982, personal communication) examined the relationship between body wave magnitude and epicentral intensity in New England and obtained the equation

$$m_b = 0.44 + 0.67(I_0) \quad (2.3)$$

The epicentral intensity I_0 is however often a poor indicator of earthquake magnitude, and some researchers have found that the total felt area of total area felt at an intensity level of IV is a much more stable estimate of the earthquake magnitude. For example, Street and Lacroix (1979) determined the following relationship for New England earthquakes

$$m_b L_g = 2.77 - 0.147[\text{Log}(A)] + 0.100[\text{Log}(A)]^2 \quad (2.4)$$

where A is the total felt area in square kilometers.

Regionalization: Returning to the cumulative seismicity map in Figure 2.2, we see that epicenters scatter across the entire study area, although some areas are more active than others. This scatter makes the visual assignment of seismic zones difficult to achieve, and often a function of the plotting parameters (i.e., symbol type or size). Also, it is impossible to delineate the occurrence of many events at a single location unless one resorts to three dimensional plots of seismicity. Thus, we seek a regionalization method to eliminate the background seismicity and provide an unbiased and quantitative assignment of seismic zonation.

Regionalization schemes fall into two general categories: frequency regionalization and energy regionalization. Frequency

regionalization is based solely on the number of earthquakes in an area (generally with aftershocks removed). Energy regionalization is based on the seismic energy release per unit area (including aftershocks). Each method provides different yet complementary information about the seismicity of an area.

Frequency Regionalization: A number of methods are available for determining the frequency of earthquake occurrence across an area. Hadley and Devine (1974) attempted to regionalize the seismicity of the eastern US by counting the number of events in 1 degree by 1 degree squares and then contouring. The problem with this method is that regions of seismicity smaller than 1 degree by 1 degree cannot be resolved, and simply dividing the area into smaller blocks may only introduce biases into the interpretation. Caputo (1974) applied a two dimensional spatial filtering procedure to eliminate the effect of the background seismicity and define seismic zones. Chiburis (1981) applied a modified version of Caputo's method to the NEUS-SEC; however his method suffers from a number of serious computational errors. In this study, we applied a corrected version of Chiburis' method with a number of improvements included to speed up the computations.

The algorithm is based on a two-dimensional spatial filter which weights each k event around point P(i,j) as

$$\Omega(i,j,k) = \begin{cases} 2^{-[10(x-u)]} & \text{for } u > x \\ 1 & \text{for } u \leq x \end{cases} \quad (2.5)$$

where i and j are latitude and longitude, x is the maximum location error and u is the distance from the epicenter to point $P(i, j)$. Then, for each point $P(i, j)$ we compute the weighted sum

$$S(i, j) = \sum_{i=1}^K \Omega(i, j, k) \quad (2.6)$$

where K is the total number of events within the region sampled by the spatial filter. Each $S(i, j)$ is then weighted in terms of the peak value $S(\max)$ by

$$S_w(i, j) = S(i, j)/S(\max) \quad (2.7)$$

Each point can then be contoured in term of the percentage of relative activity with respect to $S(\max)$.

This regionalization process was applied to the entire study area, covering the period 1534-1975 with all aftershocks removed, and with a maximum location error of 0.2 degrees. The result is shown in Figure 2.4 . Each contour has been shaded in terms of the percentage of relative activity above 10% of the maximum. The areas with the greatest frequency of earthquake occurrence are La Malbaie, PQ, southern NH, eastern MA, and central CT. The regionalization has defined three broad seismic zones in the area. The naming convention for these zones will follow previous conventions from other authors, where possible.

The first seismic zone delineated by this procedure is the

Western Quebec Seismic Zone, a broad area of seismicity stretching in a northwesterly direction from the Lake Champlain area in VT to the PQ-ONT border. The greatest amount of earthquake activity in this zone is at the NY-PQ border. The second zone delineated in the frequency regionalization is the Charlevoix Seismic Zone in the upper St. Lawrence River Valley. This zone appears to be two-lobed in the regionalization with the greatest amount of activity at the northern end near La Malbaie. The third zone is a broad band of seismicity stretching from coastal ME to central NH, then to the Boston area, through central CT and on to the NY-NJ area. We shall refer to this zone as the Coastal New England Seismic Zone. These three seismic zones are also visually apparent in the cumulative seismicity maps, such as Figures 2.1 and 2.2, but the regionalization has allowed us to better define their geometry, delineate small seismic zones, and separate zones within zones. The small zones delineated include the lower St. Lawrence area, central ME, eastern ME near Passamoquoddy Bay, three zones in the Hudson Valley, the Attica zone, and the Niagara zone.

The frequency regionalization just presented is based on our total accumulated knowledge of the seismicity of the NEUS-SEC. As discussed earlier, this knowledge is not uniformly distributed across the study area. That is, we know of more events in the populated areas than in the unpopulated ones. To account for this situation, we have recomputed the frequency regionalization over a dataset using only events of magnitude greater than or

equal to 3 1/2 (mb) or intensity greater than or equal to IV. This regionalization is shown in Figure 2.5 . There are some interesting differences in this regionalization when compared to that of the entire dataset. For one thing, there are no longer any continuous, large seismic zones in the area. The Coastal New England Seismic Zone, defined earlier, has now been broken up into a number of smaller zones. The largest is the band of seismicity stretching from Boston to central NH. The seismicity of ME has now been delineated into a number of small circular zones in the central, eastern, and southern portion of the state. Central CT is also delineated as a separate, small seismic zone. The Western Quebec Seismic Zone has been separated into a number of small zones, with the greatest frequency of activity occurring on the NY-PQ border. The greatest similarity in the two frequency regionalizations is the delineation of the Charlevoix Seismic Zone, which in both cases stands out as the most seismically active region in the study area.

Energy Regionalization: The regionalization of energy provides a dynamic characterization of the seismicity in an area. In contrast to the frequency regionalization just presented, energy mapping permits the estimation of other source parameters such as the maximum magnitude and ground acceleration, which are of engineering significance.

In order to delineate the seismic energy release in the NEUS-SEC, we will apply the "Moving-Block" method of Bath (1982). In this method, the total seismic energy release is calculated

for a succession of partially overlapping areas, or blocks. Any relationship between magnitude and seismic energy may be used, and in this case we relate the seismic energy in ergs to the body wave magnitude via the equation

$$\text{Log}(E) = 5.8 + 2.4(\text{mb}) \quad (2.8)$$

from Gutenberg and Richter (1941).

A block size of 0.25 by 0.25 degrees was chosen for the calculations. The grid spacing between blocks was chosen as 0.125 degrees, providing a 50% overlap of adjacent blocks. This overlap acts as a smoothing function to eliminate any biases which may be introduced by the grid spacing.

The seismic energy release in the study area for the period 1534-1975 has been displayed as a variable density plot in Figure 2.6. The gradations in the seismic energy release cover three distinct energy bands. The logarithms of these bands in ergs are: 16 to 18, 18 to 20, and ≥ 20 . These correspond to the equivalent energy in the magnitude ranges (mb) 4.2 to 5.0, 5.01 to 5.9, and ≥ 5.9 , respectively. The four areas with the greatest seismic energy release are the Charlevoix zone, the Cornwall, ONT - Massena, NY area, the Timiskaming, ONT area, and Cape Ann, MA. Secondary areas of seismic energy release include the lower St. Lawrence, the Montreal, PQ area, parts of western PQ, central NH in the Lakes Region, western NY at Attica, and the NY-NJ coastal area.

It is of interest to compare the results of the energy regionalization with that of the frequency regionalization. The Charlevoix Seismic Zone is distinctive in both the frequency and energy regionalizations and stands out as a unique seismic source zone in the study area. The Boston to central NH area is also delineated in both regionalizations. The extreme ends of this zone are the most active in terms of both the frequency of occurrence and the energy release. Of course, whether or not this is a continuous zone of seismicity depends on the assumed location of the 1755 Cape Ann earthquake. If this event was farther out to sea, as has been proposed by some investigators (see Appendix A), then the central NH area may be its own unique source zone separate from the activity in eastern MA. Taken together, the two regionalizations suggest, but do not prove, that the seismic source zones in the NEUS-SEC are small in extent and do not form continuous bands of seismicity.

2.2.2 Return Times and Probabilities of Earthquake Occurrence

Given the distribution and regionalization of epicenters outlined in the previous section, we now turn to the calculation of the return times and probabilities of earthquake occurrence in each of the major seismic zones. Four statistical methods will be used, with the aim of comparing and contrasting the results of each method.

The first method employs the well known relationship

$$\text{Log}[N(M)/\text{yr}] = a - b(M) \quad (2.9)$$

where $N(M)$ is the cumulative number of earthquakes of magnitude greater than or equal to M , yr is the number of years covered in the dataset, and a and b are the constants to be determined. We will use the body wave magnitude (m_b) as the source size specification for all of the calculations. The method of least squares will be used to determine the constants a and b .

Equation (2.9) can also be written in terms of intensities, with different values of a and b resulting from the process. However, we choose to perform the calculations in terms of magnitude, since the epicentral intensity is a combination of the effects of earthquake magnitude, focal depth, local soil conditions, and construction practices. Consequently, the epicentral intensity is often site-specific, and may be only loosely related to the earthquake process which we are trying to model. If the relationship between magnitude and intensity is of the form

$$M = A + B(I) \quad (2.10)$$

then equation (2.9) can be transformed by substitution to

$$\text{Log}[N(I)/yr] = (a - bA) - (bB)I \quad (2.11)$$

The second method we will use to estimate return times is the maximum likelihood estimate of " b " in equation (2.9) which is given by Aki (1965) as

$$b = \log(e)/[\underline{M} - M(\min)] \quad (2.12)$$

Here, \underline{M} is the average magnitude, $M(\min)$ is the minimum magnitude in a given sample, and e is 2.7183...

There is an abundance of worldwide and local calculations of "b" values in the literature, and the value of this constant is generally between 0.9 and 1.0 (Chinnery and North, 1975), although some departure have been noted. Nuttli (1974) applied the first and second methods to the Mississippi River Valley Seismic Zone and obtained a "b" value of 0.92 using least squares, and 0.87 using the maximum likelihood method.

In both the first and second methods, the return time, or number of years between events of magnitude at least M is given by

$$T_o(M) = 10^{[b(M)-a]} \quad (2.13)$$

If the sequence of earthquakes is a Poissonian process, then the probability that an earthquake with a return time of T_o years will occur in T years is given by

$$P[T, T_o(M)] = 1 - \exp[-T/T_o(M)] \quad (2.14)$$

One method of demonstrating the approximate Poissonian character of a sequence of earthquakes is to plot the frequency distribution of interoccurrence times (Lomnitz, 1966; Chinnery,

1979). In some cases, the Poissonian distribution has been shown to be a good description for large events (e.g., Gardner and Knopoff, 1974) whereas other studies have shown departures from Poisson statistics (e.g. Shlien and Toksöz, 1970).

The third and fourth methods we will use employ Gumbel's theory of extreme events (Gumbel, 1954, 1958). The advantage of using the extreme values of a geophysical variable is that they are more easily determined than all other occurrences in a time series of observations. However in earthquake seismology, these events have the longest return times and in many cases represent only one sample in a time series. Thus, the extreme value method is highly dependent on this poorly known parameter. Knopoff and Kagan (1977) and Weichert and Milne (1979) found that the theory of extremes gives unacceptably large errors in the determination of return times. Thus, it will be instructive to compare the results of this method with those of the previous two.

According to Gumbel, there are three types of asymptotic distributions of extremes. The Type I distribution assumes that the variable is unlimited, while the Type II includes a lower limit, and the Type III includes an upper limit. In this study, we will apply the Type I distribution as the third method, and Type III distribution as the fourth method.

For the Type I distribution, the probability that the magnitude of the largest yearly earthquake (M') will be less than M is given by

$$P(M' < M) = \exp[-\{\exp(-\alpha(M-\mu))\}] \quad (2.15)$$

where α and μ are the constants to be determined. If we take double logarithms of equation (2.15) and rearrange terms, we obtain

$$M = \mu - (1/\alpha) \ln[-\ln(P)] \quad (2.16)$$

To find α and μ , the largest observed yearly (or in any interval) magnitudes of a sequence of earthquakes $M(1), M(2), \dots, M(N)$ are arranged in order of increasing size. The value of P is then

$$P(n) = n/(N+1) \quad (2.17)$$

where N is the total number of years, and n varies from 1 to N . Equation (2.16) is a simple linear equation of the form

$$Y = Ax + B$$

where $Y=M$, $A=-(1/\alpha)$, $x=\ln[-\ln(P)]$, and $B=\mu$. Thus, μ and α can be found by simple linear least squares.

For the Type III distribution with an upper limit of $M(\max)$, the probability that the largest yearly earthquake (M') will be less than M is given by

$$P(M' < M) = \exp[-\{(M(\max)-M)/(M(\max)-\mu)\}^k] \quad (2.18)$$

where k and μ are the constants to be determined. As before, equation (2.18) can be rearranged to

$$M = M(\max) - [M(\max) - \mu] [-\ln(P)]^{1/k} \quad (2.19)$$

Further manipulation yields

$$\ln(M(\max) - M) = (1/k) \ln[-\ln(P)] + \ln(M(\max) - \mu) \quad (2.20)$$

which is also of the form

$$Y = Ax + B$$

where $Y = \ln(M(\max) - M)$, $x = -\ln(-\ln P)$, $\mu = M(\max) - \exp(B)$, and $-(1/k) = A$. Thus, μ and k are again solved by simple linear least squares. The inverse of the exceedence probability is then simply

$$P(M' \geq M) = 1 - P(M' < M) \quad (2.21)$$

To apply these equations to the seismic zones delineated in the previous section, we must first extract from the master earthquake catalog the events within each seismic zone. This can be accomplished in a number of ways. The simplest way is to approximate the seismic zone by a number of rectangles, select the events within each rectangle, and then combine the datasets.

This is a tedious and inefficient process. A fast way of selecting events within an irregularly shaped seismic zone is provided by the "Winding-Number Algorithm", which is described in Appendix B of this work.

For each catalogued earthquake, there are four possible source size specifications, and each possibility must be properly used in the calculation of return times for events of a given magnitude. Each event may be specified by 1) both magnitude and intensity, in which case we use the magnitude; 2) magnitude but no intensity, we simply use the magnitude; 3) intensity but no magnitude, in which case we convert intensity to magnitude using the equation $m_b = 1 + 0.6I$; 4) neither magnitude nor intensity given, in which case we ignore the entry unless another catalog gives a source size.

Western Quebec Seismic Zone: In this seismic zone we choose the time period 1844 - 1975 as being a representative sample of the statistical distribution of seismicity. The dataset includes 403 events, with foreshocks and aftershocks removed. Examples of larger events in this seismic zone include: 13Jul1861 Int. VII at Ottawa, 27Nov1893 Int. VII at Montreal, and 05Sep1944 magnitude 5.9 (mb) at Massena, NY.

Figure 2.7 shows a plot of the $\text{Log}[N(m_b)/\text{yr}]$ versus m_b statistics for this dataset, along with a least squares fit between magnitudes 3.7 and 5.9 and 95% confidence intervals. The equation of this line is

$$\text{Log}[N(\text{mb})/\text{yr}] = 3.076 - 0.897(+/- .030)\text{mb} \quad (2.22)$$

Before continuing, let us examine whether or not this dataset represents a Poissonian process. For this test, we select from the dataset the earthquakes of intensity at least V or magnitude at least 4.0 (again with foreshocks and aftershocks removed) and plot the interoccurrence times of these events. These are shown as a statistical distribution in Figure 2.8. The mean interoccurrence time for this dataset is 2.00 years. Also shown on Figure 2.8 is a theoretical plot of a Poissonian process with a mean return time of 2.00 years. The dataset is closely Poissonian. The only departure from this nature is the single occurrence of a 16 year period with no events. This is likely due to the incompleteness of the catalog.

The return times and probabilities of occurrence calculated from equations (2.22) and (2.13) are listed in Table 2.1a. The mean return time for an event of magnitude at least 5.0 is 23.8 years with a 99% probability of occurrence in 100 years. For an event of magnitude at least 6.0, the mean return time is 188 years with a 41% probability of occurrence in 100 years. For an event of magnitude at least 6.5, the mean return time is 526 years with a 17% probability of occurrence in 100 years. If we extend these calculations to $\text{mb}=7.0$, we obtain a mean return time of 1480 years. The errors in these calculations are quite substantial for the larger events. For a magnitude at least 6.0, the return time at a 95% confidence level is between 113 and 309

years with a probability of occurrence between 28% and 59% in 100 years. For a magnitude at least 6.5, the return time is between 310 and 895 years with a probability of occurrence between 11% and 28% in 100 years.

Table 2.1b compares these results with the maximum likelihood method and Gumbel Type I and III distributions. The maximum likelihood method with a minimum magnitude of $m_b=3.7$ yields the equation

$$\text{Log}[N(m_b)/\text{yr}] = 2.574 - 0.785(+/- .272)m_b \quad (2.23)$$

This equation predicts shorter return times for the larger events. For example, for a magnitude at least 6.0, the mean return time is 151 years, and for a magnitude at least 6.5, the mean return time is 385 years.

Figure 2.9 shows the application of Gumbel's Type I distribution to this dataset. The equation we obtain, using the largest events of magnitude at least 4.0 grouped in five year intervals is

$$P(m_b' < m_b) = \exp[-\{\exp(1.988(m_b-4.326))\}] \quad (2.24)$$

This equation predicts that the mean return time for a magnitude 6.0 event is 142 years with a 70% probability of occurrence in 100 years. Similarly, for a magnitude 6.5 event, the mean return time is 380 years with a 26% probability of occurrence in

100 years. It is interesting to note that these values lie nearly halfway between the values predicted by the maximum likelihood and least squares methods.

If we apply Gumbel's Type III distribution to this dataset with a maximum magnitude of 8.0, we obtain the equation

$$P(m_b' < m_b) = \exp\left[-\left\{\frac{8-m_b}{3.655}\right\}^{6.239}\right] \quad (2.25)$$

Because of the nature of the Type III distribution and the fact that the largest event in the sample is of magnitude $m_b=5.9$, the return times predicted by equation (2.25) are significantly longer than those predicted by the previous three methods. For an event of $m_b=6.0$, the mean return time is 218 years with a 42% probability of occurrence in 100 years. For $m_b=6.5$, the mean return time is 1230 years with an 8% probability of occurrence in 100 years. This return time is twice as long as that predicted by the simple $\text{Log}[N(m_b)/\text{yr}]$ vs. m_b method. Extrapolating to $m_b=7.0$, the mean return time is 16,200 years.

Charlevoix Seismic Zone: In this seismic zone, we chose the time period 1818 - 1975 as being a representative sample of the statistical distribution of seismicity. The dataset includes 199 events, with foreshocks and aftershocks removed. Examples of large events in this zone include: 20Dec1870 Int. IX at Baie-St-Paul and 01Mar1925 $m_b=6.6$ at La Malbaie.

Figure 2.10 shows the $\text{Log}[N(m_b)/\text{yr}]$ versus m_b statistics for

this dataset. The equation of the least squares line fit between magnitude 4.0 and 6.7 is

$$\text{Log}[N(\text{mb})/\text{yr}] = 1.619 - 0.569(+/- .015)\text{mb} \quad (2.26)$$

Note that the "b" value of 0.569 is very low when compared to that of the Western Quebec zone.

The return times in the seismic zone calculated from equations (2.26) and (2.13) are considerably shorter in this zone than in the Western Quebec zone. The mean return time for an event of magnitude at least 5.0 is 16.8 years, with a 95% confidence interval between 12.0 and 23.7 years. The probability of this event occurring within 50 years is between 89% and 98%. For an event of magnitude at least 6.0, the mean return time is 62.4 years, with a 95% confidence interval between 44.1 and 88.3 years. The probability of this event occurring within 50 years is between 43% and 68%. For an event of magnitude 7.0, the mean return time is 231 years with a 95% confidence interval between 160 and 334 years. This is an extremely short period of time for an event of this size in an intraplate area.

Table 2.2b compares these estimates with the results of the maximum likelihood and Gumbel Type I and III methods. Using the maximum likelihood method, we obtain the relationship

$$\text{Log}[N(\text{mb})/\text{yr}] = 1.578 - 0.560(+/- .162)\text{mb} \quad (2.27)$$

This method produces return times nearly equal to those of the least squares method. For an event of at least magnitude 6.0, the maximum likelihood mean return time is 60.5 years with a 56% probability of occurrence in 50 years. For an event of magnitude at least 7.0, the mean return time is 219 years with a probability of occurrence of 20% in 50 years.

Figure 2.11 shows the application of Gumbel's Type I distribution to this dataset for earthquakes greater than magnitude 4.0, and spaced into 5 year intervals. From this, we obtain the equation

$$P(mb' < mb) = \exp[-\{\exp(-1.477(mb-4.398))\}] \quad (2.28)$$

This equation yields a mean return time of 55.8 years for an event of magnitude at least 6.0 with a 98% probability of occurrence in 50 years. For an event of magnitude at least 7.0, the mean return time is 236 years with a 21% probability of occurrence in 50 years.

For the Gumbel Type III distribution with a maximum magnitude of $mb=8.0$, we obtain the equation

$$P(mb' < mb) = \exp[-\{(8.0 - mb)/(3.918)\}^{4.082}] \quad (2.29)$$

With the exception of the largest event ($mb=7.0$), the Type III distribution for this dataset yields values of return times and probabilities which are very close to the Type I distribution.

This is because there are large events in the dataset. For an event of magnitude at least 6.0, the mean return time is 55.6 years with a 90% probability of occurrence in 50 years. For an event of magnitude at least 6.5, the mean return period is 174 years with a 29% probability of occurrence in 50 years. The return time for the magnitude 7.0 event is, however, quite long, with a mean value of 902 years.

Boston - New Hampshire Seismic Zone: For this seismic zone, we will take a somewhat different approach to the calculation of return times. In the previous two seismic zones, we performed the calculations on mb datapoints with events specified only by intensities converted using the standard formula. This was a valid procedure since in both zones there were independent magnitude estimates for most of the events. However, in the Boston - NH Zone, there are few magnitudes given. Most source sizes are specified only by an intensity value. Converting the data to magnitudes before the regression is performed may only contaminate the calculations. Therefore we will perform all of the calculations on the original intensity values. These may later be converted to magnitudes if necessary. We shall use the time period 1727-1975 as a representative sample of the statistical distribution of the seismicity. This time period includes the 1727 intensity VII event and the 1755 intensity VIII event at Cape Ann, MA.

Figure (2.12) shows the $\text{Log}[N(I)/\text{yr}]$ versus I data for this

seismic zone. The equation of the least squares line fit between intensities IV and VIII is

$$\text{Log}[N(I)/\text{yr}] = 1.539 - 0.498(+/- .034)I \quad (2.30)$$

Table 2.3a summarizes the return times computed from this equation. For an intensity VII event, equation (2.30) predicts a mean return time of 88.4 years with a 90% probability of occurrence in 200 years. For an intensity VIII event, the mean return time is 278 years with a 51% probability of occurrence in 200 years. Extrapolating to intensity IX, the mean return time is 876 years with a 20% probability of occurrence in 200 years.

We can now convert equation (2.30) to the equivalent magnitude recurrence relationship, which is

$$\text{Log}[N(\text{mb})/\text{yr}] = 2.369 - 0.830(+/- .057)\text{mb} \quad (2.31)$$

For a magnitude 6.0 (mb) event, equation (2.31) predicts a mean return time of 408 years with a 39% probability of occurrence in 200 years. For a magnitude 6.5 event, the mean return time is 1060 years with a 17% probability of occurrence in 200 years.

The maximum likelihood method was not applied to this dataset since it does not work well when the discretization is large (i.e., 1 unit for intensity values).

Figure 2.13 shows the application of Gumbel's Type I distribution to the dataset. The equation we obtain is

$$P(I' < I) = \exp[-\{\exp(0.878(I-4.919))\}] \quad (2.32)$$

Table 2.3b compares the results of this method with those of the previous one. The mean return time for an intensity VII event in this zone is 168 years with a 100% probability of occurrence in 200 years. For an intensity VIII event, the mean return time is 386 years with a 52% probability of occurrence in 200 years. Extrapolating to intensity IX, the mean return time is 911 years with a 22% probability of occurrence in 200 years.

Two independent estimates of return times are available for the Boston - NH Seismic Zone. Chinnery and Rogers (1973) used the data from Smith (1962, 1966) and the $\text{Log}[N(I)/\text{yr}]$ vs. I method to estimate the return times of the large events in this zone. Their return time for an intensity VIII event was 371 years, and for an intensity IX event they obtained 1445 years. These values are somewhat longer than the return times computed in this work. This is likely due to the fact that they used the time period 1800-1959 as a statistical sample of the seismicity. This time period was after the occurrence of the 1727 and 1755 Cape Ann earthquakes, which were included in our calculations. Shakal and Toksöz (1975) used the Gumbel Type I distribution over the time period 1725 to 1974 and computed a return time of 130 years for an intensity VIII event. This is less than half the time period computed in this study. Part of the reason for this discrepancy may lie in the fact that they have used two events of intensity between VIII and IX in their calculations (probably the

1727 and 1755 Cape Ann earthquakes with overestimated epicentral intensities). The maximum intensity in our dataset is VIII. This would certainly shorten the calculated return time for an intensity IX event.

Maximum Credible Earthquakes: Given these statistical earthquake relations, we can now estimate for each seismic zone the maximum credible earthquake magnitudes. The term "maximum credible earthquake" can be defined in a number of ways, but one widely acceptable definition follows from Nuttli and Herrmann (1981) who use the corresponding earthquake magnitude or intensity for a 1000 year return period. Using this definition, the maximum credible earthquake in the Western Quebec Seismic Zone corresponds to a magnitude 6.8 (mb) event. For the Charlevoix Seismic Zone, the maximum credible earthquake corresponds to a magnitude 8.1 (mb) event. And for the Boston - NH Seismic Zone, the maximum credible earthquake corresponds to an intensity IX or magnitude 6.5 (mb) event.

2.3 Instrumental Seismicity

Nearly all of the shortcomings of historical earthquake reports are alleviated with the use of instrumental network data. The only problem to date with the instrumental data in the NEUS-SEC is the limited number of years the network has been in operation. However, the instrumental data does provide some important constraints on the interpretation of the historical dataset. In this section, we examine the results of six years of network operation in this area. This includes a short

description of the N.E.U.S.S.N., a regionalization of epicenters, discussion of the magnitude problem, and focal depth determinations for some New England earthquakes.

2.3.1 The N.E.U.S.S.N.

In 1975, a consortium of universities and private agencies was formed for the purpose of installing a dense, short period, high gain telemetered seismic network in the NEUS-SEC. This network, known as the Northeastern United States Seismic Network (or N.E.U.S.S.N.) was to provide high quality data for the determination of earthquake hypocenters and magnitudes, and provide a database for further seismological study, such as the determination of the crust and upper mantle structure of the area. The N.E.U.S.S.N. presently consists of over 120 stations in the NEUS-SEC. A map of the present network configuration is shown in Figure 2.14 . (Some of the stations in Figure 2.14 are now closed.) In many cases, the distribution and geometry of the stations has been controlled by the pattern of historical events, meaning that more stations have been placed in areas where the historical seismicity is great. Station distribution has also been controlled to some extent by access to seismically quiet areas. All station locations are given in Appendix C as well as detailed maps of the station distribution in various subareas of the NEUS-SEC.

Instrumentation at N.E.U.S.S.N. stations consists of 1 Hz vertical seismometers, with some stations having 3-component instruments. The seismometers are generally either Mark Products

L4-C or Hall Sear HS-10 instruments. The sensors are connected to preamplifiers and voltage controlled oscillators, with the data transmitted in analog format over leased voice grade telephone lines. The data are transmitted to a number of central recording stations, including Weston Observatory, M.I.T., and Lamont Doherty Geological Observatory. For many years, recording was done only in analog format on either helicorders or develocorders through 16 Hz galvanometers. This provides a peak frequency of about 8 Hz. Station gains range from about 60,000 at 1 Hz at the noisy sites to about 100,000 at 1 Hz at the quiet sites. These gains increase by about a factor of 10 up to the peak frequency. Recently, a number of institutions have converted their recording facilities to digital recording format. Appendix D describes the digital data acquisition system and event detector installed for the M.I.T. Seismic Network.

The reading accuracy of the data varies with the recording format. For helicorders recording at 30 mm/min, the best resolution is about 0.5 sec. At a recording speed of 60 mm/min, the resolution is about 0.2 sec. Enlarged develocorder records provide a reading accuracy of 0.05 sec. For digital recordings, the reading accuracy is equal to the sampling rate. At present, the M.I.T. Seismic Network digital recording system operates at a sampling rate of 25 samples per second. This provides a reading accuracy of 0.04 sec. The system is now being upgraded to record at a sampling rate of 100 Hz, which will provide a reading accuracy of 0.01 sec.

Given the distribution of seismic stations and their respective gains, we can go on to estimate the sensitivity of the network in terms of both detection and location thresholds. For an event to be detected, we assume that it can be seen on a minimum of two stations with twice the average background noise level. This can be stated in terms of Lg-wave amplitudes and their equivalent m_bL_g magnitudes as defined by Nuttli (1973). Given this definition, we find that the detection threshold across all of the study area is $m_bL_g=1.75$. For most of southern New England, the detection threshold is $m_bL_g=1.5$, and in areas with high station density, such as eastern MA, CT, and southeastern NY - northern NJ, this reduces to $m_bL_g=1.25$. In areas with special dense arrays, such as Moodus, CT, the detection threshold is as low as $m_bL_g=-2$. However, this definition of detection threshold does not necessarily mean that an event can be located. To locate an event, we need at least three stations to record the P-waves. These P-wave amplitudes can be two to ten times smaller than the corresponding Lg amplitudes, depending on the distance to the station. Using this concept, the location threshold across the study area is $m_bL_g=2.0$. In areas of higher station density, specified earlier, this reduces to $m_bL_g=1.5$.

To locate an event, we must have a crustal model to predict travel times to recording stations. A number of crustal models are used to locate NEUS-SEC earthquakes, depending on the source region. These models are discussed in Section 3.2.1 of this

work. The primary consideration in the application of these models is the difference in crustal structure between the Grenville and Appalachian Provinces. In the Grenville Province, the crust is very homogeneous, consisting of a single crustal layer of nearly constant velocity. The average crustal thickness is 37 km. However, in the Appalachian Province, the crust consists of two or three layers with some areas having a high velocity lower crustal layer. The average crustal thickness in the Appalachian Province is 40 km.

Location accuracy for the instrumental dataset varies from event to event, but is in general better than 10 km. For most events with good azimuthal station distribution, this reduces to 2 km. One way to examine the location accuracy of a network is to locate a controlled source, such as a quarry blast. This is illustrated in Figure 2.15. The quarry used in this demonstration is at the McClellan Construction Company near Manchester, NH. This quarry is located near the center of the M.I.T. Seismic Network. At the top of the figure, a record section has been plotted showing waveforms from one of their blasts. Note the prominent surface waves which are distinctive of surface or near surface sources. The azimuthal coverage for this blast is shown in the middle illustration. The maximum gap in azimuth is 86 degrees. Using this dataset to locate the blast, the location is in error by 1.4 km to the northwest. At the bottom of this figure we illustrate the use of the arrival-order-location method described by Anderson (1981). In

this method, the order of station arrivals is used to construct perpendicular bisectors between stations of increasing arrival order. This provides an estimate of the location sensitivity independent of crustal model (assuming no severe lateral heterogeneity). The location based on this method is 1.2 km from the actual location of the quarry. Thus, for events within the network with good azimuthal coverage in areas with no severe crustal velocity heterogeneity, we expect that the location accuracy is about 2 km.

2.3.2 Distribution and Regionalization of Epicenters

Figure 2.16 shows the epicentral locations of all events located by the N.E.U.S.S.N. during the instrumental period. There are approximately 700 earthquakes in this dataset. In many ways, this distribution of epicenters is a mirror image of the historical data. To provide an unbiased estimate of the distribution of seismicity, we now apply the frequency and energy regionalizations, outlined earlier, to this dataset.

Frequency Regionalization: The frequency regionalization described in Section 2.2.1 was applied to the instrumental dataset using a maximum location error of 0.1 degrees and a minimum magnitude of 2.0 (mb). The result of this regionalization is shown in Figure 2.17. The most seismically active region in the study area during the instrumental period is the Charlevoix Seismic Zone. The lateral extent of this zone is smaller for the instrumental dataset, due to the more accurate epicentral locations. Two relatively large zones delineated by

the procedure are at the NY-PQ border, and in southeastern NY and northern NJ. This second zone is also the second most seismically active area in the instrumental dataset. Other small seismic zones delineated include central ME, southwest ME, Passamoquoddy Bay, central and southern NH, central CT, and the upper Hudson Valley near Blue Mountain Lake. Note that the lateral extent of the seismic zones delineated by this regionalization are quite small.

Energy Regionalization: For the energy regionalization of the instrumental dataset, two changes will be made. The first change is that we have included the 09Jan82 New Brunswick and 19Jan82 Gaza, NH earthquakes in the calculation. This is because they have the largest effects on the results. No other events which have occurred since the defined end of the instrumental dataset (September 1981) and January 1982 have any effect on the results of the energy regionalization. The second change is that the energy bands delineated have been reduced by a factor of 100 to account for the shorter time period covered by the instrumental dataset. These energy bands are in log ergs: 14-16, 16-18, and ≥ 18 . These correspond to the equivalent seismic energy release in the magnitude ranges 3.4-4.2, 4.2-5.0, and ≥ 5.0 respectively.

The area with the greatest seismic energy release is that of the New Brunswick earthquake. Secondary areas of energy release include the Charlevoix Seismic Zone and central NH, the site of the Gaza earthquake. There is in general good agreement between

the results of the frequency and energy regionalizations. The Charlevoix Seismic Zone, New Brunswick, central NH, and the NY-PQ border area all stand out as areas of both frequent and energetic earthquake activity. There are however some important differences. The seismic zone delineated in central ME is due to low magnitude events, whereas larger, less frequent events occur along the coast of that state. Likewise, in central CT there are frequent but low magnitude events so that the area does not show up in the energy regionalization. This is also the case in southeastern NY and northern NJ.

2.3.3 Magnitudes of NEUS-SEC Earthquakes

Magnitude calculations for NEUS-SEC earthquakes have long been a point of confusion and controversy. The reasons for this situation relate to the fundamental concept of earthquake magnitude and the problem of the variation in crustal Q and earthquake source parameters between the western and eastern US. Although magnitude calculations may be internally consistent within a network, the true value of this parameter lies in the comparison of earthquake magnitudes for worldwide events. It is only in this way that we can relate strong ground motion records from one area to another.

Drawing from the concept of stellar magnitudes, Richter (1935) developed the instrumental magnitude scale for southern California earthquakes. He defined the local magnitude, M_L , as

$$ML = \text{Log}[A(\Delta)] - \text{Log}[A_0(\Delta)] \quad (2.33)$$

where $A(\Delta)$ is the maximum trace amplitude of an earthquake at a distance Δ as recorded on a Wood-Anderson torsion seismograph, and $A_0(\Delta)$ is a reference amplitude of a magnitude zero earthquake at the same distance Δ . The function $A_0(\Delta)$ was derived from plots of seismic wave amplitude versus distance in southern California, so that this function is a reflection of the attenuation characteristics in this calibration area. Thus if equation (2.33) is applied to an area where the seismic wave attenuation is significantly different, the ML value calculated will be in error, either underestimating or overestimating the actual earthquake magnitude. In addition, equation (2.33) does not specify that a particular frequency be used in the calculation, yet both seismic wave attenuation and the earthquake source spectrum are frequency dependent. For many years, ML values were calculated in the NEUS-SEC using equation (2.33) without any correction term for the difference in seismic wave attenuation. This was primarily because it was unknown at the time that any difference existed.

To aid in the calculation of magnitudes in eastern US networks, Nuttli (1973) introduced the mbLg magnitude scale. Nuttli's (1973) formulas for computing magnitudes from 1-Hz vertical Lg waves are

$$mbLg = 3.75 + 0.90[\text{Log}(\Delta)] + \text{Log}(A/T) \quad \text{for} \quad 0.5 \leq \Delta \leq 4.0 \quad (2.34a)$$

$$mbLg = 3.30 + 1.66[\text{Log}(\Delta)] + \text{Log}(A/T) \quad \text{for} \quad 4.0 \leq \Delta \leq 12.0 \quad (2.34b)$$

where A is the zero to peak amplitude in microns, T is the period in seconds, and Δ is the distance in degrees. These equations were developed by measuring (A/T) values for eastern US earthquakes and fitting straight line approximations of the equation for Airy phase propagation to the data. Since the events used to measure the attenuation were large enough to be recorded teleseismically, Nuttli (1973) was able to specify the value of the leading coefficients (3.75 and 3.30) by tying the results to teleseismic mb measurements.

Equations (2.34a, b) specify that 1.0 Hz Lg waves are to be used in the calculation of magnitudes. However, in New England, 1.0 Hz waves are generally not observed. Lg frequencies are usually greater than 5 Hz. This is likely due to the fact that earthquakes in this area have greater corner frequencies than those in the central US. Thus, dividing by the period (A/T) has the effect of overestimating the actual earthquake magnitude. Recently, magnitude calculations using Nuttli's (1973) equations have been made by using values of amplitude alone (A) rather than (A/T) to eliminate this overestimation.

In practice, it is often difficult to apply magnitude formulas such as equations (2.34a, b). This is because the analog transmission and recording systems used in most short

period networks limits the dynamic range of the seismic channels. In addition, there is poor visual resolution of the higher frequencies. In such cases, a number of investigators (e.g. Lee et al., 1972; Herrmann, 1975; Chaplin et al., 1980) found that a coda magnitude scale is appropriate. The coda length of a local event can be defined in a number of ways, but is usually the total time elapsed from the beginning of the P-wave arrival to the point in the tail of the seismogram where the signal to noise ratio becomes one. The coda magnitude formula is then of the form

$$M_c = A + B[\text{Log}(\tau)] + C(\Delta) + D[\text{Log}(\Delta)] \quad (2.35)$$

where τ is the coda duration, Δ is the epicentral distance, and A, B, C, and D are constants. It is usually the case that these constants C and D are very small, so that there is little distance dependence of the coda length. Chaplin et al., (1980) determined a coda length magnitude formula New England by correlating the coda lengths with mbLg magnitudes as reported in the N.E.U.S.S.N. Bulletins. Their resulting equation was

$$M_c = 2.21[\text{Log}(\tau)] - 1.70 \quad (2.36)$$

However, as discussed earlier, the magnitudes reported in the N.E.U.S.S.N. Bulletins may be overestimated, since high frequency Lg waves were used in the calculations. Thus, equation

(2.36) will be likewise biased toward the high end of the magnitude scale. To overcome this problem, we have recomputed the coda length magnitude scale using the ML values from Ebel (1982). In this paper, Ebel (1982) computed ML values for New England earthquakes by applying a correction term to Richter's (1935) formula (equation 2.33) to account for the difference in seismic wave attenuation between the western and eastern US. The equation we have obtained is

$$ML = 2.08[\text{Log}(\tau)] - 1.91 \quad (2.37)$$

Magnitudes determined from equation (2.37) can thus be directly compared with those calculated for western US earthquakes.

2.3.4 Focal Depths of NEUS-SEC Earthquakes

Focal depth information is very important in the estimation of earthquake hazards. For one thing, the distribution of earthquake hypocenters allows us to delineate the three dimensional structure of the seismic zones, and aids in the correlation of the earthquake activity with geologically known faults. Also, the focal depth is an important source property in the calculation of potential ground motion, for a shallow earthquake will generate more surface waves and crustal reverberations than a deeper event (e.g., Bouchon, 1976). However, focal depths are generally unknown for most NEUS-SEC earthquakes, because of the large station to epicenter distances. For many years it was thought that most NEUS-SEC earthquakes were

deep because they were felt over broad areas and never produced surface faulting. This is discussed in detail in Appendix A of this work. In this section, we review available focal depth information in the NEUS-SEC and compute focal depths for some New England earthquakes by examining the depth convergence of station residuals.

Western NY: Focal depths are available for two earthquakes in this area. Herrmann (1978) studied the Attica, NY earthquakes of January 1, 1966 and June 12, 1967 by using surface wave radiation patterns and P-wave polarities. The focal depths computed for these events were both between 2 and 3 km. This area was the site of an intensity VIII earthquake in 1929, which was of magnitude 5.2 (mb). If the 1929 event was as shallow as the 1966 and 1967 events, this would account for the relatively high epicentral intensity for a magnitude 5.2 event.

Northern NY - western PQ: Focal depth information in this area is available from both aftershock studies and surface wave radiation patterns for the larger events.

Schlesinger-Miller et al. (1981) studied the aftershocks of the 1981 Cornwall, ONT earthquakes using an array of portable seismographs and determined that the aftershocks were concentrated in a small source volume at a depth of of 16 km. At Blue Mountain Lake, NY, Sbar et al. (1975) studied earthquake swarms using both temporary and permanent stations and delineated conjugate dipping fault zones striking NW. The focal depths ranged from 0.5 to 2.0 km. At nearby Racquette Lake, NY,

Aggarwal et al. (1975) studied the aftershocks of the November 3, 1975 earthquake and found a similarly oriented fault plane with focal depths ranging from 1 to 3 km. At Plattsburgh, NY, Aggarwal et al. (1975) located earthquake aftershocks and delineated focal depths ranging from the surface to 20 km.

Canadian seismologists have studied the surface wave radiation patterns of the 1975 Maniwaki, PQ earthquake and the 1978 St. Donat, PQ earthquake. The computed focal depths from these studies were 17 and 7 km, respectively (Horner et al., 1978 and Horner et al., 1979).

La Malbaie, PQ: This area has been intensively studied by Canadian seismologists since the destructive 1925 earthquake. There is presently a multi-element seismic array operating in this zone. In addition, and two reconnaissance microearthquake studies have been conducted by Leblanc et al. (1973) and Leblanc and Buchbinder (1977). Focal depths in this area range from the near surface to 20 km and all occur within the Paleozoic structure. Hasegawa and Wetmiller (1980) studied the surface wave radiation pattern of the August 19, 1979 La Malbaie earthquake and determined a focal depth of 15 km.

New Brunswick: The January 1982 earthquake sequence in New Brunswick provided a wealth of data for the delineation of earthquake hypocenters. The main shock was studied by Nabelek et al. (1982) by modeling teleseismic P- and SH- waveforms, and the surface wave radiation pattern. The focal depth determined from this study was 7 km. Wetmiller et al. (1982) studied the

aftershocks of this event and found that they define a V-shaped pattern in an area 4 km NS by 6 km EW, and ranging in depth from 0 to 7 km.

Southeastern NY - northern NJ: This area has been intensely studied because of the large number of earthquakes (both recently and historically), the population density, and the location of nearby critical facilities. Aggarwal and Sykes (1978) reported on a study of the seismicity in this area and found that the focal depths of earthquakes range from the near surface to about 10 km.

New England: In this area, well determined focal depths are available in three regions from aftershock studies. At Moodus, CT a dense array of seismic stations has delineated focal depths from 1 to 3 km. Aftershocks of the Bath, ME earthquake range in depth from 2 to 6 km, and aftershocks of the January 1982 Gaza, NH earthquake ranged from 2 to 7 km.

Before continuing, some general comments on the calculation of earthquake hypocenters in New England are in order. Experience has shown that the location programs (e.g., HYPOINVERSE by Klein, 1978) tend to place earthquake hypocenters at the surface or shallower than 10 km. This does not provide much of a constraint, however if the events were deeper in the lower crust, better resolution would be expected.

One way to examine the convergence to a particular focal depth is to compute the RMS errors for a given event over a grid of fixed hypocenters. As a further constraint, we would like a

station to be located within ten kilometers of the epicenter so that the travel time of the upgoing portion of the raypath would be at least 10% of the total travel time. The N.E.U.S.S.N. catalog was searched for events in New England that occurred within 10 km of a station and in addition had good azimuthal coverage. Six events were selected. These events are shown in Figure 2.19 and were located in southern NH, eastern MA, and central CT near Moodus. In Figure 2.20, we have for each event computed the RMS error by first fixing the focal depth at 1 km intervals and allowing the latitude, longitude, and origin time to vary freely. These are shown as open circles for each event. Then, we computed RMS errors by fixing the latitude, longitude, and origin time to the values computed in the depth free calculation and then vary the focal depths in 1 km intervals. These are shown as the solid circles. Focal depths examined in the way are listed in Table 2.4. Event No. 1 in E. Haddam, CT had a focal depth of 1 km, while the events in NH had focal depths of 4, 7, and 7 km. In eastern MA, the focal depths were 3 and 2 km. In each calculation, a crustal model was chosen which was appropriate for each source area. Some experiments were performed in which these crustal models were perturbed by changing the top layer velocity or thickness. In all cases, the computed focal depths varied somewhat, but were still confined to the top crustal layer.

The general picture which emerges from this review is that earthquakes in the Grenville Province have focal depths which

range from the near surface to 20 km. In the Appalachian Province, earthquake focal depths range from the near surface to only 10 km. However, this is based on a limited dataset, so that it cannot be precluded that deeper events will not occur in New England.

2.4 Comparison of Instrumental and Historical Seismicity

We now compare and contrast the results of our study for the historical and instrumental datasets in the NEUS-SEC. We begin with the distribution of epicenters.

There is a remarkable degree of similarity between the frequency regionalizations in Figure 2.5 and Figure 2.17. The Charlevoix Seismic Zone stands out as the most seismically active area in both datasets. The seismic zone at the NY-PQ border is also common to both datasets, as are the small seismic zones in ME and NY. The NY-NJ border also stands out in both regionalizations. However, an important difference in the datasets is the absence of events in eastern MA for the instrumental dataset. This could be caused by either the short length of time covered in Figure 2.17 (i.e. the return times are much longer than the time period considered in this figure) or the historical events are mislocated due to population biases. A further possibility is that the rate of occurrence of earthquakes in this area is not constant with time. This was suggested in the study by Shakal and Toksöz (1975).

Another way we can compare the instrumental and historical seismicity is via the earthquake statistics. Since accurate

magnitudes are available for the instrumentally recorded events, the statistics based on these events should provide useful insights into the historical record.

For the Western Quebec Seismic Zone, defined earlier, the earthquake statistics over the past six years yield the equation

$$\text{Log}[N(\text{mb})/\text{yr}] = 2.919 - 0.876(+/- .063)\text{mb} \quad (2.38)$$

This equation is remarkably similar to its counterpart for the historical dataset. The return times versus magnitude predicted by this equation and equation (2.22) are summarized in Table 2.5. Equation (2.38) predicts a mean return time for an $\text{mb}=5.0$ event of 29 years with a 97% probability of occurrence in 100 years, while the historical dataset predicts a return time of 24 years with a 99% probability of occurrence in 100 years. For an $\text{mb}=6.0$ event, equation (2.38) yields a mean return time of 217 years with a 37% probability of occurrence in 100 years, while the historical dataset predicts a return time of 188 years with a 41% probability of occurrence in 100 years. Extrapolating to an $\text{mb}=6.5$ event, equation (2.38) predicts a mean return time of 595 years with a 15% probability of occurrence in 100 years, while the historical dataset yields a return time of 526 years with a 17% probability of occurrence in 100 years. The similarity of the results likely means a number of things. For one thing, it means that the instrumental dataset is a statistically valid

sample of the seismicity in this seismic zone. In other words, the seismicity is uniform in time. The similarity also validates our intensity - magnitude relationships for this zone.

For the Charlevoix Seismic Zone, the instrumental dataset yields the equation

$$\text{Log}[N(\text{mb})/\text{yr}] = 2.479 - 0.741(+/- .032)\text{mb} \quad (2.39)$$

Note that again the "b" value is anomalously low (0.741), although not as low as that calculated from the historical dataset. Return times based on the instrumental and historical data in this zone are summarized in Table 2.5 . The mean return times based on this equation for an mb=5.0 event is 17 years with 100% probability of occurrence in 100 years, whereas from the historical dataset we obtain a return time of 17 years with again a 100 % probability of occurrence in 100 years. For an mb=6.0 event, equation (2.39) predicts a mean return time of 93 years with a 66% probability of occurrence in 100 years, while the historical dataset predicts a return time of 62 years with an 80% probability of occurrence in 100 years. Extrapolating to mb=6.5, equation (2.39) yields a mean return time of 218 years. The historical dataset predicts a mean return time of 120 years, roughly half the time predicted by the instrumental data. This is likely due to the overestimation of the earthquake size for many early events based in intensity data.

For the Boston to NH Seismic Zone, the dataset yields the equation

$$\text{Log}[N(\text{mb})/\text{yr}] = 2.142 - 0.829(+/- .071)\text{mb} \quad (2.40)$$

This equation predicts a mean return time for a magnitude 6.0 event of 679 years with a 26% probability of occurrence in 200 years. The historical dataset predicts 408 years with a 39% probability of occurrence in 200 years. For a magnitude 6.5 event, the instrumental dataset predicts 1760 years with an 11% probability of occurrence in 200 years, while the historical dataset predicts 1060 years with a 17% probability of occurrence in 200 years.

In conclusion, both the historical and instrumental datasets provide important constraints on the location and frequency of earthquake occurrence in the NEUS-SEC. Continued network monitoring will allow many of the uncertainties in seismic zonation to be reduced.

Table 2.1a

Earthquake Statistics in the Western Quebec Seismic Zone

(Based on the Period 1844 - 1975 and Least Squares "b" Value)

$$\text{Log}[N(\text{mb})/\text{yr}] = 3.076 - 0.897(+/- .030)\text{mb}$$

Return Time in Years

(95% Confidence Intervals)

<u>mb</u>	<u>Minimum</u>	<u>Mean</u>	<u>Maximum</u>
4.5	5.3	8.5	13.6
5.0	14.8	23.8	38.1
5.5	41.3	66.8	108.
6.0	113.	188.	309.
6.5	310.	526.	895.
7.0	838.	1480.	2610.

Probability of at Least 1 Event in T Years (%)

T = 200 years

T = 100 years

<u>mb</u>	<u>Minimum</u>	<u>Mean</u>	<u>Maximum</u>		<u>Minimum</u>	<u>Mean</u>	<u>Maximum</u>
4.5	100	100	100		100	100	100
5.0	99	100	100		93	99	100
5.5	84	95	99		60	78	91
6.0	48	66	83		28	41	59
6.5	20	32	48		11	17	28
7.0	7	13	21		4	7	11

Table 2.1b

*Earthquake Statistics in the Western Quebec Seismic Zone**Comparison of Four Statistical Methods*

(Based on the Period 1844 - 1975)

Mean Return Time in Years

<u>mb</u>	<u>Least Squares</u>	<u>Maximum Likelihood</u>	<u>Gumbel I (5 yr int)</u>	<u>Gumbel III (5 yr int)</u>
4.5	8.5	9.2	9.9	9.4
5.0	23.8	23.4	21.7	19.8
5.5	66.8	59.5	54.2	56.0
6.0	188.	151.	142.	218.
6.5	526.	385.	380.	1230.
7.0	1480.	980.	1020.	16200.

Mean Probability of at Least 1 Event in 100 Years (%)

<u>mb</u>	<u>Least Squares</u>	<u>Maximum Likelihood</u>	<u>Gumbel I (5 yr int)</u>	<u>Gumbel III (5 yr int)</u>
4.5	100	100	99	99
5.0	99	99	99	99
5.5	78	81	99	99
6.0	41	48	70	46
6.5	17	23	26	8
7.0	7	10	10	1

Table 2.2a

Earthquake Statistics in the Charlevoix Seismic Zone

(Based on the Period 1818 - 1975 and Least Squares "b" Value)

$$\text{Log}[N(\text{mb})/\text{yr}] = 1.619 - 0.569(+/- .015)\text{mb}$$

Return Time in Years

(95% Confidence Intervals)

<u>mb</u>	<u>Minimum</u>	<u>Mean</u>	<u>Maximum</u>
4.5	6.2	8.7	12.3
5.0	12.0	16.8	23.7
5.5	23.0	32.4	45.7
6.0	44.1	62.4	88.3
6.5	84.3	120.	171.
7.0	160.	231.	334.

Probability of at Least 1 Event in T Years (%)

T=100 years

T=50 years

<u>mb</u>	<u>Minimum</u>	<u>Mean</u>	<u>Maximum</u>		<u>Minimum</u>	<u>Mean</u>	<u>Maximum</u>
4.5	100	100	100		98	100	100
5.0	99	100	100		89	95	98
5.5	88	95	99		67	79	89
6.0	68	80	90		43	55	68
6.5	44	56	69		25	34	45
7.0	26	35	46		14	19	27

Table 2.2b

*Earthquake Statistics in the Charlevoix Seismic Zone**Comparison of Four Statistical Methods*

(Based on the Period 1818 - 1975)

Mean Return Time in Years

<u>mb</u>	<u>Least Squares</u>	<u>Maximum Likelihood</u>	<u>Gumbel I (5 yr int)</u>	<u>Gumbel III (5 yr int)</u>
4.5	8.7	8.7	8.7	8.3
5.0	16.8	16.7	14.8	12.9
5.5	32.4	31.8	28.0	24.0
6.0	62.4	60.5	55.8	55.6
6.5	120.	115.	114.	174.
7.0	231.	219.	236.	902.

Mean Probability of at Least 1 Event in 50 Years (%)

<u>mb</u>	<u>Least Squares</u>	<u>Maximum Likelihood</u>	<u>Gumbel I (5 yr int)</u>	<u>Gumbel III (5 yr int)</u>
4.5	100	100	98	98
5.0	95	95	98	98
5.5	79	79	98	98
6.0	55	56	90	90
6.5	34	35	44	29
7.0	19	20	21	6

Table 2.3a

Earthquake Statistics in the Boston - NH Seismic Zone
 (Based on the Period 1727 - 1975 and Least Squares "b" Value)

$$\text{Log}[N(I)/\text{yr}] = 1.539 - 0.498(+/- .034)I$$

Return Time in Years
 (95% Confidence Intervals)

<u>Int</u>	<u>Minimum</u>	<u>Mean</u>	<u>Maximum</u>
V	3.6	8.9	22.1
VI	11.8	28.1	67.2
VII	35.7	88.4	219.
VIII	102.	278.	761.
IX	276.	876.	2770.

 Probability of at Least 1 Event in T Years (%)

T=300 years

T=200 years

<u>Int</u>	<u>Minimum</u>	<u>Mean</u>	<u>Maximum</u>		<u>Minimum</u>	<u>Mean</u>	<u>Maximum</u>
V	100	100	100		100	100	100
VI	99	100	100		95	100	100
VII	75	97	100		60	90	100
VIII	33	66	95		23	51	86
IX	10	29	66		7	20	52

Table 2.3b

Earthquake Statistics in the Boston - NH Seismic Zone
 Comparison of Two Statistical Methods
 (Based on the Period 1727-1975)

Mean Return Time in Years

<u>Int</u>	<u>Least Squares</u>	<u>Gumbel Type I (25 yr int.)</u>
V	8.9	41.3
VI	28.1	77.9
VII	88.4	168.
VIII	278.	386.
IX	876.	911.

 Mean Probability of at Least 1 Event in 200 Years (%)

<u>Int</u>	<u>Least Squares</u>	<u>Gumbel Type I (25 yr int)</u>
V	100	100
VI	100	100
VII	90	100
VIII	51	52
IX	20	22

Table 2.4

Focal Depth Calculations for New England Earthquakes
Using RMS Error Versus Depth

<u>No.</u>	<u>Date</u>	<u>Lat.</u>	<u>Long.</u>	<u>mbLg</u>	<u>Area</u>	<u>Depth km</u>
1	24Mar76	41.46	-72.49	2.2	E. Haddam, CT	1.
2	17Aug78	43.52	-71.56	1.9	Winnisquam, NH	4.
3	21Jun78	43.66	-71.38	1.8	Lake Winn., NH	7.
4	01Sep78	42.48	-71.46	2.0	Acton, MA	3.
5	23Nov80	42.62	-71.39	2.9	Lowell, MA	2.
6	09Feb81	43.26	-71.56	1.9	Concord, NH	7.

Table 2.5

Comparison of Historical and Instrumental Seismicity

Western Quebec Seismic Zone

<u>mb</u>	<u>Instrumental</u>			<u>Historical</u>	
	Mean Return <u>Time</u>	P(1 event) <u>in 100 yrs</u>		Mean Return <u>Time</u>	P(1 event) <u>in 100 yrs</u>
5.0	29	97		24	99
5.5	79	72		67	78
6.0	217	37		188	41
6.5	595	15		526	17
7.0	1630	6		1480	7

Charlevoix Seismic Zone

<u>mb</u>	<u>Instrumental</u>			<u>Historical</u>	
	Mean Return <u>Time</u>	P(1 event) <u>in 100 yrs</u>		Mean Return <u>Time</u>	P(1 event) <u>in 100 yrs</u>
5.0	17	100		17	100
5.5	40	92		32	95
6.0	93	66		62	80
6.5	218	37		120	56
7.0	510	18		231	35

Table 2.5 cont.

Boston - NH Seismic Zone

<u>mb</u>	<u>Instrumental</u>			<u>Historical</u>	
	Mean Return <u>Time</u>	P(1 event) <u>in 200 yrs</u>		Mean Return <u>Time</u>	P(1 event) <u>in 200 yrs</u>
5.0	101	86		60	96
5.5	262	53		157	72
6.0	679	26		408	39
6.5	1760	11		1060	17

Figure Captions

Figure 2.1 The seismicity of the NEUS-SEC for the period 1534 - 1959, reproduced from Smith (1966).

Figure 2.2 The seismicity of the NEUS-SEC for the period 1534 - 1975. The epicenters plotted are from the catalog of Chiburis (1981).

Figure 2.3 The seismicity of the NEUS-SEC over four time periods. a) 1534-1700, b) 1700-1800, c) 1800-1900, and d) 1900-1975. The source of data for each of these plots is the catalog of Chiburis (1981).

Figure 2.4 Seismic frequency regionalization of the NEUS-SEC over the period 1534-1975, using the regionalization algorithm outlined in Section 2.2.1 . The shading is in terms of the percentage of relative activity with respect to the peak.

Figure 2.5 Seismic frequency regionalization of the NEUS-SEC for the period 1534-1975 using only events of magnitude greater than or equal to 3 1/2 (mb) or intensity greater than or equal to IV (M.M.). The shading used in this figure is the same as that in Figure 2.4 .

Figure 2.6 Seismic energy release in the NEUS-SEC over the period 1534-1975, determined using the Moving-Block method of Bath (1982), outlined in Section 2.2.1 . Three energy levels are delineated in the plot. These bands correspond to an

equivalent energy in Log ergs of 16-18, 18-20, and ≥ 20 . The equivalent magnitude ranges are mb 4.2-5.0, 5.01-5.9, and ≥ 5.9 .

Figure 2.7 Cumulative frequency-magnitude plot for the Western Quebec Seismic Zone for the period 1844 - 1975. Aftershocks have been removed from the calculation. A least squares fit to the data plus the standard deviations are shown. The interval over which the calculation has been performed is indicated by the horizontal bar.

Figure 2.8 Frequency-interoccurrence time plot for the Western Quebec seismic zone, for the period 1844-1975. Events of intensity $\geq V$ or mb ≥ 4.0 have been chosen for the calculation. The mean interoccurrence time is 2.0 years. Also shown is a theoretical plot of a Poissonian process with an interoccurrence time of 2.0 years.

Figure 2.9 Application of the Gumbel Type I distribution for events in the Western Quebec seismic zone, covering the years 1844-1975, and grouped into 5 year intervals.

Figure 2.10 Cumulative frequency-magnitude statistics for the Charlevoix seismic zone, covering the years 1818-1975, as well as a least squares fit and error bars. The interval over which the calculations have been performed is indicated by the horizontal bar.

Figure 2.11 Application of the Gumbel Type I distribution for events in the Charlevoix seismic zone, covering the years 1818-1975 and grouped into 5 year intervals.

Figure 2.12 Cumulative frequency-intensity statistics for the Boston-NH seismic zone, covering the years 1727-1975, with a least squares fit and error bars. The interval over which the calculation has been performed is indicated by the horizontal bar.

Figure 2.13 Application of the Gumbel Type I distribution for events in the Boston-NH seismic zone, covering the years 1727-1975 and grouped into 25 year intervals.

Figure 2.14 Seismic stations in the NEUS-SEC. Some of these stations are now closed. See Appendix C for detailed maps of the station distribution, as well as coordinate locations.

Figure 2.15 Example of the location of a controlled source by the M.I.T. Seismic Network in order to estimate location accuracy. The source is a quarry blast at the McClellan Construction Company near Manchester, NH. The top figure shows a record section from a representative blast. Note the surface waves indicative of a surface or near surface source. The azimuthal station coverage is indicated in the middle figure. At the bottom, the arrival-order location method has been illustrated which uses only the order of

P-wave arrivals to construct perpendicular bisectors between stations of increasing arrival order. The error in location is 1.2 km.

Figure 2.16 Instrumentally located earthquakes in the study area, covering the period October 1975 through September 1981. The source for the epicentral locations is the N.E.U.S.S.N. quarterly bulletins.

Figure 2.17 Seismic frequency regionalization of the NEUS-SEC using instrumental data covering the time period October 1975 through September 1981.

Figure 2.18 Seismic energy regionalization of the NEUS-SEC The time period October 1975 through January 1982.

Figure 2.19 Locations of six earthquakes whose focal depths were estimated using the RMS error versus depth method.

Figure 2.20 RMS error versus depth for six New England earthquakes. The open circles indicate computed RMS errors for a fixed focal depth, but with the latitude, longitude, and origin time unconstrained. The solid circles are the computed RMS errors for fixed depth, latitude, longitude, and origin time.

**EARTHQUAKES
OF
EASTERN CANADA
AND ADJACENT AREAS
1534-1959**

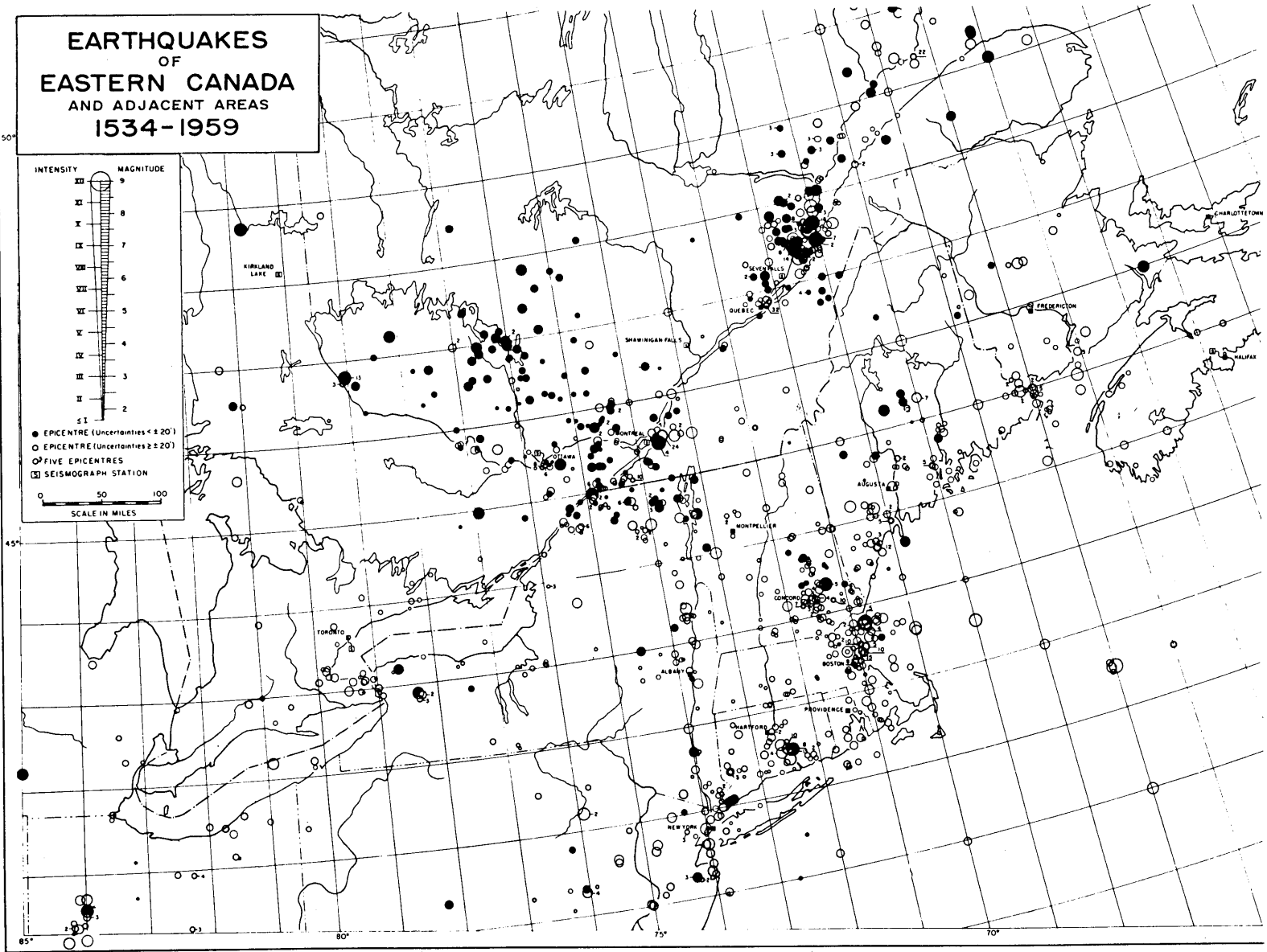
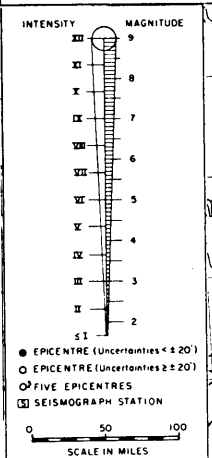


FIGURE 2.1

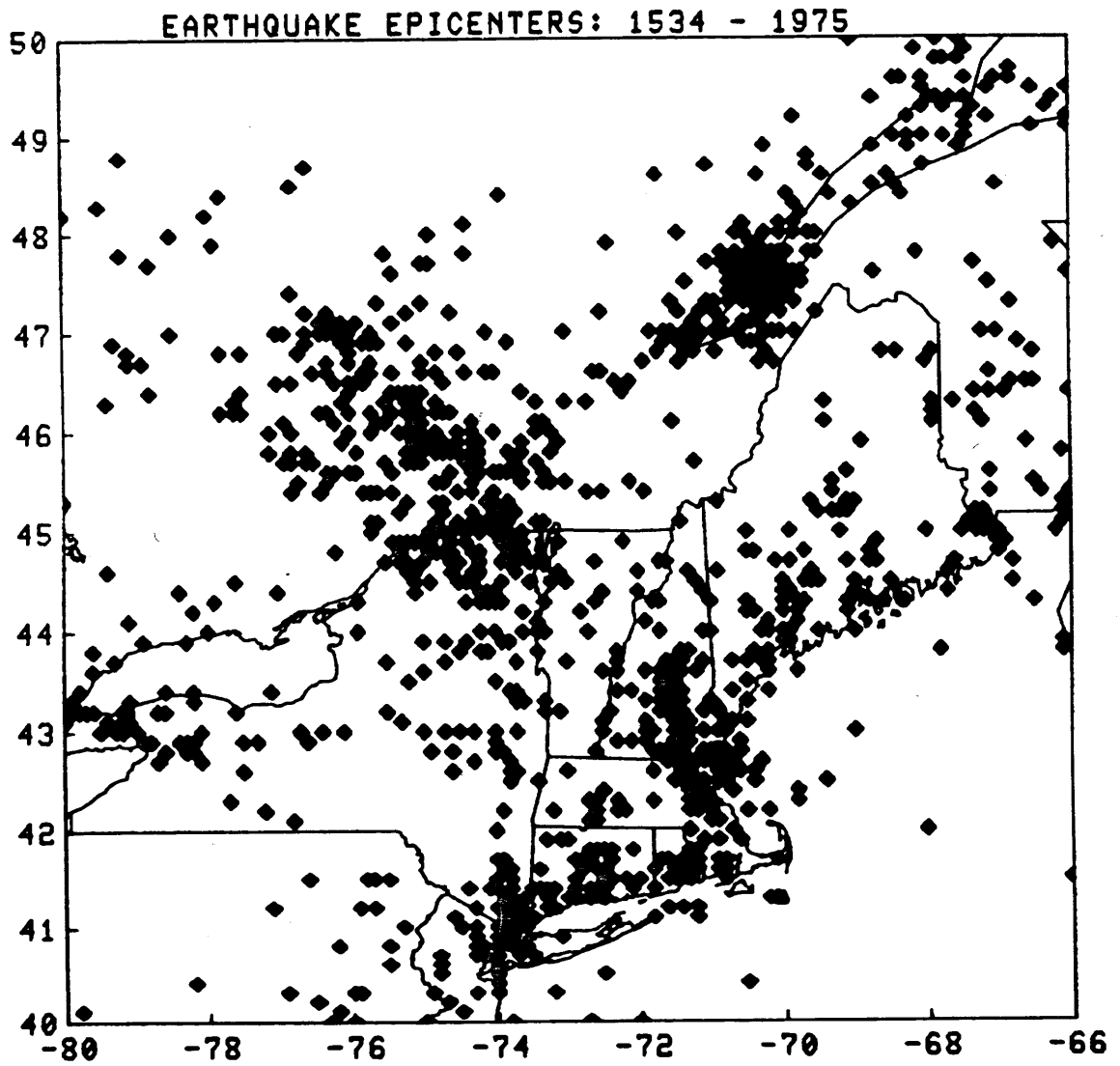


FIGURE 2.2

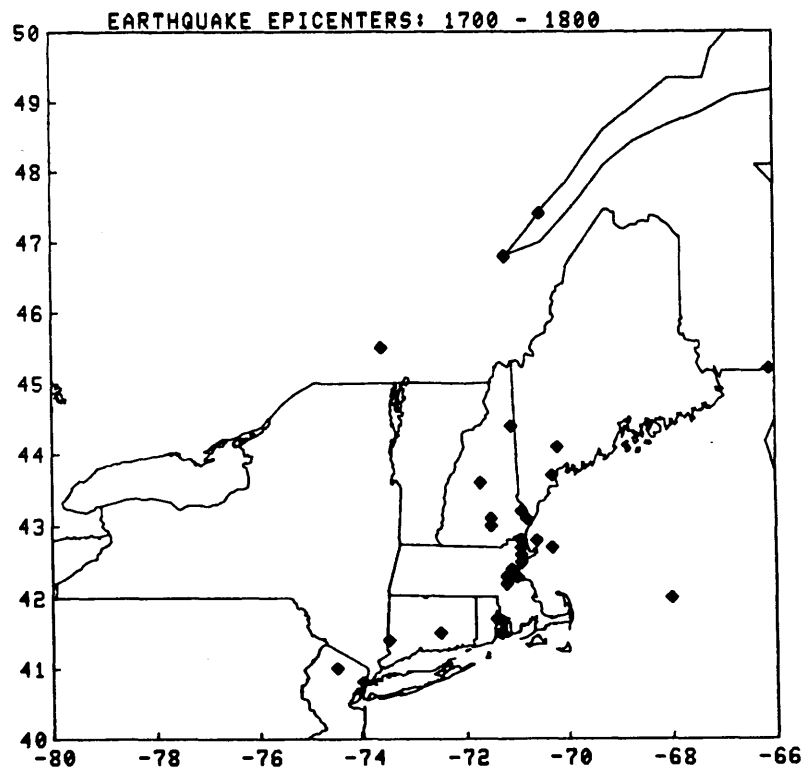
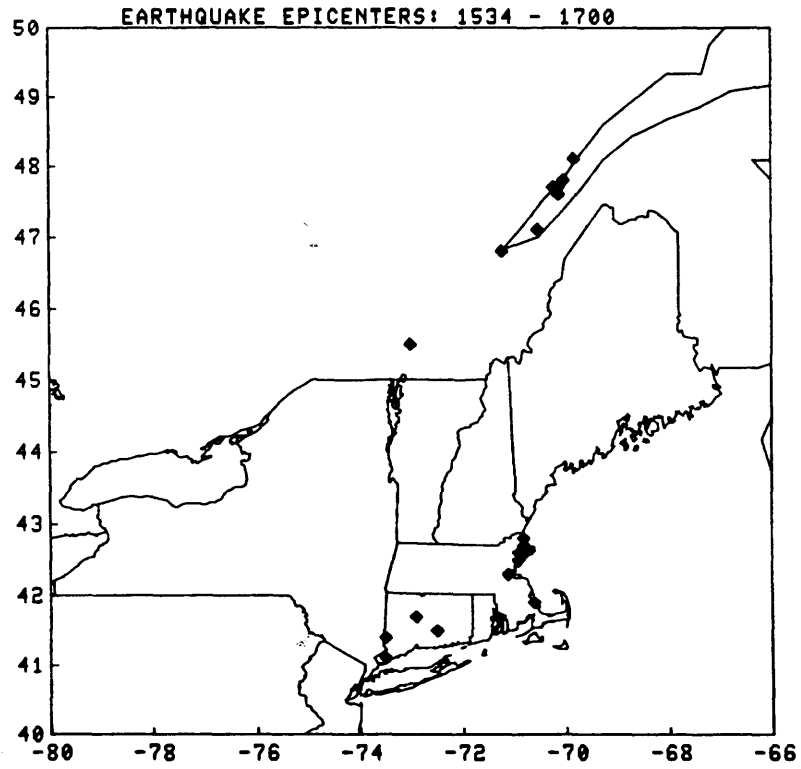


FIGURE 2.3

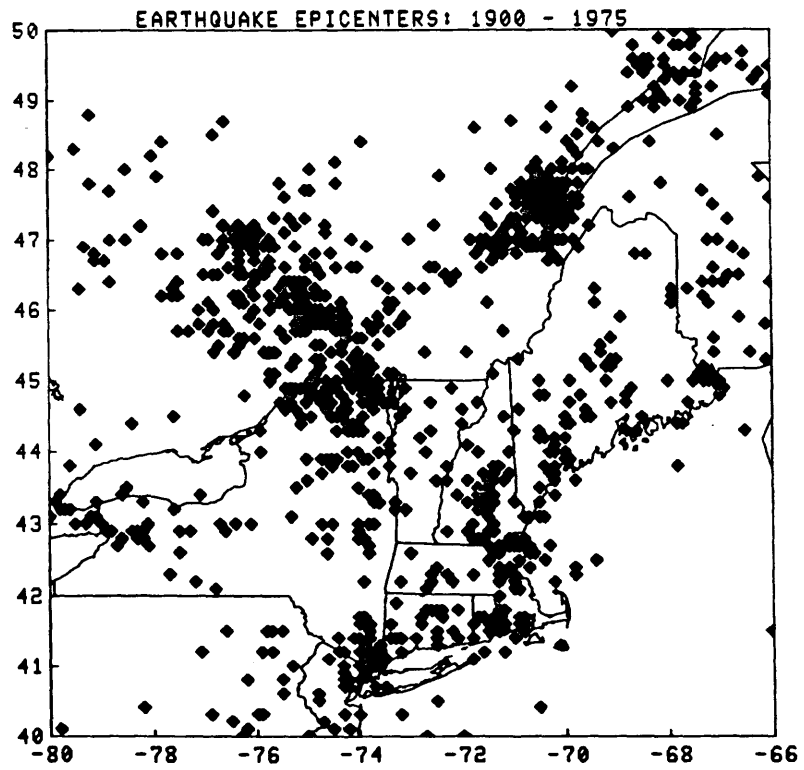
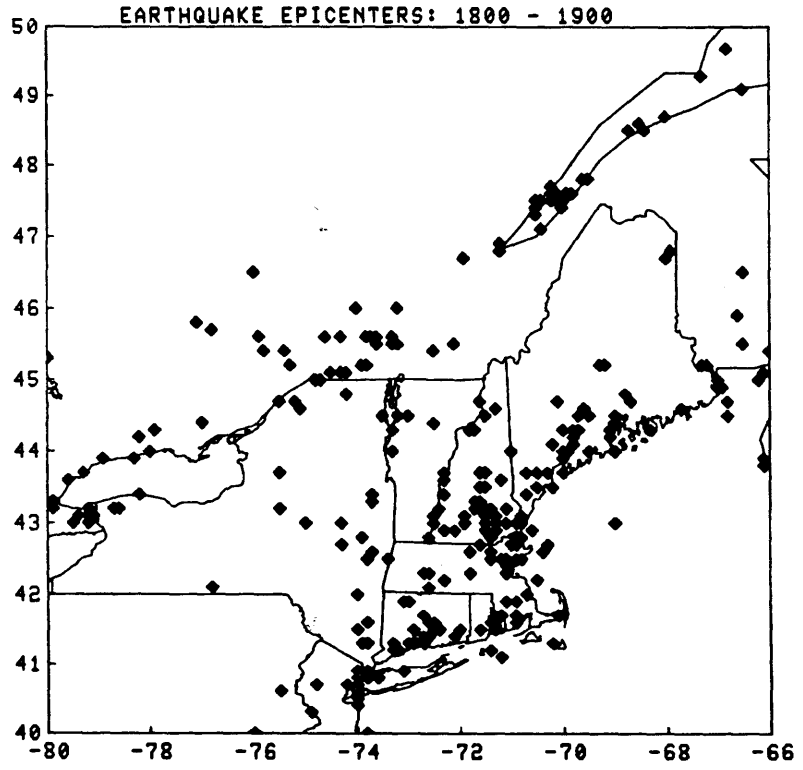


FIGURE 2.3 cont.

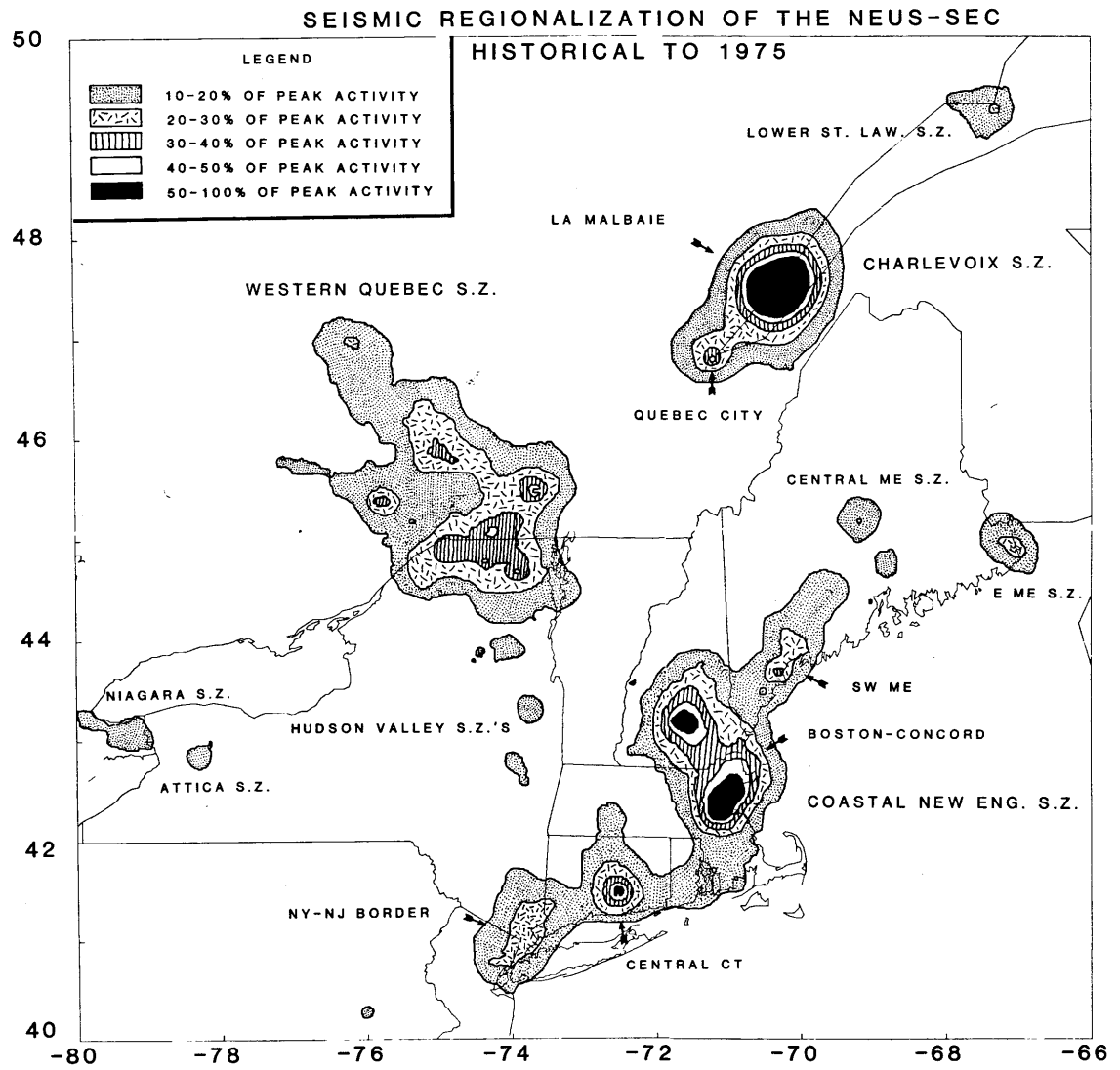


FIGURE 2.4

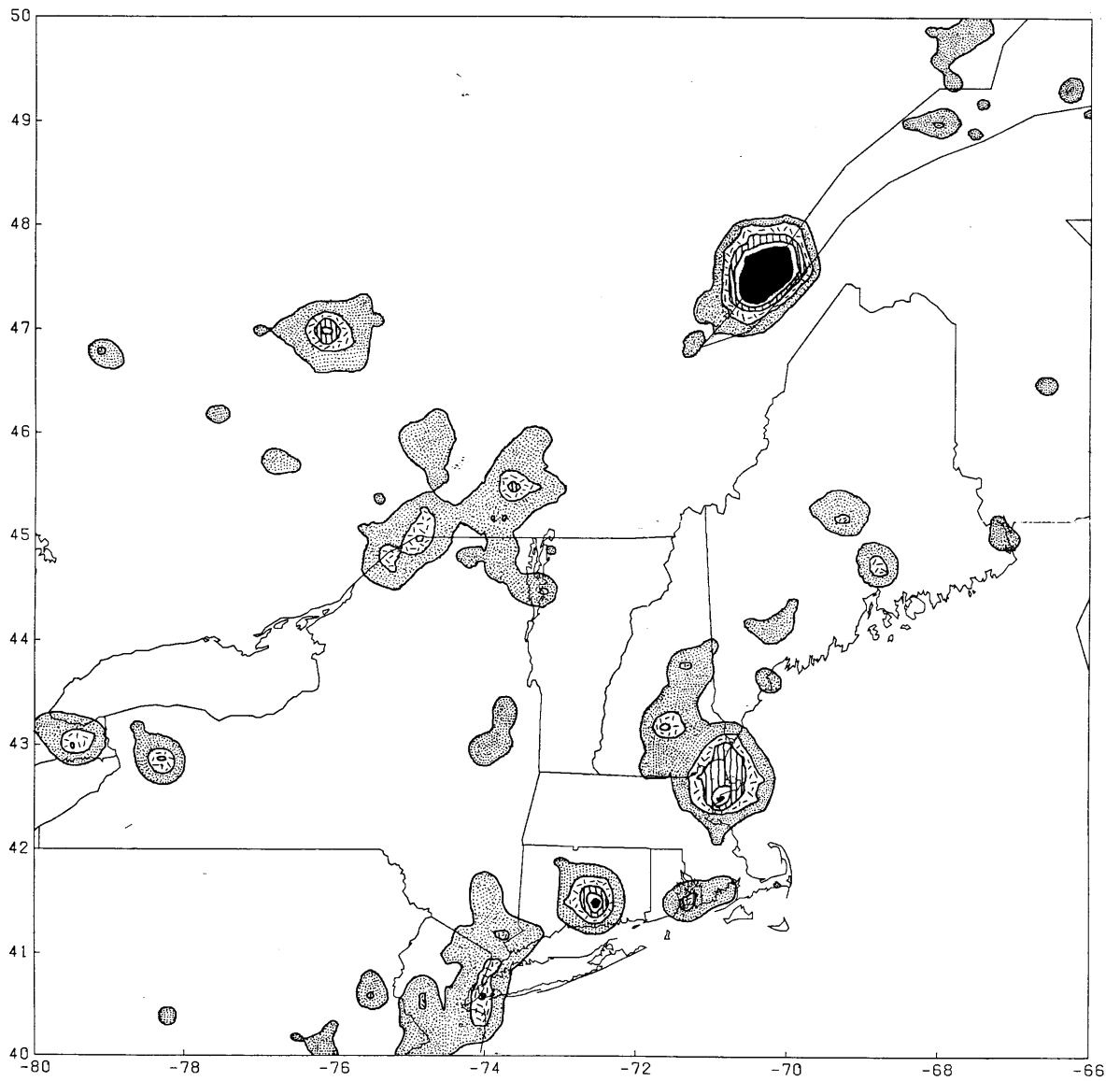


FIGURE 2.5

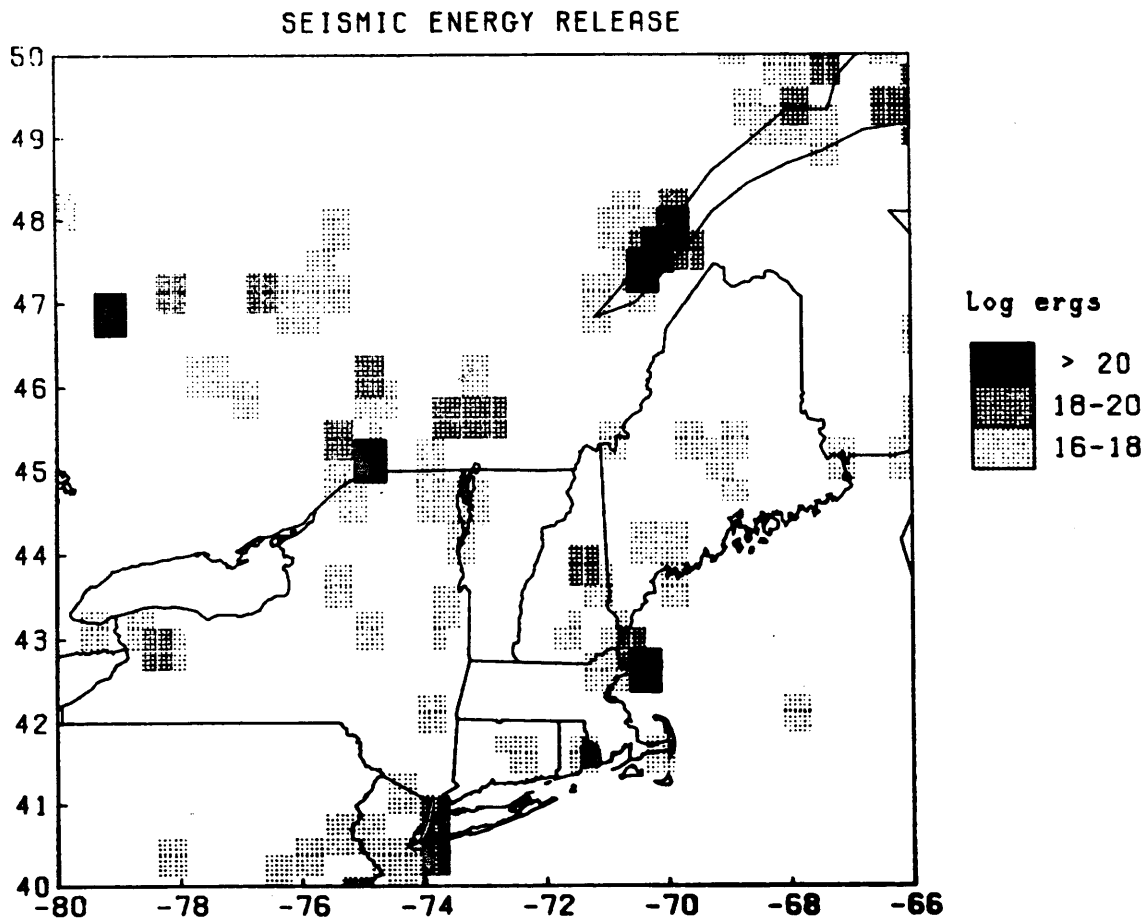


FIGURE 2.6

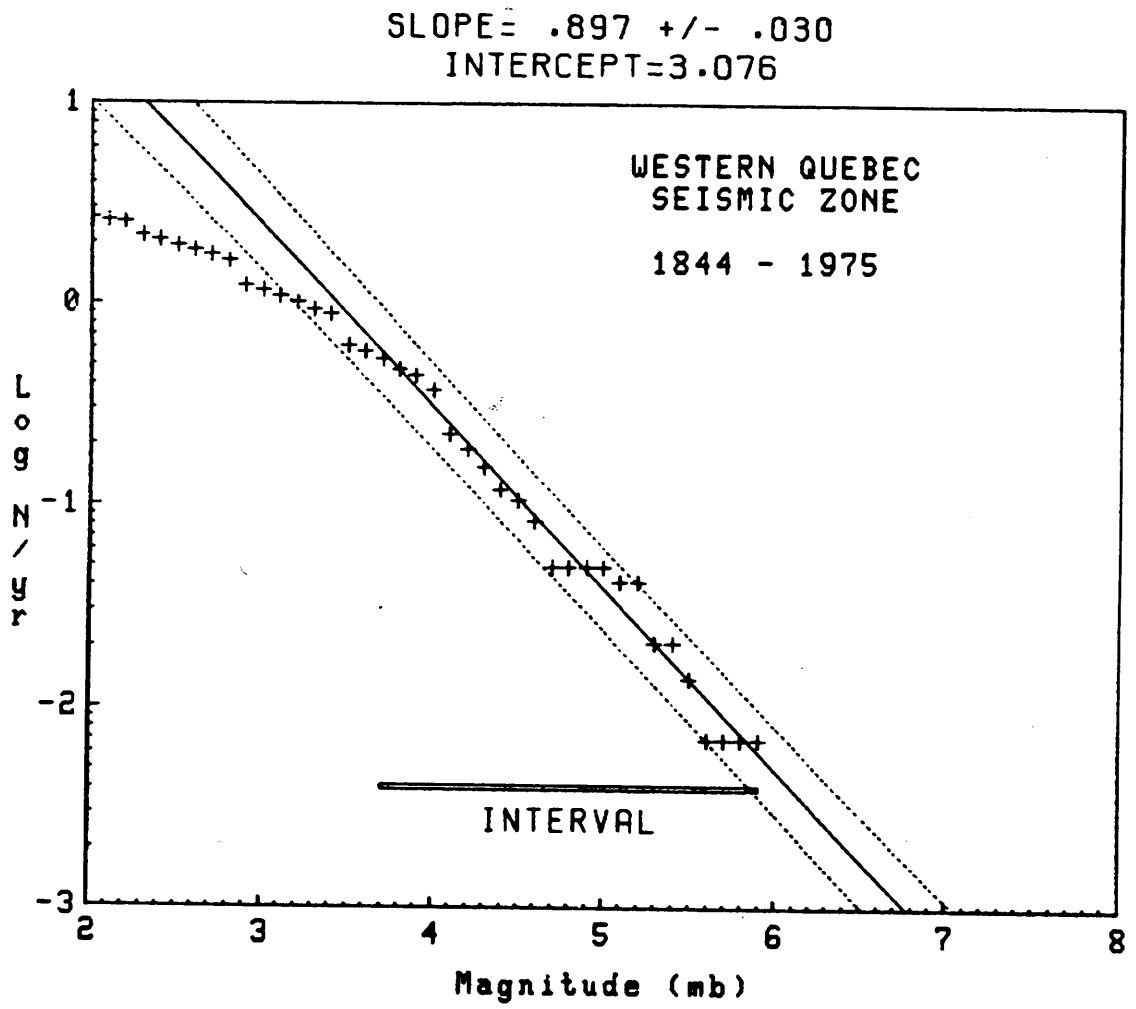


FIGURE 2.7

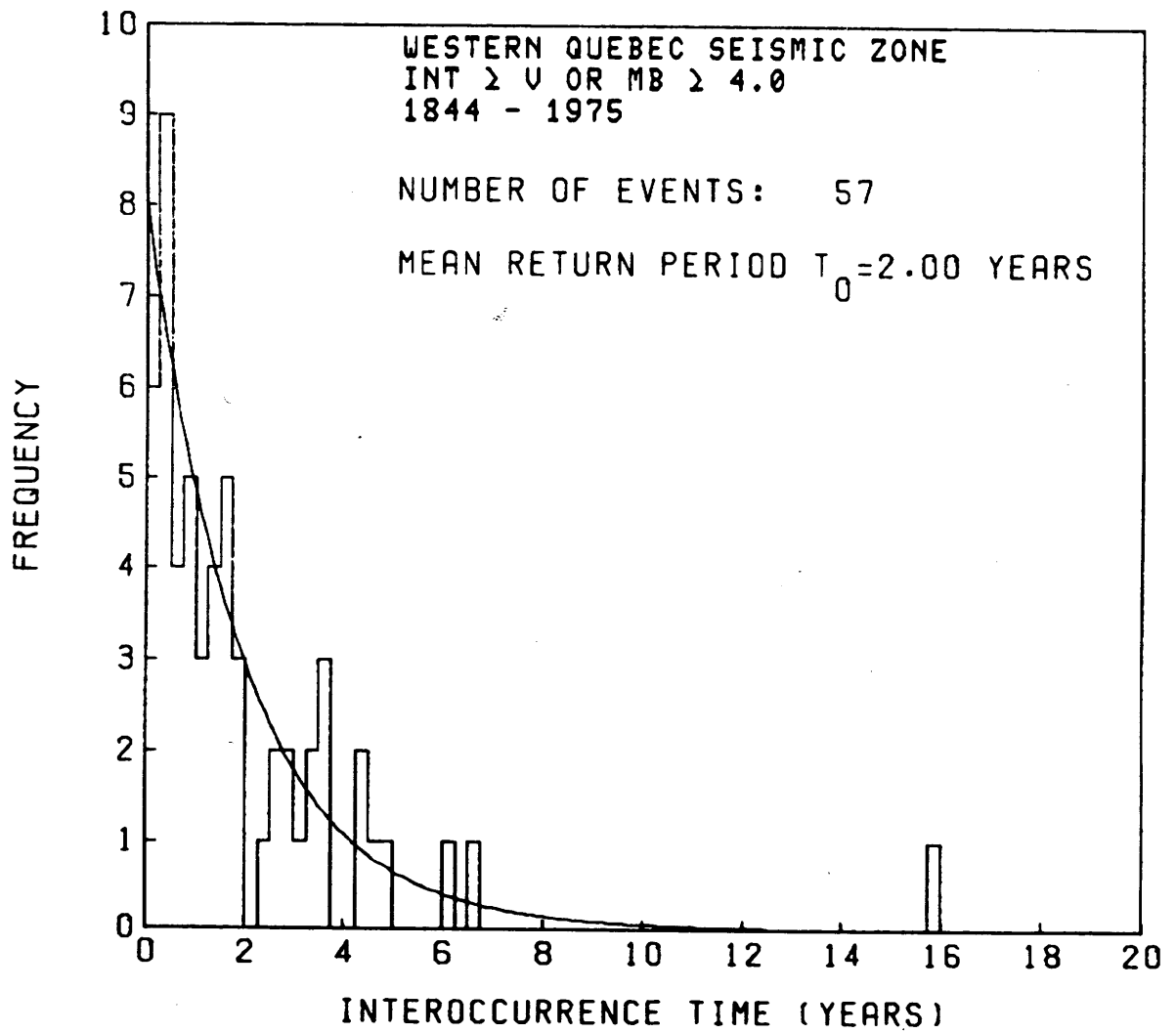


FIGURE 2.8

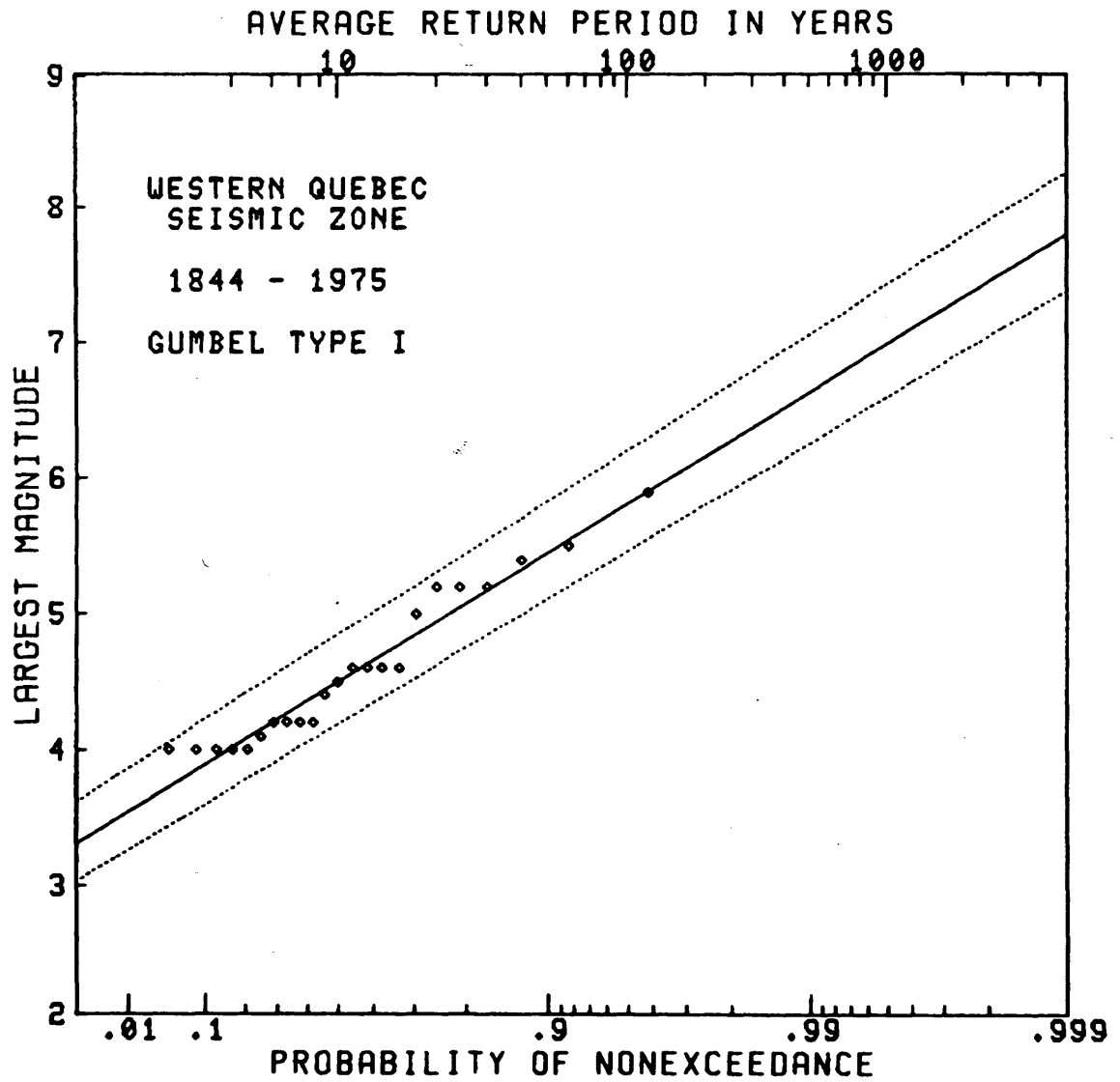


FIGURE 2.9

SLOPE = .569 +/- .015
INTERCEPT = 1.619

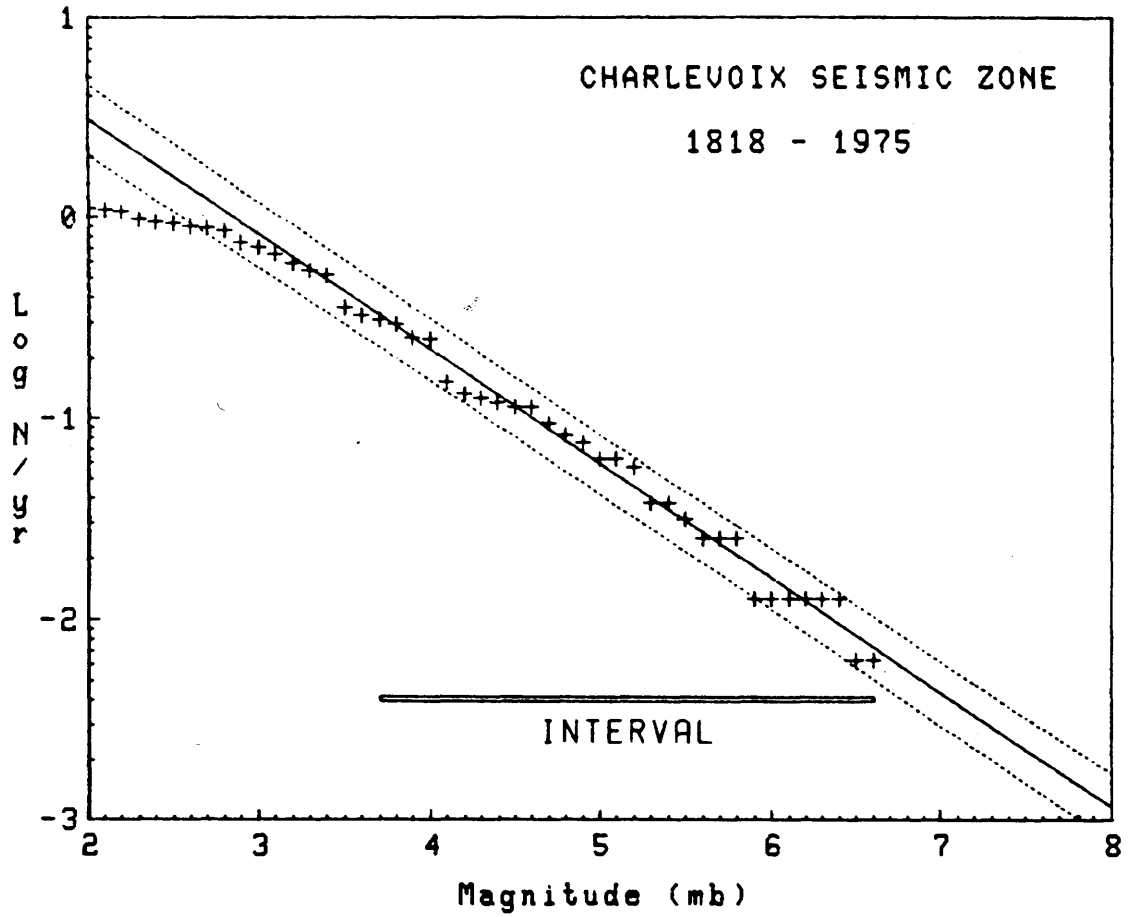


FIGURE 2.10

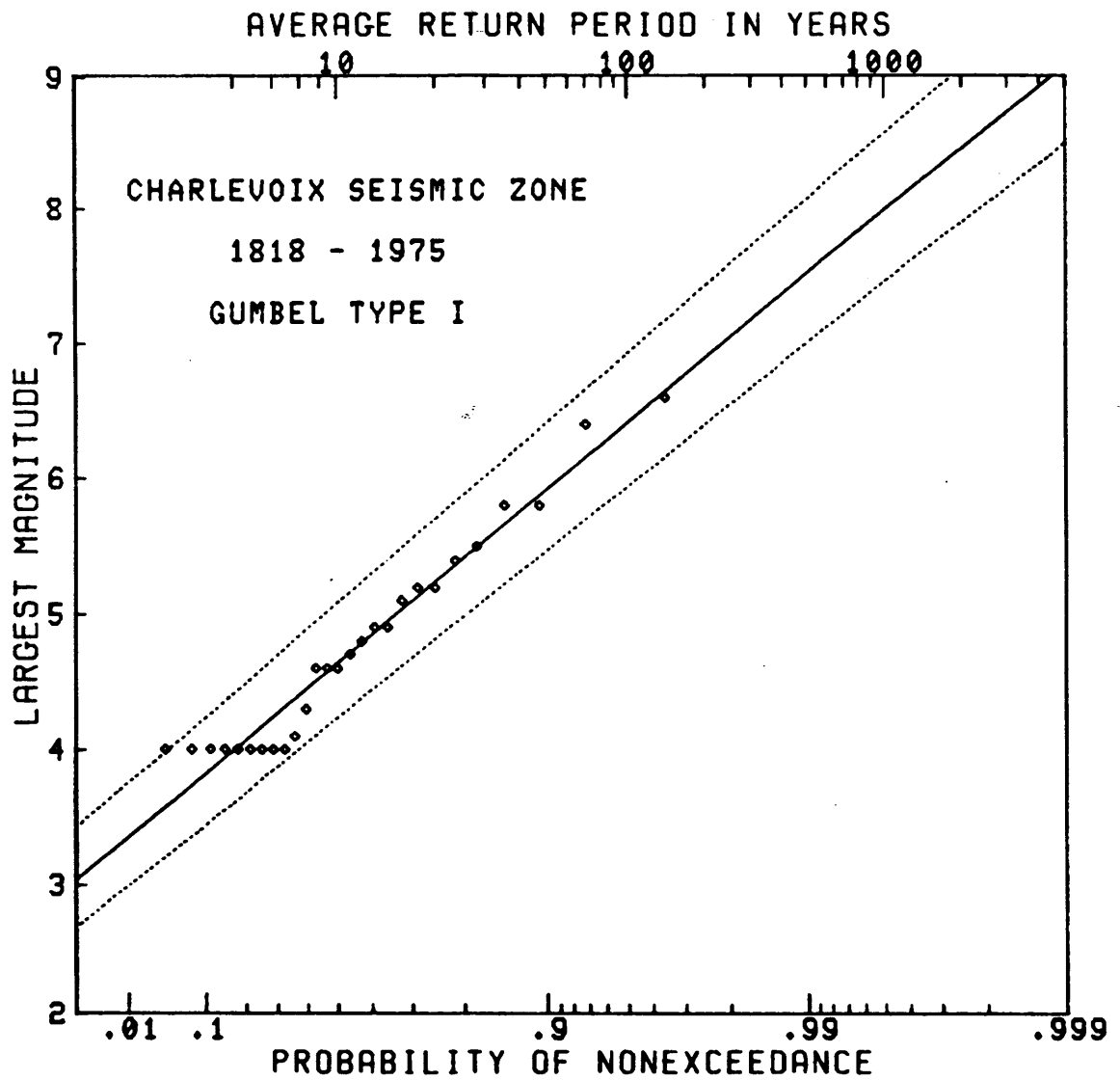


FIGURE 2.11

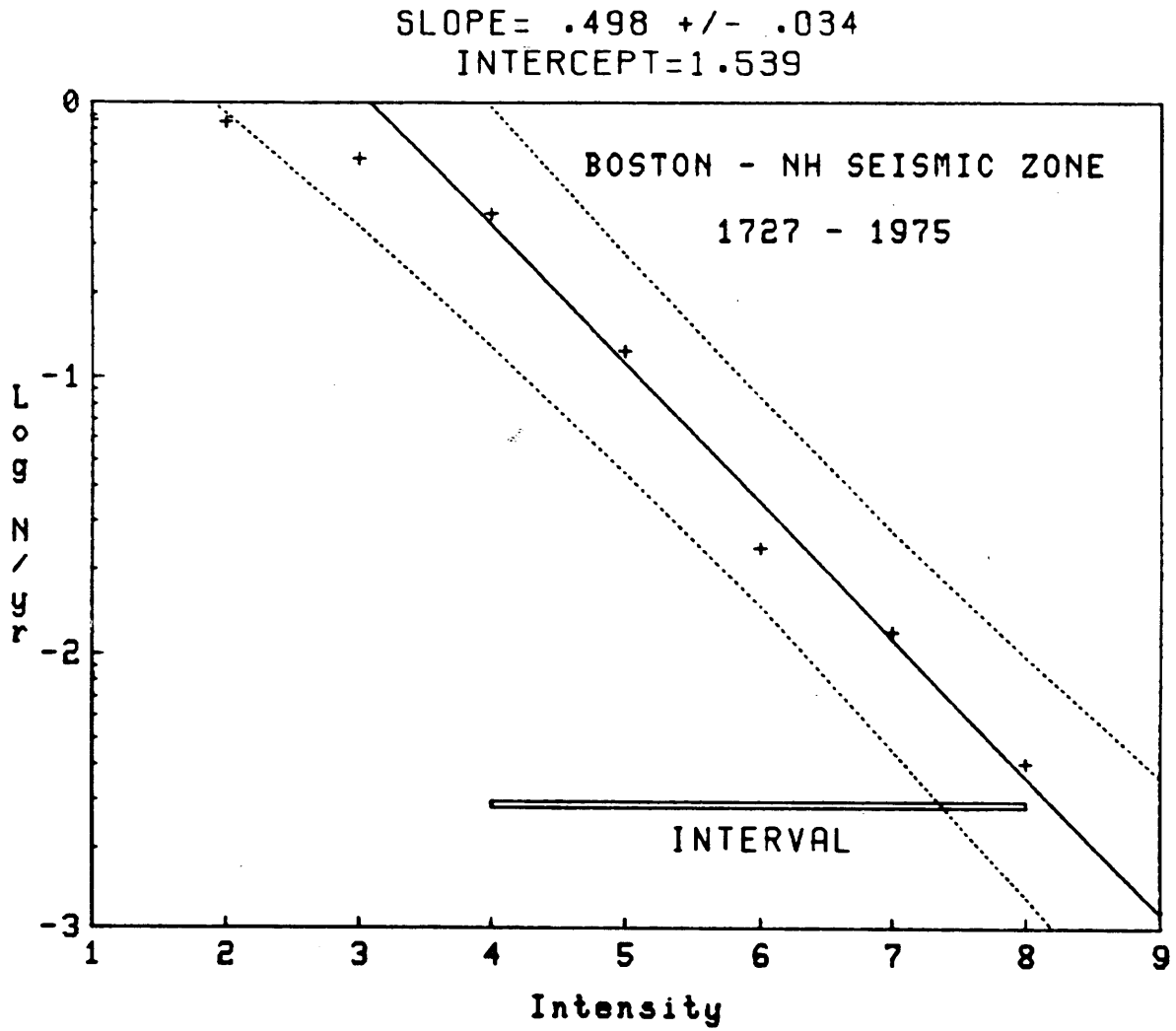


FIGURE 2.12

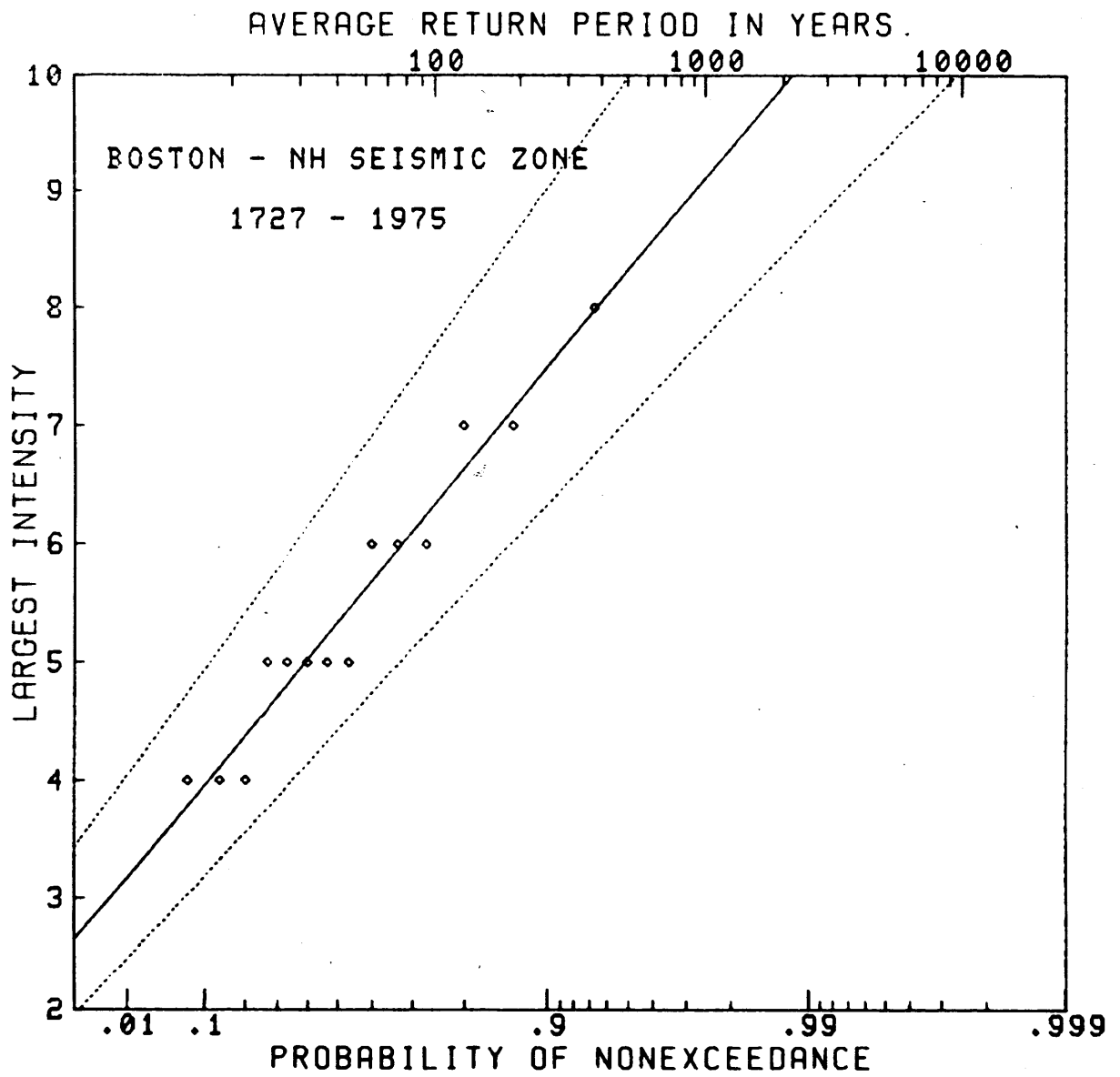


FIGURE 2.13

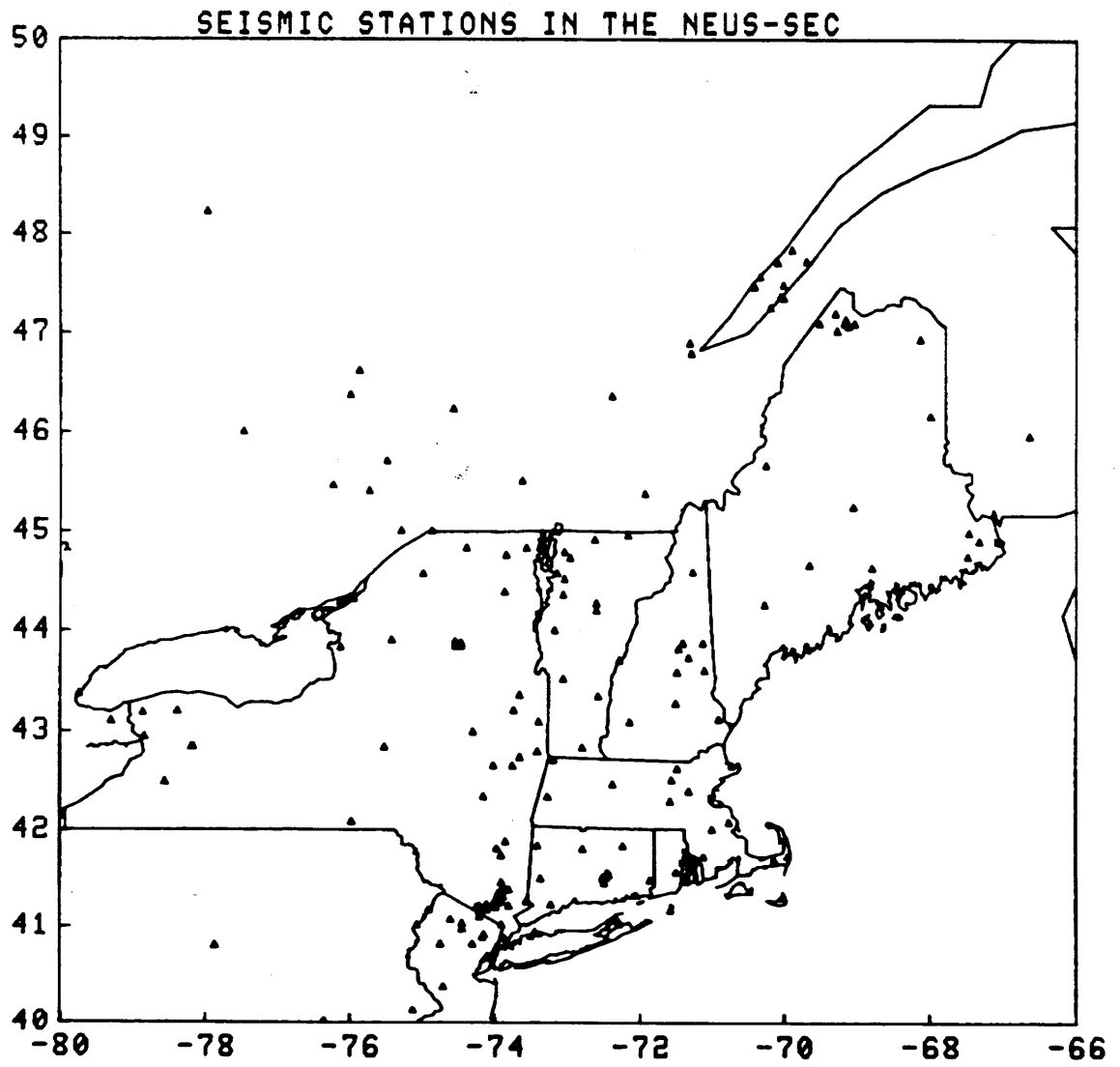
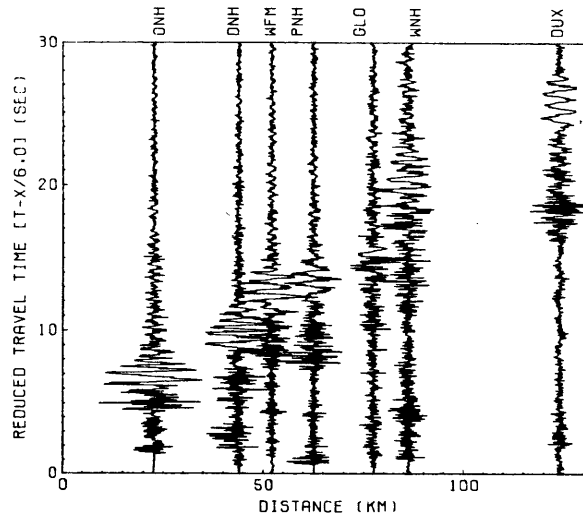


FIGURE 2.14



Blast, McClellan Const Co., Manchester NH Mc(2.5) CH34AB

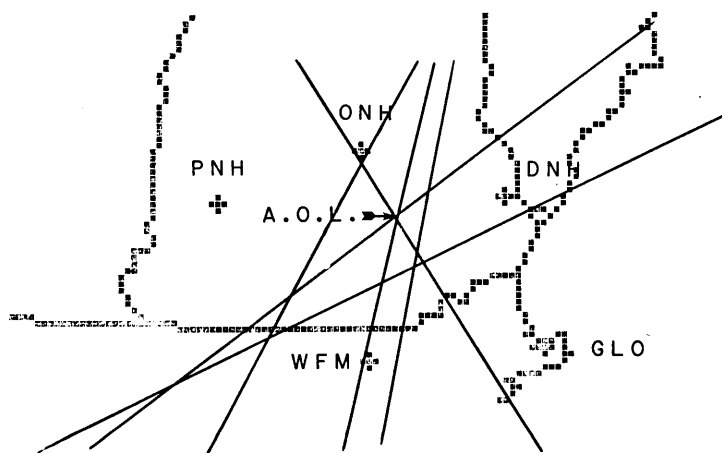
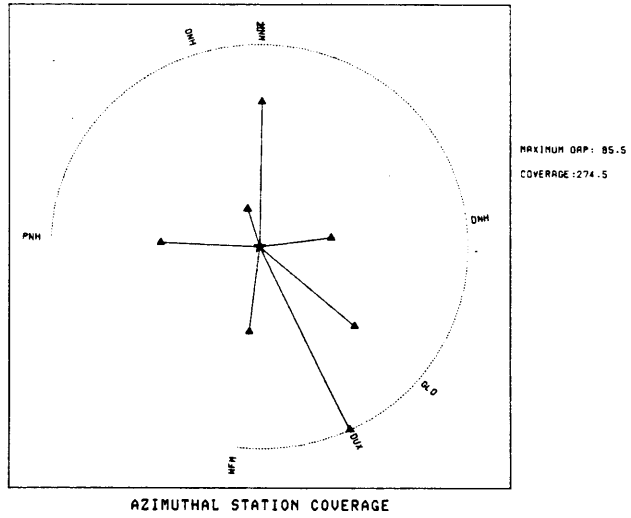


FIGURE 2.15

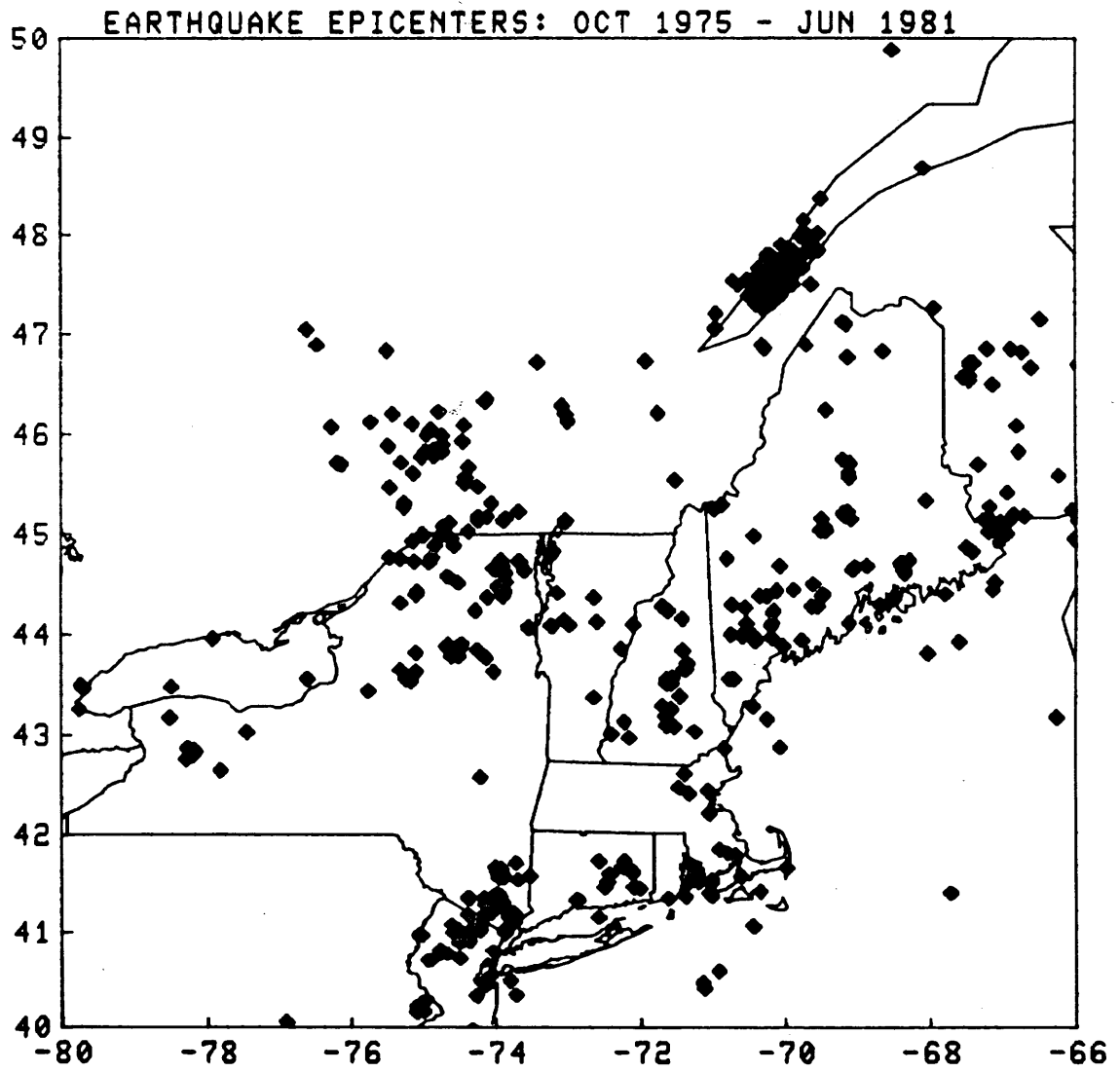


FIGURE 2.16

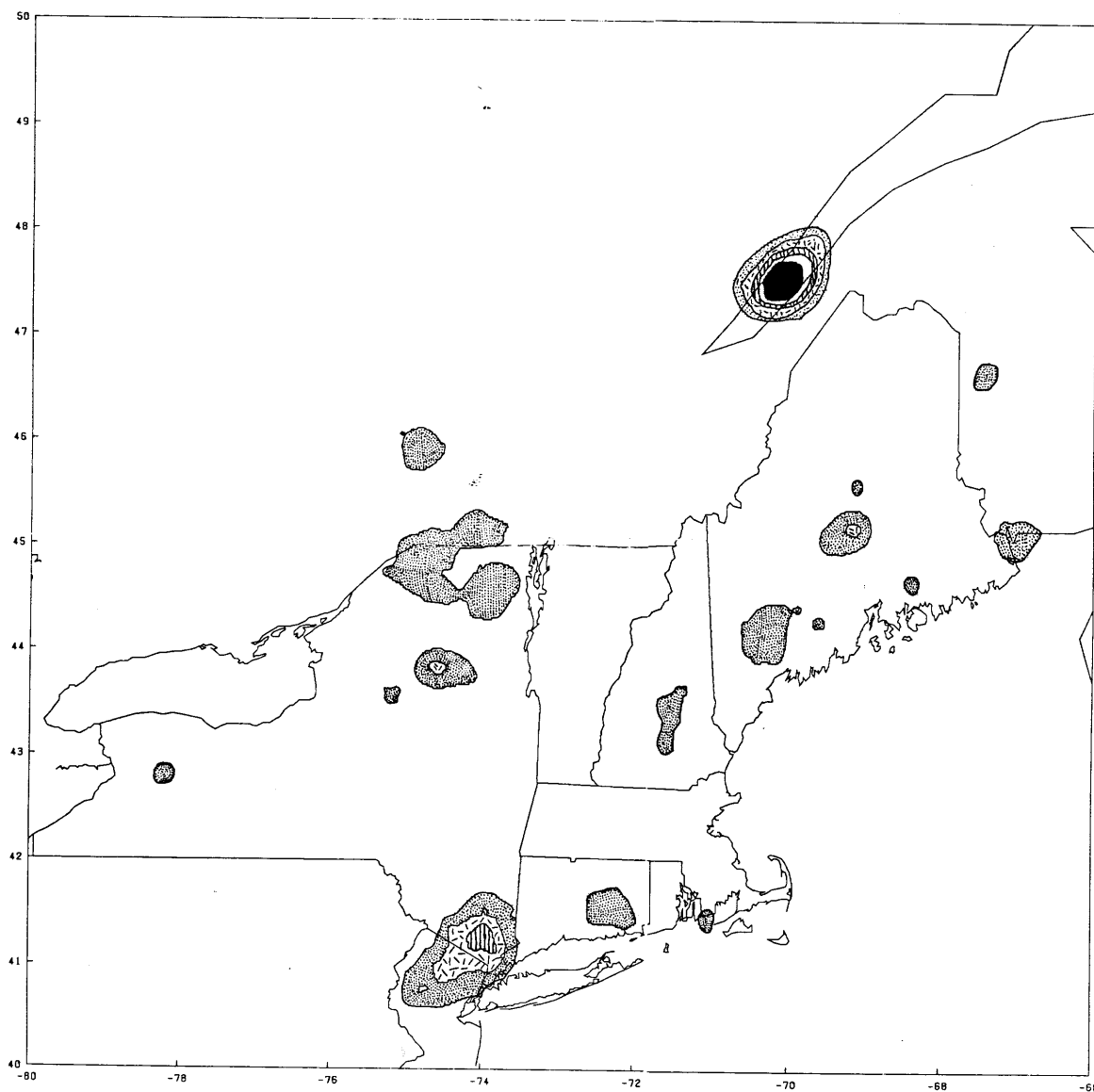


FIGURE 2.17

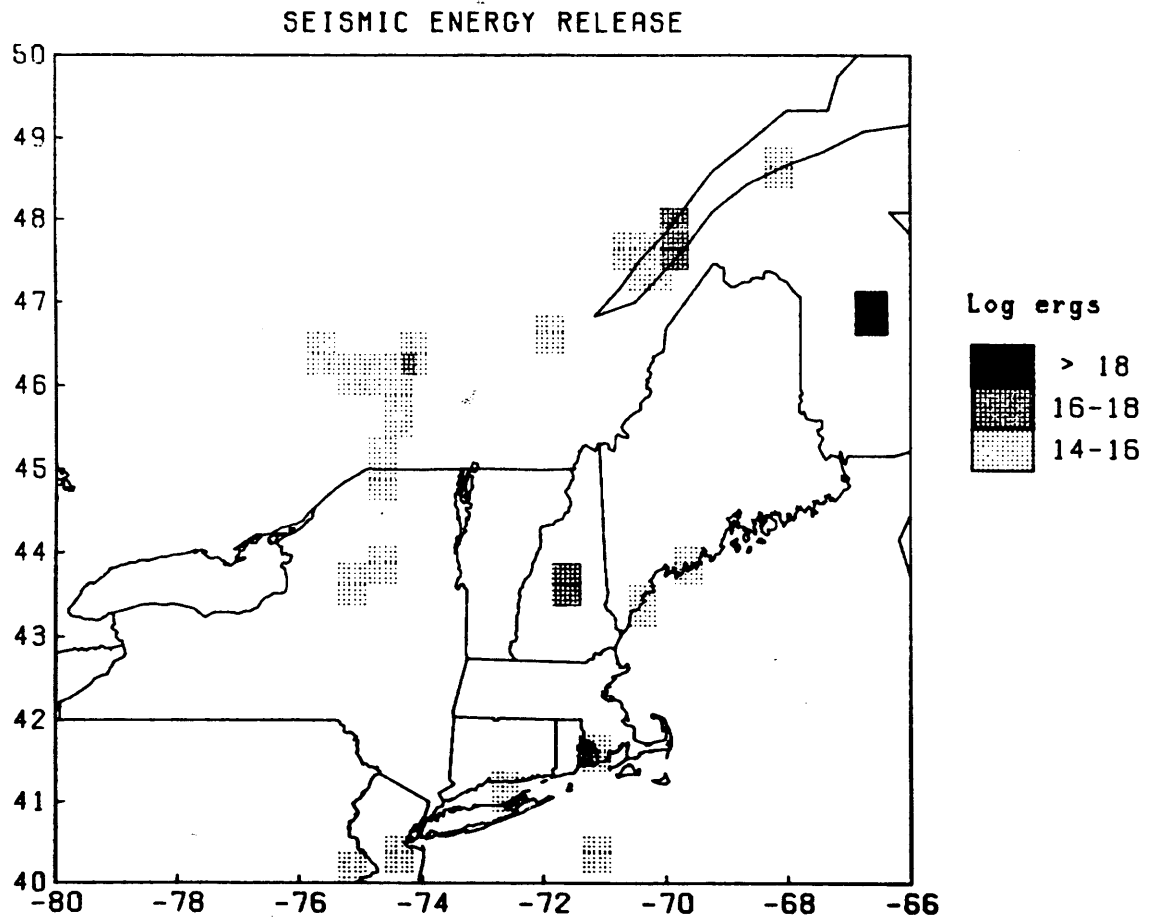


FIGURE 2.18

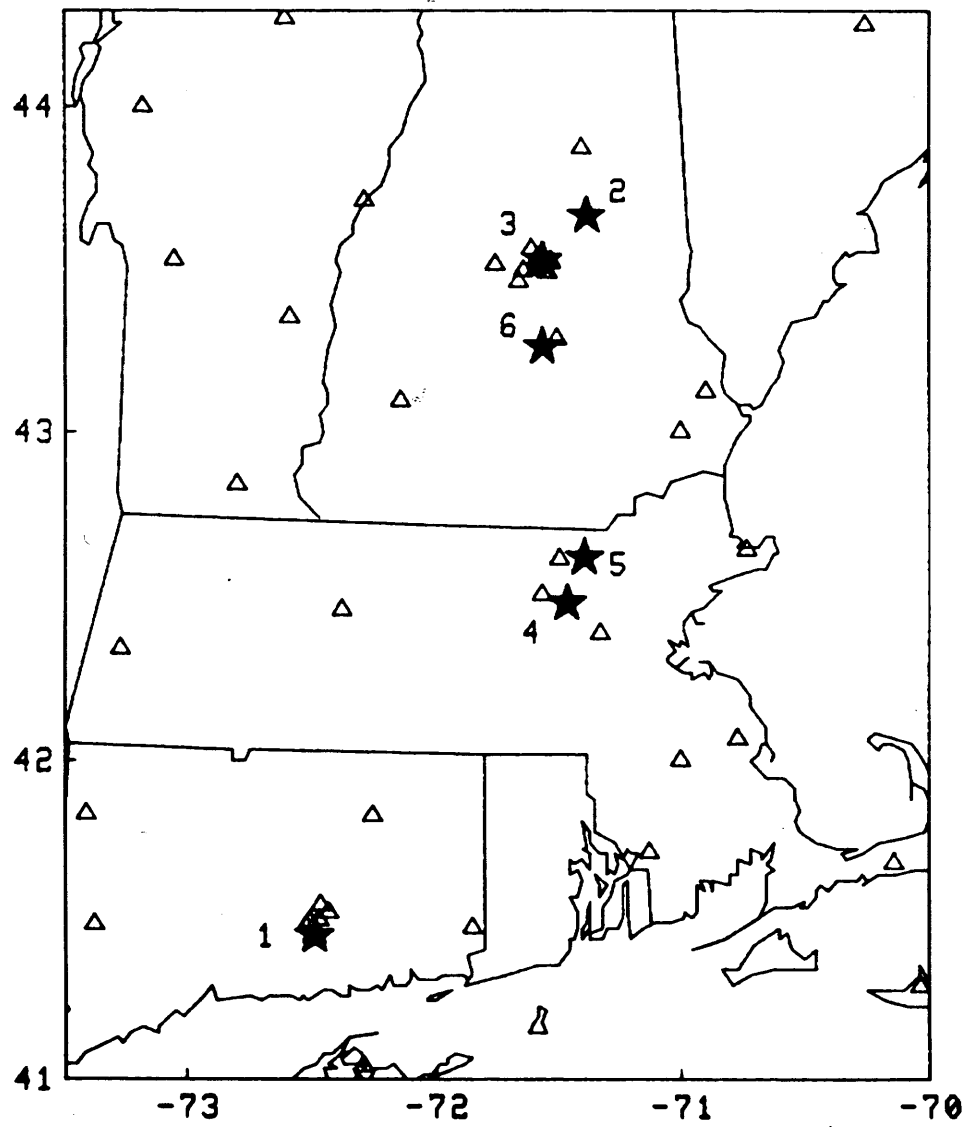


FIGURE 2.19

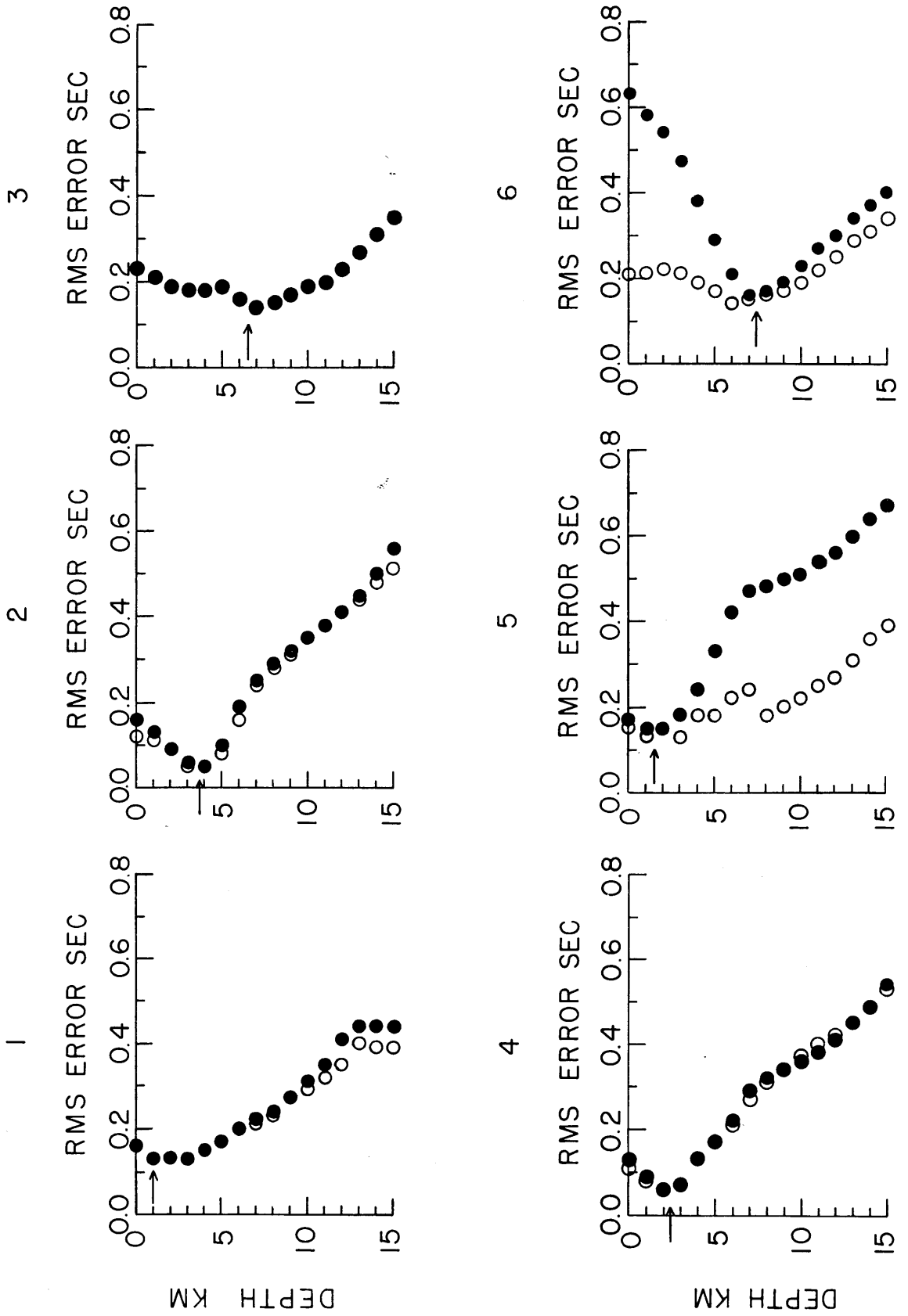


FIGURE 2.20

CHAPTER 3
FAULT PLANE SOLUTIONS AND CRUSTAL STRESSES
IN THE NORTHEASTERN UNITED STATES
AND SOUTHEASTERN CANADA

3.1 Introduction

The distribution of earthquake hypocenters generally does not provide sufficient information to determine the tectonic origin of the seismicity in an area. This is especially true in intraplate areas such as the NEUS-SEC where the pattern of seismicity defines broad seismic zones, as was shown in Chapter 2, rather than linear seismogenic features such as faults. These seismic zones may be indicative of areas of large scale crustal weakness, subsidence or uplift, or the release of residual strains from previous tectonic episodes. In some cases, these seismic zones may cross, rather than parallel, the structural grain of the area. Thus, it is difficult to correlate the seismicity with the structural geology, and we must turn to other source parameters for an understanding of the earthquake processes.

After the hypocentral location and magnitude, the next relevant characterization of the earthquake source is its fault plane solution. From the fault plane solution we obtain the type of faulting (i.e., the sense of relative motion), the orientation of the two possible fault planes, and by implication, the state of stress at the focus. By examining the geographic distribution of many fault plane solutions, we can delineate the state of

stress within the crust and possibly identify the surface expressions of geologic structures which may be the sources of the earthquakes. Detailed knowledge of the pattern of intraplate stresses also provides important constraints on models of global tectonic processes and the mechanisms of plate motions. Moreover, in tectonically and seismically stable areas such as the NEUS, knowledge of the stress field is required for the delineation of potential earthquake hazards associated with preexisting zones of weakness in the crust.

An example of an intraplate area where fault plane solutions have supplemented hypocentral data in the delineation of earthquake hazards is the New Madrid seismic zone. The events in this area define a 120 kilometer long earthquake zone (Stauder et al., 1976). Herrmann and Canas (1978) studied the focal mechanisms of the larger earthquakes in this zone and found that many events share the common feature of a NE-SW trending nodal plane which parallels the trend of the seismic zone. In addition, nearly all of the events in this zone with resolvable mechanisms have P-axes trending NE to E. With this information, the regional stress field in the central US has been delineated, and it is now possible to identify the faults which are preferentially oriented to respond to this stress field. These studies, as well as the use of deep crustal reflection surveys (Zoback et al., 1980) have greatly increased our understanding of the earthquake hazard in the central US (Johnston, 1982).

Until recently, little information has been available

regarding crustal stresses in the NEUS-SEC. Since most of the earthquakes are small, the number of clear P-wave first motions on the few permanent stations was insufficient to constrain the focal mechanisms. Most events were also too small to generate observable surface waves, which have been successfully used in other areas to study the earthquake mechanisms (e.g., Herrmann, 1979; Patton, 1976; Mitchell, 1973). (Recently, this situation has changed with the occurrence of the New Brunswick earthquake of January 9, 1982. This event, which was of magnitude 5.7 (mb), has been studied teleseismically by Nabelek et al., 1982 using both body and surface waves.) Early investigators resorted to the study of in-situ stress measurements such as hydrofracturing and strain relief, and geologic stress indicators, such as pop-ups and rockbursts (Hooker and Johnson, 1969; Sbar and Sykes, 1973). These measurements are generally indicative of the stress field near the surface, which may be decoupled from the stress field in the mid-to-lower crust. Thus, their usefulness in the study of earthquake generating stresses is limited. The installation of the Northeastern United States Seismic Network (N.E.U.S.S.N.) in 1975 meant that, for the first time, fault plane solutions could be determined for many events of magnitude greater than 3 (mb), and for some events of magnitude greater than 2 which are located in areas of high station density.

In this chapter, fault plane solutions will be determined for ten NEUS earthquakes using P-wave first motions recorded on N.E.U.S.S.N. and other short period seismic stations. A variety

of crustal models are used to project these surface observations back to the earthquake source. Then, published fault plane solutions and geologic (non-seismic) stress measurements in the NEUS-SEC are reviewed to form a basic dataset for interpretation. When possible, these fault plane solutions will be compared with the structural geology and the mapped faults in each area. Finally, a comprehensive examination of crustal stresses in the NEUS-SEC will be made with the objective of defining the state of stress in the crust on a regional and a local scale.

3.2 Determination of Fault Plane Solutions

In this section, fault plane solutions are determined for ten NEUS earthquakes using P-wave first motions. Particular attention will be paid to the effects of focal depth and crustal structure on the resulting fault plane solutions. (Many of the results from this section have been previously published in Pulli *et al.*, 1980; Pulli and Toksöz, 1981; Pulli and Guenette, 1981a, b; and Pulli and Godkin, 1981.)

3.2.1 Data and Analysis

Figure 3.1 shows the configuration of short period seismic stations in this area as well as the locations of the ten earthquakes studied in this chapter. (Some of the stations in Figure 3.1 are now closed. Station coordinates are listed in Appendix C of this work.) Epicentral information for these events are given in Table 3.1 and were determined using data from all participating members of the N.E.U.S.S.N., as well as other

short period seismic stations operating in this area. However, it must be stressed that the network was assembled over a period of five years (1975 - 1980) so that Figure 3.1 exaggerates the azimuthal coverage for the earlier earthquakes. Also, the smaller events will only have clear P-wave first motions on the closest stations.

Studies of the crust and upper mantle structure in the NEUS (Taylor and Toksöz, 1979, 1982b; Taylor et al., 1980) have shown that significant structural variations exist in this area. For example, the crust in the Grenville Province (i.e., west of the Appalachian - Precambrian contact) is quite uniform and consists of a single crustal layer of nearly constant velocity. However, in the Appalachian Province, the crust consists of two or three layers with some areas having a high velocity lower crustal layer. Thus, if we are to properly project the seismic rays back to the lower focal sphere, we must use a number of different crustal models depending on the source area. The effect of crustal structure is especially important for shallow events and close stations. The models used in this study are shown in Figure 3.2 and were obtained from 1) Chiburis et al. (1980), 2) Taylor and Toksöz (1979), 3) Weston Geophysical Corporation (personal communication), and 4), 5), and 6) Yang and Aggarwal (1981). The areas over which these models are judged to be applicable by this author are shown in Figure 3.3. Crustal models were chosen according to the source (epicentral) area. An interactive computer program was developed which allows the user

to change the crustal structure or focal depth and immediately see the effect of the change on the fault plane solution via a graphics terminal. In this way, the stability of the ten fault plane solutions could be tested. This step is important since accurate focal depths are known for only a few NEUS earthquakes.

Given the crustal model and the epicentral distance Δ , the takeoff angles were computed by calculating the travel times of all refracted rays and the direct ray, and then choosing the raypath of least travel time. For a crustal model consisting of N horizontal layers over a halfspace, where $v(i)$ and $\lambda(i)$ are the velocity and thickness of layer i respectively, with the source in layer η at a depth of ζ from the top of layer η , the travel time for a ray refracted along the top of layer κ is given by (Lee and Stewart, 1981)

$$\begin{aligned}
 T(\eta, \kappa, \Delta) = & \Delta/v(\kappa) - \zeta\Omega(\kappa, \eta)/v(\eta)v(\kappa) \\
 & + \sum_{i=1}^{\eta-1} [\lambda(i)\Omega(\kappa, i)/v(i)v(\kappa)] \\
 & + 2 \sum_{i=\eta}^{\kappa-1} [\lambda(i)\Omega(\kappa, i)/v(i)v(\kappa)] \quad (3.1)
 \end{aligned}$$

where

$$\Omega(\kappa, i) = [v(\kappa)^2 - v(i)^2]^{1/2}, \quad (3.2a)$$

and

$$\Omega(\kappa, \eta) = [v(\kappa)^2 - v(\eta)^2]^{1/2} \quad (3.2b)$$

The corresponding takeoff angle for this ray is

$$\theta(\eta, \kappa) = \sin^{-1} [v(\eta)/v(\kappa)] \quad (3.3)$$

and the crossover distance is

$$\begin{aligned} \chi(\eta, \kappa) = & - \zeta v(\eta)/\Omega(\kappa, \eta) \\ & + \sum_{i=1}^{\eta-1} [\lambda(i)v(i)/\Omega(\kappa, i)] \\ & + 2 \sum_{i=\eta}^{\kappa-1} [\lambda(i)v(i)/\Omega(\kappa, i)] \end{aligned} \quad (3.4)$$

If the source is in the first layer, the travel time of the direct (upgoing) ray is simply

$$T(u, \Delta) = [\Delta^2 + \zeta^2]^{1/2} / v(1) \quad (3.5)$$

with a corresponding upward takeoff angle of

$$\theta(u) = \tan^{-1} [\Delta/\zeta] \quad (3.6)$$

However, if the source is in the second or deeper layer, there is no explicit expression for computing the travel time of the

direct ray. In this case, an iterative procedure must be used to trace the ray from the source to the receiver. Starting with a trial takeoff angle θ_ϵ , Snell's law is used to compute successive incident angles to each overlying layer until the trial ray reaches the surface at an epicentral distance Δ_ϵ given by

$$\Delta_\epsilon = z[\tan(\theta_\epsilon)] + \sum_{i=\eta-1}^1 [\lambda(i)\tan(\theta(i))] \quad (3.7)$$

where $\theta(\eta) = \theta_\epsilon$. The incident angles are related by

$$\sin[\theta(i)]/v(i) = \sin[\theta(i+1)]/v(i+1) \quad (3.8)$$

for $1 \leq i < \eta$. The trial angle θ_ϵ is then varied, and the procedure is repeated. This trial takeoff angle converges rapidly to the angle whose associated raypath reaches the station within a defined error limit. Since the raypath consists of j segments of a straight line in each of the j layers, we can sum the travel time in each layer to obtain the travel time from the source to the station. This travel time is then compared with the travel times of the refracted rays, and the raypath of minimum travel time is selected.

Since many of the earthquakes studied here are small, or near the coast, and since we are using discrete velocity models, the coverage of the lower focal sphere can be non-uniform. To avoid any bias in the picking of the fault plane solutions, or

visually missing a valid solution, the algorithm of Guinn and Long (1977) was used which searches the lower focal sphere for all valid areas of P, T, and B axes with a specified number of possible errors. The P (pressure) and T (tension) axes are defined as the normal axes to the two nodal planes, whereas the B (null) axis lies at their intersection. In earthquake seismology, the P axis is commonly assumed to represent the axis of maximum compressive stress, σ_1 , and the T axis is assumed to represent the axis of minimum compressive stress, σ_3 . (Here we use the convention that compressive stresses are positive, so that the relationship between the principal stresses is $\sigma_1 > \sigma_2 > \sigma_3$.) The association of the P, T, and B axes with the σ_1 , σ_3 , and σ_2 axes, respectively, is reasonable if the earthquake occurs in a homogeneous medium. If the earthquake occurs on a preexisting fault, these assumptions are invalid on theoretical grounds. For example, McKenzie (1969) showed that the σ_1 -axis could be located up to +/- 90 degrees from the P-axis when the motion occurs on a preexisting fault. This would render fault plane solutions useless for the study of crustal stresses. However, Raleigh et al. (1972) experimentally derived faulting relations which show that only preexisting planes lying at 10 to 50 degrees from the σ_1 -axis would slip, so that the P-axis could be in error by no more than 35 to 40 degrees when sliding on a preexisting fault produces the earthquake. Also, the range of variation is only within the plane containing the slip vector and the P and T axes. For a thrust or normal fault with no

strike-slip component, or any case where the B axis is horizontal, this plane is vertical so that the errors in the σ_1 - and σ_3 -axes are small. The usual way of avoiding these errors is to average the P, T, and B directions obtained from a number of fault plane solutions in a given area and assume that this average approximates the actual stress orientation in the area.

The principal advantage of estimating stress orientations from fault plane solutions is that the inferred directions represent the stress conditions at considerable depths in the crust over a region comparable to the size of the earthquake (i.e., the smaller events are indicative of the local stress field, whereas the larger earthquakes are indicative of the long wavelength state of stress). The principal drawback of fault plane solutions is that only stress directions, and not magnitudes, are estimated from this procedure.

The procedure for the determination of the fault plane solutions may be summarized as follows: 1) An input dataset is created which consists of an event name or other identification, source latitude, longitude, and depth, and a list of station names and first motions. 2) A crustal model is selected. 3) After distances and azimuths are calculated and sorted, the travel times of all refracted P-waves and the direct P-wave are calculated. The ray of minimum travel time is then selected, and its takeoff angle is determined. If the ray of minimum travel time has been determined as leaving the upper hemisphere, the azimuth is increased by 180 degrees. 4) The first motions are

displayed on a lower hemisphere Schmitt projection via a graphics terminal. (For a Schmitt projection, the distance from the center of the plot, r , is related to the takeoff angle, θ , by $r=1.414(D)[\sin(\theta/2)]$, where D is the radius of the projection.) This allows a visual examination of the P-wave data. 5) The first motion data are examined by the Guinn and Long (1977) subroutine for all possible combinations of P, T, and B axes. The first run is for zero first motion errors. If no solutions are found, the number of possible errors is increased by one, and the procedure is repeated. When solutions are found, these are displayed on a lower hemisphere projection. 6) The stability of the solution is next tested by looping through this procedure for different focal depths and crustal models.

3.2.2 Fault Plane Solutions

All fault plane solutions determined in this Chapter are shown in Figures 3.4a and b. Individual P-wave first motions are listed in Table 3.2 for reference. First motions were used only from stations with known polarities. These polarities were checked using impulsive arrivals from nuclear blasts or teleseisms, or in some cases, instrumental weight lifts. This step is important since it was found during the course of this study that nearly 30% of the short period stations in the NEUS have been improperly wired at some point in the data channel. A short discussion of each solution is now presented.

1) 11Mar76 Portsmouth, RI: Since this earthquake occurred during the early phase of network installation and was located

close to the coast, the data are not numerous but do constrain the mechanism. The intensity of this earthquake was extensively studied by Albert et al. (1976). The relatively high epicentral intensity (V) and rapid decay of intensity with distance suggest that the event was shallow. The focal mechanism shows thrust faulting on NW-SE striking fault planes. The P-axis trends NE-SW.

2) 10May76 New Bedford, MA: Again, the early occurrence and coastal location of this event limited the number of available first motions. Intensity data for this earthquake suggest that the focal depth was shallow. The mechanism is similar to that of event No. 1, though less well constrained. The fault planes trend N-S to NW-SE. The P-axis trends NE-SW, similar to that of event No. 1.

3) 25Dec77 Hopkinton, NH: This earthquake occurred near the center of the network, so that the azimuthal coverage is quite good. The event was also recorded on a temporary short period seismic network operated in the Lake Winnepesaukee, NH area by Weston Geophysical Corporation. The mechanism shows thrust faulting with a small component of strike-slip motion. Fault planes strike NE-SW and NW-SE. The P-axis trends nearly E-W.

4) 01Sep78 Acton, MA: This very small earthquake was felt and heard by most residents within an area of approximately 2 square kilometers. A well constrained focal depth of 3 km was determined for this event which explains the sound and intensity pattern. Fundamental mode Rayleigh waves of 1/2 second period

could also be seen on the closer stations. The fault plane solution shows either strike-slip or dip-slip faulting, depending on which fault plane is chosen. The P-axis trends nearly N-S.

5) 18Apr79 Bath, ME: This event was extensively studied by Pulli et al. (1980) and is also described in Appendix F of this work. Although the focal depth cannot be accurately determined, the travel times indicate that the event was shallower than 5 km. The mechanism did not change significantly for depths from 0 to 5 km. The mechanism shows thrust faulting on nearly N-S striking fault planes. The P-axis trends E-W.

6) 23Apr79 Candia, NH: Fundamental mode Rayleigh waves of 1/2 to 1 second period were observable on some close stations, which indicates a very shallow focus. This event shows thrust faulting; however, the data permit varying components of strike-slip motion. The significance of the result is the fact that the P-axis trends nearly E-W for all possible solutions.

7) 06Jun80 Booneville, NY: This earthquake, located near the southwestern Adirondacks, exhibits pure thrust faulting on NNW-SSE striking fault planes. The P-axis trends ENE-WSW. The mechanism is similar to those of other nearby events, discussed later (Yang and Aggarwal, 1981).

8) 23Nov80 Chelmsford-Lowell, MA: This earthquake was studied in detail by Pulli and Guenette (1981a, 1981b) and is also described in Appendix F of this work. They obtained a well constrained focal depth of 1.5 km. The fault plane solution shows either strike-slip or dip-slip faulting, and the P-axis

trends NE-SW. The mechanism is similar to that of the nearby event No. 4.

9) 21Oct81 Long Island Sound, NY: Because of its relatively large size ($m_b L_g=3.4$) and proximity to some special seismic arrays, this earthquake provided an abundance of first motion data. Using 27 P-wave polarities, the mechanism obtained shows thrust faulting on NE-SW trending fault planes. This event was studied in detail by Pulli and Godkin (1981) and is also discussed in Appendix F of this work.

10) 19Jan82 Gaza, NH: This earthquake was the largest event to occur within the New England states since the installation of the N.E.U.S.S.N. ($m_b L_g=4.6$). Twenty four clear P-wave first motions were recorded. The mechanism shows strike-slip faulting on faults oriented nearly N-S or E-W. This mechanism is somewhat different from those of the nine other earthquakes studied here. The P-axis trends NE-SW.

Events 1, 2, 3, 5, and 6 were also studied by Graham and Chiburis (1980). They used crustal model No. 1 for all the solutions and greater focal depths for events 1 and 3 (15 km and 6 km, respectively). Their solutions are essentially the same as those presented in this work. Yang and Aggarwal (1981) also studied events 1 and 3. Their mechanism for event No. 1 shows the same mode of faulting (i.e., thrust faulting); however, the orientation of the fault planes is NE-SW rather than the NW-SE direction obtained here and by Graham and Chiburis (1980). Yang

and Aggarwal's (1981) mechanism for event No. 3 is the same as that presented here.

3.2.3 Discussion and Error Analysis

The ten fault plane solutions obtained here are arranged geographically in Figure 3.5. It is apparent from this dataset that the predominant earthquake mechanism in the NEUS is thrust faulting, with some events showing components of strike-slip motion. However, the direction of the P-axis is not uniform throughout the entire area. For instance, in the Maine-New Hampshire area (events 3, 5, 6, and 10) the P-axis trends NE-SW to E-W. In northeastern Massachusetts (events 4 and 8), the P-axis trends N-S to NE-SW. In eastern New York and southeastern New England (event 7), the P-axis trends NE-SW. In Long Island Sound, the P-axis trends NW-SE. These variations in stress directions are discussed in detail in Section 3.4 of this Chapter.

The determination of fault plane solutions for small local earthquakes presents a number of complications not associated with the corresponding procedure for the teleseismic case. Perhaps the most significant complication arises from the use of layered crustal models. Since we assume that all first arrivals are either direct (upgoing) or refracted, the number of possible takeoff angles equals the number of crustal layers plus one. With layered models, the selection of the takeoff angles is based solely on the calculation of the travel times and crossover distances. This becomes a crude approximation when the source is

in one crustal model and the receiver is on top of another. Also, for a source in the lowest crustal layer, only one takeoff angle will be observable unless there is a close station which will record the upgoing ray. For dip-slip faulting, this represents a serious resolution problem. Fortunately, all the events studied here were shallow, with at least two different takeoff angles possible.

The idea that the crust of the earth consists of horizontal layers is a useful concept supported by refraction experiments. However, it is becoming increasingly apparent that the crust is much more heterogeneous than the layered models imply. In such cases we must turn to alternative methods of relating the surface observations to the earthquake sources. For example, if we can specify the P-wave velocity at regularly spaced intervals (both laterally and in depth), we can use ray tracing techniques (Thurber, 1981). In other cases, we can assume a linear or parabolic increase in P-wave velocity with depth down to the mantle and use integral representations to calculate travel times and takeoff angles. However, in order to apply these techniques, our understanding of the crust and upper mantle structure in this area must be refined on a much finer scale than is presently available.

Instrumental considerations are also important to the determination of fault plane solutions for local earthquakes. A seismic channel in a local earthquake network is a multi-component data line, consisting of a seismometer,

preamplifier, amplifier, voltage controlled oscillator (VCO), transmission line, discriminator, and a recorder which may be a galvanometer, helicorder, an A/D converter and computer, or a tape recorder. At each component, the possibility of a phase reversal exists. Modern seismometers are also compact and sealed, so that the mass is inaccessible, and weight lifts are not possible. Thus, the channel polarities are best confirmed using impulsive teleseismic arrivals, preferably from large nuclear explosions. (During this study, it was found that nuclear explosions from the Semipalatinsk area of the Soviet Union provided the clearest arrivals for checking the polarities. This is due to the simple crustal structure in the area, and the fact that the blasts were usually shot at approximately 02:00 UTC, which is a time of minimum cultural noise at our stations.) Another problem is that at high frequencies, some telemetry units exhibit phase shifts which may render the response at teleseismic frequencies useless for the determination of high frequency polarities. Thus, it is advisable to test the phase response of the telemetry units prior to installation.

The fault plane solutions presented here represent a "best effort" to project the surface observations of P-wave first motions back to the source, given our present knowledge of the crust and upper mantle structure. In many areas of the NEUS, this knowledge is inadequate, and should be the focus of future research. As more data on the crustal structure become

available, these fault plane solutions should be studied again using ray tracing techniques.

3.3 Literature Review of Fault Plane Solutions and Geologic Stress Measurements

Fault plane solutions have been published for a number of earthquakes in the NEUS-SEC during recent years. There are also a number of in-situ stress measurements available, as well as geologic stress indicators such as fault offsets and pop-ups. In this section, a review is conducted of these data before an examination of the crustal stresses is made in the next section.

3.3.1 Fault Plane Solutions

This review of published fault plane solutions is presented by region. Table 3.3 lists the epicentral and stress data in chronological order. This table includes the results from Section 3.2. Figures showing the nodal planes and P and T axes for these earthquakes are presented in Appendix E.

Western NY: This area includes the site of the August 12, 1929 Attica, NY earthquake. This event was of magnitude 5.2 (mb) (Street and Turcotte, 1977) and had an epicentral intensity of VIII (Fox and Spiker, 1977). Chadwick (1920) inferred from the surface geology the presence of a N-S striking, deeply dipping fault in this area, known as the Clarendon-Linden structure. Whether or not this structure was responsible for the 1929 earthquake remains an unsolved problem. The seismicity in this area is rather diffuse and appears to follow an E-W rather than a

N-S trend. The seismicity and geology of this area have been extensively outlined by Fletcher and Sykes (1977).

Herrmann (1978) studied the Attica, NY earthquakes of January 1, 1966 and June 12, 1967 using both surface wave radiation patterns and P-wave first motions. These events were of mb 4.6 and 4.4 respectively. Both events exhibit predominantly strike-slip motion on N-S and NW-SE trending fault planes. The P-axes trend at 62 and 74 degrees. The N-S striking fault plane is parallel to the trend of the Clarendon-Linden structure. However, since these events occurred prior to the network installation, an accurate location is not possible (accurate to within 10 km) and thus the association of these events with the Clarendon-Linden Fault cannot be definitively established. Herrmann (1978) was able to determine that these events occurred at focal depths between 2 and 3 km. If the 1929 earthquake occurred at a similar focal depth, this would account for the relatively high epicentral intensity for an event of mb 5.2 .

Northern NY - western PQ: This area encompasses a broad band of seismicity stretching from Lake Champlain, VT to Timiskaming, ONT. A number of fault plane solutions are available for this area from various investigators.

Schlessinger-Miller et al. (1981) studied the focal mechanisms of two recent earthquakes in the Cornwall, ONT area. This area was the site of an intensity VIII earthquake on September 4, 1944. The present events occurred on July 4 and 5,

1981. Both events were of magnitude 3.4 (mbLg) and had a well determined focal depth of 16 km. These events show primarily thrust faulting on N-S or E-W fault planes, with a small component of strike-slip motion. The P-axes trend NE-SW.

Further northwest, the mechanisms of two moderate earthquakes are available from Canadian seismologists. The mechanisms of both events were studied using P-wave first motions and surface wave excitation. The 12Jul75 Maniwaki, PQ earthquake (mbLg=4.2, depth=17km) was studied by Horner et al. (1978) and shows thrust faulting on NW-SE trending fault planes. The 18Feb78 St. Donat, PQ earthquake (mbLg=4.1, depth=7km), studied by Horner et al. (1979) shows pure thrust faulting on fault planes trending just west of N-S.

Yang and Aggarwal (1981) studied the focal mechanisms of a number of earthquakes in this area ranging in magnitude from 2.0 to 4.2 (mb). The events show thrust faulting with some earthquakes having small components of strike-slip motion. All events are characterized by a fault plane trending NW-SE and have P-axes trending NE-SW to nearly E-W. In addition, Sbar et al. (1972) compiled a composite fault plane solution for the Blue Mountain Lake earthquakes of 1971-73 and found thrust faulting on NW-SE trending fault planes with a P-axis trending ENE-WSW.

Throughout this area, the mechanisms and stress directions for most of the earthquakes are very uniform, showing thrust faulting on NW-SE trending fault planes with P-axes in the NE-SW to ENE-WSW direction. The NW-SE trend of the fault planes is

parallel to the trend of the seismicity in this area. However, the predominant trend of the mapped faults is NE in northern NY and WNW in western PQ (King, 1969). Sbar and Sykes (1977) suggested that this meant the earthquakes in this area were occurring on structures deeper than those seen in the surficial geology.

La Malbaie, PQ: This region is one of the most seismically active areas in the NEUS-SEC. (The region is often referred to as the Charlevoix seismic zone (Basham et al., 1979). On March 1, 1925 a magnitude 6.7 earthquake (Street and Turcotte, 1977) occurred in this area, producing intensity IX effects (see Appendix A). Consequently, it has been the subject of close scrutiny by Canadian seismologists (Stevens, 1980a) and there is presently a permanent microearthquake array surrounding this zone. The seismotectonic environment is very complex and includes an impact crater which extends over two-thirds of the seismic zone (Rondot, 1971), an anomalous zone of subsidence, and broad scale features such as rifting (Kumarapeli, 1978) and post-glacial uplift (Andrews, 1970). The current seismicity is confined by sharply defined, steeply dipping boundaries on both sides of the St. Lawrence River (Basham et al., 1979).

Two reconnaissance microearthquake studies have been conducted in this area by Leblanc et al. (1973) and Leblanc and Buchbinder (1977). During the latter study, fault plane solutions were obtained for six microearthquakes ranging in magnitude from -0.3 to 2.0 (ML). The mechanisms range from pure

thrusting to predominantly strike-slip motion to one case of normal faulting. The direction of the P-axis varies considerably from event to event, which is to be expected in a tectonically complex region. Also, since the events are relatively small, they are probably indicative of small scale stress concentrations rather than a reflection of the long wavelength state of stress in this area. However, a common feature of these six fault plane solutions is the presence of a N-S to NE-SW trending fault plane which parallels the trend of the St. Lawrence River Valley and Logan's Line (the Appalachian-Grenville surface contact).

On August 19, 1979 an mbLg 5.0 earthquake occurred in this seismic zone and was studied in detail by Hasegawa and Wetmiller (1980). This larger event provided the first opportunity to establish the predominant response to the regional stress field in this area. The mechanism shows predominantly thrust faulting with a small component of strike-slip motion. The fault planes strike NE-SW and NW-SE. The P-axis trends NW-SE. The NE-SW trending fault plane was also seen in the fault plane solutions of the microearthquakes and the surface geology.

New Brunswick: On January 9, 1982 a magnitude 5.7 (mb) earthquake occurred in the central portion of this province. The focal mechanism of this earthquake, determined by an inversion of P- and SH-waves and the Rayleigh wave radiation pattern (Nabelek et al., 1982), shows thrust faulting on nearly N-S striking fault planes. The P-axis trends E-W. The primary structural feature in this area is the Appalachian Highlands, which strike NE-SW.

This is the only fault plane solution available in this area, and thus the stress orientation may not be entirely representative of the actual stress conditions in this area. The earthquake was followed by a number of aftershocks of magnitude greater than 4.5 (mb) and the mechanisms of these events, when available, will provide additional information on the state of stress in this area.

New England: The structural geology of New England is dominated by the Appalachian orogen. This ancient mountain belt consists of alternating synclinoria and anticlinoria which trend N-S to NE-SW across the region. The area has experienced alternating episodes of compressional and extensional tectonics, resulting in complicated structures whose expressions may reach to 200 km in depth (Taylor and Toksöz, 1979).

Graham and Chiburis (1980) studied the mechanisms of eighteen New England earthquakes which occurred between March 1976 and April 1979. Five of these events were studied in Section 3.2 of this work (events No. 1, 2, 3, 5 and 6 in Table 3.1), and the mechanisms obtained are essentially the same. Seven of the eighteen events studied by Graham and Chiburis (1980) have either non-unique focal mechanisms or were based on sparse station distributions. These seven events will not be considered here. The six remaining mechanisms are well constrained and will be included in this compilation. The earthquakes in Crescent Lake, ME (29Oct78) and Otisfield, ME (04Jan78) both reveal thrust faulting on NE-SW trending fault

planes. This is in contrast to the nearby Bath, ME earthquake of 09Apr79 which shows thrust faulting on N-S striking fault planes. The Lake Winnepesaukee, NH earthquake of 21Jun78 shows strike-slip faulting on NE-SW and NW-SE trending fault planes. The Wareham, MA (20Dec77) earthquake shows thrust faulting on NE-SW trending fault planes, differing from those of the nearby New Bedford, MA and Portsmouth, RI earthquakes. The earthquake in Norwich, CT (17Dec76) shows either thrust or strike-slip faulting, whereas the East Haddam, CT earthquake (17Dec76) shows pure thrust faulting on E-W trending fault planes.

The Maine-Quebec border earthquake of 15Jun73 was one of the largest events to occur in the New England area in recent years ($m_b L_g=4.8$, depth=6km). Since this event occurred prior to the network installation, the amount of P-wave data is not great and different mechanisms have been published by various authors. Wetmiller (1975) used reported P-wave first motions and found a strike-slip mechanism on NE-SW and NW-SE fault planes, with a large component of normal faulting. Herrmann (1979) used the surface wave radiation patterns with some P-wave first motions and also found a strike-slip mechanism with a large component of thrust faulting on N-S and NW-SE fault planes. Yang and Aggarwal (1981) used aftershock data as well as main shock surface wave data and found a thrust mechanism on nearly N-S striking fault planes. Although these mechanisms differ considerably, the directions of the P-axes are similar and reveal a NE-SW direction.

Southeastern NY - northern NJ: The primary structural feature in this area is the Ramapo Fault system, a NE-SW trending feature just west of New York City. Aggarwal and Sykes (1978) and Yang and Aggarwal (1981) studied the focal mechanisms of a number of earthquakes believed to be associated with this feature. All of their mechanisms show thrust faulting on NE-SW trending fault planes and have P-axes trending NW-SE.

However, on the northern end of this feature the stress distribution is apparently more complicated. On 07Jun74 a magnitude 3.3 (mb) earthquake occurred in Wappinger Falls, NY and again, different investigators have published significantly different fault plane solutions. Pomeroy et al. (1976) found a thrusting mechanism on NW-SE trending fault planes. However, Yang and Aggarwal (1981) found thrust faulting on NE-SE trending fault planes, which matches the mechanisms of the events on the Ramapo system. It is nearly impossible to assess which solution is correct. If the solution of Pomeroy et al. (1976) is correct, then this implies that a rapid change in the direction of maximum compressive stress exists over a small area. If the solution of Yang and Aggarwal (1981) is correct, then the state of stress is uniform over this area.

Recently, two composite fault plane solutions have been made available for this area by Seborowski et al. (1982) which shed some light onto the controversy. The earthquakes they studied occurred in Annsville, NY, just south of Wappinger Falls. Both mechanisms show thrust faulting on NW-SE fault planes, similar to

Pomeroy's mechanism for the Wappinger Falls earthquake. Thus, it appears that the stress distribution in this area is much more complicated than was first assumed.

On the south end of the Ramapo Fault zone, Sbar et al. (1970) determined a composite fault plane solution for a series of earthquakes near Lake Hopatcong, NJ. Their mechanism reveals normal faulting on NE-SW trending fault planes with a P-axis oriented NE-SW and nearly vertical. This event is one of the few normal faulting earthquakes known in the NEUS-SEC.

3.3.2 *Geologic and In-Situ Stress Measurements*

We now present a review and brief discussion of the available geologic stress measurements in the NEUS-SEC, including hydrofracturing, strain relief measurements, fault and core offset data, and pop-ups. The data from this section are summarized by type in Table 3.4. (Again, the principal stress convention is $\sigma_1 > \sigma_2 > \sigma_3$.)

Hydrofracturing: This technique consists of hydraulically isolating a section of a well using inflatable rubber packers, and then pressuring the isolated section with a fluid while recording the time history of the fluid pressure. The pressure is then increased to the level at which a tensile fracture occurs. The orientation of the fracture can then be determined using a borehole televiewer. For a vertical borehole, the tensile fracture should be oriented in a direction perpendicular to that of the minimum horizontal stress.

Haimson and Lee (1979), Haimson (1974), and Overbey and

Rough (1968) cite hydrofracturing measurements in Quebec, New York, and Pennsylvania. In Quebec, the maximum horizontal compressive stress is oriented in a NE-SW direction. In New York, the σ_1 direction is oriented in a NE and ENE direction. The measurements in these areas are consistent with the inferred stress directions from the fault plane solutions.

Strain Relief Data: This method involves the measurement of the change in strain that occurs after relieving the ambient stress on the rock. The strain relief is accomplished by drilling an annulus in a rock mass and attaching strain gauges to the exposed surface. The deformation associated with the stress relief can then be measured and related to the ambient stress field.

The most serious drawback of strain-relief measurements is that they are operationally limited to the upper 50 meters of the free surface. Also, to obtain reliable results that are not influenced by small-scale inhomogeneities in the rock, a number of measurements must be taken at each hole, which is a time consuming and expensive process. Accurate determinations of the elastic constants of the rock are also required to relate the strain relief to the stresses. Ideally, these should be determined under the confining pressure and temperature conditions that exist at the point of measurement.

Hooker and Johnson (1969) conducted a number of strain relief measurements in New England. In northeastern Massachusetts, their results indicate a direction of maximum

compressive stress ranging from 0 to 56 degrees (from N). This agrees with nearby earthquake focal mechanisms. In central Vermont, their results show a direction of maximum compressive stress from 0 to 14 degrees. There are no focal mechanisms in this area to substantiate this result.

Fault Slip and Core Offset Data: If the direction of slip on a preexisting fault can be measured in the field, we can then determine the direction of the principal stresses. Woodworth (1907) and Oliver et al. (1970) cite the occurrence of postglacial vertical offsets in high-angle reverse faults in Attleboro, MA, indicating a direction of maximum compressive stress oriented at 157 degrees. Oliver et al. (1970) also cite reverse faults cutting Pleistocene gravels in Pumpkin Hollow, NY indicating a σ_1 direction of 130 degrees.

Drill holes from road excavations are sometimes found offset after the excavation is complete. The direction of the offset, as in the case of fault slip, can be used to determine the orientation of the principal stresses. Block et al. (1979) found core offsets in a roadcut in Colchester, CT indicating thrust motion on a preexisting fault. The direction of the σ_1 axis was determined to be 122 degrees. Schäfer (1979) also found offset drill holes in Port Matilda and Millerstown, PA, indicating a maximum compressive stress direction at 140 and 100 degrees, respectively.

Pop-ups: Pop-ups have been frequently found in northern and western New York where the lithostatic load has been reduced by

glacial unloading and quarrying activities. Since pop-ups are compressional features, the axis of maximum compression, σ_1 , is taken to be perpendicular to the strike of the feature.

Cushing et al. (1910) noted several pop-ups in the Thousand Islands area of northern New York. The largest feature, which was 40 meters long and 4 meters high, struck N28W, indicating a σ_1 -axis trending NE. Sbar and Sykes (1973, 1977) describe the occurrence of similar features in western New York. All of these pop-ups in New York indicate a direction of maximum compression trending NE to ENE.

As with strain relief data, pop-ups indicate the state of stress at the near surface, and thus the extension of the stress field to depths may not be valid. In such cases, the pop-up data should be used as a supplement to earthquake fault plane solutions.

3.4 Crustal Stresses in the Northeastern United States

We have now compiled a dataset consisting of 53 earthquake fault plane solutions and 18 non-seismic stress measurements. However, before an interpretation is attempted on this dataset, let us review the conclusions of previous works on crustal stresses in the NEUS-SEC.

Sbar and Sykes (1973) studied the distribution of crustal stress measurements in the central and eastern US using primarily in-situ measurements and a few earthquake fault plane solutions. They concluded that much of the central and eastern US was presently under a horizontal compressive stress oriented ENE to

E. This area of uniform stress extended from west of the Appalachians to the middle of the continent. The only data available for the New England area at that time were the strain relief data from Hooker and Johnson (1969) which indicated a nearly N-S oriented horizontal compression in Vermont and eastern Massachusetts. Thus, the Appalachians marked a transition zone across which the axis of maximum compressive stress (σ_1) rotated from ENE to N (moving west to east). However, Sbar and Sykes (1973) cautioned that the in-situ measurements should be confirmed with fault plane solutions before a definitive change in the direction of σ_1 was accepted.

Later, Sbar and Sykes (1977) utilized the new data from the Lamont-Doherty Seismic Network to determine more fault plane solutions for this area and drew the same conclusion regarding crustal stresses west of the Appalachians. However, based largely on the data accumulated in SE New York and N New Jersey, they concluded that the area east of the Appalachians was characterized by a horizontal compressive stress oriented WNW-ESE. This change in the direction of the σ_1 -axis means that earthquakes west of the Appalachians should occur on preexisting faults oriented in a NW direction, whereas east of the Appalachians, the earthquakes should occur on NE trending faults. In both areas, the predominant earthquake mechanism should be thrust faulting.

Recently, Zoback and Zoback (1980) compiled crustal stress data for all of the conterminous US in order to define stress

provinces. They divided the eastern US into two stress provinces. These are the Mid-continent province, characterized by a horizontal compressive stress trending ENE, and the Atlantic Coastal province, characterized by a horizontal compressive stress trending NW. As in the previous two studies, the boundary marking the transition between these two stress provinces coincided with the Appalachian Mountains.

Finally, Yang and Aggarwal (1981) used fault plane solutions of NEUS-SEC earthquakes to define the stress regime in this area. As in the previous studies, they divided the area into two stress provinces. West of the Appalachians, they concluded that the compressive stress field is horizontal and oriented ENE-WSW. East of the Appalachians, they found that the compressional stress field is oriented WNW-ESE.

We now turn to the interpretation of the stress data compiled in this chapter. The interpretation will be carried out over two datasets. The first dataset consists of all the data from Tables 3.3 and 3.4. The second dataset is a subset of the first and includes only earthquake fault plane solutions for events of magnitude greater than or equal to 3.0 (mb). This second dataset is used for two reasons. First, the in-situ and geologic stress indicators are indicative of the state of stress at very shallow depths. This shallow stress field may be decoupled from the stress field at greater depths (i.e., greater than a few hundred meters) at which depths the earthquakes are occurring. The shallow stress field is also greatly influenced

by crustal inhomogeneities and topographic features (McTigue and Mei, 1981). Thus, we exclude this sensitive data. Second, earthquakes of magnitude less than 3.0 (mb) are excluded since these events are of very small source dimensions and may represent the response to localized stress concentrations. All of these factors may contribute to scatter in the stress field data, and may cloud our understanding of the long wavelength state of stress in the crust.

We begin with no previous assumptions about the stress field, and will statistically test for regional uniformity. This will be accomplished using rose diagrams which indicate the frequency distribution of principal stress direction with azimuth.

Figure 3.6a shows the horizontal projections of the P-axes for the 53 earthquakes in Table 3.3 as well as the trends of the σ_1 -axes for the 18 non-seismic stress measurements from Table 3.4. Figure 3.6b is the corresponding figure for the abridged dataset. Figure 3.6c shows the horizontal projections of the T-axes for the 53 earthquakes in Table 3.3 as well as the trends of the σ_3 -axes for the non-seismic stress measurements. Figure 3.6d is the corresponding figure for the second dataset. In Figures 3.6 a,b,c, and d the approximate trend of the Appalachian - Precambrian contact is indicated by the dotted line (King, 1969). As a first observation, we see that the predominant stress field is compressive in nature, as indicated by the vast majority of thrust faulting events. Therefore the interpretation

will be carried out using only the P- and σ_1 -axes. Second, we find that there is a general agreement between the seismic and non-seismic measurements in areas where both measurements are available. This agreement can be seen in western NY, northern NY, and northeastern MA. However, in southeastern MA and CT, the agreement is weak. This may be due to a decoupling of the shallow stress field from that at greater depths. Third, we see that when the entire dataset is considered, there is no uniform state of stress across the entire study area, although some regional patterns appear to visually stand out. If we consider the abridged dataset, the stress field is more uniform, but there is still considerable scatter in the data, especially in the Appalachian Province.

To test for a uniform regional stress field, we have plotted the stress measurements for both datasets on rose diagrams, shown in Figure 3.7 a and b. The mean direction of the P- and S_1 -axes for the study area is 86 ± 39 degrees for the entire dataset, and for the abridged dataset we obtain a mean of 78 ± 33 degrees. Although a mean regional stress field oriented ENE-WSW may be present across the study area, the standard deviation of the field amounts to nearly 40% of the possible values.

In Figure 3.6a, we see that a uniform compressive stress field may exist in some areas of the NEUS-SEC. Visually, the boundary marking a transition appears to coincide with the trend of the Appalachians. Next, we test for a uniform compressive stress field on both sides of the Appalachians, again using rose

diagrams. These are shown in Figures 3.8 a,b,c, and d. West of the Appalachians (which includes northern NY, western PQ, and western NY), the compressive stress field is remarkably uniform, with a maximum compressive stress direction trending at 64 ± 18 degrees for the entire dataset, and 60 ± 19 degrees for the abridged dataset. However, east of and including the Appalachians (which includes New England, New Brunswick, La Malbaie, southeastern NY, northern NJ, and PA), the compressive stress field is oriented at 98 ± 41 degrees for the entire dataset, and 96 ± 34 degrees for the abridged dataset. Although the stress field in the Appalachian Province may have an underlying E-W component, it is nonetheless highly variable.

Let us now further subdivide the study area and examine the stress field on a local basis. Rose diagrams showing these stress measurements are presented in Figure 3.9 . (This interpretation is carried out over the entire dataset.) In western NY and adjacent areas of Canada, the maximum compressive stress field is oriented at 65 ± 17 degrees. In northern NY and western PQ, the compressive stress field is oriented at 60 ± 18 degrees. These two subregions demonstrate the remarkable uniformity of the stress field west of the Appalachians. In the La Malbaie, PQ area, the compressive stress field is oriented at 94 ± 28 degrees. The larger variation in the mean stress field is likely a result of the complicated tectonics and wide range of earthquake magnitudes in this subregion. In New England, we find the largest variations in the stress field, trending at 93 ± 53

degrees. This stress field is essentially random. In southeastern NY and northern NJ, the mean compressive stress field is oriented at 98 degrees, but is again highly variable with a standard deviation of 30 degrees.

Given these results, we can go on to describe the crustal stress field in the following way: West of the Appalachians, in the Precambrian Grenville Province, the compressive stress field is highly uniform, horizontal, and oriented in an ENE-WSW direction. East of and including the Appalachians, the compressive stress field is non-uniform, although an underlying E-W regional trend may exist in this area. Thus, our conclusion about the stress field west of the Appalachians is the same as those of previous investigators (Sbar and Sykes, 1977; Zoback and Zoback, 1980; Yang and Aggarwal, 1981). However, in the Appalachian Province, our conclusions disagree with those of the aforementioned authors.

The next question we ask is, what are the sources of this stress field? If the stress field is regionally uniform over a broad area, as appears to be the case west of the Appalachians (and extending to the central US), then the forces which give rise to these long wavelength stresses are likely to be plate tectonic in origin (Richardson et al., 1979). These forces originate at the mid-ocean ridges, the subduction zones, at the base of the lithosphere (drag forces), at the transform faults, and also from the cooling of the lithosphere and the movement of elastic plates over the elliptical earth. Richardson et al.

(1979) modeled worldwide intraplate stresses in terms of the above forces and used the observed intraplate stress field to estimate the relative contribution of each force. For the stress field in the central US, the best fit was obtained from equal contributions of the ridge force (from the Mid-Atlantic Ridge), the trench force (from the Cocos - North American plate boundary), and partially from a drag force at the base of the continental lithosphere.

If the stress field east of the Appalachians is random or highly non-uniform, then there are a number of possible reasons for this situation. First, the Appalachians may be modifying any regional stress field which does exist in the area. This is possible if the Appalachians consist of numerous small crustal blocks of varying physical properties. These blocks may rub against one another as they respond to any regional stress field. Strain energy is then built up along the block boundaries and is eventually released as earthquake activity. Block tectonics has been successfully applied to the California and Nevada region by Hill (1982) and has been used in the interpretation of regional travel time anomalies in the eastern US by Alexander (1981). Additional support for the block model comes from recent interpretations of spatially filtered gravity data (Simpson and Godson, 1981; Simpson et al., 1981). A second possibility is that gravity induced stresses from topographic features may be significantly modifying the local stress field. McTigue and Mei (1981) showed that regional horizontal compressive stresses can

be significantly reduced, or even changed to extension, in the neighborhood of a topographic high. This topographic effect is greatest at shallow depths. A final possibility is that the earthquake activity represents the release of paleostresses which accumulated in the area during the closing of the Proto-Atlantic and subsequent opening of the present Atlantic.

Given the tectonic histories of both areas, there is little reason to believe that the stress field in the Appalachian Province should be uniform like that of the Grenville. The area west of the Appalachians is part of the continental craton, consisting of old, stable lithosphere which has not seen significant tectonic activity during the last 600 million years. In contrast, the Appalachian Province consists of accreted material from alternate episodes of compressional and extensional tectonics over the last 400 million years. This complicated geologic history has resulted in a heterogeneous crust and upper mantle (Taylor and Toksöz, 1979). Consequently, even the application of a uniform compressive stress field at the boundary of the region would still result in a non-uniform stress distribution within the area.

As a related problem, we may ask how this stress field influences the pattern of faulting in both areas. This can be investigated by performing a similar statistical analysis on the strikes of the fault planes for events in Table 3.3. Each fault plane solution presented in this chapter yields two possible fault planes, and without auxiliary information it is impossible

to determine on which fault plane the motion has occurred. In Figure 3.10 we have plotted the frequency distribution of fault plane strike versus azimuth for both fault planes of each mechanism, again separated by region. Since we are plotting the strike of both fault planes, the mean and standard deviation are meaningless and are thus not given in the figure. West of the Appalachians, there is a significant portion of fault planes which strike NNW, and east of and including the Appalachians the predominant trend is NNE, with a larger variation. The uniformity of fault plane strikes in the Grenville Province is a reflection of the vast majority of pure thrust faulting events, whereas in the Appalachian Province many events have a strike-slip component of faulting.

If we go on to map the fault planes geographically in Figure 3.11, plotting the fault plane closest to the mean as a solid line, we find that the pattern of faulting closely resembles the pattern of faulting seen in the surface geology. That is, in the Grenville Province, the majority of the earthquakes occur on NW trending faults. Amazingly, the strikes of the fault planes in the Appalachian Province are much more uniform than the stress distribution. Here, the fault planes trend northeasterly, parallel to the structural trend of the area. If this observation is to have any significance, we must make the following assumption: in an area where both thrust faulting and strike-slip faulting are present, the plane on which the motion occurs will be that closest to the mean strike of all the fault

planes. There are some seismological data to support this assumption. Herrmann and Canas (1978) studied the focal mechanisms of earthquakes in the New Madrid seismic zone and found that, although all three fault mechanisms are present, each solution shares the common feature of a NE-SW trending fault plane parallel to the trend of the seismicity and the structural geology. Similarly, in the La Malbaie, PQ area, we saw that the focal mechanisms change drastically from event to event, yet each solution shares the common feature of a fault plane striking parallel to Logan's Line (the Appalachian-Grenville surface contact)(Leblanc and Buchbinder, 1977).

Finally, what are the implications of this stress distribution for the earthquake hazard in the NEUS-SEC? For the uniform stress field west of the Appalachians, we expect that ancient faults which are preferentially oriented would be reactivated under this stress field. The range of orientations depends not only on the magnitude of the stress field but also the degree of fault healing which has taken place. East of and including the Appalachians, where the stress field is complicated, the predominant earthquake mechanism would be difficult to predict. However, if our observation and assumption concerning the strikes of the fault planes are correct, then we expect that the motion would occur on northerly or northeasterly striking fault planes.

Table 3.1
Epicenter and Source Data for the
Ten Earthquakes Studied in this Chapter

<u>No.</u>	<u>Date</u>	<u>Lat</u>	<u>Long</u>	<u>Depth</u> <u>km</u>	<u>mbLg</u>	<u>Area</u>
1	11Mar76	41.56	-71.21	<5	2.7	Portsmouth, RI
2	10May76	41.54	-71.01	<5	2.7	New Bedford, MA
3	25Dec77	43.19	-71.65	<5	3.2	Hopkinton, NH
4	01Sep78	42.48	-71.46	3	1.8	Acton, MA
5	18Apr79	43.98	-69.80	3	4.0	Bath, ME
6	23Apr79	43.04	-71.24	2	3.1	Candia, NH
7	06Jun80	43.60	-75.10	2	3.5	Booneville, NY
8	23Nov80	42.63	-71.36	1.5	2.9	Chelmsford, MA
9	21Oct81	41.14	-72.57	<5	3.4	L.I. Sound, NY
10	19Jan82	43.51	-71.62	<5	4.6	Gaza, NH

Table 3.2

First Motion Data for the Ten Events Studied
+1.=compression, -1.=dilatation
(see Appendix C for station coordinates)

1) 11Mar76 Portsmouth, RI

flr -1. apt -1. uct -1. hdm -1. tmt -1. bct +1. bpt -1.
 wfm -1. hrv +1.

2) 10May76 New Bedford, MA

flr +1. laf -1. apt -1. uct -1. hdm -1. bpt +1. ect +1.
 bct +1. hrv -1.

3) 25Dec77 Hopkinton, NH

hnh -1. qua -1. wes +1. uct +1. ect +1. bct +1. trm -1.
 emm +1. mim +1. dnh -1. wfm +1. csnh+1. wnh -1. mbnh+1.
 lanh+1. wbnh+1.

4) 01Sep78 Acton, MA.

hrv +1. wfm -1. glo -1. pnh -1. wnh -1. dnh -1. wes +1.
 uct +1.

5) 18Apr79 02:34 Bath, ME

trm -1. hkm +1. wnh -1. mim +1. emm -1. wfm +1. ivt +1.
 qua +1. flr +1. hnme+1. d6a +1. d3a +1. agm +1. cbm +1.
 dnh -1. d4a +1.

6) 23Apr79 Candia, NH

dnh -1. wnh +1. pnh -1. glo -1. wfm -1. hrv -1. qua -1.
 ect +1. uct +1.

7) 06Jun80 Booneville, NY

wnh -1. onh +1. dnh -1. pnh +1. hrv +1. bing+1. crog+1.
 ptn +1. marl+1. pny +1. wnd +1. pqn +1. flet-1. msny+1.
 alx +1. medy+1. cly -1. ctr -1.

8) 23Nov80 Chelmsford-Lowell, MA

wnh -1. onh -1. dnh -1. dux +1. glo -1. wfm -1. hrv -1.
 wes +1. bvt +1. hnh +1. ect +1. qua -1. ivt -1. bnh -1.

9) 21Oct81 Long Island Sound, NY

dux +1.	dnh +1.	glo +1.	cod +1.	onh +1.	wnh +1.	lvnj+1.
pal -1.	wpy-1.	wpr -1.	clin-1.	pqn +1.	aph +1.	crog+1.
mash-1.	ldny-1.	osny-1.	rlsp-1.	clar-1.	have-1.	putn-1.
anns-1.	garn-1.	gsc -1.	denj-1.	hdm +1.		

10) 19Jan82 Gaza, NH

bpm -1.	bgr +1.	com -1.	rpi -1.	hkm -1.	bnh +1.	dvt +1.
hnh +1.	bvt -1.	ivt -1.	lnx -1.	wes +1.	mcb -1.	uct -1.
qua +1.	bct -1.	ect -1.	hdm -1.	emm +1.	onh -1.	wnh -1.
wfm +1.	pnh -1.	glo +1.	wgma+1.	sch -1.	mnt +1.	unb +1.

Table 3.3

*Fault Plane Solutions for NEUS-SEC Earthquakes
(Note: "C" in Column 2 Indicates Composite FPS)*

<u>MoDyYr</u>	<u>HrMn</u>	<u>Lat</u>	<u>Long</u>	<u>Dp</u>	<u>Mag</u>	<u>P-Axis</u>		<u>T-Axis</u>		<u>Area</u>	<u>Ref.</u>
						<u>Tr</u>	<u>Pl</u>	<u>Tr</u>	<u>Pl</u>		
010166	1323	42.8	-78.2	2	4.6	62	1	331	28	Attica, NY	1
061367	1908	42.9	-78.2	3	4.4	74	11	336	53	Attica, NY	1
	69	C 41.1	-74.6	2	2.5	235	65	130	10	Hopatcong, NJ	2
	71	C 43.81	-74.45	3	3.2	251	18	70	73	Blue Mt Lake, NY	3
061573	0109	45.32	-70.91	6	4.8	47	32	187	51	ME-QUE Border	4
060974	0301	47.43	-70.36	19	- .3	256	7	351	37	La Malbaie, PQ	5
062074	1336	47.41	-70.18	17	1.7	219	58	353	24	La Malbaie, PQ	5
062374	0906	47.51	-70.22	15	0.5	317	1	217	83	La Malbaie, PQ	5
063074	1155	47.72	-69.84	15	2.0	94	5	310	83	La Malbaie, PQ	5
070274	0230	47.56	-70.23	4	0.3	100	3	191	25	La Malbaie, PQ	5
071374	1929	47.49	-69.97	13	0.6	110	17	246	67	La Malbaie, PQ	5
060774	1945	41.63	-73.94	1	3.3	225	10	45	70	Wap. Falls, NY	6
122174	1451	45.04	-74.03	3	2.9	249	6	140	83	Valleyfield, PQ	7
010475	2040	44.89	-74.55	0	2.8	259	16	56	72	Massena, NY	7
060975	1839	44.89	-73.57	13	4.2	253	8	75	84	Altona, NY	7
071275	1237	46.45	-76.21	17	4.2	210	15	5	50	Maniwaki, PQ	8
171975	2059	41.43	-73.79	3	2.3	135	30	333	58	Mahopoc, NY	7
082275	1749	41.14	-73.95	3	2.3	276	18	96	72	Lake de For, NY	7
110375	2054	43.91	-74.64	4	3.9	250	7	65	85	Racquette, NY	7
031176	2107	41.56	-71.21	2	3.2	220	1	40	89	Portsmouth, RI	9
031176	2107	40.95	-74.35	1	2.6	118	38	303	52	Pomp Lake, NY	7
051076	0134	41.54	-71.01	0	2.7	55	15	175	45	New Bedford, MA	9
041376	1539	40.83	-74.05	3	3.0	260	32	133	45	Ridgefield, NJ	7
042476	1022	41.46	-72.49	0	2.2	205	5	30	65	E. Haddam, CT	10
042876	2132	44.58	-74.63	1	2.8	250	15	61	82	Potsdam, NY	7
082076	2208	41.13	-73.76	5	2.5	285	30	158	47	Mt. Pleasant, NY	7
092276	0904	41.29	-73.95	8	1.8	120	15	311	71	Indian Pt, NY	7
112276	0443	40.99	-73.86	5	1.9	294	25	37	64	Yonkers, NY	7
121776	1030	41.47	-72.07	0	2.2	90	45	295	40	Norwich, CT	10
031077	1622	41.18	-74.15	6	2.2	116	23	322	59	Sufferin, NY	7
09 77		C 41.31	-73.95	0	2.5	220	15	10	65	Annsville, NY	11
092877	1721	44.39	-73.89	3	3.1	64	36	180	34	Wilmington, NY	7
120477	2350	40.80	-74.77	1	2.3	311	7	80	77	Schooley Mt, NJ	7
122077	1744	41.78	-70.66	0	3.1	120	5	300	85	Wareham, MA	10
122577	1535	43.19	-71.65	0	3.2	285	15	180	35	Hopkinton, NH	9
010478	1928	44.04	-70.51	0	3.2	340	20	150	70	Otisfield, ME	10
021878	1448	46.35	-74.12	7	4.1	255	5	75	85	St. Donat, PQ	12
062178	1831	43.66	-71.38	0	1.8	100	5	10	25	Lake Winn, NH	10
073078	1054	45.64	-74.37	3	3.8	35	8	269	78	Lachutte, PQ	7
082178	0847	44.52	-74.51	1	1.9	53	28	279	62	Bay Pond, NY	7
090178	0333	42.48	-71.46	3	1.8	20	30	65	45	Acton, MA	8
102978	2359	43.94	-70.40	0	2.5	340	5	160	85	Crescent Lake, ME	10
041879	0234	43.95	-69.75	4	4.0	90	5	270	85	Bath, ME	9
042379	0005	43.04	-71.24	1	3.1	90	5	270	85	Candia, NH	9
080979	2249	47.67	-69.90	10	5.0	105	15	355	45	La Malbaie, PQ	13

01	80	C	41.31	-73.95	0	2.9	260	15	55	75	Annsville, NY	11
060680	1315		43.60	-75.10	2	3.5	85	5	265	85	Booneville, NY	9
112380	0039		42.63	-71.36	2	2.9	45	30	165	25	Lowell, MA	9
070481	2316		45.11	-74.61	16	3.3	45	20	150	45	Cornwall, ONT	14
070581	2147		45.11	-74.61	16	3.3	20	13	140	40	Cornwall, ONT	14
102181	1649		41.14	-72.57	5	3.4	135	15	20	70	Long Island, NY	15
010982	1253		46.98	-66.66	10	5.7	93	0	273	90	New Brunswick	16
011982	0014		43.52	-71.61	5	4.7	240	20	150	10	Gaza, NH	15

References: 1, Herrmann (1978); 2, Sbar et al. (1970); 3, Sbar et al. (1972); 4, Herrmann (1979); 5, Leblanc and Buchbinder (1977); 6, Pomeroy et al. (1975); 7, Yang and Aggarwal (1981); 8, Horner et al. (1978); 9, Pulli and Toksöz (1981) and this work; 10, Graham and Chiburis (1980); 11, Horner et al. (1978); 12, Hasegawa and Wetmiller (1981); 13, Horner et al. (1979) 14, Schlessinger-Miller et al. (1981); 15, Pulli and Godkin (1982) and this work; 16, Nabelek et al. (1982).

Table 3.4
Geologic (non-seismic) Stress Measurements

<u>Hydrofracturing Data</u>						
<u>Area</u>	<u>Lat</u>	<u>Long</u>	<u>Depth m</u>	<u>Trend of σ_1</u>	<u>Ref.</u>	
Oshawa, PQ	43.88	-78.85	230-300	25	1	
Alma Township, NY	42.08	-78.00	510	77	2	
Allegany Cty, NY	42.08	-78.00	-	60	3	
Bradford, PA	41.97	-78.65	-	70	3	
<u>Strain Relief Data</u>						
W. Chelmsford, MA	42.60	-71.41	19	56	4	
Tewksbury, MA	42.61	-71.23	12	358	4	
Barre, VT	44.21	-72.49	46	14	4	
Proctor, VT	43.65	-73.06	0.3	356	4	
Oswego, NY	43.45	-76.52	810	67	5	
<u>Fault Slip and Core Offset Data</u>						
Colchester, CT	41.5	-72.25	surface	122	6	
Attleboro, MA	41.94	-71.32	surface	157	7,8	
Pumpkin Hollow, NY	42.83	-73.66	surface	130	8	
Port Matilda, PA	40.78	-78.07	surface	140	9	
Millerstown, PA	40.55	-77.58	surface	100	9	
<u>Pop-up Data</u>						
Alexandria Bay, NY	45.53	-74.37	surface	60	10	
Ogdensburg, NY	44.81	-75.45	surface	70	11	
Cheektowaga, NY	42.94	-78.77	surface	90	11	
Niagara Falls, NY	43.08	-79.12	surface	70	11	

References: 1, Haimson and Lee (1979); 2, Haimson (1974); 3, Overbey and Rough (1968); 4, Hooker and Johnson (1969); 5, Zoback and Zoback (1980); 6, Block et al. (1979); 7, Woodworth (1907); 8, Oliver et al. (1970); 9, Schäfer (1979); 10, Cushing et al. (1910); 11, Sbar and Sykes (1973, 1977).

Figure Captions

Figure 3.1 Present network configuration in the NEUS. Solid circles indicate stations, open circles are the locations of the earthquakes studied in this paper. Numbers refer to events in Table 3.1. Since the network has been assembled during the past five years, the azimuthal coverage for the earlier events is exaggerated by this figure.

Figure 3.2 Northeastern U.S. crustal models used to project the seismic rays back to the lower focal sphere. See Figure 3.3 for areas of applicability. References are: 1) Chiburis et al. (1980), 2) Taylor and Toksöz (1979), 3) Weston Geophysical Research (personal communication), and 4), 5), 6) Yang and Aggarwal (1981)

Figure 3.3 Areas of applicability of the six crustal models in Figure 3.2. The judgement of applicability was made by this author.

Figure 3.4 a,b Fault plane solutions for the ten earthquakes studied in this chapter. All are lower hemisphere projections. Solid circles are compressions, open circles are dilatations, and P, T, and B are the valid areas of pressure, tension, and null axes, respectively, as determined by the algorithm of Guinn and Long (1977).

Figure 3.5 Map of fault plane solutions in the NEUS, from Figure 3.4. The shaded areas are compressions. Lower hemisphere projections used throughout.

Figure 3.6 Crustal stress field in the NEUS-SEC. a) Horizontal projections of the P-axes for the fault plane solutions in Table 3.3 as well as the trend of the σ_1 -axes for the geologic stress measurements in Table 3.4. b) Horizontal projections of the P-axes for the fault plane solutions in Table 3.3 for events of magnitude greater than or equal to 3.0 (mb). c) Horizontal projections of the T-axes for the fault plane solutions in Table 3.3 as well as the trend of the σ_1 -axes for the geologic stress measurements in Table 3.4. d) Horizontal projections of the T-axes for the fault plane solutions in Table 3.3 for events of magnitude greater than or equal to 3.0 (mb). In Figures 3.6 a,b,c, and d the approximate trend of the Appalachian - Precambrian contact is indicated by the dotted line.

Figure 3.7 Rose diagrams showing the frequency distribution of compressive stress directions in the study area. The distribution has been blocked into 10 degree increments. The top figure is for entire dataset. The lower figure is for abridged dataset. The mean and standard deviations are also indicated next to each plot.

Figure 3.8 Rose diagrams showing the distribution of P- and σ_1 -axes for the areas west of the Appalachians and east of and including the Appalachians.

Figure 3.9 Rose diagrams showing the distribution of P- and σ_1 -axes in various sub-regions of the study area.

Figure 3.10 Rose diagrams showing the distribution of fault plane strikes for the areas west of the Appalachians (above) and east of and including the Appalachians (below).

Figure 3.11 Map of fault plane strikes in the study area from the fault plane solutions in Table 3.3 .

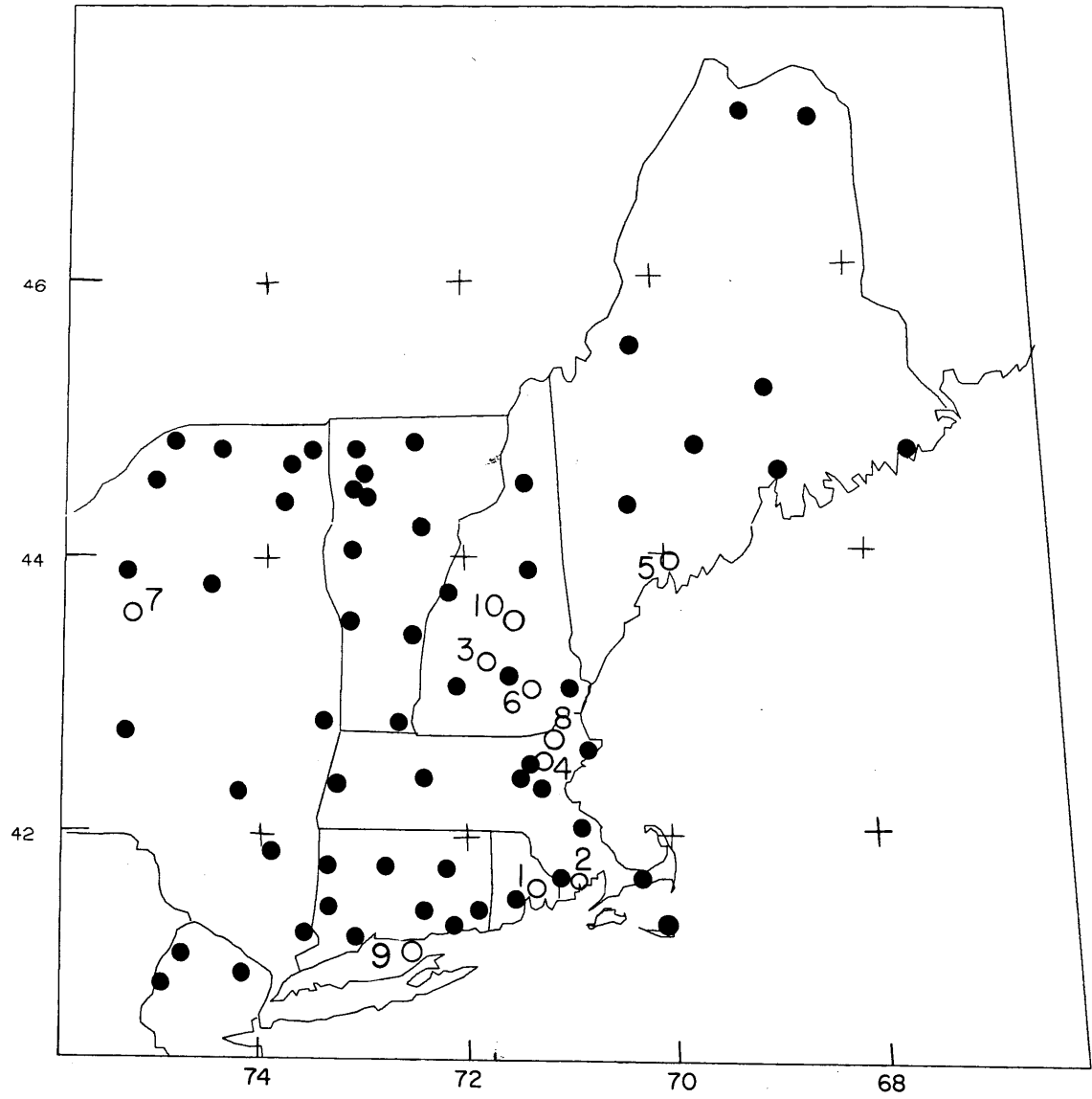


FIGURE 3.1

NEUS CRUSTAL MODELS

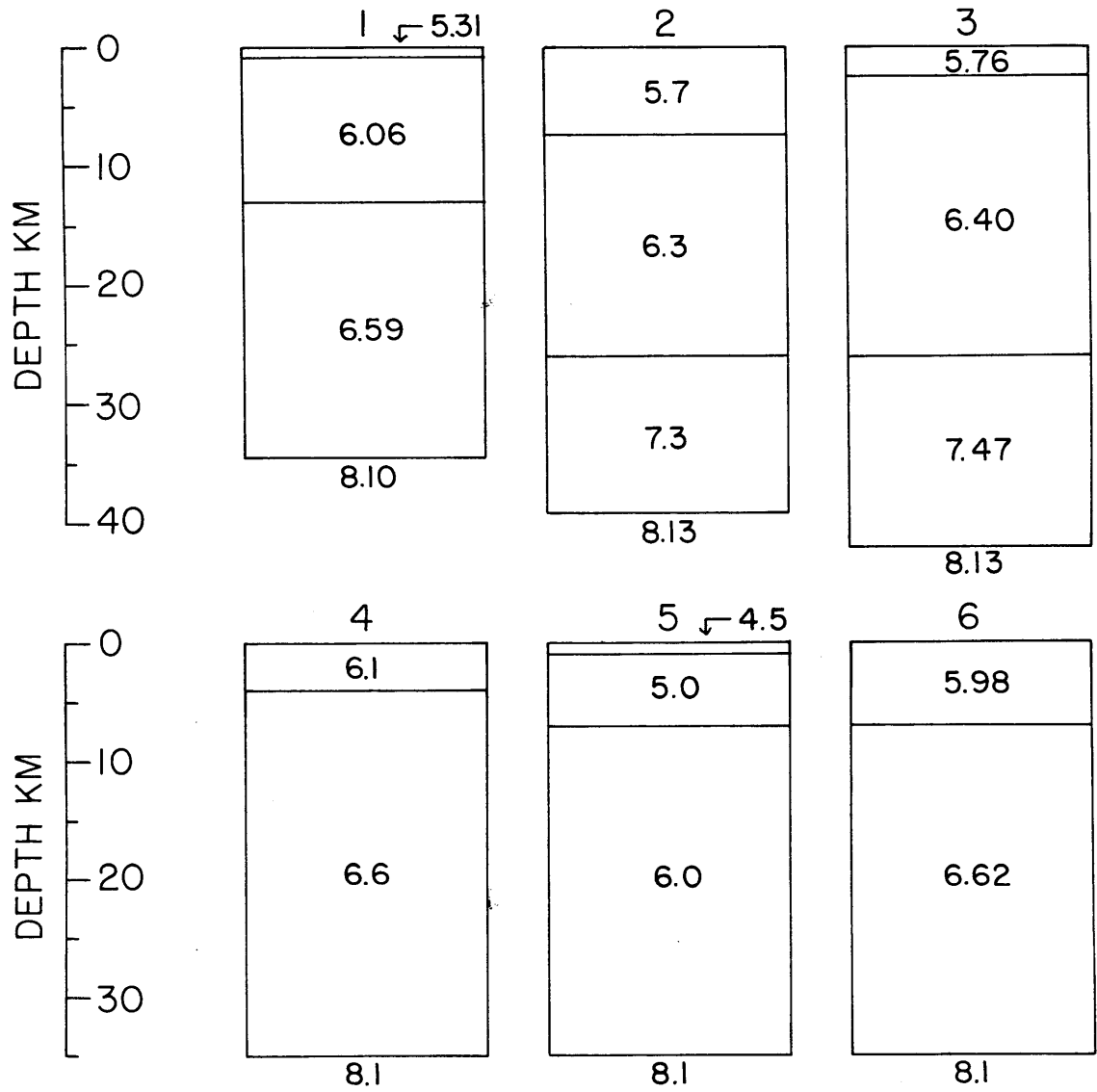


FIGURE 3.2

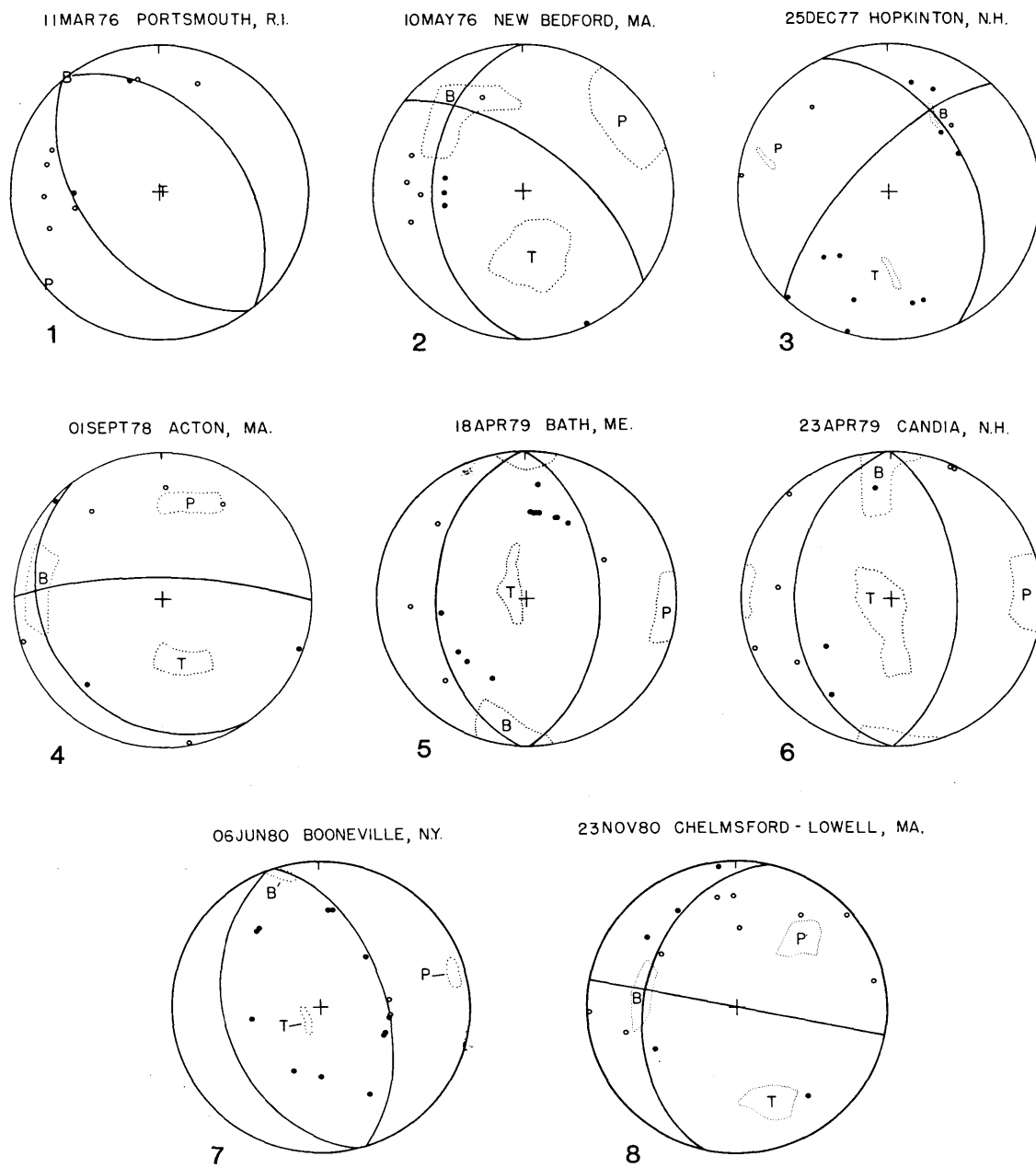
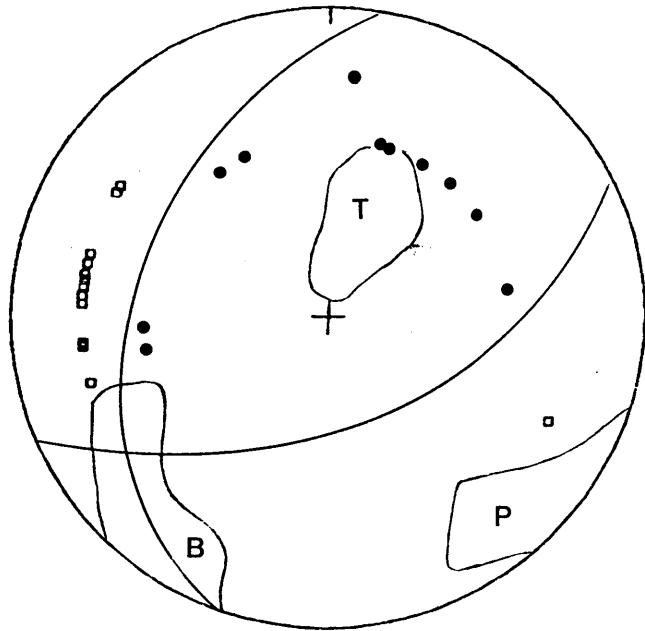


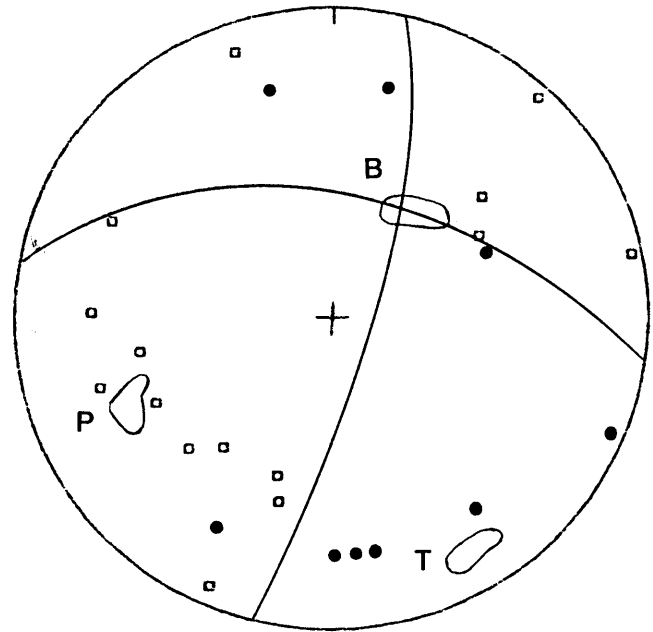
FIGURE 3.4a

21OCT81 LONG ISLAND SOUND, NY



9

19JAN82 GAZA, NH



10

FIGURE 3.4b

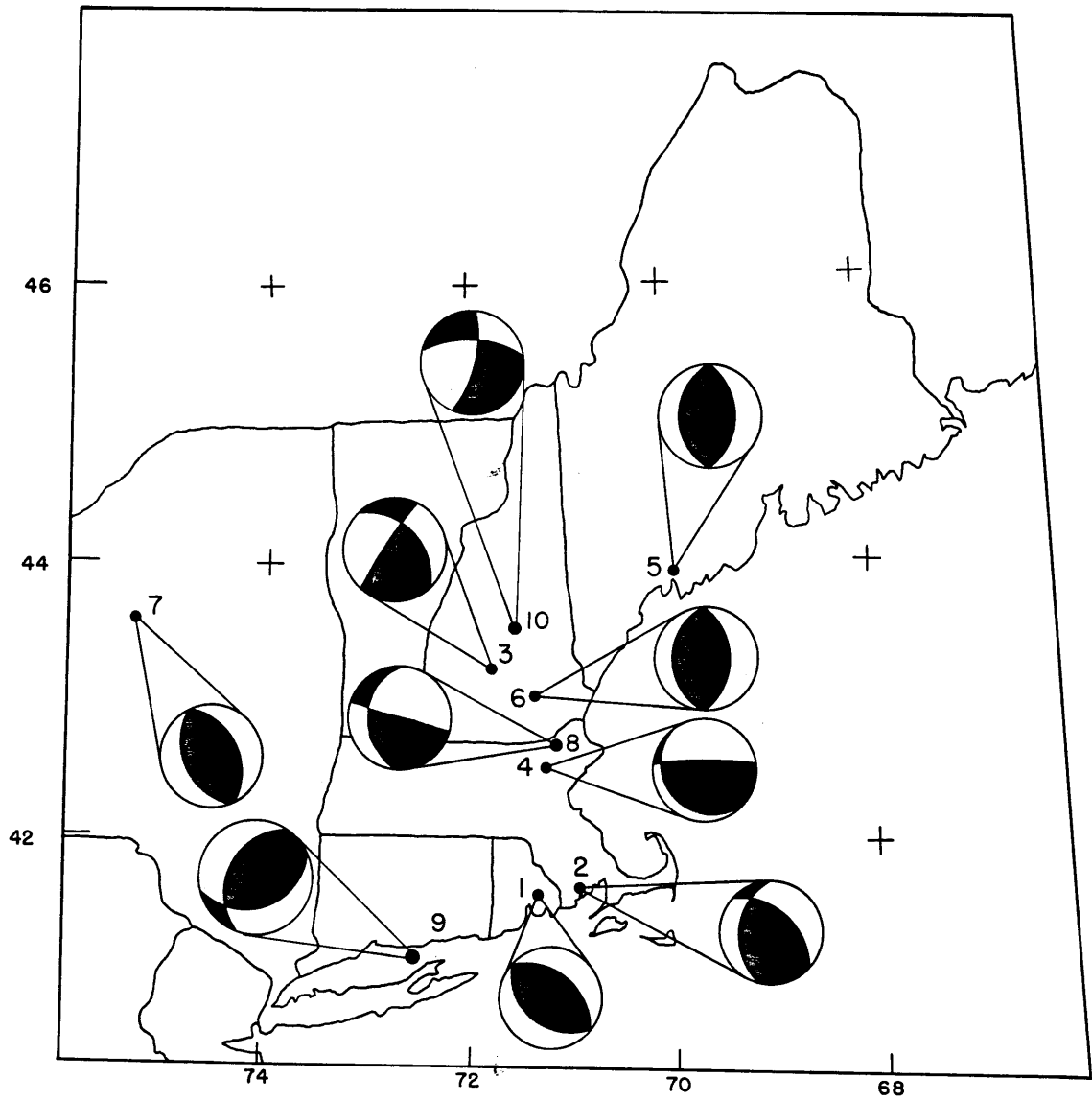


FIGURE 3.5

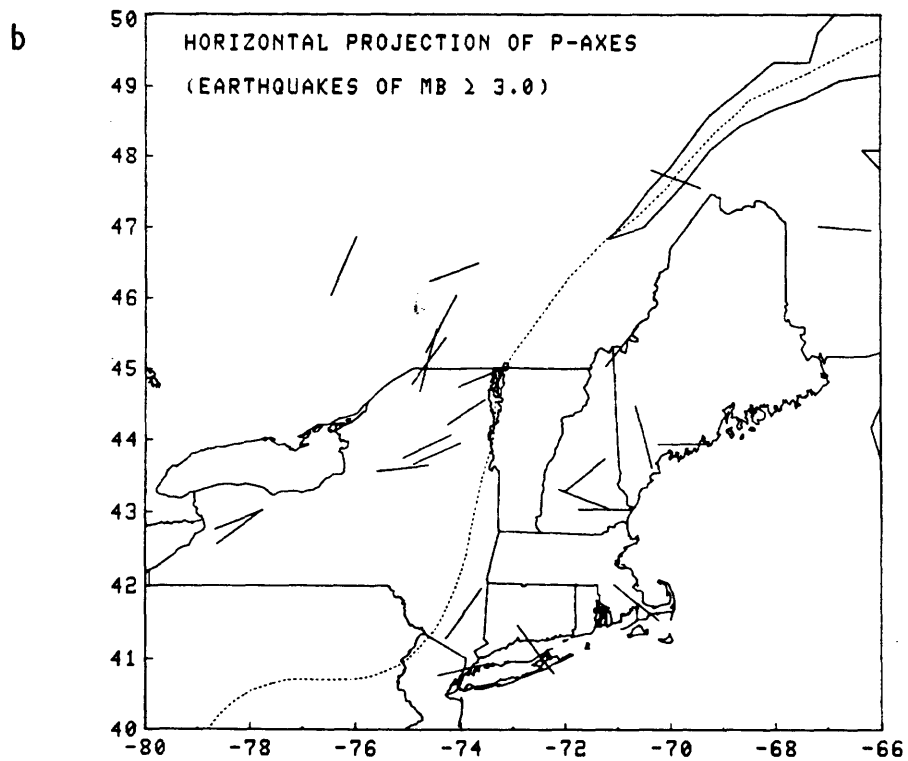
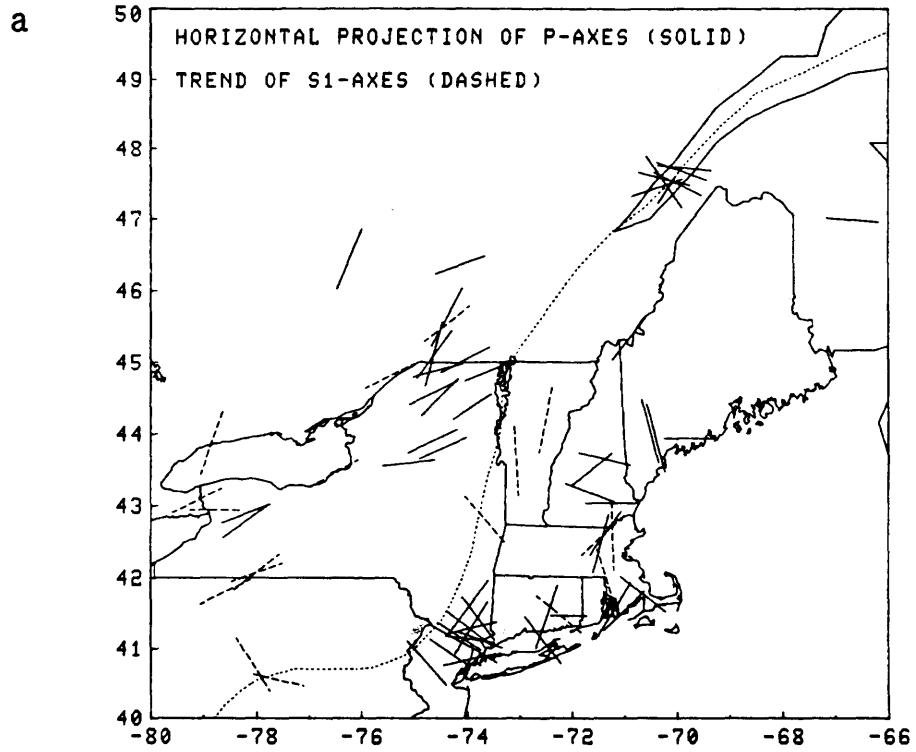


FIGURE 3.6

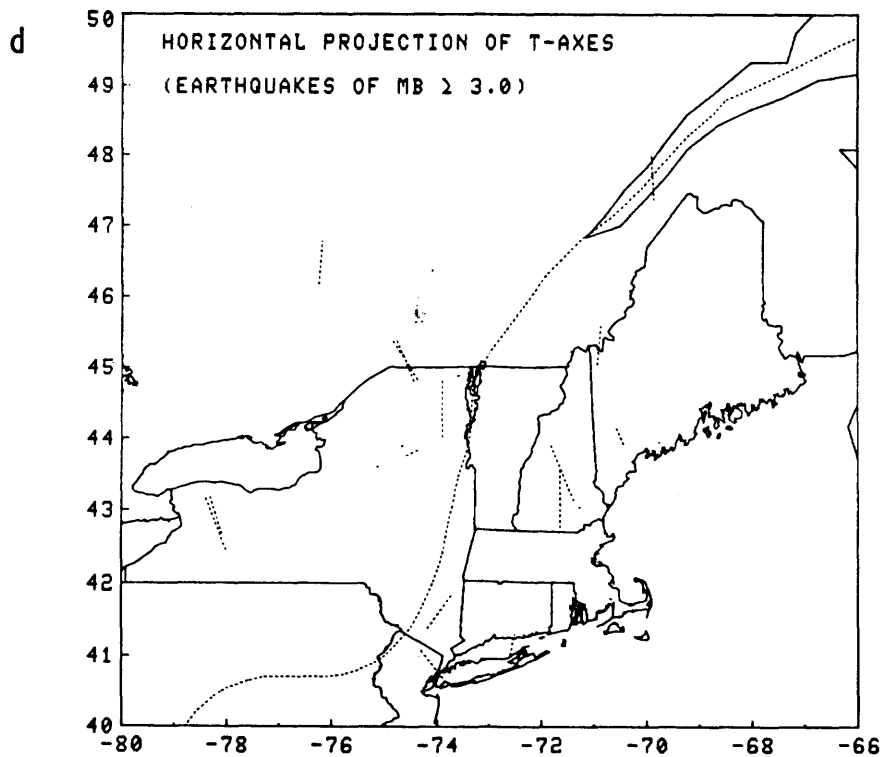
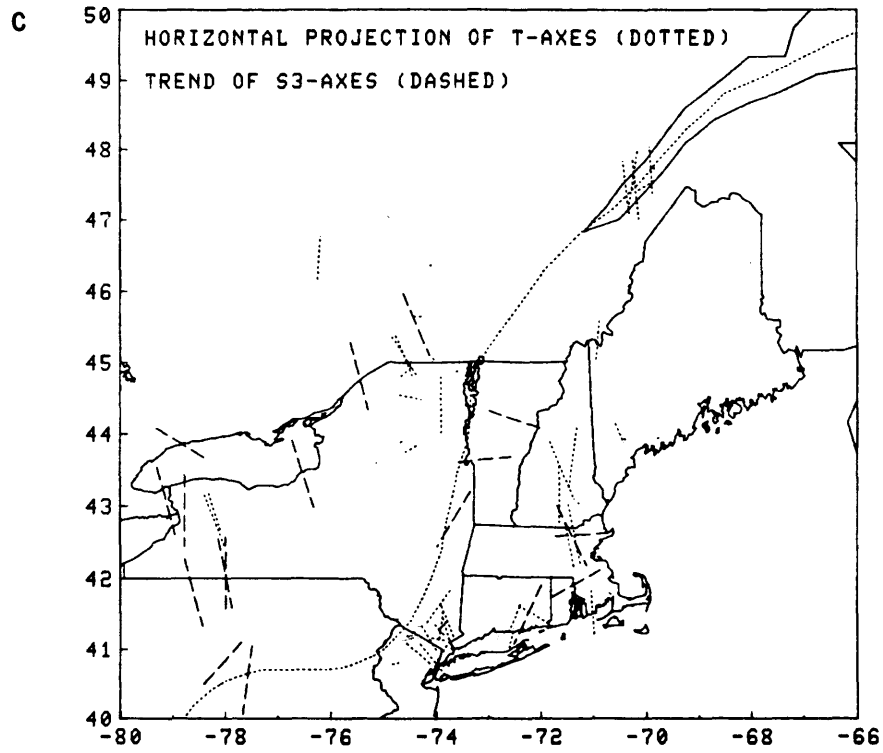


FIGURE 3.6

COMPRESSIONAL STRESS FIELD
(ENTIRE STUDY AREA)

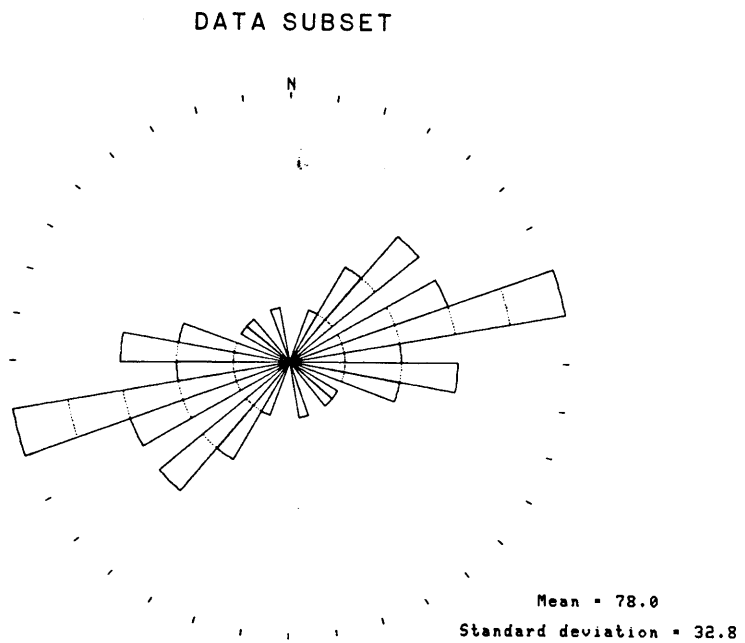
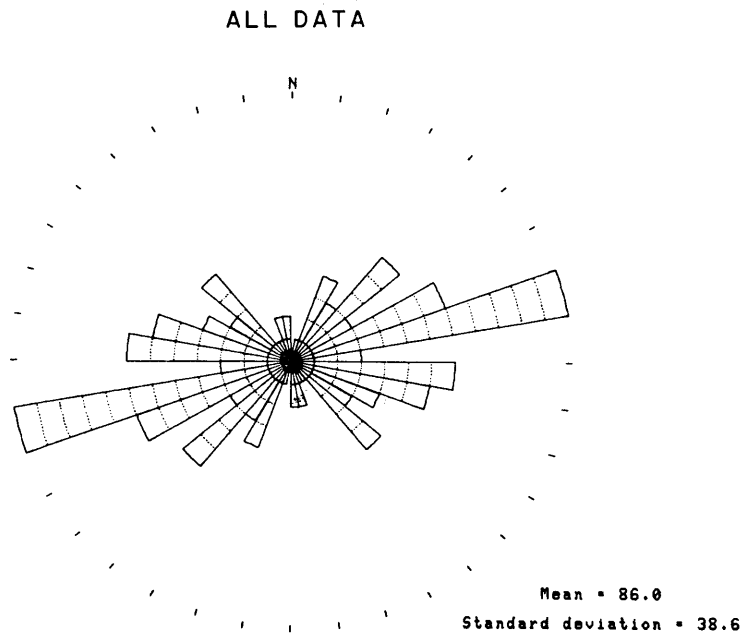


FIGURE 3.7

COMPRESSIVE STRESS FIELD

WEST OF APPALACHIANS

EAST OF AND INCLUDING APPALACHIANS

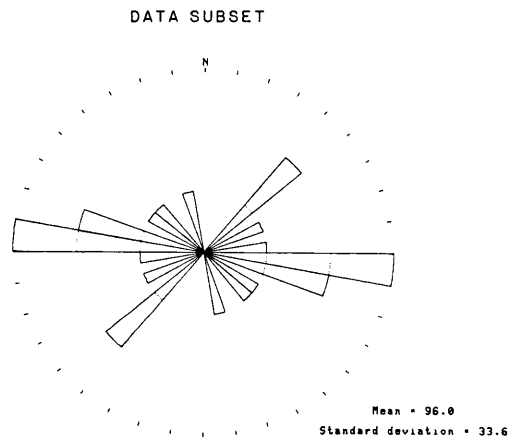
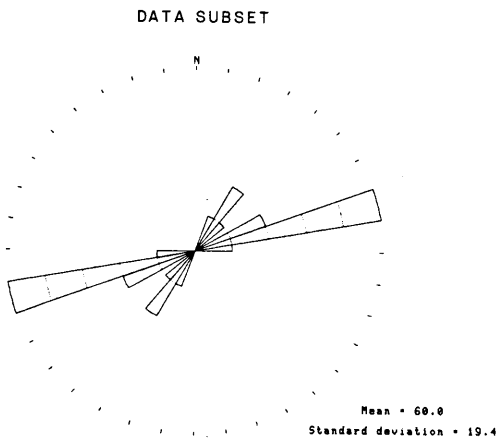
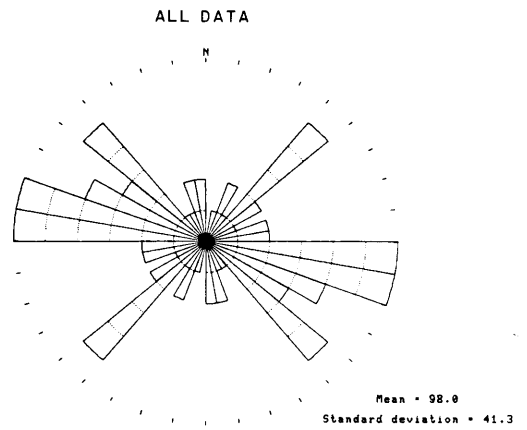
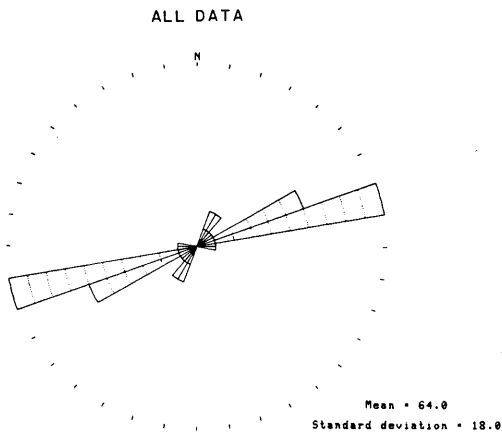


FIGURE 3.8

P- AND S1-AXES

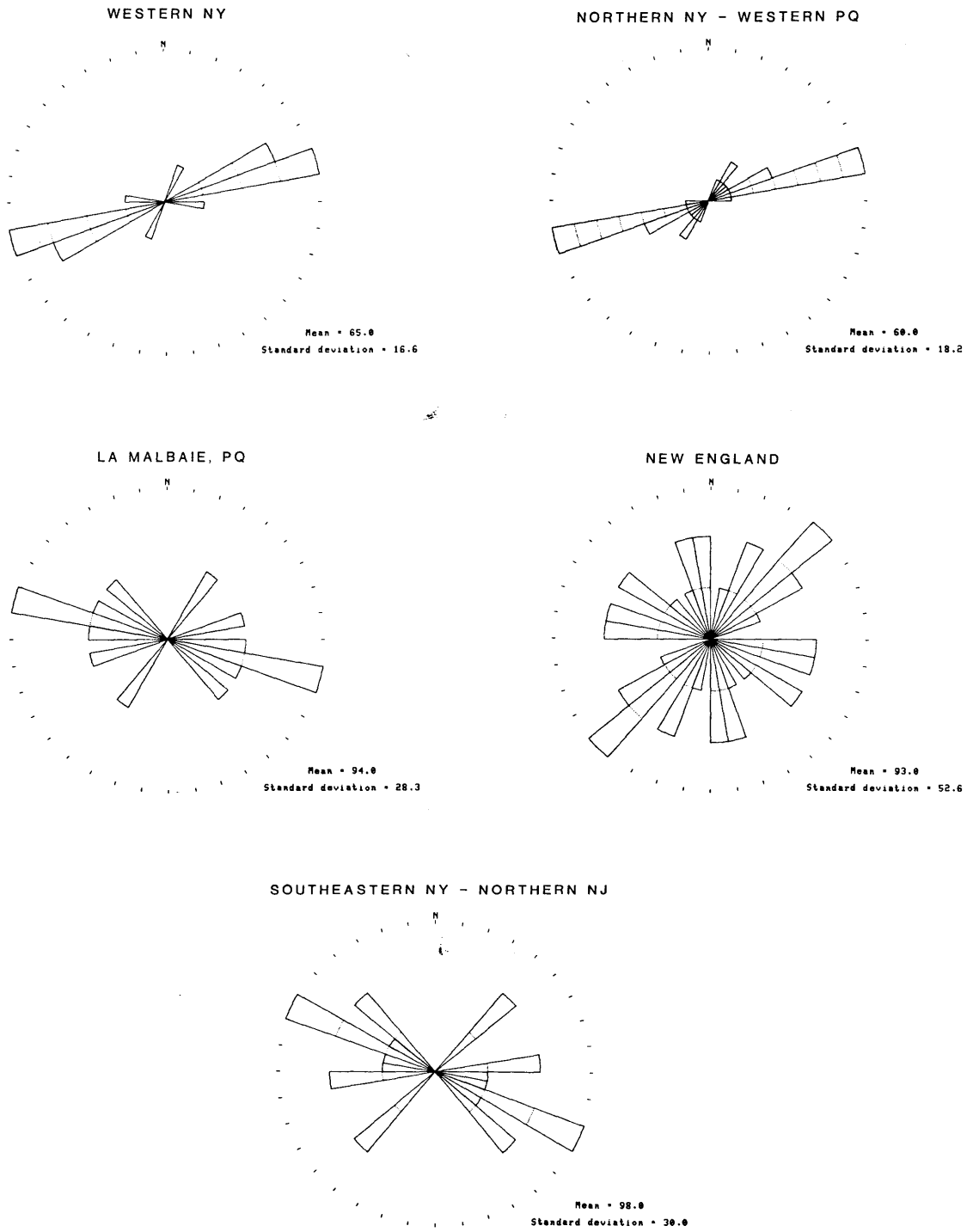
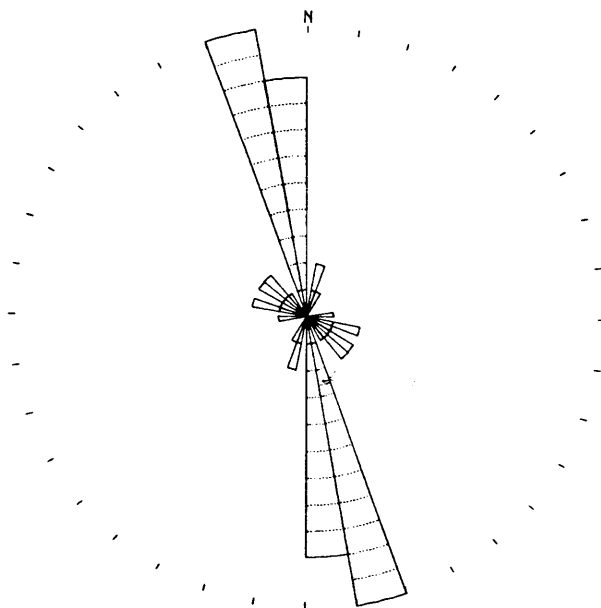


FIGURE 3.9

STRIKE OF FAULT PLANES

WEST OF APPALACHIANS



EAST OF AND INCLUDING APPALACHIANS

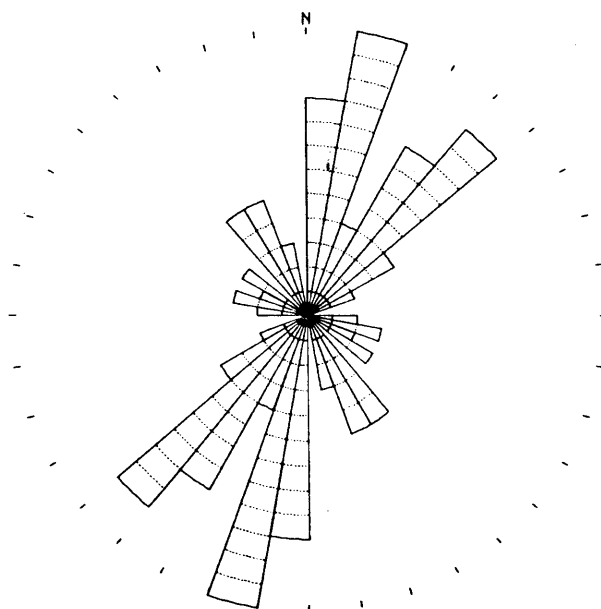


FIGURE 3.10

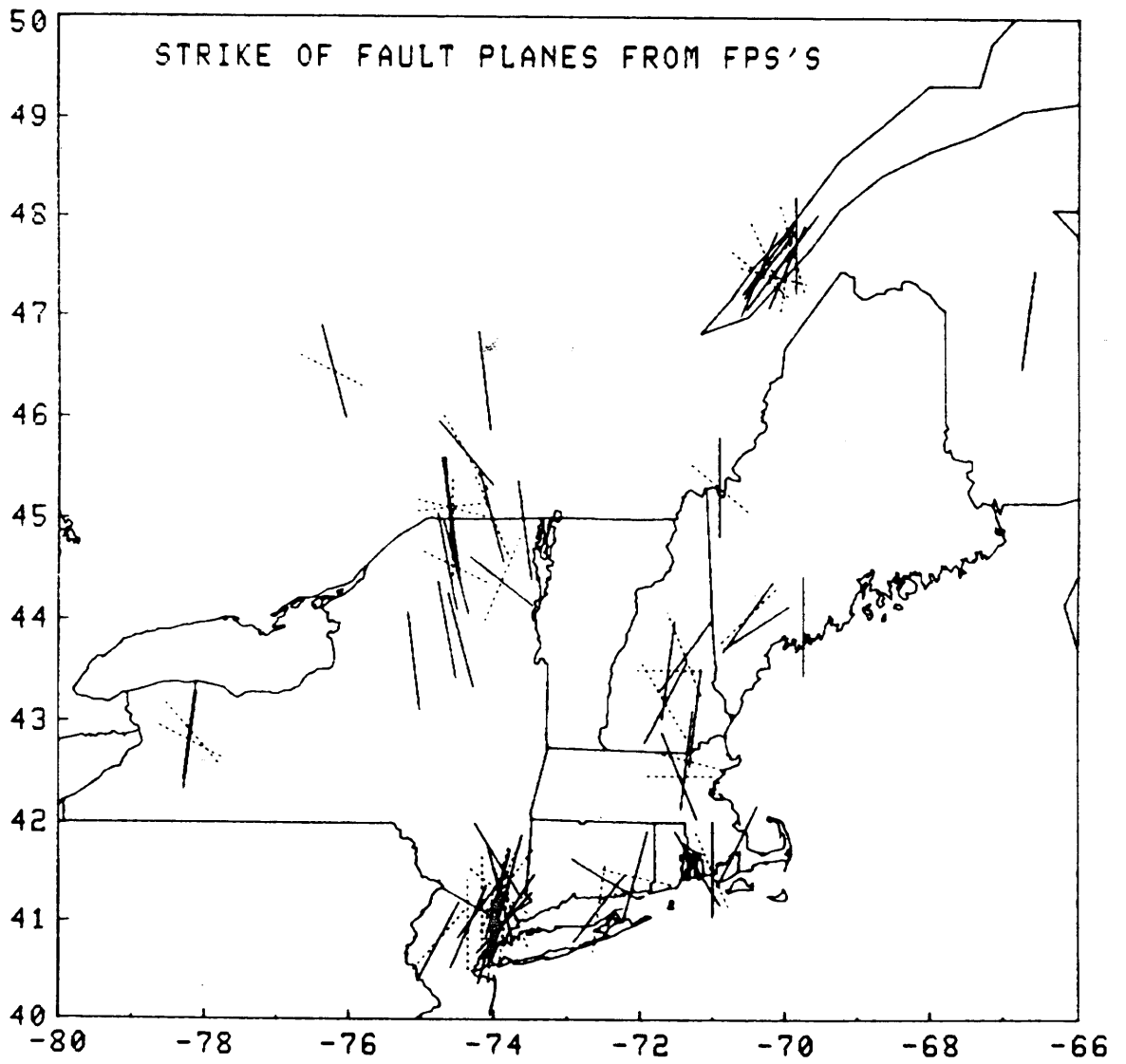


FIGURE 3.11

CHAPTER 4
Q MEASUREMENTS AND STRONG MOTION ATTENUATION MODELS
FOR NEW ENGLAND

4.1 Introduction

The estimation of the earthquake hazard in an area is a twofold process. First, we must understand the nature of the earthquake sources that generate potentially hazardous ground motion. This includes knowledge of the distribution of the seismic source zones, the return times of large events, and the predominant earthquake mechanisms within each zone. Second, we must understand the effects of the transmitting medium (the earth) on the seismic waves. Then, a synthesis of the source and path effects will allow us to calculate the ground motion at a given site. In the previous two chapters of this thesis, we have been concerned with the earthquake sources in the NEUS-SEC. We now turn our attention to the study of the path effect, namely the measurement of seismic wave attenuation.

There are two physical properties that are important in considering the propagation of seismic waves in the transmitting medium. The first is the velocity of wave propagation, which depends on the type of wave and its location within the medium. The second is the seismic wave attenuation, which is a combination of anelastic wave damping and the scattering properties of the medium. The attenuation also varies spatially, and may be frequency dependent. The seismic wave velocity is generally the more straightforward of the two properties to

determine, since the measurement of travel time involves fewer assumptions than the measurement of relative amplitudes. Thus, our knowledge of the distribution of seismic velocities in the earth is more complete than our knowledge of attenuation.

To illustrate the importance of seismic wave attenuation to the estimation of earthquake hazards, consider the example of the variation in attenuation across the United States. It is well known that earthquakes in the eastern US (that is, east of the Rocky Mountains) are felt more widely than earthquakes of comparable magnitude in the west (Nuttli and Zollweg, 1974). For example, the New Madrid, Missouri earthquake of 1811 was felt over five million square kilometers and is believed to have been of magnitude 7.2 (mb) ($M_s \sim 8.0$) (Nuttli, 1973b). In contrast, the San Francisco earthquake of 1906 was felt over one million square kilometers, yet was also of magnitude $M_s \sim 8$. The primary factor which contributes to this difference in felt areas is the significantly lower seismic wave attenuation in the eastern US (Nuttli, 1973a).

Seismic wave attenuation can be measured using a number of different methods, depending on the frequency band of interest. At high frequencies ($0.1 < f < 1.0$ MHz), attenuation can be measured in the laboratory using the pulse transmission technique (Toksöz et al., 1979). At low frequencies ($f < 0.05$ Hz), attenuation can be measured from the propagation of surface waves over a great circle path that includes two stations (e.g., Kovach, 1978; Taylor and Toksöz, 1982a). However, at the

frequencies of interest in short period seismology and structural engineering ($0.75 < f < 25$ Hz), the measurement of attenuation is difficult to accomplish. Much of this difficulty arises from the sensitivity of seismic waves in this frequency band to both earth structure and the presence of small scale heterogeneities in the crust and upper mantle. In addition, most short period seismic stations are presently recorded in analog format at slow speed which makes the high frequency waves difficult to resolve. Thus, both temporal and spectral measurements of the decay of seismic wave amplitudes with distance in the short period band often show great inconsistencies. This inconsistency is reflected in the large scatter of magnitude calculations across seismic arrays (Chang and von Seggern, 1980).

One way to cope with the sensitivity of short period waves to earth structure is to measure seismic wave amplitudes statistically rather than deterministically. Such an approach has been applied to the study of coda waves generated by local earthquakes. Coda waves compose the latter part of a seismogram of a local event and are assumed to consist of backscattered S-waves from many randomly distributed heterogeneities in the earth's lithosphere. Aki (1969) studied the coda waves of local earthquakes and found that the source and path effects could be separated using these waves. Later, Aki and Chouet (1975), Rautian and Khalturin (1978), Herrmann (1980), Aki (1980a), Singh and Herrmann (1983), and Roecker et al. (1982) measured the attenuation of coda waves and S-waves in a number of tectonically

stable and active areas around the globe and correlated the results with the degree of tectonic activity in each area.

In this chapter, the attenuation of coda waves will be measured as a function of frequency using data from local earthquakes recorded digitally by the M.I.T. Seismic Network. We will also examine the regional and depth dependence of Q_c by measuring the coda decay at different lapse times in the tail of the seismogram. The results will be compared with other Q measurements in the northeast, as well as from other tectonically stable and active areas. We will then use the model of Dainty (1981) to separate the scattering and anelastic attenuation components in the observed Q_c values. Next, we turn to the development of a strong ground motion attenuation model for use in earthquake hazards studies in New England. To accomplish this, we will combine the Q_c measurements with studies of intensity attenuation and the strong motion data from the January 19, 1982 Gaza, NH earthquake. This model will then be used to estimate the distribution of ground motions for a number of large hypothetical NEUS-SEC earthquakes.

4.2 Q Measurements Using Coda Waves

In this section, we present the measurement of coda wave attenuation in New England using digital data from the M.I.T. Seismic Network. (A detailed description of the Network and the digital data acquisition system is given in Appendix E of this work.) We begin by describing some properties of coda waves and by examining the single scattering model of coda wave generation

and propagation. Then, the details of the Q measurement procedure will be outlined, and the results presented. These results will be compared with other published measurements of seismic wave attenuation in tectonically active and stable areas. Finally, we will apply the scattering model of Dainty (1981) to separate the contributions of scattering and anelastic attenuation to the Q values.

4.2.1 Some Properties of Coda Waves

Figure 4.1 shows a recording of a local earthquake which occurred east of Gloucester, MA and was recorded on the M.I.T. seismic station GLO. The event has been played out in terms of lapse time measured from the earthquake origin time. The P-, S-, and coda waves have been indicated on this figure. These coda waves exhibit a number of interesting properties which make them ideal for the estimation of both source and medium parameters. These properties have been extensively outlined in a number of recent publications, which we review below.

Aki and Chouet (1975) listed several important observations concerning coda waves.

1. Although the spectral content of the early part of a local earthquake seismogram depends strongly on the epicentral distance and wavepath, the spectra of coda waves at various stations are very uniform (Aki, 1969).

2. For a local earthquake at epicentral distance shorter than about 100 km, the total coda length is nearly independent of distance and can be effectively used as a measure of earthquake

magnitude (Lee et al., 1972; Real and Teng, 1973; Herrmann, 1975; Suteau and Whitcomb, 1979). It has since been demonstrated that the distance dependence in some areas is negligible out to 300 km (Chaplin et al., 1980).

3. The power spectra of coda waves from different earthquakes decay as a function of lapse time, independent of the distance and the nature of the path (Aki, 1969; Aki and Chouet, 1975).

4. This time dependence is also independent of earthquake magnitude, at least for earthquakes of magnitude less than 6 (Aki, 1969; Aki and Chouet, 1975).

5. The coda excitation does depend on the local geology at the receiver. It can be 5 - 8 times larger on sediments than on granite (Aki, 1969).

6. Studies of coda waves by small aperture seismic arrays show that they are not regular plane waves coming from the epicenter (Scheimer and Landers, 1974).

Given these observations, Aki (1969) and Aki and Chouet (1975) considered a number of possible mechanisms for the generation and propagation of coda waves and concluded that the coda consists of backscattered waves generated when the primary S-waves encounter velocity and structural heterogeneities in the crust and upper mantle. Two backscattering models have been used to explain the coda wave amplitudes on a seismogram. The first is the single-scattering model, which assumes that the scattered wavefield is "weak" and does not produce secondary scattering

when it encounters another scatterer. (This is the so-called "Born approximation".) The second model is the diffusion model, which does assume secondary scattering. Some hybrid models include the effects of both single and multiple scattering. Dainty and Toksöz (1981) and other investigators have argued that the diffusion model does not apply to the earth, yet does successfully explain the coda wave amplitudes on the Moon. Thus, we will apply the single-scattering model of coda wave propagation in this study.

Following Aki and Chouet (1975), let the source and the receiver be located at the same point in an infinite medium. This is a valid assumption for coda waves which arrive at the receiver long after the passage of the primary P- and S-waves. Let $\phi(\omega|r)$ be the Fourier transform at the circular frequency ω of the displacement due to a backscattered wavelet from a single scatterer at a distance r , and let N be the number of scatterers per unit volume. The energy carried by all of the backscattered waves arriving at time $(t, t+\Delta t)$ from a distance $(r, r+\Delta r)$ will be equal to Δt times the power spectral density $P(\omega|t)$. Thus

$$P(\omega|t)\Delta t = |\phi(\omega|r)|^2 4N\pi r^2 \Delta r \quad (4.1)$$

If we now incorporate geometrical spreading of body waves and attenuation, and note that $r = vt/2$, where v is the seismic wave velocity and $\Delta r = v\Delta t/2$, we obtain

$$P(\omega|t) = |\phi(\omega|r)|^2 \frac{4}{8r} \frac{1}{\pi N v} t^{-1-2} \exp[-\omega t/Qc(\omega)] \quad (4.2)$$

A simplified form of this equation is

$$P(\omega|t) = S(\omega) t^{-2} \exp[-\omega t/Qc(\omega)] \quad (4.3)$$

where all of the source terms have been lumped into the parameter $S(\omega)$. It is this separation of the source and path terms which makes coda wave measurement a powerful tool in short period seismology. Equation (4.3) can be related to the RMS amplitude of the coda waves on a narrow bandpass filtered seismogram using the relation

$$A(\omega|t) = 2[2P(r,\omega|t)\Delta f]^{1/2} \quad (4.4)$$

from Aki and Chouet (1975). Here, Δf is the bandwidth of the filter with a center frequency at ω . Substituting equation (4.4) into (4.3), we obtain

$$A(\omega|t) = C(\omega) t^{-1} \exp[-\omega t/2Qc(\omega)] \quad (4.5)$$

The term $C(\omega)$ is often called the "coda source factor". Equation (4.5) can be used to estimate the Qc of coda waves as a function of frequency by taking natural logarithms and rearranging terms to obtain

$$\ln[A(\omega|t)t] = C - [\omega/2Q_c(\omega)]t \quad (4.6)$$

Since the term $C(\omega)$ is dependent only on frequency and we are using narrow bandpass filtered seismograms, it has been replaced by the constant "C". Thus, there is a linear relationship between $\ln[A(\omega|t)t]$ and t , the slope of which is $-\omega/2Q_c(\omega)$. Note that in this derivation we have used the term $Q_c(\omega)$ to specify the attenuation of coda waves, rather than $Q(\omega)$ since the attenuation which we are measuring cannot be definitively associated with the Q of P- or S-waves. However, a number of studies (e.g., Aki, 1980b; Herrmann, 1980) have shown that independent measurements of Q_c and the Q_β of S-waves are equivalent, supporting the theory that the coda consists of backscattered S-waves. Also note that $Q_c(\omega)$ is a combination of both anelastic attenuation, Q_i , and scattering, $Q_s = \omega L/v$, where L is the mean free path and v is the velocity. We cannot directly separate the effects of anelastic attenuation and scattering, since both physical processes are of the mathematical form $\exp(-\delta r)$, where r is the propagation distance. However, Dainty (1981) has suggested the following expression

$$1/Q(\omega) = 1/Q_i + v/\omega L \quad (4.7)$$

to explain the frequency dependence of Q in terms of both anelastic attenuation and scattering. Here, Q_i is assumed to be frequency independent. Thus, in Dainty's (1981) model it is the

scattering component, Q_s , which is responsible for the frequency dependence of the apparent Q_c . Later, we will apply this model to our observations of frequency dependent Q_c in New England in order to estimate L and the size of the scatterers in the study area.

As mentioned earlier, the coda wave theory of Aki and Chouet (1975) assumes that the source and receiver are at the same point in the earth. This is a viable approximation for signals which arrive long after the primary waves (i.e. after twice the S-wave lapse time). However, one is sometimes restricted to measurements of coda waves close to the S-wave arrival. For example, in seismically noisy environments, the amplitudes of the coda waves from small events are often below the background noise level after twice the S-wave lapse time. In other circumstances, the digital recordings of local earthquakes may be truncated due to data storage restrictions or problems with the triggering algorithm. In such cases, it is necessary to measure the coda waves early in the wavetrain, and thus the source-receiver distance must be taken into account. Such a separation is included in the single scattering model of Sato (1977) which was applied to the analysis of coda waves in central Asia by Roecker et al. (1982). A brief review of this model is now presented.

Imagine a source and receiver embedded in an infinite medium populated by a random distribution of N scatterers per unit volume and of cross-sectional area σ . The sum of the energy

scattered by the inhomogeneities on the surface of an expanding ellipsoid whose foci are the source and receiver is

$$E(r, \omega | t) = [N\sigma\Omega(\omega)/4\pi r^2] K(a) \quad (4.8)$$

where r is the source-receiver distance, $a = t/t_s$, t_s is the S-wave lapse time, $\Omega(\omega)$ is the total energy radiated by the source within a unit angular frequency band, and

$$K(a) = (1/a) \ln[(a+1)/(a-1)] \quad (4.9)$$

In order to relate equation (4.8) to the coda wave amplitude data, we use the following relation from Aki and Chouet (1975) for band-pass filtered seismograms

$$E(r, \omega | t) = \rho \omega^2 P(r, \omega | t) \quad (4.10)$$

as well as equation (4.4), where $P(r, \omega | t)$ is the power spectral density, and ρ is the density. Substituting equations (4.10) and (4.4) into equation (4.8) and rearranging terms, we obtain

$$A(r, \omega | t) = \frac{1}{\omega} \left| \frac{\Omega(\omega) \Delta f}{2\pi \rho L} \right|^{1/2} \frac{|K(a)|^{1/2}}{r} \exp[-\omega t / 2Qc(\omega)] \quad (4.11)$$

where $L = 1/N\sigma$. A simplified form of this equation, separating source and path terms, is

$$A(r, \omega | t) = C(\omega)k(r, a)\exp[-\omega t/2Q_c(\omega)] \quad (4.12)$$

As before, we can take natural logarithms of equation (4.12) and rearranging terms, we obtain

$$\ln[A(r, \omega | t)/k(r, a)] = C - [\omega/2Q_c(\omega)]t \quad (4.13)$$

The term $k(r, a)$ has the effect of increasing the coda wave amplitudes at lapse times near that of the S-wave. Again, we find that for bandpass filtered seismograms, there is a linear relationship between $\ln[A(r, \omega | t)/k(r, a)]$ and t , the slope of which is $-\omega/2Q_c(\omega)$.

This formulation will now be used for the measurement of coda wave attenuation versus frequency in New England. In the next section, the details of the analysis procedure will be outlined.

4.2.2 Data and Analysis

Figure 4.2 shows a map of the M.I.T. Seismic Network as well as the locations of the twelve earthquakes used as coda wave sources in this study. Epicentral data for these twelve earthquakes are given in Table 4.1. These earthquakes are distributed across the study area, and the regions sampled by the coda wave propagation both parallel and cross the structural

grain of the area (northeasterly). The magnitudes of the events range from mb 2.0 to 5.5. This wide range of magnitudes allows us to measure the coda decay at both short and long lapse times. For example, the small earthquakes at short epicentral distances (such as event No. 3 in Table 4.1) allow us to measure the coda decay at lapse times from 25 to 60 seconds. The larger, more distant events (such as event No. 6) allow us to measure the coda wave decay at lapse times of 100 to 500 seconds. The lapse time is related to the region of sampling, since for any given lapse time t , the scatterers responsible for the generation of coda waves are located on the surface of an ellipsoid whose surface projection is defined by the equation

$$\left[\frac{x}{(vt/2)} \right]^2 + \frac{y^2}{[(vt/2)^2 - R^2/4]} = 1 \quad (4.14)$$

for a surface source. Here, R is the source-receiver distance, v is the velocity (which we shall take as the S-wave velocity, 3.5 km/sec), t is the lapse time, and x and y are the surface coordinates. Figure 4.3 shows the evaluation of this equation for four cases which are similar to those encountered in this study. In Figure 4.3a, an epicentral distance of 15 km has been chosen along with a lapse time of 40 seconds. The coda waves in this case sample a small zone of about 100 km in extent, 50 km in depth, and 15,000 square km in surface area. Thus, we would be measuring the Q_c in a localized area surrounding the source and

station. At a greater epicentral distance and lapse time (Figure 4.3b), the coda waves sample a correspondingly larger zone. For an epicentral distance of 300 km and lapse time of 200 seconds (Figure 4.3c), the coda waves would sample an area the size of New England (350,000 sq km). In the last case (Figure 4.3d) the coda waves would sample an area the size of the NEUS-SEC (700,000 sq km). In each of these cases, the Q_c which we measure is an average $Q(\text{ave})$ for the region given by

$$t/Q(\text{ave}) = \sum_{i=1}^N [t_i/Q_i] \quad (4.15)$$

where t_i are the times the wave spreads in each ellipsoidal region of local attenuation Q_i .

The analysis of the data proceeds as follows:

Step 1: The seismic data are time shifted so that the signal is expressed in terms of lapse time. The seismogram is then displayed on a graphics terminal. The S-wave lapse time is entered, and a window length is chosen over which the RMS amplitudes will be calculated. The length of the window is chosen so as to smooth-out any irregularities in the seismogram. For close events of small magnitude, this window is generally chosen to be 5 seconds long. For larger, more distant events, the window length is 10 to 15 seconds.

Step 2: A representative noise sample before the onset of the P-wave is visually chosen. This will be used to correct the

coda amplitudes at each frequency.

Step 3: The seismogram is then filtered. A three-pole phase-free Butterworth bandpass (low-pass then high-pass) filter is used. Six frequency bands were chosen for analysis, with the filter parameters given in Table 4.2. The filter parameters were chosen to be the same as those used in other studies of coda wave attenuation (Aki and Chouet, 1975; Aki, 1980; Roecker, 1981) so that the results would be directly comparable. (The exception to this is at the high frequency end. The sampling rate of data for the M.I.T. Network is presently 25 samples per second, so that the Nyquist frequency is 12.5 Hz.) The filtered seismogram is then displayed on the graphics terminal.

Step 4: The amplitudes in each window are calculated by sliding the window across the time series at 1.0 second intervals. The noise sample is then subtracted from the seismogram. If the seismogram consists of a linear superposition of the signal $s(t)$ and a noise component $n(t)$, both at frequency ω , then

$$S(t) = s(t) + n(t) \quad (4.16)$$

If the signal and the noise are uncorrelated, then

$$\langle S(t) \rangle_{\tau}^2 = \langle s(t) \rangle_{\tau}^2 + \langle n(t) \rangle_{\tau}^2 \quad (4.17)$$

where $\langle \rangle$ refers to the mean of the quantity in the brackets over the time interval τ . Thus,

$$\langle s(t) \rangle_{\tau}^2 = \langle S(t) \rangle_{\tau}^2 - \langle n(t) \rangle_{\tau}^2 \quad (4.18)$$

The RMS amplitude of the signal is then

$$A(r, \omega | t) = [\langle s(t) \rangle_{\tau}^2]^{1/2} \quad (4.19)$$

Step 5: The function $A(r, \omega | t)$ is then multiplied by $1/k(r, \alpha)$ and the natural logarithm is taken. We are left with $\ln[A(r, \omega | t)/k(r, \alpha)]$ versus t . This function is then displayed on the graphics terminal.

Step 6: The linear portion of $\ln[A(r, \omega | t)/k(r, \alpha)]$ is visually chosen and a linear regression is performed to calculate the slope, from which $Q_c(\omega)$ is obtained.

An example of this procedure is shown in Figure 4.4. The event (No. 9 in Table 4.1) occurred east of Gloucester, MA and was recorded at the M.I.T. station PNH (epicentral distance = 172 km). The unfiltered signal is shown at the top left of this figure. Note that the seismogram has been played out in terms of lapse time measured from the earthquake origin time. The S-wave lapse time is 45 seconds, and a window size of 5 seconds has been chosen for computation of the RMS coda wave amplitudes. Below the unfiltered playback are shown the bandpass filtered

seismograms over five frequency bands. To the right of each filtered seismogram is shown the quantity $\ln[A(r, \omega | t)/k(r, \omega)]$ versus lapse time, t . The linear portion of this function is visually chosen, and a linear regression is performed to determine the slope, s . Given the slope and the center frequency of the filter, the Q_c value at that frequency is simply

$$Q_c(\omega) = \omega/2s \quad (4.20)$$

This value is shown at the top right corner of each amplitude display.

4.2.3 Results

Using the method outlined in the previous section, values of $Q_c(\omega)$ were determined using all of the events in Table 4.1. However, because of varying noise conditions and sizes of the events, $Q_c(\omega)$ could not be determined for all event - station - band combinations. In particular, M.I.T. Network stations are very noisy at frequencies below 1.0 Hz, so that the Q_c at low frequencies could only be measured for the largest events where the signal to noise ratio was high. The event - station pairs that were used in this study are shown in Figure 4.5. In all, 67 Q_c measurements were made. All of the results are tabulated in Table 4.3 including the standard errors and values of $1000/Q_c$. The distribution of Q_c measurements with frequency is given in Table 4.4. Since there are many more Q_c measurements at middle and high frequencies than at low, these measurements are the most

reliable.

All values of $1000/Q_c$ versus frequency have been plotted in Figure 4.6 . Two observations may be noticed from this figure. First, there is a definite frequency dependence of Q_c in the study area. At high frequencies (10.0 Hz), Q_c is approximately 1300, whereas at low frequencies (1.5 Hz), Q_c is lower and ranges from 300 to 1000. The second observation is that the greatest scatter in the Q_c values is at the low frequency end of the spectrum. As we shall show, this scatter is not due to errors in the analysis, but is due to the varying regions of sampling of the coda waves, indicating that significant variations in Q_c are present across the area.

If we fit all of the Q_c data in Figure 4.6 to a power law of the form

$$Q_c(f) = a(f)^b \quad (4.21)$$

we obtain the equation

$$Q_c(f) = 460(f)^{0.40} \quad (4.22)$$

Values of this equation are superimposed onto the data in Figure 4.6 . We can compare this result with the frequency dependence of Q_c in the central US, which Singh and Herrmann (1983) have determined to be

$$Q_c(f) = 1000(f)^{0.20} \quad (4.23)$$

and that of the western US (Singh and Herrmann, 1983)

$$Q_c(f) = 150(f)^{0.45} \quad (4.24)$$

Since the attenuation is proportional to $1/Q_c$, our measurements show that the seismic wave attenuation in the study area is about twice that of the central US, and is only $1/3$ that of the West. This result is supported by the work of Solomon and Toksöz (1970). They measured the S-wave differential attenuation across the continental US using arrivals from deep focus earthquakes in South America. Their results indicate that the total S-wave attenuation in the western US is at least as large as the difference in attenuation between the central and eastern US.

As mentioned earlier, Figure 4.6 shows that there is a large amount of scatter in the Q_c measurements. This scatter arises because we have included Q_c measurements over a broad area and for both short and long lapse times. By combining all of the results at both short and long lapse times, we have determined an average Q_c across a broad area the size of the NEUS-SEC, and over a depth range of 0 to 500 km. Clearly, the Q_c values must vary significantly over this volume within the earth.

We can see this variation if we plot the Q_c measurements at short lapse times (< 100 sec) differently from those at long lapse times (> 100 sec). This is illustrated in Figure 4.7 where we have plotted the Q_c measurements at short lapse times as crosses, and those at long lapse times as diamonds. We see from

this figure that the attenuation measured at short lapse times is not only greater at low frequencies than that measured at long lapse times, but also shows a greater frequency dependence. If we fit the data for lapse times less than 100 seconds, we obtain the equation

$$Q_c(f) = 140(f)^{0.95} \quad (4.25)$$

and the corresponding equation for lapse times greater than 100 seconds is

$$Q_c(f) = 660(f)^{0.40} \quad (4.26)$$

Values of $Q_c(f)$ from equations (4.26) and (4.27) have been listed in Table 4.4, and are also plotted in Figure 4.7. In Table 4.4 we have also listed the corresponding value of the coefficient of anelastic attenuation, γ . The relationship between γ and Q is $\gamma = \pi f / QU$, where f is the frequency and U is the group velocity. For the calculation in Table 4.4, we have used a value of U equal to the S-wave velocity (3.5 km/sec).

To aid in the interpretation of this dataset, we will examine the regions of coda wave sampling versus lapse time, which are graphically outlined in Figure 4.3. Let us first consider the short lapse time dataset. There are two separate effects which influence these results. The first effect is controlled simply by the lapse time. By measuring the coda decay

at short lapse times, the resulting Q_c measurements are valid only over a small source volume surrounding the source and receiver. Therefore, the short lapse time Q_c measurements are valid only for southern NH and eastern MA. The second effect present in the dataset results from the fact that the raypaths tend to cross rather than parallel the structural grain of the study area. Thus, the attenuation measurements may be biased by this raypath effect. The long lapse time measurements do not suffer from these effects. This is because the raypaths both cross and parallel all of the major structural features in the NEUS. Thus the average Q_c for the NEUS should be taken as that of the long lapse time measurements.

Let us now compare the results of this study with other attenuation measurements conducted in this area. Street (1976) measured the spatial attenuation of 1.0 Hz Lg waves in the eastern US for four NEUS earthquakes. Street's (1976) amplitude measurements were made over a distance range out to 3000 km, which corresponds to the coda measurements at long lapse times in this study. His results indicate that the coefficient of anelastic attenuation, γ , is 0.001/km at 1.0 Hz. This value of γ is very close to the result of this work, which indicates a value of 0.0015/km. The small discrepancy is probably due to Street's (1976) measurement of γ over a much broader region which included parts of the Canadian Shield.

Singh (1981) measured the Q of coda waves in the NEUS using the peak frequency versus lapse time method developed by Herrmann

(1980). Singh's (1981) results indicate that at 1.0 Hz, Q varies from 700 near the coast to 900 inland. This increase in Q_c as one goes inland from the coast was also seen in the data from this section.

4.2.4 Attenuation and Scattering of Seismic Waves

Our observation of frequency dependent Q_c in New England has also been found in other areas around the world. Recently, Aki (1980b), Pulli and Aki (1981), and Roecker *et al.* (1982) compiled measurements of frequency dependent Q and found a strong correlation between the degree of frequency dependence and the level of tectonic activity in the area of measurement. For example, in the tectonically stable central US, Q was found to be nearly frequency independent over the band of interest, while in the subduction area of Japan, Q was found to vary by a factor of ten between 1.5 and 25 Hz. Aki (1980b) used this evidence to conclude that the scattering of seismic waves was the principal contributor to the frequency dependence of Q . This is a natural conclusion, since in areas of active tectonics, the lithosphere is highly heterogeneous, whereas in old, stable areas, the lithosphere is generally uniform.

We can estimate the relative contributions of anelastic attenuation and scattering in our data by applying the model of Dainty (1981). In this model, the anelastic attenuation Q_i is assumed to be frequency independent, and the apparent Q_c takes on the value

$$1/Q_c(\omega) = 1/Q_i + v/\omega L \quad (4.27)$$

where v is the seismic wave velocity (3.5 km/sec) and L is the mean free path. Dainty's (1981) argument for frequency independent Q_i follows from the assumption that scattering dominates at frequencies near 1 Hz. Accordingly, the assumption that Q_i is constant may be replaced by the weaker assumption that Q_i does not decrease substantially between 30 and 1 Hz. The value of L can thus be estimated by choosing a high frequency value of Q_i and visually fitting the resulting Q_c values to those of our results. We have done this in Figure 4.8. The value of Q_i chosen for the fits was 1800. For the long lapse time case (> 100 sec), we obtain a mean free path of 400 km. For the short lapse time data (< 100 sec), we obtain a mean free path of 80 km. This result makes physical sense since the greater frequency dependence of Q at shallow depths implies that the crust is much more heterogeneous than the mantle.

Another way in which we can interpret this dataset is to assume that scattering is the only contribution to the apparent Q_c values and that Q_i is infinite. This approach was taken in the study of Q_c in Afghanistan by Roecker et al., (1982). Since $Q_c = Q_i Q_s / (Q_i + Q_s)$, an infinite Q_i leads to a "minimum mean free path" of $v Q_c / \omega$. In Table 4.5, we have calculated values of L_{min} from the Q_c measurements at both short and long lapse times. At long lapse times, corresponding to greater depths within the earth (> 100 km), the minimum mean free path decreases from 437

km at 0.75 Hz to 92 km at 10 Hz. However, at short lapse times, corresponding to shallow crustal depths, L_{min} is essentially constant (70 km) between 1.5 Hz and 10 Hz. (The L_{min} at 0.75 Hz, which is 79 km, is in parentheses in Table 4.5 since this value is extrapolated outside of the data range and thus may be in error.) This result has some interesting implications. At greater depths within the earth, the average distance between scatterers decreases with the decreasing size of the scatterers. This result is consistent with the idea that the earth becomes more homogeneous with depth. At shallow depths, the frequency independent L_{min} implies that scatterers of varying sizes are equally present through the crust. Of course, this interpretation assumes that the size of the scatterers is directly proportional to the wavelength of the coda waves. A similar observation of frequency independent L_{min} at shallow depths was also found by Roecker *et al.* (1982) who studied coda wave propagation in Afghanistan.

4.2.5 Discussion of Possible Errors

In this chapter, we have used the coda wave theories of Aki (1969), Aki and Chouet (1975), and Sato (1977) to measure the frequency dependence of Q_c in the NEUS. Our results are thus highly dependent on the assumptions and validity of these models. In this section, we briefly review these assumptions as possible sources of error in the data.

The first source of error arises from the fact that the coda wave models used here assume that the coda consists of

backscattered body waves (actually S-waves), so that the geometrical spreading term goes as t^{-1} , where t is the lapse time. If the coda consists of backscattered surface waves, then the geometrical spreading term will be $t^{-1/2}$. An incorrect assumption that the coda consists of body waves leads to an overcorrection of the amplitudes, resulting in Q_c values which are too high.

There is reason to believe that surface wave scattering is a significant contribution to the development of coda waves in the New England area. Earthquakes in New England are shallow, generally occurring in the upper ten kilometers of the crust (see Chapter 2). These shallow earthquakes are efficient generators of surface waves. In addition, the L_g phase, which is a higher mode surface wave consisting of both Love and Rayleigh wave components, is usually the largest phase observed on short period seismograms in this area. These facts, combined with the complicated surface topography of the area, suggest that surface wave scattering may need to be examined in detail in future studies. Here, we will briefly examine its effects.

To investigate the importance of surface wave scattering in our Q_c values, we recalculated the Q_c values for a representative sample of event-station pairs in our dataset assuming that surface wave scattering dominated over body wave scattering. Thus, the geometrical spreading correction was $t^{1/2}$ rather than t^1 . These calculations were made over frequencies from 1.5 to 10.0 Hz and at both short and long lapse times. Let us first

consider the short lapse time data.

For the short lapse time data ($t < 100$ sec), Q_c was found to obey the relationship $Q_c(f) = 115(f)^{0.95}$. This compares with the equation $Q_c(f) = 140(f)^{0.95}$ assuming body wave scattering. Thus, for surface wave scattering, the Q_c at 1.5 Hz is 170, versus a Q_c of 206 assuming body wave scattering. This represents a 25% increase in attenuation at this frequency. At 10 Hz, Q_c is 1025 assuming surface wave scattering versus 1250 assuming body wave scattering. This difference is insignificant in its effect on wave amplitudes at the distances considered here.

For the long lapse time data ($t > 100$ sec), Q_c was found to obey the relationship $Q_c(f) = 570(f)^{0.40}$. This compares with the equation $Q_c(f) = 660(f)^{0.40}$ assuming body wave scattering. Thus, for surface wave scattering, Q_c at 1.5 Hz is 670, whereas for body wave scattering Q_c is 764. This represents approximately 15% greater attenuation assuming surface wave scattering. At 10 Hz, Q_c assuming surface wave scattering is 1430, whereas Q_c is 1660 assuming body wave scattering. Again, this difference is insignificant over the distance range of consideration in this study.

This exercise suggests that surface wave scattering may be important when measuring Q_c values at low frequencies and at short lapse times. The resolution of the composition of the coda is a difficult problem; however, we are encouraged by the results of Sato (1977) who measured the coda simultaneously at the

surface and in a deep borehole (depth ~ 3 km) and found no difference in the statistical character of the coda amplitudes.

Another source of error in the models is that they assume an infinite, unbounded propagation medium, whereas a halfspace is a more accurate representation of the problem. Roecker (1981) estimated this error by modifying Sato's (1977) coda wave theory for a halfspace, and found that for lapse times between t_s and $2t_s$, the ratio of the halfspace Q_c to that of the unbounded Q_c was 1.03. Thus, we do not expect any large errors in our results from the assumption of an infinite medium.

We have also neglected the effect of multiple scattering of the coda waves since we are using the "weak scattering" Born approximation. To estimate the errors, we need to know the values of σ and N separately. However, we can only measure the product $N\sigma$ from our data. Dainty and Toksöz (1981) have suggested that the critical parameter for determining whether multiple or single scattering is applicable in an area is the ratio of the "attenuation distance" to the mean free path, L . The attenuation distance x^* is defined as the average distance the seismic energy travels before being attenuated by $1/e$, and is equal to Qv/ω . For $x^*/L \leq 1$, Dainty and Toksöz (1981) state that single scattering applies, whereas if $x^*/L \gg 1$, then multiple (strong) scattering applies. For our dataset, $x^*/L \sim 1$ for all cases. Thus, the effects of multiple scattering should be minimal in our dataset.

Recently, Gao et al., (1983) compared the effects of single

and multiple scattering on the coda waves of local earthquakes. They found that at short lapse times, the coda power is well explained by single scattering, but at long lapse times the effects of multiple scattering need to be considered. Neglecting multiple scattering gives rise to an overestimation of Q_c by a factor of 1.4 .

4.3 Ground Motion Attenuation Models for New England

The Q measurements presented in the previous section enable us to accomplish two important tasks in New England seismology. First, they allow us to correct instrumental seismic observations for propagation effects in order to retrieve the source parameters of earthquakes and other events. Second, they allow us to apply a propagation term to a specific earthquake source spectrum and thereby estimate the ground motion at sites of interest. However, in many situations we do not have enough information to specify the earthquake source spectrum, yet we must still provide an estimate of the potential ground motion at a specific site. For example, in earthquake risk studies, we need to know the distribution of the seismic source zones, the maximum earthquake magnitude in each zone, the return times for this event in each zone, and a ground motion attenuation model in order to calculate the ground motion as a function of probability (Cornell, 1968). Similarly, we may need to know the statistical distribution of accelerations or velocities in Boston due to all of the known historical earthquakes in the Massachusetts area. To answer these questions, we must use a ground motion

attenuation model. (Note that in this section we will frequently interchange natural and common logarithms. Natural logarithms are designated as $\ln(u)$, whereas common logarithms are designated as $\text{Log}(u)$.)

Such a model is of the form

$$G = F(M,R) \quad (4.28)$$

where G is the ground motion parameter, M is the earthquake magnitude or other source size specification, and R is the distance. The parameters G , M , and R must be explicitly defined in order to properly apply such a relation. For example, G may be the ground acceleration, velocity, or displacement and may be the vertical, vector resolved horizontal, or average horizontal component of the ground motion. In addition, G may be the peak or 3-cycle sustained value of the ground motion parameter. The magnitude specification may be the local (M_L), body wave (m_b), or moment derived magnitude (M_w), each corresponding to a different frequency range of the source spectrum. The distance R may be the epicentral, hypocentral, or other distance specification.

As examples of ground motion attenuation models, we cite the velocity attenuation model of Joyner and Boore (1981) developed for the California area using strong motion records,

$$\begin{aligned} \text{Log}(v) = & - 0.67 + 0.489(M_w) - \text{Log}(r) \\ & - 0.00256(r) + 0.17(S) + 0.22(P) \end{aligned} \quad (4.29)$$

where v is the peak ground velocity in cm/sec, r is defined by

$$r = (d^2 + 16.0)^{1/2}, \quad (4.30)$$

d is the closest distance to the surface projection of the fault rupture in kilometers, S takes on the value of zero at rock sites and one at soil sites, and P is zero for 50 percentile values and one for 84 percentile values. Similarly, Street (1982) derived a relationship between the vector resolved horizontal particle velocity at 1.0 Hz, the $mbLg$ magnitude, and the epicentral distance r in kilometers using data from the July 1980 Sharpsburg, KY earthquake, which is

$$\text{Log}(v) = - 3.56 + mbLg - \text{Log}(r) \quad (4.31)$$

Ground motion attenuation models like these may be derived in a number of ways. The first way is by a multiple regression analysis of a strong ground motion parameter measured for a number of earthquakes of varying sizes and at a wide range of epicentral distances. To accomplish this task, we must have a voluminous dataset of strong motion records. As we shall see in the next section, such a dataset does not exist for the New England area. In fact, the only area in the continental U.S. where such a dataset does exist is in the West. A second way we can derive a ground motion attenuation model is by taking near field strong motion records and applying the measured Q values

determined in the previous section to propagate the values to greater distances. This method requires less data, but still assumes that some strong motion records exist over a wide range of magnitudes. Again, the limited dataset for New England precludes the use of this technique. A final way that we can develop a strong motion attenuation model is to take advantage of the numerous intensity surveys which have been conducted in this area for a wide range of earthquake magnitudes. If a correspondence can be found between the seismic intensity and a measureable ground motion parameter, such as the ground acceleration, velocity, or displacement, then the intensity attenuation function can be converted to the corresponding ground motion attenuation relation. We can then test this relation by comparing the results with the theoretical ground motion attenuation from the measured Q values, and with whatever strong motion data does exist in the area.

It is this third approach which we will use to develop a strong ground motion attenuation model for New England. We begin by reviewing the strong motion data in this area, which at present consist of recordings at six sites of the January 19, 1982 Gaza, NH earthquake. Then, we examine the intensity attenuation relationships determined by Klimkiewicz (1980, 1982); and by combining this relation with a velocity-intensity correlation, we obtain a particle velocity attenuation function for New England. Next, we test this relation against the strong motion data and the theoretical seismic wave attenuation from the

derived Q measurements presented earlier. Finally, we will use this relation to calculate the distribution of ground motions for some hypothetical NEUS-SEC earthquakes.

4.3.1 Strong Motion Data

The Gaza, NH earthquake of January 19, 1982 produced the first strong motion dataset for New England. This earthquake was of body wave magnitude 4.6 and occurred at latitude 43.52 N, and longitude 71.61 W. The focal depth of this event is not precisely known at this time, but the travel-time data from the permanent stations around the epicenters limit the depth to less than 5 kilometers. The focal depths of the aftershocks, determined from P- and S-wave arrival times on a portable microearthquake network setup around the epicenter, are all less than 5 kilometers. The focal mechanism of this event, determined in Chapter 3 of this work, shows predominantly strike-slip faulting on fault planes oriented nearly N-S or E-W.

The US Army Corps of Engineers Waterways Experiment Station in Vicksburg, MS operates a number of strong motion instruments at flood control dams in the area of the Gaza earthquake. Figure 4.9 shows the location of these sites with respect to the epicenter of the Gaza event. Most dam sites have three installations of 3-component Kinometrics SMA-1 accelerographs. There is an instrument at the dam crest, at the top of the abutment, and downstream from the dam. The closest accelerograph site to the epicenter was at the Franklin Falls Dam, a distance of 7 km to the southwest. The farthest known site triggered by

the event was at the Ball Mountain Dam, a distance of 105 km to the southwest.

The accelerograms were digitized and processed under the direction of the Army Corps of Engineers. Table 4.6 summarizes their results (personal communication, 1982). (When available, we have used the downstream record values of strong ground motion in Table 4.6. The accelerations at these sites should be the closest to the free field accelerations, that is the accelerations uninfluenced by the dam structure or sediment accumulation around the dam.) The most remarkable feature of Table 4.6 is the very high ground accelerations recorded at the closest site, the Franklin Falls Dam. Here, the peak transverse acceleration was 378 cm/sec/sec, and the peak longitudinal acceleration was 141 cm/sec/sec. (Coincidentally, the accelerographs were placed on azimuth with the Gaza earthquake, so that the L and T components were nearly naturally rotated.) Thus, the mean peak horizontal ground acceleration was approximately 260 cm/sec/sec. These accelerations are much higher than one would expect from an earthquake of magnitude 4.6 (mb). For example, the acceleration attenuation model of Herrmann (1981) predicts a mean peak horizontal acceleration of about 70 cm/sec/sec for a central US earthquake of mb 4.6. Similarly, the model of Joyner and Boore (1981) predicts a peak horizontal acceleration of only 30 cm/sec/sec on a rock site in the California area. The far field accelerations for the Gaza earthquake are more typical of the values predicted by these

equations. At 60 km, the Gaza event produced accelerations of about 25 cm/sec/sec. Herrmann's (1981) central US model also predicts a value of 25 cm/sec/sec at this distance.

Why did the Gaza earthquake produce such high near field accelerations? Part of the answer may lie in the complex nature of the rupture process and the high stress drops of New England earthquakes.

Evidence is accumulating which indicates that the stress drops of New England earthquakes are significantly higher than those of similar sized events in both California and the central US. For example, Nabelek et al. (1982) studied the source parameters of the January 9, 1982 New Brunswick earthquake and found a stress drop between 60 and 900 bars (depending on the choice of t^* used in the calculation of the source time function). Similarly, Mueller and Cranswick (1982) studied the source parameters of the aftershocks of this event, and found that their S-wave corner frequencies were between 40 and 50 Hz. Thus, the stress drops were on average ten times greater than the stress drops of California events. Other evidence, such as the large number of audibly perceptible earthquakes in this area, indicate that New England earthquakes are of small source dimensions and high stress drop. If we assume an idealized earthquake source spectrum where the displacement spectral density is flat below the corner frequency (f_c) and decays as the second power of frequency above f_c , then the acceleration spectrum is flat at frequencies above f_c (up to an f_{max}). Thus

for a given seismic moment, the higher the stress drop, the higher the frequencies of the peak accelerations. (A discussion of the effects of the earthquake source properties on the acceleration spectrum is given in Hasegawa, 1974.)

Finally, what are the engineering implications of this dataset? From the peak ground acceleration values alone, we would expect some structural damage in the epicentral region. However, the Gaza earthquake produced intensities of only V (M.M.). The answer to this dilemma lies in the frequency content and duration of the observed accelerations. These values, where available, are listed in Table 4.5. The peak ground accelerations at the Franklin Falls Dam site were of a frequency around 20 Hz, and occurred over a duration of 0.4 seconds. These high frequency, short duration accelerations will not produce damage in ordinary structures. (Site effects are also important in the determination of the frequency of the strong motion. The site effects at the Army Corp of Engineers strong motion instruments for the Gaza, NH earthquake are now being investigated.) In addition, if these accelerations are integrated to produce ground velocities, the resulting values are low. For example, at the Franklin Falls Dam, the velocities were on the order of 2 to 3 cm/sec (see Table 4.5). At greater distances, the velocities are all below 0.5 cm/sec. These values of ground velocity are considerably below the level at which damage would be expected (approximately 10 cm/sec).

These observations confirm the correspondence between

Modified Mercalli intensity and ground velocity. This correspondence will be used in the next section to convert an intensity attenuation model to a velocity attenuation model for New England.

4.3.2 Seismic Intensity and Strong Ground Motion

Before the development of the seismograph (circa 1880) and the instrumental magnitude scale (Richter, 1935), seismic intensity data provided the only quantitative measure of the relative size of an earthquake. The concept of seismic intensity is simple but useful. In general, the greater the earthquake "size", the greater the resulting intensities. (A number of other factors influence the seismic intensity at a given site, including the geologic and site conditions, and the quality of the construction.) Furthermore, the measurement of the attenuation of seismic intensity with distance from the earthquake provided some of the first evidence that the seismic wave attenuation was significantly lower in the eastern US than in the West (Nuttli and Zollweg, 1974).

Although the earthquake magnitude and seismic moment are better indicators of the earthquake "size", we continue to study the intensities of present-day earthquakes for a number of reasons. First, the intensity value provides a readily identifiable indicator of the damage or degree of ground shaking produced by an earthquake at a given site. Second, since an intensity value can be determined wherever there is a structure or a person, an intensity map is similar to having a dense array

of "peak ground motion" sensors surrounding the earthquake. This information can be extremely useful when instrumental data are unavailable in an area. A third reason is that there already exists a voluminous dataset on the distribution of seismic intensities for many important historical NEUS-SEC earthquakes. Thus, by studying the intensities of present-day earthquakes with known locations and magnitudes, we gain further insight into the source parameters of historical events (e.g., Street and Lacroix, 1979).

Klimkiewicz (1980, 1982) studied the attenuation of seismic intensities with distance for six NEUS earthquakes with known body wave magnitudes. These events include the Gaza, NH earthquake and the New Brunswick earthquake of January 9, 1982. The magnitudes of these events ranged from 3.0 to 5.8 (mb). The regression analysis used by Klimkiewicz (1980, 1982) differs from those of earlier intensity attenuation studies in that the regression was performed on individual site intensity-mb-distance datapoints. Other investigators (e.g., Chandra, 1979) measured the intensities at various distances using isoseismal maps, which tend to average the intensity effects over broad areas. Chandra's (1979) method is also equivalent to predicting a distance associated with a particular seismic intensity, whereas we wish to predict the intensity at a given distance. These two procedures are not statistically equivalent. Klimkiewicz (1980, 1982) used this second method in his study, which has the added advantage of providing a direct estimate of the variability of

intensity with epicentral distance and magnitude.

The result of the regression is

$$I(r,mb) = - 1.43 + 1.79(mb) - 0.0018(r) - 1.83[\text{Log}(r)] \quad (4.32)$$

where r is the epicentral distance in km. It must be remembered that the site intensities predicted by equation (4.32) correspond to those observed on average foundation conditions. At an alluvial site, the intensity may increase by one or two MMI units.

Figure 4.10 shows the evaluation of this equation out to an epicentral distance of 1000 km for magnitudes 3.0 to 6.5 (mb). Also included in Figure 4.10 is a horizontal line at intensity VII which we shall take as the damage threshold. (Further discussion on the choice of a damage threshold in earthquake hazards studies is presented in Appendix A of this work.) The inclusion of this threshold points out a number of interesting facts about the damage potential of NEUS earthquakes. First, it appears that the smallest earthquake capable of producing damage in this area is of magnitude 5.2 (mb). An event of this size would produce intensities of VII out to a distance of 3 km. Assuming circular isoseismals, this corresponds to an area of potential damage of 30 square km. Second, we can compute the areas of potential damage for much larger earthquakes. For a magnitude 6.0 (mb) earthquake, the area of potential damage is

approximately 1000 square kilometers, whereas for an mb 6.5 earthquake, the area of potential damage is about 8000 square kilometers. Extrapolating these results to an mb 7.2 earthquake, the corresponding area of damage is just over 100,000 square kilometers. We can compare this potential damage area with the actual intensity VII area of the 1811 New Madrid earthquake, which Nuttli (1973b) estimates to be 600,000 square km. The smaller potential damage area in the NEUS is a reflection of the higher attenuation in this area as compared with the central US. In contrast, the 1906 San Francisco earthquake had an area of intensity VII of about 30,000 square km.

In Figure 4.11, we have used equation (4.32) to compute the theoretical distribution of isoseismals for four hypothetical NEUS-SEC earthquakes. The locations of these earthquakes have been chosen to be coincident with those of large historical events in this area. The magnitudes used in the calculations were chosen to be 1/2 mb unit greater than the largest known historical event at each site. Thus, they represent the "maximum credible earthquake" for each site (Nuttli and Herrmann, 1981; An alternate definition of the maximum credible earthquake presented by Nuttli and Herrmann (1981) is to extrapolate the frequency-magnitude statistics to a return time of 1000 years, and use the magnitude which corresponds to this return time.) The epicentral data used in each of these calculations are summarized in Table 4.7. Also included in Table 4.7 are the values of the epicentral intensity, I_0 , determined for each

hypothetical event. (See Appendix A for a discussion of the effects of three large NEUS-SEC earthquakes.)

In the case of the Cape Ann event, we see that this hypothetical earthquake of mb 6.5 would alarm the general public (V) across most of New England, and would produce intensity VI and VII effects along the coast of Massachusetts. The smaller hypothetical event at Ossipee, NH would alarm the public in New Hampshire and Vermont, and would produce intensity VII effects only in the Lakes Region of NH. The large (mb=7.2) La Malbaie, PQ earthquake would produce intensity V effects across the NEUS-SEC, and cause damage at the intensity VIII level over a broad area of the St. Lawrence River Valley. This event would also likely reach the intensity IX level in the vicinity of the epicenter. In the last case, the hypothetical Massena, NY earthquake would produce damage (VII) in a confined area at the Canadian border, but would likely be felt across the NEUS-SEC (IV).

We now convert equation (4.32) to an equivalent ground motion attenuation model using an intensity ground motion correlation. We must first decide which ground motion parameter (acceleration, velocity, or displacement) most closely corresponds with Modified Mercalli intensity. In the previous section, we saw that for the Gaza, NH earthquake, the near field accelerations were very high, but since the accelerations were of high frequency and short duration, there was little damage in the epicentral area (intensity V). However, when the accelerations

were integrated to velocities, the values were well below the damage threshold. Thus, the ground velocity showed a much better correspondence with Modified Mercalli intensity than the acceleration. A number of other investigators (Nuttli, 1973b; Crandell, 1949; Wiggins, 1964) also found that particle velocity, rather than acceleration or displacement, is a better indicator of MMI.

McGuire (1977) performed a detailed study on the correlation of seismic intensity with ground acceleration, velocity, and displacement versus epicentral distance. He used 68 horizontal strong motion records from California earthquakes. McGuire (1977) concluded that both peak ground acceleration and displacement, when related to site intensity, are also a function of epicentral distance, whereas the peak particle velocity can be considered independent of distance. This effect was recognized long ago by Neumann (1954) who found that at large epicentral distances, higher than expected intensities for low ground accelerations are often attributed to the long duration of ground shaking. McGuire's (1977) correlations between peak horizontal ground velocity and intensity yield the following relationships

$$\ln(v) = - 4.02 + 0.952(I) \quad (4.33a)$$

for "medium sites" (i.e., sedimentary rock), and

$$\ln(v) = - 1.51 + 0.543(I) \quad (4.33b)$$

for "soft sites" (i.e., alluvium). In equations (4.33a and b), v is in cm/sec. Combining the relation for "medium" sites with equation (4.32) we obtain the velocity attenuation relation

$$\begin{aligned} \text{Log}[v(r,mb)] = & - 2.34 + 0.739(mb) \\ & - 0.001(r) - 0.756[\text{Log}(r)] \end{aligned} \quad (4.34)$$

where v is in cm/sec and r is in km. Figure 4.12 shows the evaluation of this equation out to an epicentral distance of 1000 km for body wave magnitudes 3.0 to 6.0. From this plot, we see that in the near field, velocities of approximately 10 cm/sec will be produced by an mb 5.0 earthquake. For an mb 6.5 event, velocities in the near field will reach 100 cm/sec, and will produce velocities greater than 10 cm/sec out to 100 km.

Nuttli and Herrmann (1981) have recently published a velocity attenuation model, similar to equation (4.34), for the central US. Their equation is

$$\begin{aligned} \text{Log}[v(r,mb)] = & - 3.60 + 1.000(mb) \\ & - 0.0011(r) - 0.83[\text{Log}(r)] \end{aligned} \quad (4.35)$$

This equation has been developed using both empirical and theoretical concepts. As we shall show in the next section, the term $0.83[\text{Log}(r)]$ derives from the theoretical expression for the geometrical spreading of an Airy phase at close distances ($r < 10,000$ km). The term $0.0011(r)$ corresponds to the anelastic

attenuation. However, a striking difference between equation (4.35) for the central US and equation (4.34) for New England is the coefficient of magnitude scaling. For the central US, the coefficient is 1.000, meaning that the ground velocity scales by a factor of 10 with m_b . In New England, this coefficient is 0.739. If this difference is real, then it implies that the scaling relations, and thus the source properties, of New England earthquakes are different from those in the central US.

Equation (4.34) by itself provides no information on the frequency content of the peak ground velocity. The frequency, as well as the duration, of the peak velocity must be known if we are to estimate the damage potential of the ground motion. The frequency of the peak velocity will depend on both the source characteristics of the earthquake and the frequency dependence of attenuation in the area. Intuitively, we would expect that the frequency of the peak velocity would be much greater near the source than at large epicentral distances. We can model the velocity spectrum versus distance by starting with an appropriate source model and applying an attenuation operator based on the results of the previous section. The source model we will use assumes that the far field displacement spectrum is flat for frequencies below the corner frequency f_c , and decays as the second power of frequency for frequencies above f_c . Thus, the normalized far field velocity spectrum is of the form

$$\begin{aligned}
 v(f,0) &= f/f_c & f < f_c \\
 &= f_c/f & f \geq f_c
 \end{aligned} \tag{4.36}$$

At an epicentral distance r , the velocity spectrum is

$$\begin{aligned}
 v(f,r) &= (f/f_c)\exp(-\pi fr/Q(f)U) & f < f_c \\
 &= (f_c/f)\exp(-\pi fr/Q(f)U) & f \geq f_c
 \end{aligned} \tag{4.37}$$

where we have ignored the effect of geometrical spreading, since it is frequency independent. The value of $Q(f)$ can be taken from equation (4.26).

In Figure 4.13, we have plotted the values of equation (4.37) for five epicentral distances (0, 100, 500, 1000, and 2500 km) and three values of f_c (0.3, 1.0, and 10.0 Hz). For $f_c=0.3$ Hz, we see that there is little frequency shift in the peak velocity over the distances considered. This is because the low frequencies generated by an event with $f_c=0.3$ Hz are minimally attenuated, whereas the high frequencies attenuate quickly. For $f_c=1.0$ Hz, there is again no frequency shift in the peak velocity over the distance range of 0 to 1000 km. However, at 2500 km, the attenuation term dominates and the peak frequency of the velocity has shifted to 0.3 Hz. In the last case, we have used $f_c=10$ Hz and we begin to see significant shifts in the velocity spectrum. At 500 km, the peak frequency has shifted to 5 Hz, and at 1000 km the peak frequency is at 1.5 Hz.

In Figure 4.14, we have calculated the theoretical horizontal velocity distribution for the four "maximum credible earthquakes" of Table 4.7. The velocity contours are given for each power of 10 cm/sec. Also included in Table 4.7 are the values of the near field horizontal velocities, V_0 . To estimate the frequencies of the peak velocities, we must first specify a value of f_c for each event. Nuttli (1983) has recently provided estimates of f_c for intraplate earthquakes of a given body wave magnitude. In Table 4.7, we have included a column of f_c values taken from this paper. Since the events in Table 4.7 are large, f_c is less than 1 Hz for all events, so that the peak frequencies of the velocities are the same as the f_c for each event.

4.3.3 *Testing of the Ground Motion Attenuation Model*

We now test the applicability of the velocity attenuation model derived in the previous section by comparing it with the strong motion data for the Gaza, NH earthquake, and the theoretical attenuation from our measured Q values. We begin with the strong motion data.

In Figure 4.15 we have plotted the predicted velocity attenuation from equation (4.34) for an mb 4.6 earthquake (the magnitude of the Gaza, NH event). Also shown are the predicted velocities for 1 mb unit lower and higher for comparison. Superimposed on this figure are the integrated peak horizontal velocity values for the Gaza, NH earthquake from Table 4.6. The only value of ground velocity not used on Figure 4.15 was the abutment record from N. Hartland Dam, since it appears that this

record has been greatly influenced by the structure and is thus not a reflection of the free field velocity predicted by equation (4.34). What we find from this comparison is that equation (4.34) successfully predicts the peak horizontal velocity in both the near field and far field. The scatter in the data corresponds to at most 1/2 mb unit.

Next, we test equation (4.34) against the theoretical velocity attenuation from our measured Q values. We must first decide which seismic phase is responsible for the strong ground motion. A number of studies (Nuttli, 1973a; Street et al., 1975; Press and Ewing, 1952; Street, 1976) have shown that the largest short period seismic phase which propagates in the eastern US is the L_g phase. Nuttli (1973a, 1978) demonstrated that the L_g phase is a higher mode surface wave which propagates as an Airy phase. The amplitude of the Airy phase of a propagating surface wave can be expressed by the equation (Ewing, Jardetsky, and Press, 1959)

$$A(\Delta) = A_0 |\sin(\Delta)|^{-1/2} (\Delta)^{-1/3} \exp(-\gamma\Delta) \quad (4.38)$$

where Δ is the epicentral distance in degrees and γ is the coefficient of anelastic attenuation which is related to Q by $\gamma = \pi f / QU$. In this equation, f is the frequency and U is the group velocity. Note that equation (4.38) is a point source model and thus may not be applicable in the near field where the effects of the finite size of the fault may dominate.

In Figure 4.16, we have evaluated equation (4.38) for three values of anelastic attenuation in order to illustrate the relative importance of attenuation and geometrical spreading. These values correspond to no attenuation ($\gamma = 0.000/\text{km}$), the average 1 Hz attenuation in New England ($\gamma = 0.0015/\text{km}$), and the 1 Hz attenuation in California from Herrmann (1980) ($\gamma = 0.005/\text{km}$). This figure illustrates that in areas of high attenuation, such as California, the attenuation becomes important with respect to geometrical spreading at distances as short as 10 km. In New England where the attenuation is much less, attenuation becomes important after 50 km. When one approaches large distances from the source, we see the significant departure in ground motion attenuation between California and New England. At approximately 500 km distance, the ground motion in California is approximately ten times lower than that in New England.

For short distances ($\Delta < 10$ degrees), $\sin(\Delta) \sim \Delta$ so that equation (4.38) simplifies to

$$A(r) = A_0(r)^{-5/6} \exp[-\gamma r] \quad (4.39)$$

where r is now in kilometers. The amplitude is related to the particle velocity by

$$V(r) = 2\pi f[A(r)] \quad (4.40)$$

Substituting equation (4.40) into (4.39) and taking natural logarithms, we obtain

$$\ln(V) = V_0 - 0.833[\ln(r)] - \gamma r \quad (4.41)$$

The form of this equation, separating the source (V_0), geometrical spreading ($0.833[\ln(r)]$), and attenuation (γr) terms, allows us to test the applicability of equation (4.34) to the New England area. Substituting a value of $\gamma = 0.0015/\text{km}$ for New England from Table 4.4, converting to natural logarithms, and placing the equations side by side, we have

$$\ln(V) = V_0 - 0.833[\ln(r)] - 0.0015(r) \quad (4.42)$$

$$\ln[V(r,mb)] = - 5.38 + 1.70(mb) - 0.756[\ln(r)] - 0.001(r) \quad (4.43)$$

This comparison shows that the intensity-derived velocity attenuation model successfully predicts both the geometrical spreading and attenuation terms to a useable degree of accuracy. Here we see that the theoretical geometrical spreading leading coefficient is 0.833, while the intensity derived coefficient is 0.756. The anelastic attenuation leading coefficient from the observed data, 0.001, is very close to that from the measured Q values. We can also visually compare the models by tying the near field velocity term (V_0) to that of the intensity derived model. This is shown in Figure 4.17. Here, we see that the

error in the geometrical spreading term makes little difference in the decay of seismic wave amplitudes over the distance range of interest.

The testing of the New England velocity attenuation model outlined here suggests a general method by which we can develop a velocity attenuation model for any region which lacks strong motion data. The method depends on two assumptions. First, we assume that the correspondence between Modified Mercalli intensity and peak horizontal ground velocity is of the form

$$\ln(v) = A + B(I) \quad (4.44)$$

and second that this relationship is regionally invariant. Then, if the regional relationship between intensity and magnitude is

$$m = C + D(I) \quad (4.45)$$

then near field peak horizontal velocity is approximately

$$\ln(v) = (A + BC/D) - B(m) \quad (4.46)$$

Applying geometrical spreading and attenuation with a regional value of γ , we obtain

$$\ln(v) = (A + BC/D) - B(m) - 0.833[\ln(r)] - \gamma r \quad (4.47)$$

Thus, an appropriate equation for New England would be

$$\begin{aligned} \ln[v(r,mb)] = & - 5.38 + 1.70(mb) \\ & - 0.833[\ln(r)] - 0.0015r \end{aligned} \quad (4.48)$$

An equation derived in this manner should only serve as a guide to the actual ground motion attenuation in the area of interest. However, when complete seismological data are lacking, an equation of this form may provide the only available information on expected ground motions for a designer.

Table 4.1

Events used in the Study of Coda Wave Attenuation

<u>Event No.</u>	<u>Date</u>	<u>Latitude</u>	<u>Longitude</u>	<u>mb</u>	<u>Area</u>
1	13Apr1981	45.90	-65.73	3.7	New Brunswick
2	28Jun1981	43.58	-71.58	3.0	Winnisquam, NH
3	04Sep1981	43.29	-71.68	2.2	Webster, NH
4	18Sep1981	46.09	-75.03	3.5	Mont. Tremblant, PQ
5	21Oct1981	41.14	-72.57	3.4	Long Isl. Sound, NY
6	11Jan1982	46.98	-66.66	5.5	New Brunswick
7	27Jan1982	43.53	-71.60	2.8	Gaza, NH
8	31Mar1982	47.00	-66.60	4.8	New Brunswick
9	27Oct1982	42.74	-70.09	2.8	Cape Ann, MA
10	01Nov1982	42.74	-70.09	2.4	Cape Ann, MA
11	24Nov1982	45.34	-73.43	3.0	Montreal, PQ
12	01Dec1982	43.61	-71.51	3.2	Meredith, NH

Table 4.2
Filter Parameters for the Coda Wave Analysis

<u>Band</u>	<u>Center Frequency (Hz)</u>	<u>Bandwidth (Hz)</u>
1	0.75	0.5
2	1.50	1.0
3	3.00	2.0
4	6.00	4.0
5	8.00	4.0
6	10.00	4.0

Table 4.3

Summary of Coda Wave Attenuation Measurements

Event No. 1 New Brunswick

Station WNH Distance = 525 km
Lapse time = 225 - 350 sec

f (Hz)	Q	$1000/Q$
1.5	500 +/- 40	2.00
3.0	1090 +/- 55	0.92
6.0	1300 +/- 30	0.77

Event No. 2 Winnisquam, NH

Station WNH Distance = 35 km
Lapse time = 100 - 160 sec

Station HRV Distance = 119 km
Lapse time = 70 - 120 sec

f (Hz)	Q	$1000/Q$	f (Hz)	Q	$1000/Q$
3.0	725 +/- 55	1.38	1.5	330 +/- 35	3.03
6.0	1100 +/- 21	0.91	3.0	460 +/- 40	2.17
			6.0	1010 +/- 45	0.99

Event No. 3 Webster, NH

Station ONH Distance = 14 km
Lapse time = 25 - 60 sec

f (Hz)	Q	$1000/Q$
3.0	635 +/- 130	1.57
6.0	1340 +/- 280	0.75

Event No. 4 Mont. Tremblant, PQ

Station WNH Distance = 378 km
Lapse time = 125 - 300 sec

Station PNH Distance = 404 km
Lapse time = 125 - 300 sec

f (Hz)	Q	$1000/Q$	f (Hz)	Q	$1000/Q$
1.5	630 +/- 45	1.59	1.5	1060 +/- 215	0.94
3.0	970 +/- 35	1.03	3.0	1700 +/- 65	0.59
6.0	1530 +/- 21	0.65	6.0	1735 +/- 40	0.58

Event No. 5 Long Island Sound, NY

Station DNH Distance = 260 km
Lapse time = 175 - 260 sec

f (Hz)	Q	$\frac{1000}{Q}$
3.0	1000 +/- 40	1.00
6.0	1400 +/- 25	0.71

Station GLO Distance = 226 km
Lapse time = 175 - 275 sec

f (Hz)	Q	$\frac{1000}{Q}$
3.0	1210 +/- 50	0.83
6.0	1350 +/- 20	0.74

Station PNH Distance = 220 km
Lapse time = 175 - 250 sec

f (Hz)	Q	$\frac{1000}{Q}$
3.0	1150 +/- 150	0.87
6.0	1360 +/- 20	0.74

Station WNH Distance = 318 km
Lapse time = 150 - 300 sec

f (Hz)	Q	$\frac{1000}{Q}$
1.5	810 +/- 40	1.23
3.0	1045 +/- 15	0.96
6.0	1280 +/- 10	0.78

Event No. 6 New Brunswick

Station WFM Distance = 617 km
Lapse time = 250 - 500 sec

f (Hz)	Q	$\frac{1000}{Q}$
0.75	700 +/- 50	1.43
1.5	910 +/- 24	1.10
3.0	1100 +/- 75	0.91

Event No. 7 Gaza, NH

Station ONH Distance = 29 km
Lapse time = 50 - 100 sec

f (Hz)	Q	$\frac{1000}{Q}$
3.0	345 +/- 34	2.92
6.0	690 +/- 30	1.45

Station PNH Distance = 65 km
Lapse time = 50 - 100

f (Hz)	Q	$\frac{1000}{Q}$
3.0	230 +/- 18	4.39
6.0	1050 +/- 70	0.96

Event No. 8 New Brunswick

Station WFM Distance = 622
Lapse time = 200 - 325 sec

f (Hz)	Q	$\frac{1000}{Q}$
0.75	500 +/- 70	2.00
1.5	620 +/- 45	1.62
3.0	960 +/- 60	1.04
6.0	1150 +/- 25	0.87

Event No. 9 Cape Ann, MAStation GLO Distance = 53 km
Lapse time = 30 - 60 sec

<u>f (Hz)</u>	<u>Q</u>	<u>1000/Q</u>
3.0	275 +/- 30	3.64
6.0	750 +/- 80	1.33
8.0	1020 +/- 100	0.98
10.0	1040 +/- 90	0.96

Station WNH Distance = 164 km
Lapse time = 70 - 110 sec

<u>f (Hz)</u>	<u>Q</u>	<u>1000/Q</u>
3.0	240 +/- 15	4.17
6.0	825 +/- 40	1.21
8.0	1210 +/- 80	0.83
10.0	1400 +/- 80	0.71

Station PNH Distance = 172 km
Lapse time = 70 - 110 sec

<u>f (Hz)</u>	<u>Q</u>	<u>1000/Q</u>
1.5	150 +/- 10	6.67
3.0	310 +/- 20	3.23
6.0	650 +/- 30	1.54
8.0	960 +/- 35	1.04
10.0	1280 +/- 50	0.78

Event No. 10 Cape Ann, MAStation GLO Distance = 53 km
Lapse time = 20 - 45 sec

<u>f (Hz)</u>	<u>Q</u>	<u>1000/Q</u>
3.0	275 +/- 55	3.64
6.0	340 +/- 45	2.94
8.0	525 +/- 45	1.90
10.0	620 +/- 50	1.61

Event No. 11 Montreal, PQStation WNH Distance = 252 km
Lapse time = 100 - 160 sec

<u>f (Hz)</u>	<u>Q</u>	<u>1000/Q</u>
3.0	610 +/- 45	1.64
6.0	850 +/- 25	1.18
8.0	1140 +/- 40	0.88
10.0	1400 +/- 40	0.71

Event No. 12 Meredith, NH

Station WNH Distance = 31 km
Lapse time = 70 - 140 sec

f (Hz)	Q	$\frac{1000}{Q}$
6.0	1220 +/- 40	0.82
8.0	1400 +/- 37	0.71
10.0	1500 +/- 45	0.67

Station ONH Distance = 36 km
Lapse time = 70 - 110

f (Hz)	Q	$\frac{1000}{Q}$
3.0	890 +/- 91	1.12
6.0	940 +/- 36	1.06
8.0	1040 +/- 34	0.96
10.0	1210 +/- 40	0.83

Station PNH Distance = 77 km
Lapse time = 55 - 110 sec

f (Hz)	Q	$\frac{1000}{Q}$
6.0	960 +/- 65	1.04
8.0	1220 +/- 35	0.82
10.0	1310 +/- 42	0.76

Table 4.4
Mean Values of Attenuation

<u>f (Hz)</u>	<u>No. of Qc Measurements</u>	<u>Short Lapse Times</u> <u>Qc</u>	<u>γ 1/km</u>	<u>Long Lapse Times</u> <u>Qc</u>	<u>γ 1/km</u>
0.75	2	(105)	(0.006)	594	0.001
1.5	8	204	0.007	764	0.002
3.0	20	395	0.007	982	0.003
6.0	20	765	0.007	1264	0.004
8.0	8	1007	0.007	1403	0.005
10.0	8	1264	0.007	1521	0.006
	—				
Total	67				

Table 4.5
Calculation of Minimum Mean Free Paths

f (Hz)	Short Lapse Times <u>L_{min}</u> (km)	Long Lapse Times <u>L_{min}</u> (km)
0.75	(79)	437
1.5	76	288
3.0	74	190
6.0	71	125
8.0	70	106
10.0	70	92

Table 4.6
Summary of Accelerograph Data for the
January 19, 1982 Gaza, NH Earthquake

	<u>Component</u>	<u>Accel.</u> <u>cm/sec/sec</u>	<u>Freq.</u> <u>Hz</u>	<u>Dur.</u> <u>sec</u>	<u>Velocity</u> <u>cm/sec</u>
Franklin Falls Dam Distance = 7 km Downstream Record (43.469, -71.660)	L-225	140.70	21	0.4	2.03
	Up	271.00	21	0.4	1.73
	T-135	377.86	16	0.4	2.87
Union Village Dam Distance = 61 km Downstream Record (43.793, -72.259)	L-245	37.01	10	0.3	0.82
	Up	28.90	10	0.3	0.45
	T-155	22.58	10	0.3	0.47
N. Springfield Dam Distance = 75 km Downstream Record (43.371, -72.510)	L-275	31.08	10	0.5	0.41
	Up	13.66	10	0.5	0.21
	T-185	22.59	10	0.5	0.29
White River Jctn Distance = 61 km Basement of VA Hosp. (on glacial till) (43.648, -72.343)	L-27	15.00			0.33
	Up	21.81			0.38
	T-180	31.00			0.57
Ball Mountain Dam Distance = 104 km Crest Record (43.126, -72.772)	L-30	8.80	5	2.	0.37
	Up	11.97	5	2.	0.34
	T-300	10.03	5	2.	0.37
N. Hartland Dam Distance = 62 km Abutment Record (43.605, -72.361)	L-15	11.08			0.20
	Up	3.75			0.14
	T-285	6.84			0.22

Table 4.7

Maximum Credible Earthquakes for the NEUS-SEC

<u>Site</u>	<u>Lat.</u>	<u>Long.</u>	<u>Largest Hist. mb</u>	<u>Maximum Cred. mb</u>	<u>fc Hz</u>	<u>Predicted Io</u>	<u>Vo***</u>
Cape Ann, MA	42.7	-70.3	6.0*	6.5	0.13	IX	85
Ossipee, NH	43.8	-71.3	5.4**	6.0	0.22	VIII	36
La Malbaie, PQ	47.7	-69.9	6.6**	7.3	0.06	XI	280
Massena, NY	45.0	-74.9	5.7**	6.3	0.17	IX	60

* Street and Lacroix (1979)

** Street and Turcotte (1977)

*** Vo in cm/sec

Figure Captions

Figure 4.1 Analog playback of a digitally recorded local earthquake. The earthquake (event No. 9 in Table 4.1) occurred approximately 50 km east of Gloucester, MA and was recorded at the M.I.T. station GLO (epicentral distance=53 km). The event has been plotted in terms of lapse time measured from the earthquake origin time. Indicated on the plot are the primary P- and S-wave arrivals, and the coda waves which are used in this chapter for attenuation measurements.

Figure 4.2 Map of earthquake epicenters used in the study of coda wave attenuation. The epicentral data for these events are given in Table 4.1. Also shown on this figure are the locations of the M.I.T. Seismic Network stations.

Figure 4.3 Horizontal projections of the ellipsoidal regions of coda wave sampling versus lapse time. The ellipses have been calculated using equation (4.14). Indicated on each figure are the lapse time, epicentral distance, velocity, and surface area.

Figure 4.4 Example of the coda wave measurements determined in this chapter. The event (No. 9 in Table 4.1) occurred east of Cape Ann, MA and was recorded on the M.I.T. station PNH (epicentral distance=172 km). At the top left is shown the unfiltered seismogram played out in terms of lapse time.

Below this figure are the band pass filtered seismograms using the filter parameters from Table 4.2 . To the right of each filtered seismogram is shown the quantity $\ln[A(r, \omega | t) / K(r, a)]$ versus lapse time t . The slope of this function is proportional to the Q_c at each frequency. The intervals over which the slopes have been calculated are indicated by the horizontal lines.

Figure 4.5 Map showing the locations of the 13 events used in this study as well as the station-event pairs used in the measurement of Q_c .

Figure 4.6 Plot of all Q_c measurements as a function of frequency, taken from Table 4.3 . The data obey the relationship $Q_c(f) = 460(f)**0.40$. The value of this function is plotted in the figure.

Figure 4.7 Plot of Q_c measurements as a function of frequency, separated by lapse time. The measurements at short lapse times (< 100 sec) are indicated by the crosses and obey the relationship $Q_c(f) = 140(f)**0.95$. The measurements at long lapse times (> 100 sec) are indicated by the diamonds and obey the relationship $Q_c(f) = 660(f)**0.40$.

Figure 4.8 Fits of the observed Q_c data to the scattering model of Dainty (1981). The short lapse time data can be fit by a value of L of 80 km. The long lapse time data are fit by a value of L of 400 km.

Figure 4.9 Map of central New Hampshire and adjacent areas showing the location of the January 19, 1982 Gaza, NH earthquake (star) and the locations of the US Army Corps of Engineers accelerograph sites (hourglasses) used in this study. See Table 4.6 for a summary of the accelerograph data.

Figure 4.10 Modified Mercalli intensity versus epicentral distance and body wave magnitude for the New England area, from Klimkiewicz (1982) (equation 4.33). A horizontal line has been placed at intensity VII to indicate the damage threshold.

Figure 4.11 Distribution of Modified Mercalli intensities for four hypothetical NEUS-SEC earthquakes, using equation (4.33). See Table 4.7 for the epicentral data used in the calculations.

Figure 4.12 Peak ground velocity in cm/sec versus epicentral distance and body wave magnitude for the New England area, formed by combining the intensity attenuation relation of Klimkiewicz (1982) with the intensity-velocity correlation of McGuire (1977).

Figure 4.13 Theoretical velocity spectra for events with corner frequencies of 0.3, 1.0, and 10.0 Hz at distances of 0, 100, 500, 1000, and 2500 km. The spectra were calculated using equation (4.36).

Figure 4.14 Distribution of peak horizontal ground velocities for four hypothetical NEUS-SEC earthquakes. See Table 4.7 for the epicentral data used in the calculations.

Figure 4.15 Comparison of the strong motion data for the January 19, 1982 Gaza, NH earthquake with the predicted velocities from equation 4.35. Shown are the theoretical curves for mb 3.6, 4.6, and 5.6 earthquakes.

Figure 4.16 Plot of the theoretical decay of seismic wave amplitudes for an Airy phase for three values of anelastic attenuation. The values of anelastic attenuation are 0.000/km, 0.001/km, and 0.005/km. The amplitudes have been calculated using equation 4.36 .

Figure 4.17 Comparison of the velocity attenuation model for New England (equation 4.35) with the theoretical velocity attenuation using a nominal value of gamma for New England (0.0015/km).

27OCT1982 EAST OF GLOUCESTER, MA MC=2.8

GLO SPZ

UNFILTERED SIGNAL

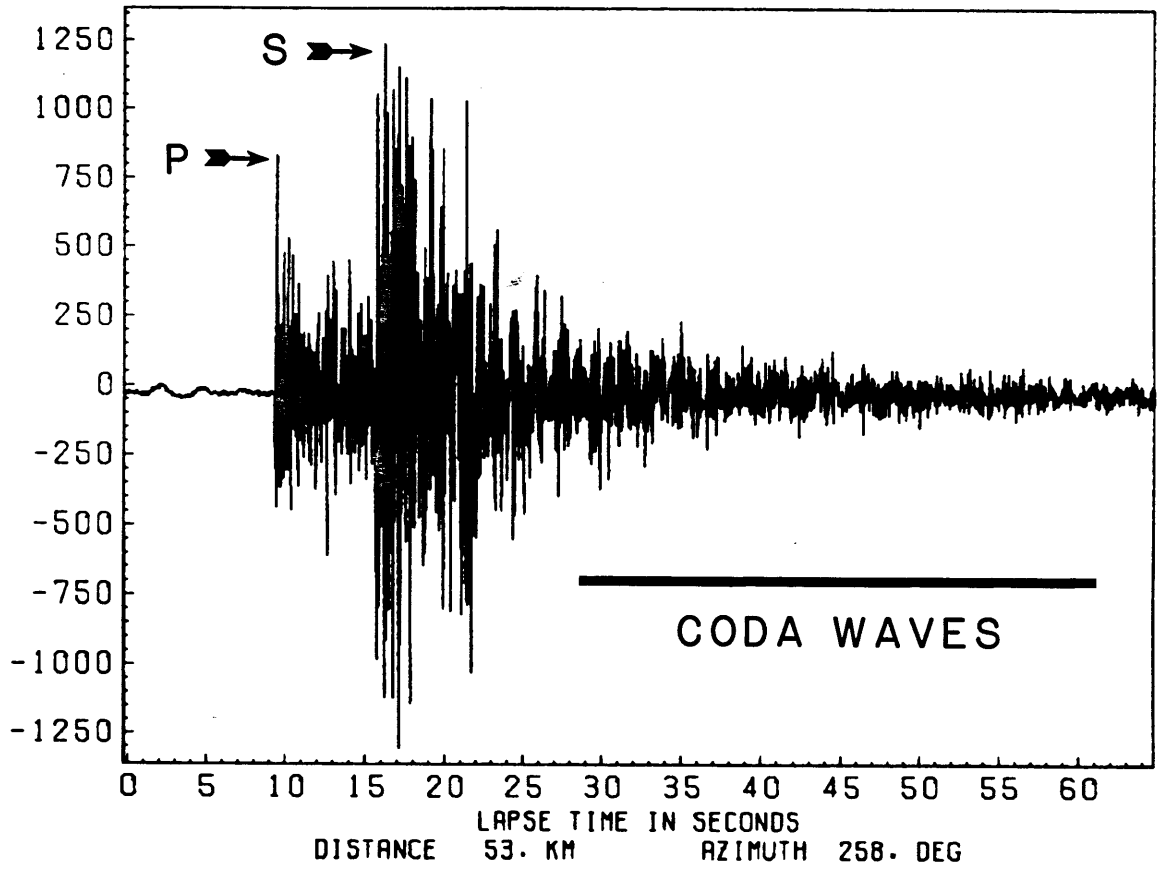


FIGURE 4.1

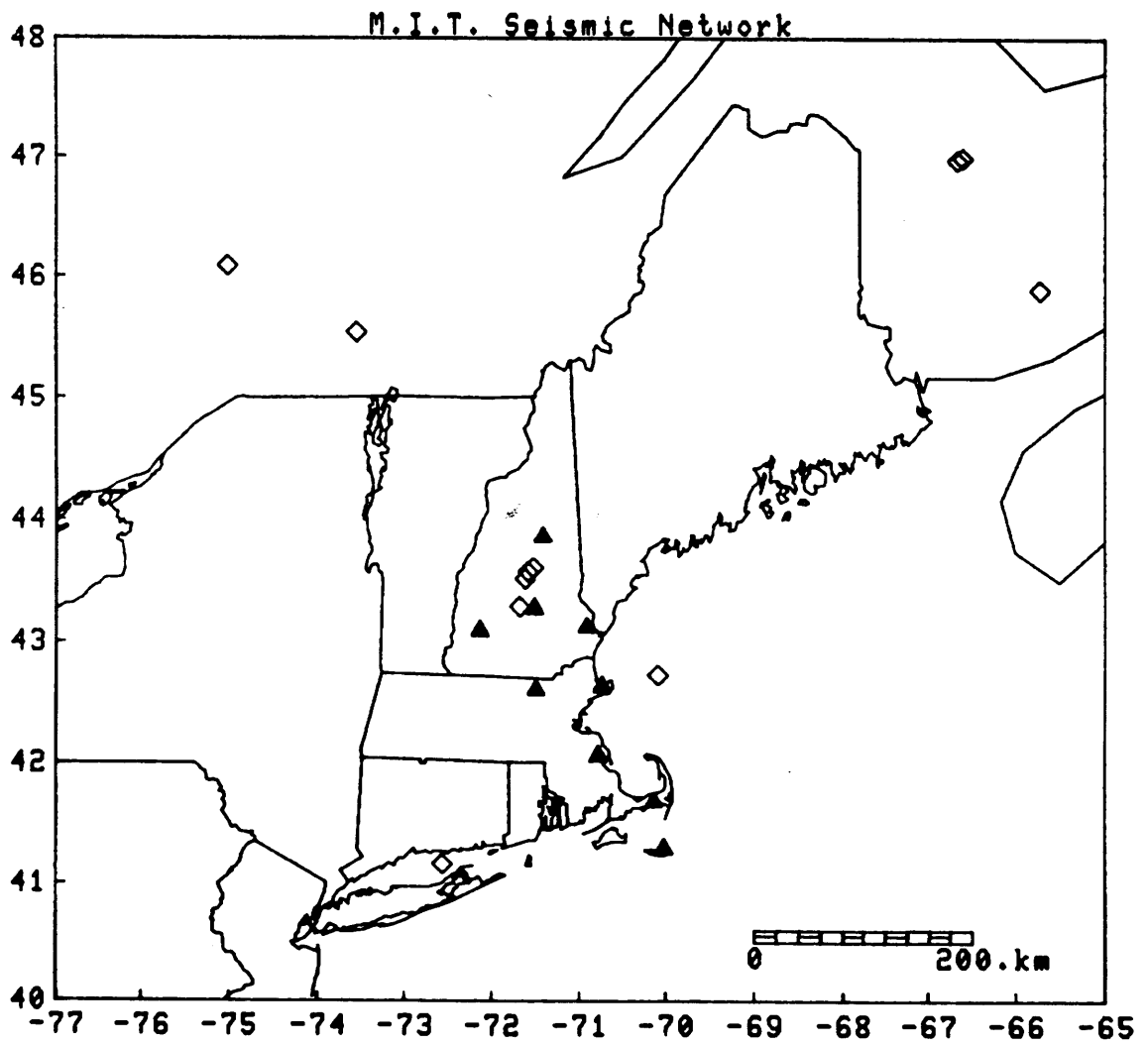


FIGURE 4.2

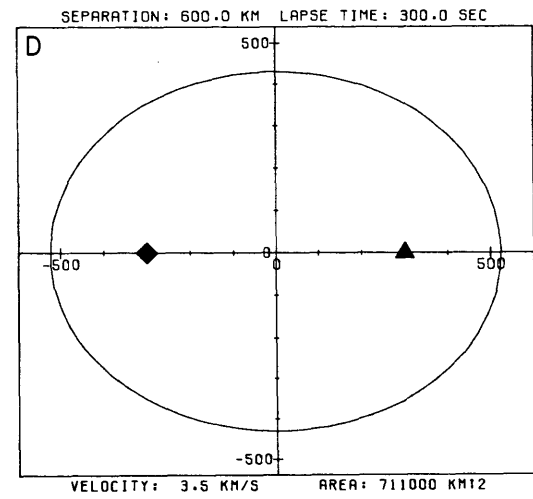
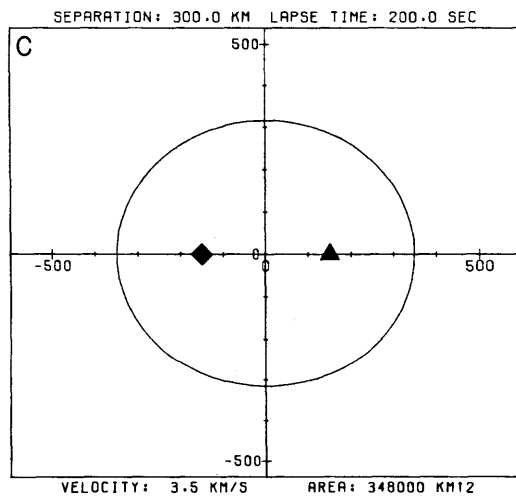
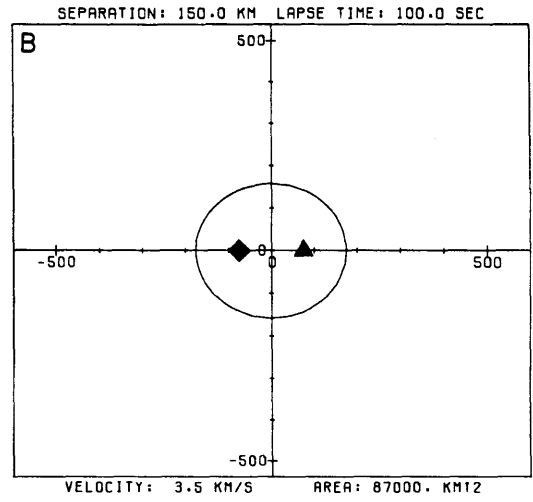
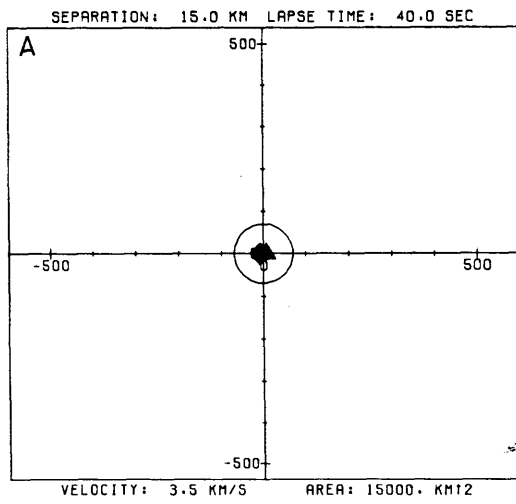


FIGURE 4.3

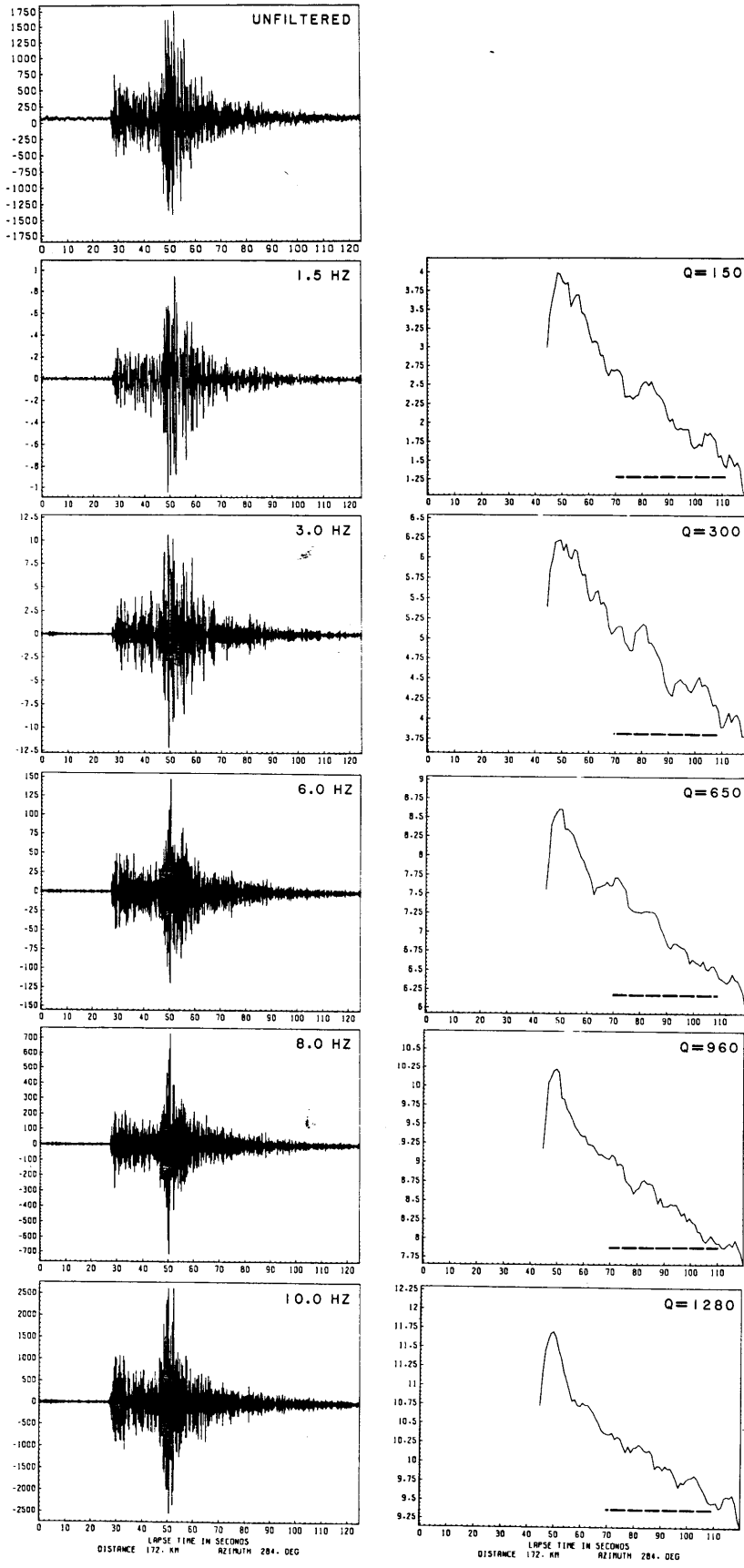


FIGURE 4.4

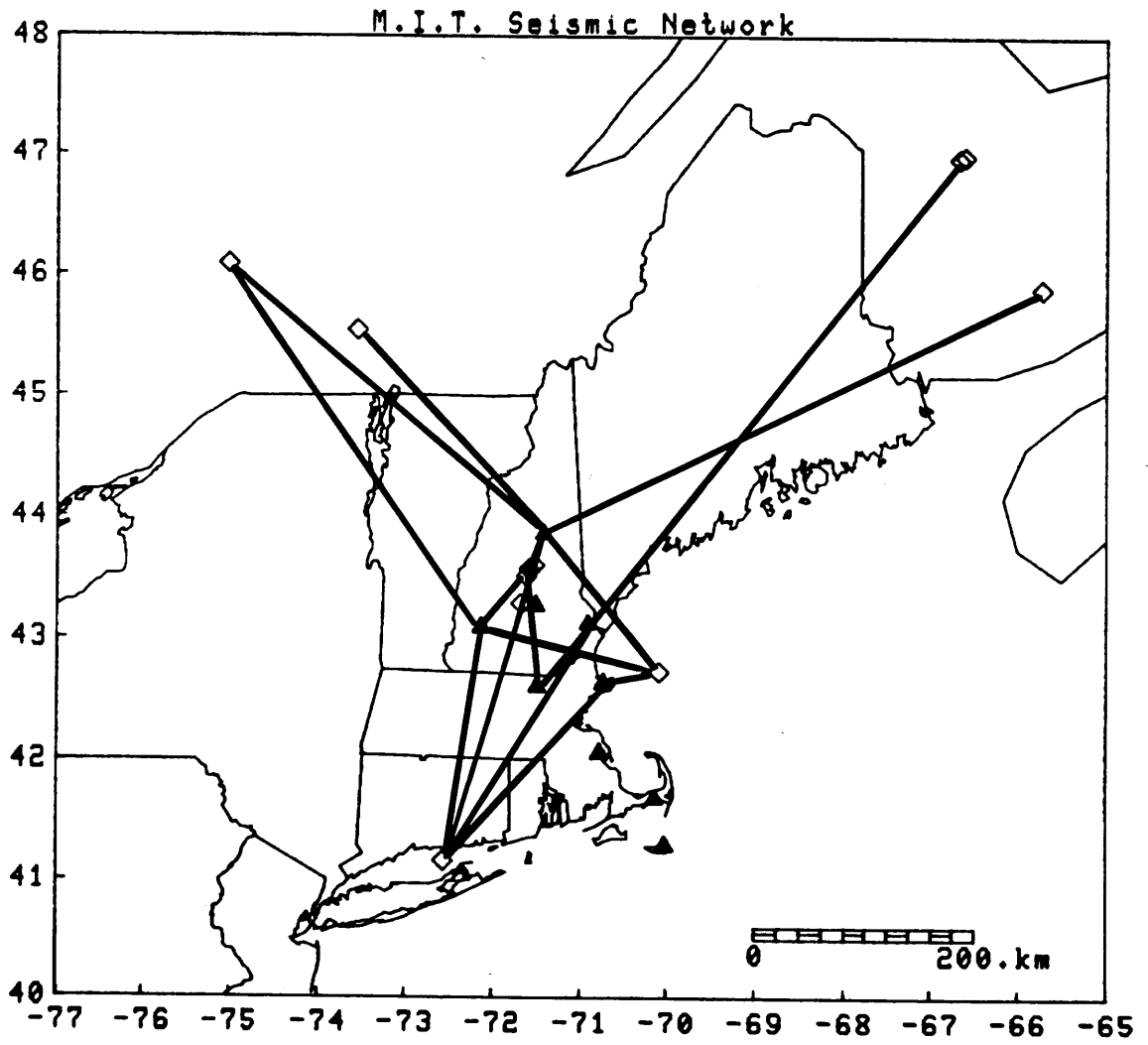


FIGURE 4.5

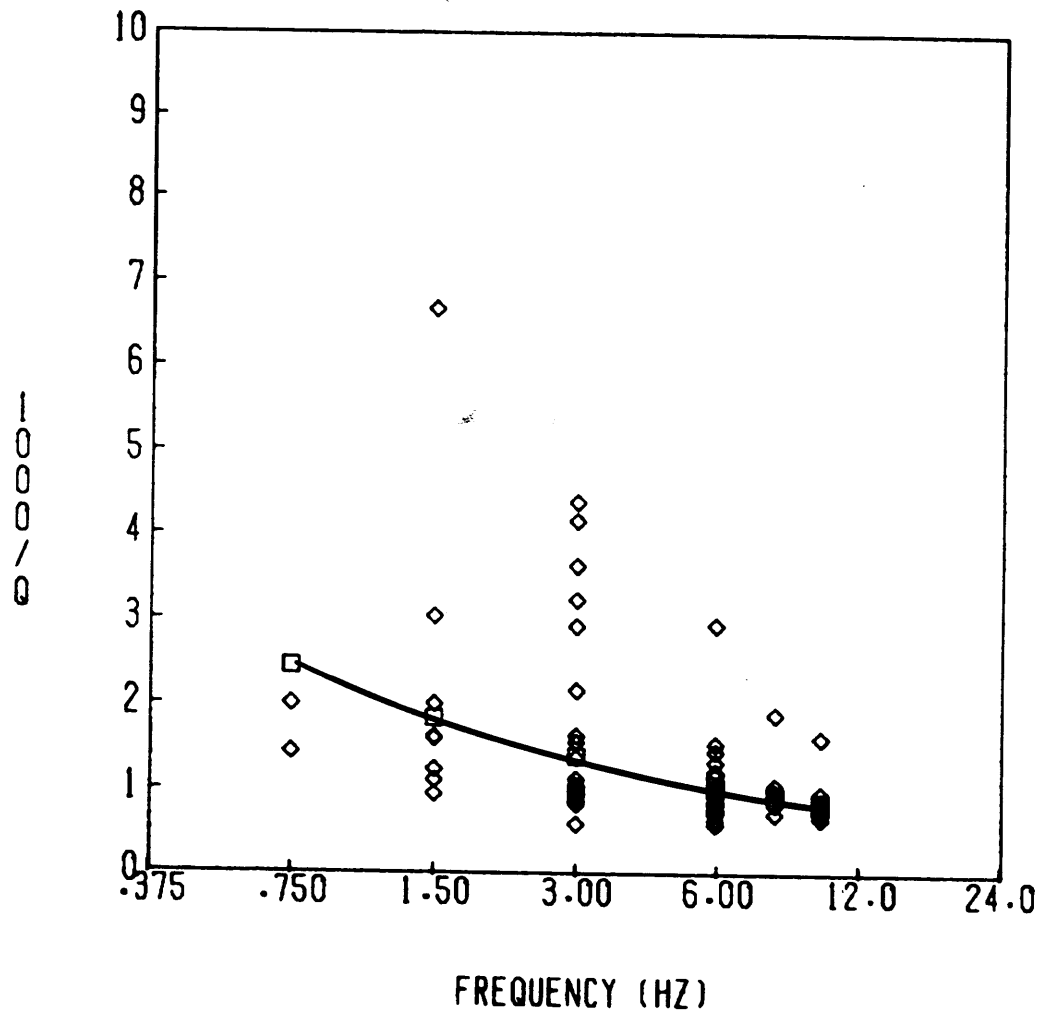


FIGURE 4.6

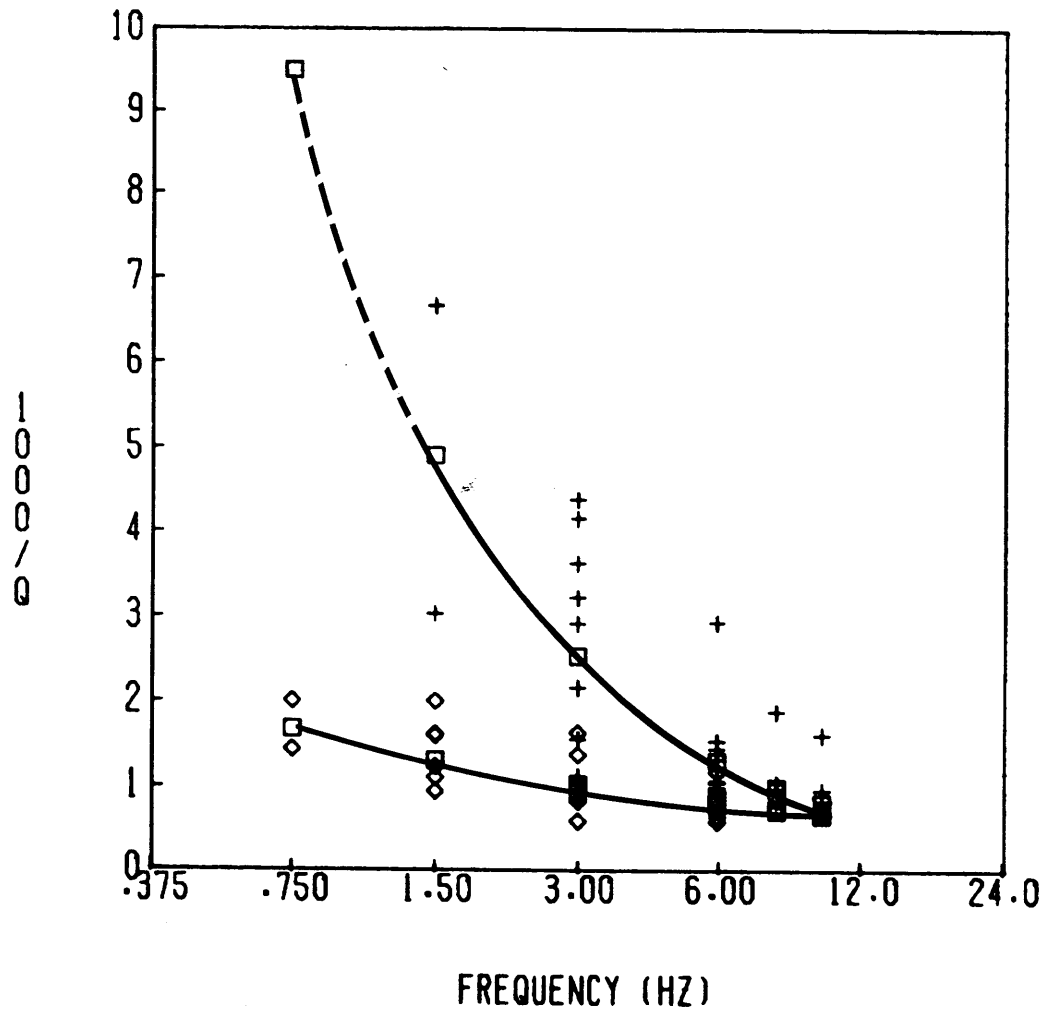


FIGURE 4.7

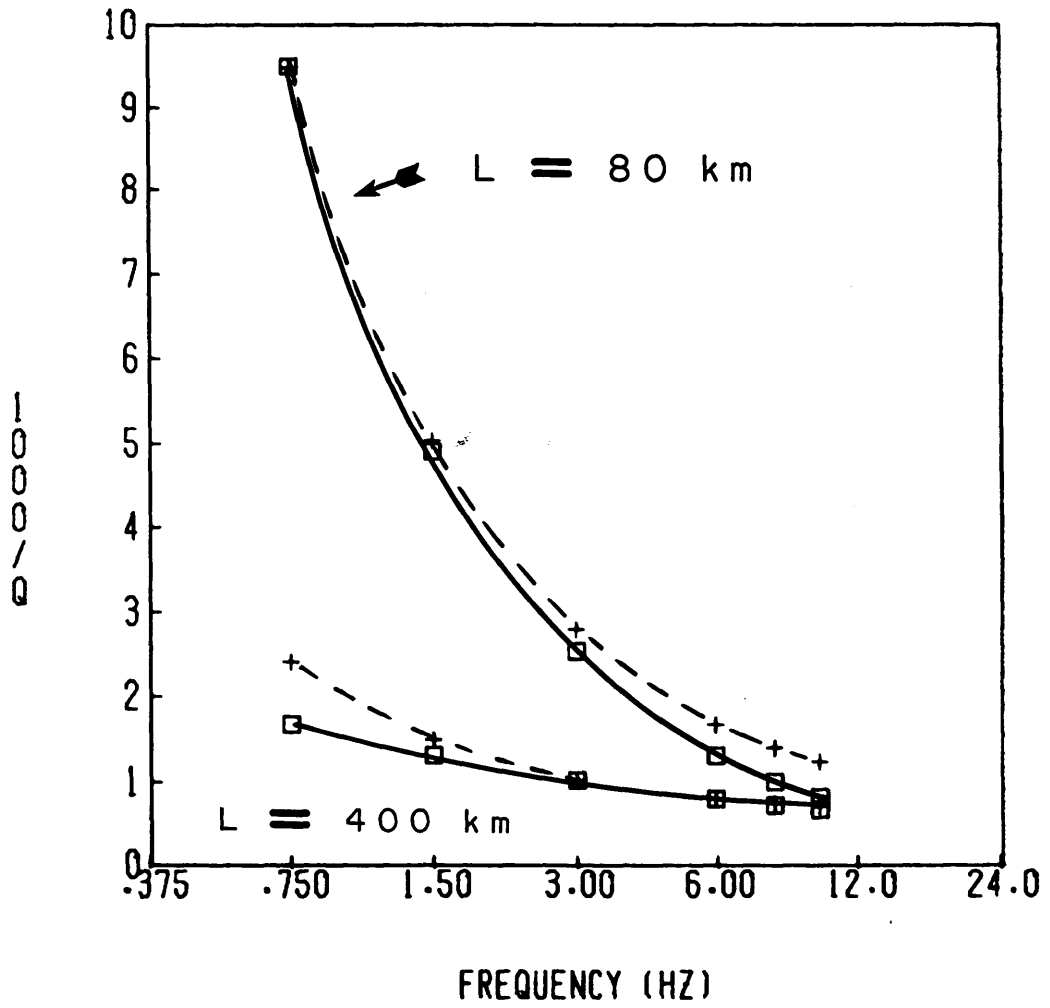


FIGURE 4.8

SMA SITES

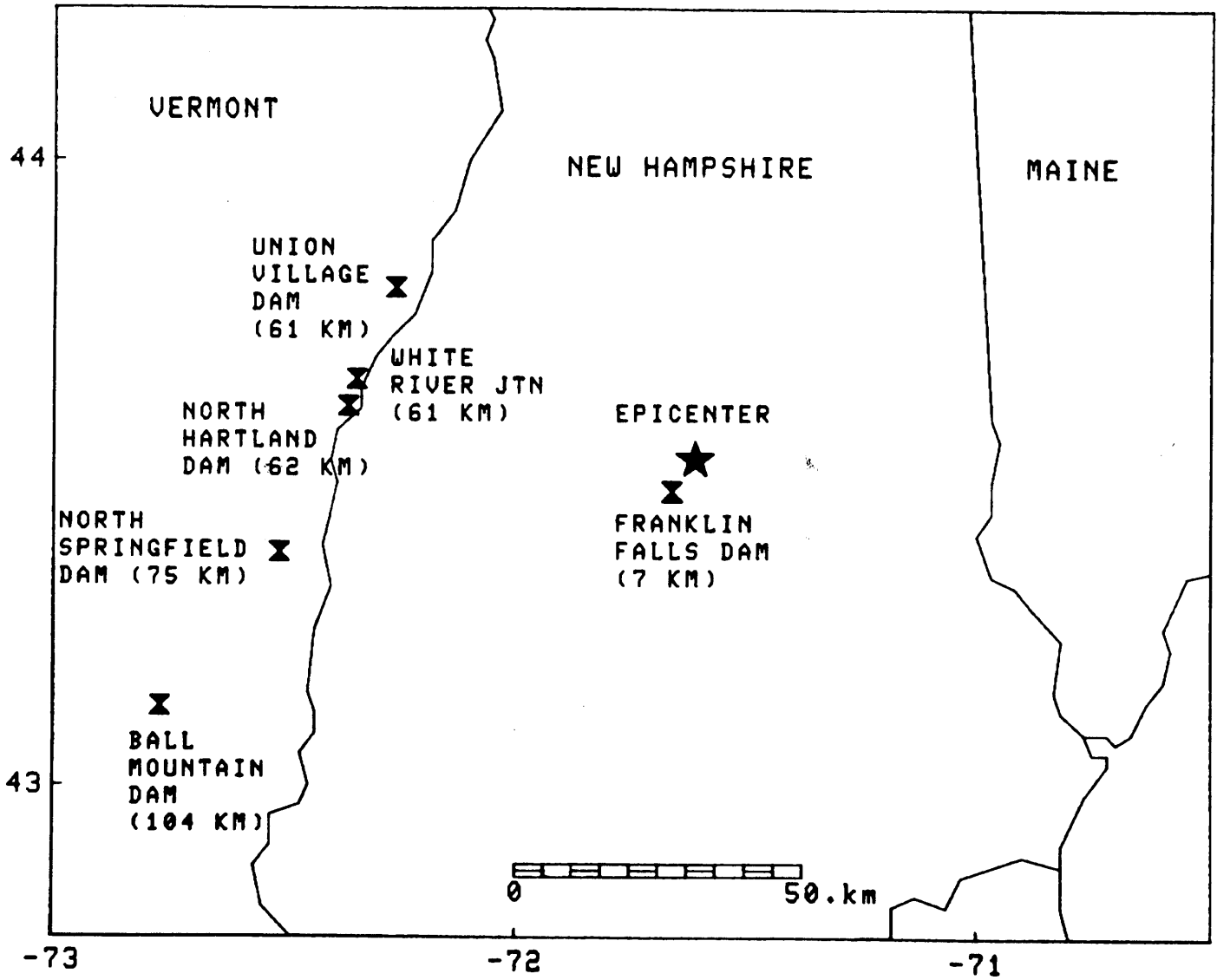


FIGURE 4.9

KLIMKIEWICZ (1982)

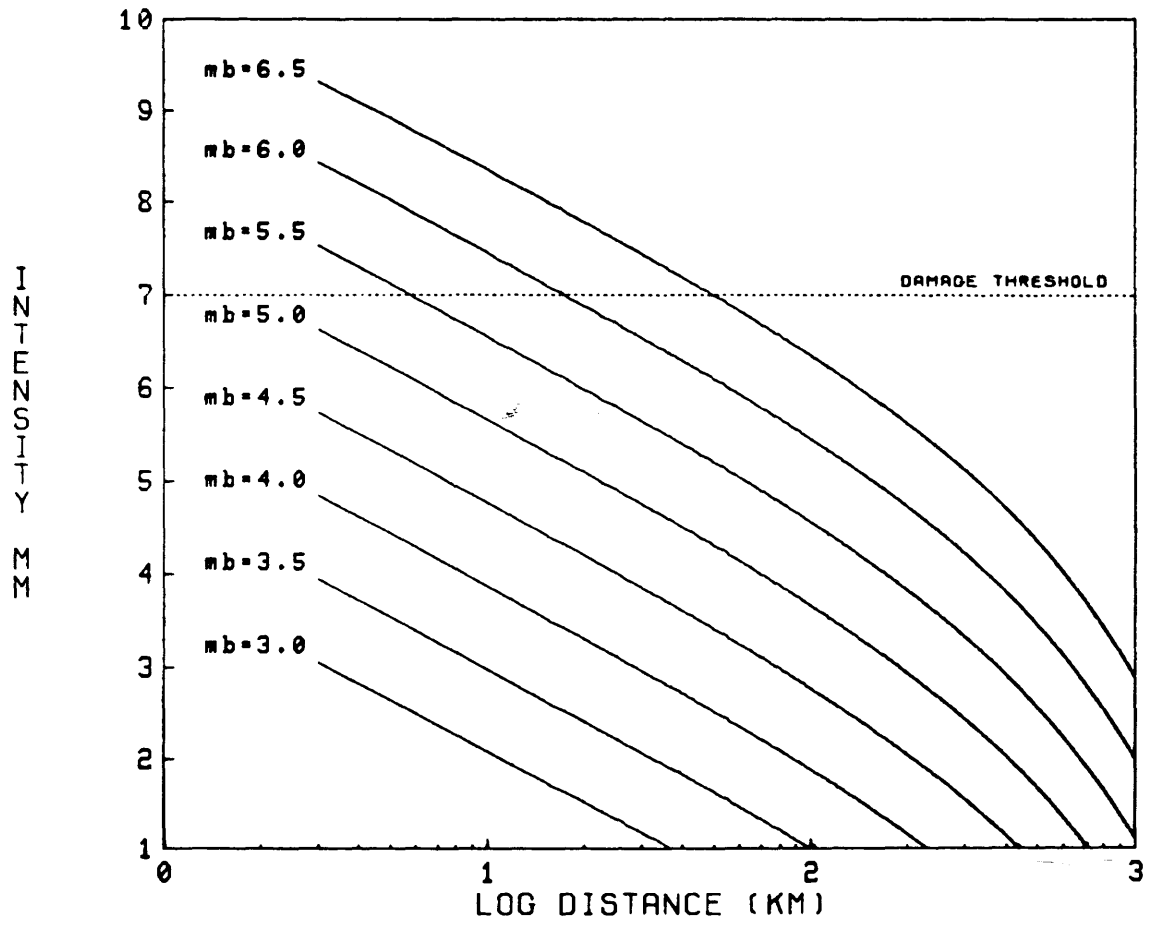


FIGURE 4.10

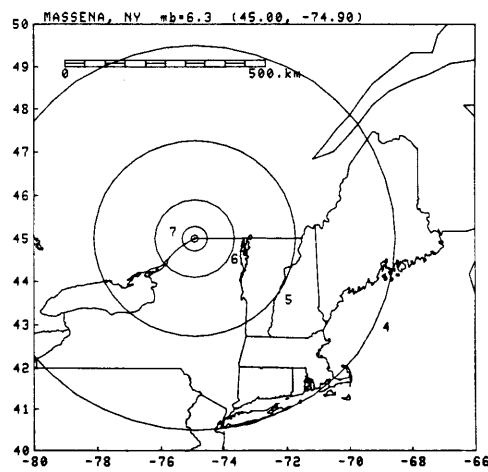
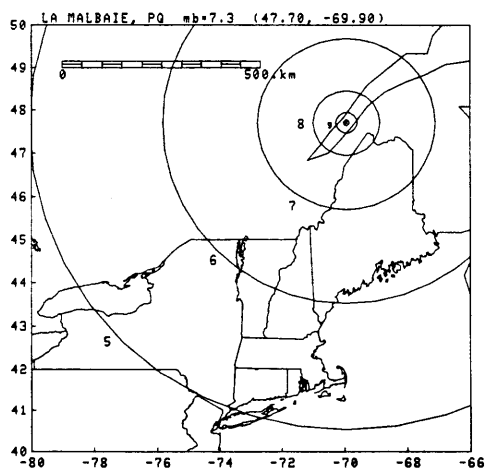
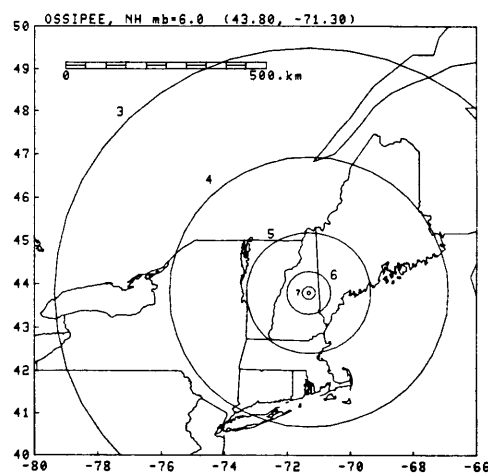
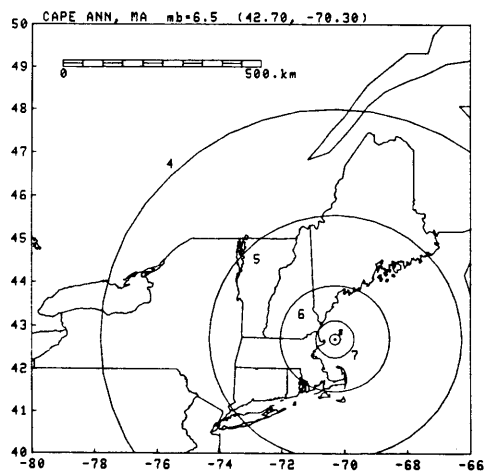


FIGURE 4.11

Klimkiewicz-McGuire

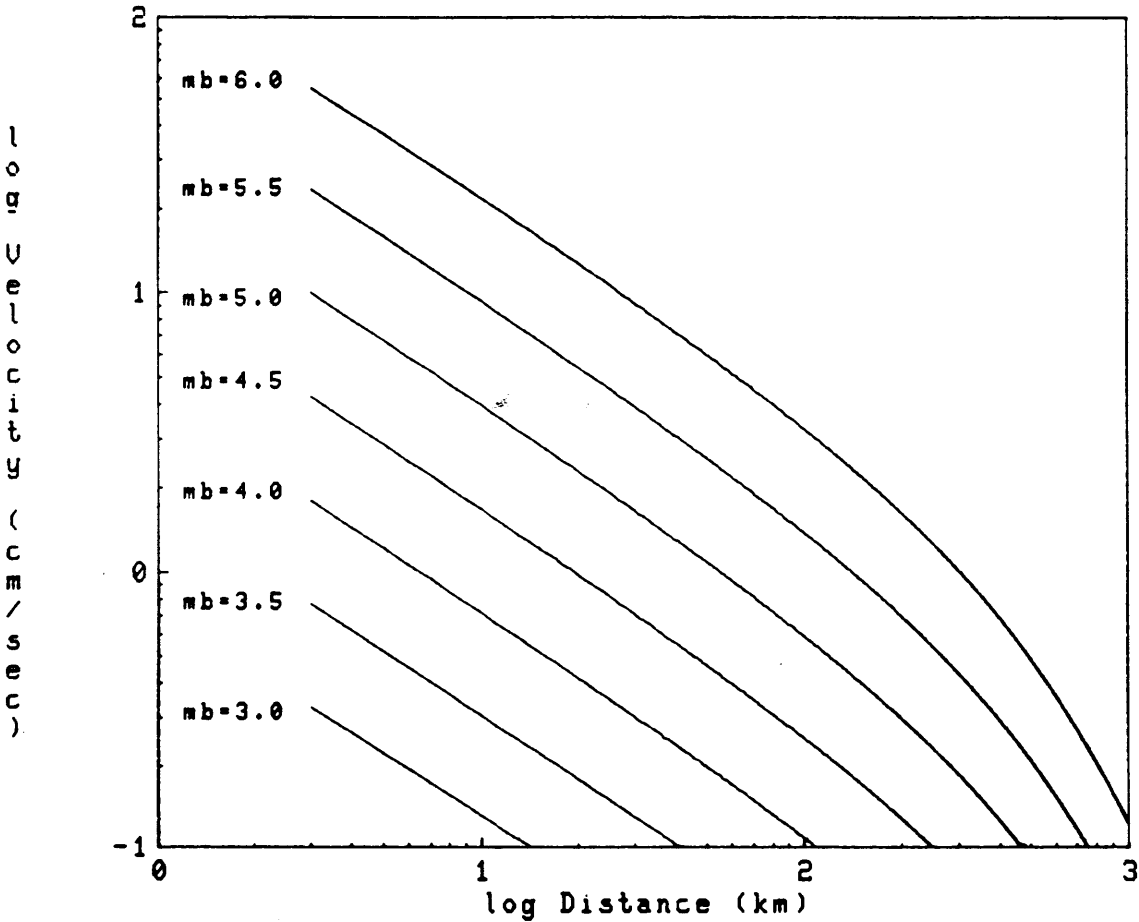


FIGURE 4.12

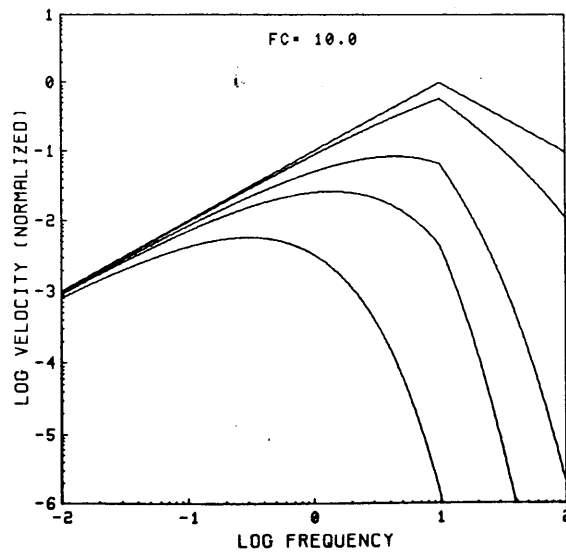
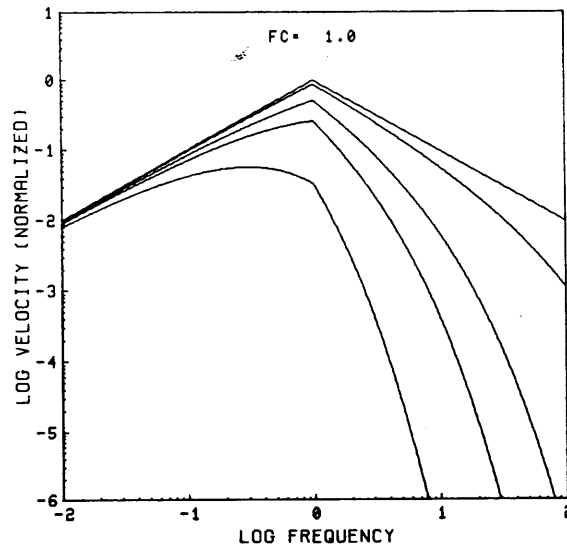
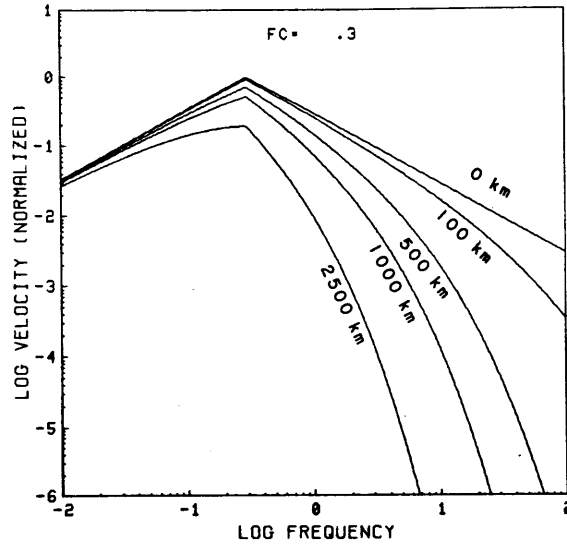


FIGURE 4.13

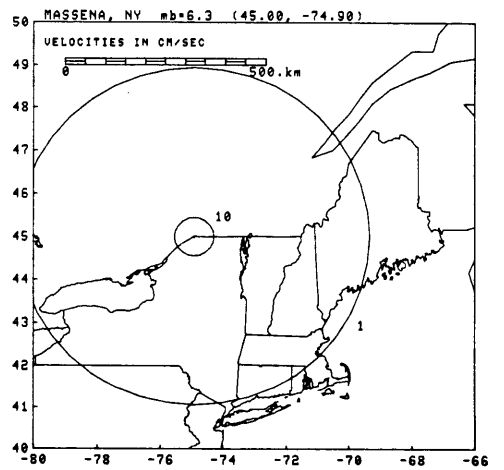
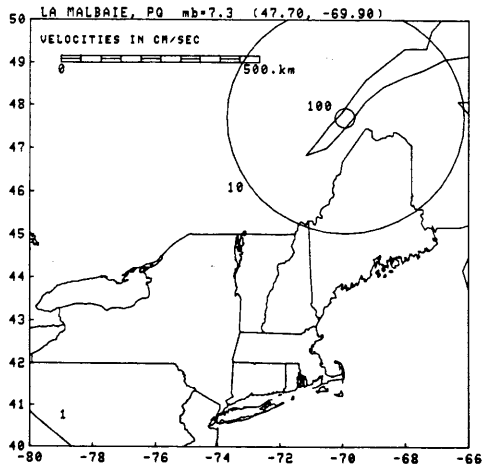
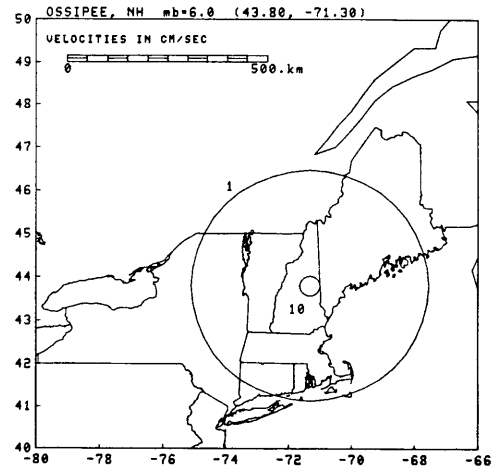
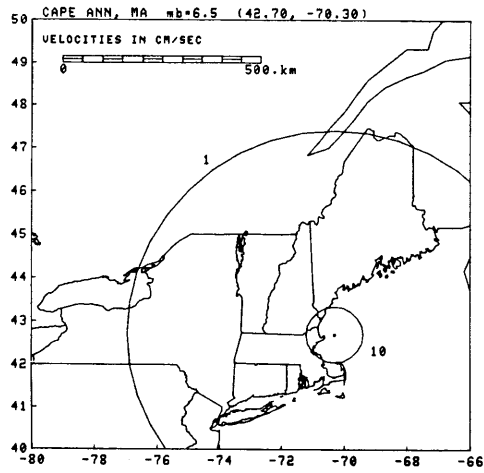


FIGURE 4.14

Klimkiewicz-McGuire

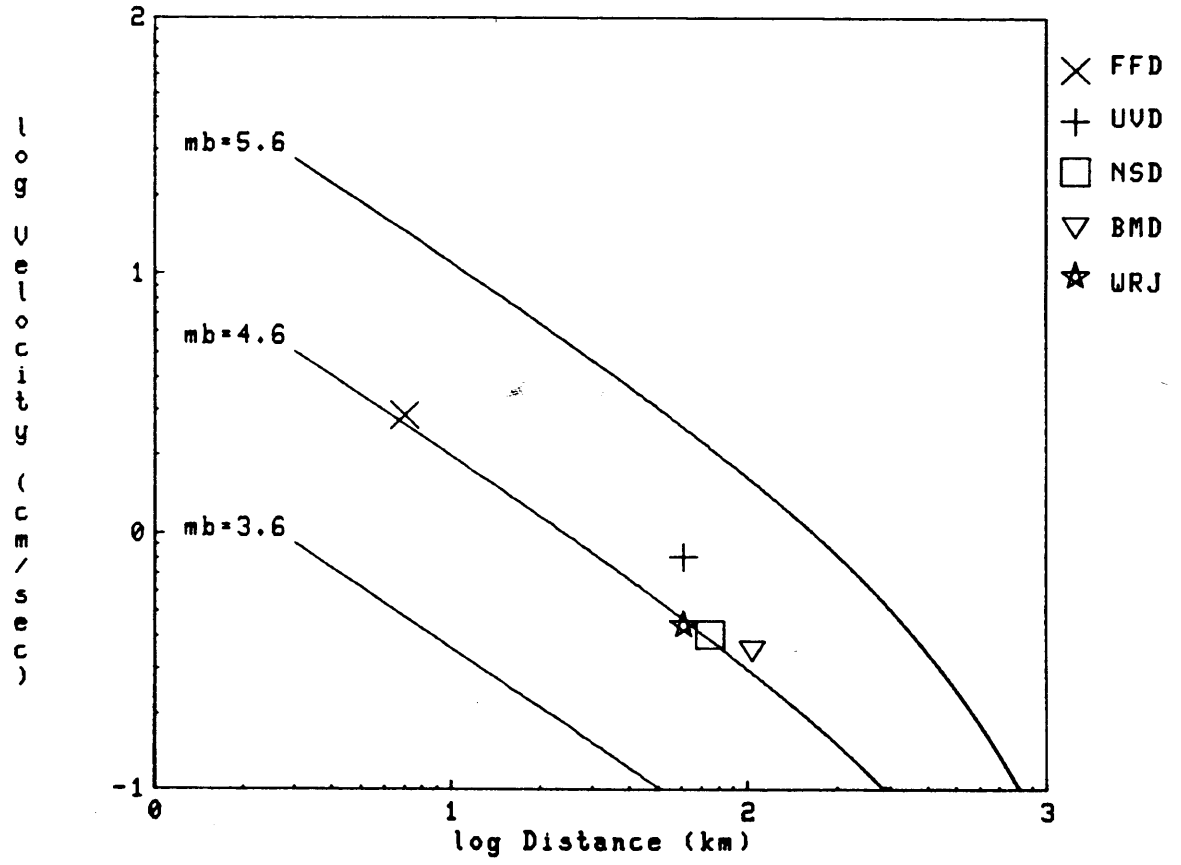


FIGURE 4.15

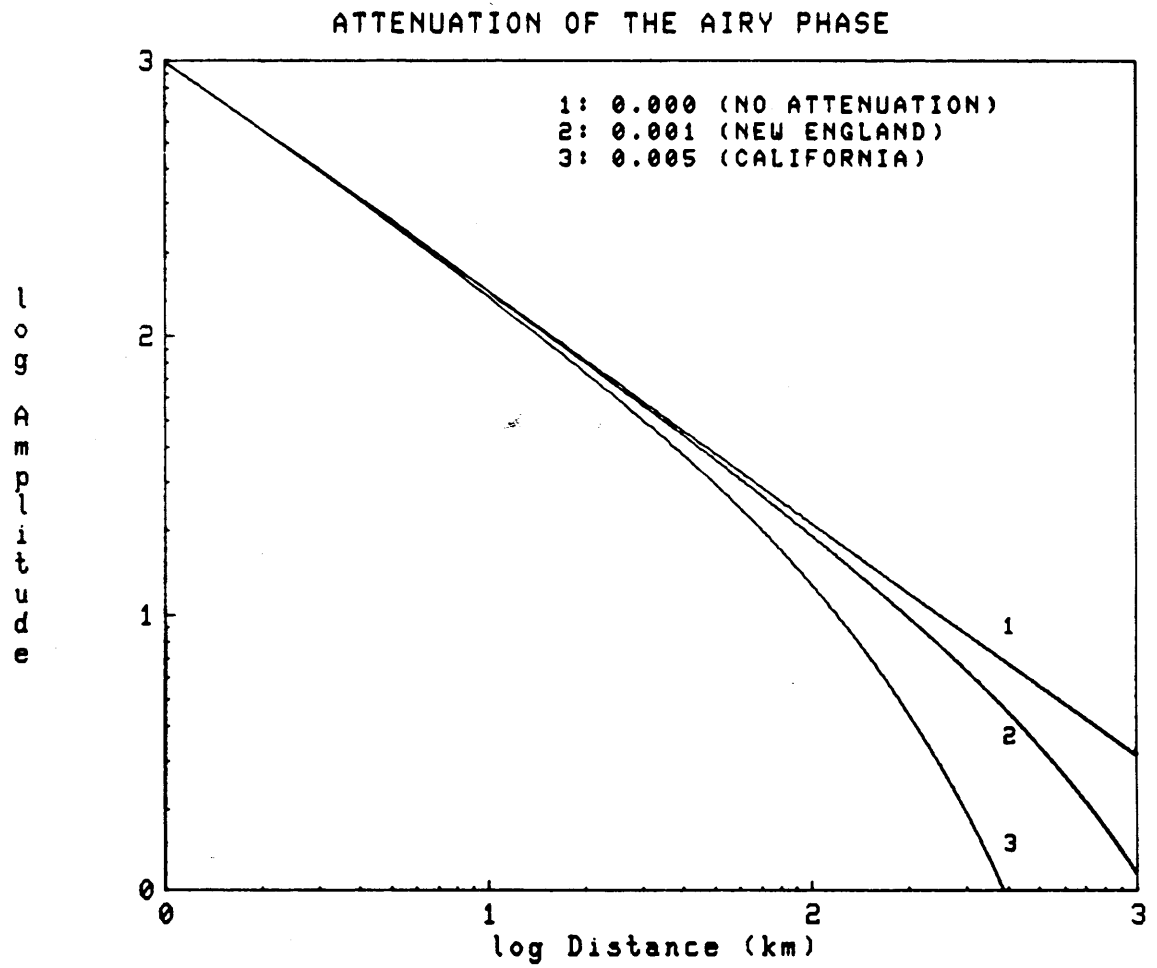


FIGURE 4.16

Klimkiewicz-McGuire

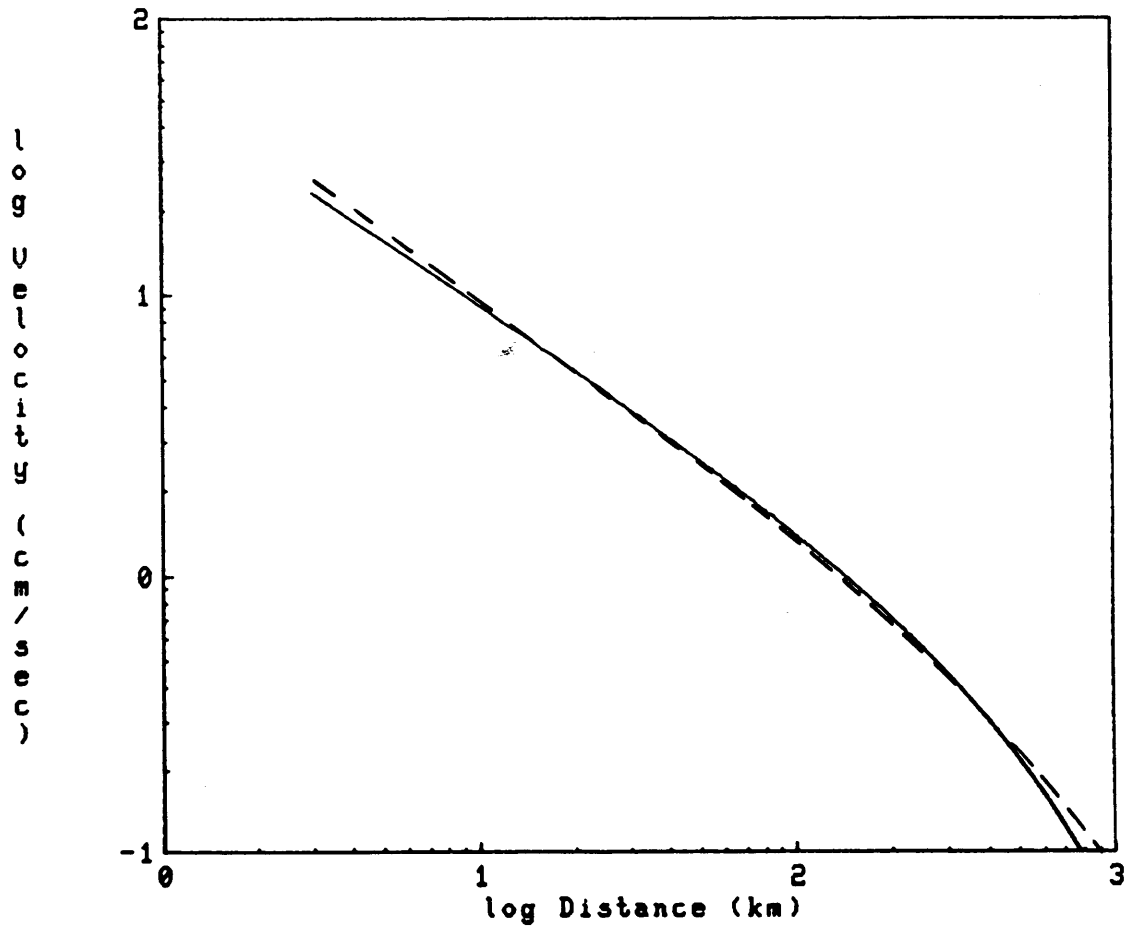


FIGURE 4.17

CHAPTER 5
SEISMOTECTONICS OF NORTHEASTERN NORTH AMERICA

5.1 Introduction

We now end our presentation of the analysis of NEUS-SEC seismicity, earthquake mechanisms, and seismic wave attenuation and turn our attention to summarization and interpretation. In this chapter, we examine the seismotectonic setting of northeastern North America and attempt to place the results of this thesis in geologic perspective. We begin with a review of the Paleozoic evolution of the northern Appalachians, which will lead us to a discussion of the crust and upper mantle structure of the area. Then, we compare and contrast the seismotectonic settings of the Grenville and Appalachian Provinces. Finally, we compare the seismotectonic setting of the NEUS-SEC with those of the central and southeastern US, two other areas where significant earthquake activity has taken place during the historical record.

5.2 Tectonic History and Crustal Structure

In this section, we examine the tectonic evolution of the northern Appalachians and discuss how this evolution has resulted in the variation of crustal structure across the study area. Then, we compare and contrast the seismic characteristics of the Grenville and Appalachian Provinces. For this comparison, we will examine the crustal structure, crustal stress regime, earthquake focal depths, earthquake mechanisms, seismic wave

attenuation, and the scattering properties of the crust and upper mantle.

5.2.1 *Tectonic History*

We now outline a possible scenario for the tectonic evolution of the northern Appalachians, drawing from both geological and geophysical evidence. For further information, the reader is advised to see the works of Taylor and Toksöz (1982b), Dietz (1972), Dott and Batten (1976), and Rogers (1970). The tectonic history outlined here is illustrated in Figure 5.1, reproduced from Taylor and Toksöz (1982b).

The tectonic development of the Appalachians begins about 800 million years ago (M.Y.A.) in the Late Precambrian when the North American-African continent split apart and the Iapetus Ocean (or proto-Atlantic) opened. As the North American plate receded from Africa and Europe, a continental margin developed (Figure 5.1a). This stable margin received sediments from the northwest and eventually developed into a miogeosyncline filled with shallow water sediments. A thick sequence of deep-sea volcanic deposits formed a eugeosyncline along the continental rise beyond the shelf, which was also likely fed from the African side.

At about 500 M.Y.A. in the early Ordovician, the Iapetus Ocean reversed its spreading trend and began to close. Subduction was initiated with an eastward dipping Benioff zone (Figure 5.1b) forming the Bronson Hill Anticlinorium, which was a site of major volcanic activity during this time period. In the

Middle and Late Ordovician, arc-continent collision resulted in the suturing of the island arc and inner arc basins with the continental lithosphere. This marked the climax of the so-called Taconic orogeny. This deformation affected rocks within and west of the Bronson Hill Anticlinorium (Figure 5.1c), overthrusting miogeosynclinal and eugeosynclinal sediments. At this time, the polarity of subduction reversed from southeast to northwest. This probably marks the beginning of the convergence of North America with the Avalon Block.

In the early Devonian (Figure 5.1d), increased tectonic activity took place as turbidite sequences were deposited in the major synclinoria of the area (such as the Littleton Formation of New Hampshire). This episode of activity climaxed with the Acadian Orogeny in the mid-Devonian when the Avalon Block collided with North America (Figure 5.1e). The compressive stresses of convergence collapsed the eugeosyncline of the continental rise and the deep-sea sediments were thrust up to form the ancient Appalachians.

Continued subduction during the Permian resulted in the collision of Gondwanaland with the North American plate. This episode, known as the Appalachian Orogeny, sutured all of the continents in the formation of Pangaea.

About 200 M.Y.A., rifting of the eastern margin of Pangaea formed the present Atlantic Ocean basin. New geosynclines formed, and the present continental shelf now occupies the site of the late Precambrian and early Paleozoic continental rise.

5.2.2 Crustal Structure

The complex evolution of the northern Appalachians and adjacent areas of the Grenville Province has resulted in significant variations in crustal structure. The crust and upper mantle in this area have been studied using P- and S- wave arrival times from local and regional earthquakes, teleseismic P-wave residuals, and surface wave dispersion (Taylor and Toksöz, 1979; Taylor *et al.*, 1980; Taylor and Toksöz, 1982b; Chiburis *et al.*, 1980; Curtin *et al.*, 1983).

These studies indicate that significant structural differences exist between the Grenville and Appalachian Provinces, and within the Appalachian Province itself. Some representative crustal models for the study area are shown in Figure 5.2. Models 1, 2, and 3 were determined for various subareas of the Appalachian Province, while models 4, 5, and 6 were determined in NY state west of the Appalachian-Grenville contact. A number of important differences are readily apparent in these models. For one thing, the models determined in the Appalachian Province show variations in both crustal thickness and velocity versus depth. Model 1, derived for CT and eastern MA (Chiburis *et al.*, 1980) shows that the crust in this area is thin (~ 35 km) with a thin, slow top layer of 5.31 km/sec (V_p) overlying layers of 6.06 and 6.59 km/sec. Model 2, from Taylor and Toksöz (1979), was determined for central New England (southern NH, northern MA, and western ME) and shows that the crust is thicker (~ 42 km), and has a deeper, slow top layer (5.7

km/sec) which overlies layers of 6.3 and 7.3 km/sec (V_p). Note that this high velocity lower layer is absent in Model 1 for southern New England. Model 3 was derived for northern New England using quarry blast sources in southern PQ and northern NH (Street, personal communication). This model is very similar to model 2 in terms of the sequence of layer velocities, yet the crust is somewhat thicker (~ 45 km). Note again the presence of the fast lower crustal layer.

Recent analyses of travel time data for earthquakes and quarry blasts in central NH confirms the general structure of models 2 and 3 (Curtin et al., 1983). Since the amount of data used in Curtin et al., (1983) is greater by a factor of 20, the results are more reliable. This study indicates that the top crustal layer is about 10 km thick with a P-wave velocity of 5.98 km/sec. This overlies a midcrustal layer of 6.5 km/sec, somewhat faster than those of models 2 and 3. The fast lower layer (~ 7.3 km/sec) can also be seen in this dataset, but the limited distance range precludes the determination of the total crustal thickness. However, a lower bound for this value would be 40 km.

Models 4, 5, and 6 were determined for the NY state area. These models show similarities in crustal thickness and velocity versus depth which appear to be fairly uniform across the Grenville Province. The models are very homogeneous with a nearly constant crustal velocity and thickness (~ 35 km). Model 5 which was derived for western NY does show some departures in

structure. Here, the average crustal velocity is somewhat lower than in the rest of the area (~ 6 km/sec).

5.2.3 *Contrasts Between Grenville and Appalachian Provinces*

We now compare and contrast the seismotectonic environments of the Grenville and Appalachian Provinces. For this comparison, we will consider the crustal structure, crustal stress regime, earthquake mechanisms, earthquake focal depths, and the seismic wave attenuation and scattering properties of the crust and upper mantle. We will discuss each of these subjects separately, however a summary is presented in Table 5.1 for quick reference and comparison.

Crustal Structure: As reviewed in the previous section, there are significant differences in the crustal structure of the Grenville and Appalachian Provinces. The crust of the Grenville Province is vertically homogeneous with nearly constant P- and S-wave velocities of 6.6 and 3.7 km/sec, respectively. The average crustal thickness is 37 km. However, the Appalachians are characterized by a two or three layer crust, with a relatively high velocity lower layer. The upper crustal layer is approximately 15 km thick and has P- and S-wave velocities of 6.1 and 3.6 km/sec, respectively. This layer overlies a high velocity lower crust with P- and S-wave velocities of 7.0 and 4.1 km/sec, respectively. The average crustal thickness in the Appalachians is 40 km.

Crustal Stress Regime: In Chapter 3, we determined fault plane solutions for ten NEUS earthquakes and reviewed published

data on fault plane solutions and in-situ stress measurements. The dataset compiled included 53 earthquake fault plane solutions and 18 non-seismic stress measurements. From this dataset, the crustal stress field in the Grenville Province has been determined to be compressive, horizontal, and oriented in an ENE-WSW direction (N64E). This stress field is highly uniform, with a standard deviation of +/- 18 degrees. In the Appalachian Province, the stress field is also compressive and horizontal, but trends in an approximate E-W direction (N98E) and is highly variable (+/- 41 degrees). This complicated stress field is likely due to a combination of factors, such as the complicated topography, crustal structure, and the presence of small crustal blocks formed during the complex tectonic history of the area.

Earthquake Mechanisms: The earthquake mechanisms in each area will be a reflection of both the local stress field and the orientation of pre-existing faults and weak zones with respect to this stress field. In the Grenville Province, earthquake mechanisms are uniform over broad areas. For example, in the Western Quebec Seismic Zone where the faults are oriented in a northwesterly direction, the earthquake mechanisms are generally pure thrust faulting with slip vectors parallel to the present stress field. In western NY where the faults are oriented more N-S and NE-SW, the resulting earthquake mechanisms exhibit some degree of strike-slip motion in response to the uniform stress field. In the Appalachian Province, where the stress field and the geology are very complicated, the earthquake mechanisms

change from thrust faulting to strike-slip faulting over short distances. However, most events share the common feature of a N-S or NE-SW trending fault plane as one of the two possibilities resulting from each fault plane solution. In other words, most events may be occurring on N-S or NE-SW fault planes parallel to the principal trend of the geology, but the complicated stress pattern results in a wide variety of faulting mechanisms.

Earthquake Focal Depths: In Chapter 2, we reviewed the available focal depth information in the NEUS-SEC, drawing from published works in a number of subareas and our own estimates of focal depths for six New England earthquakes. The general picture which emerged from this review was that in the Grenville Province, earthquake focal depths range from the near surface to as much as 20 km. However, in the Appalachian Province, known focal depths are all less than 10 km with the majority of events occurring in the upper 5 km of the crust.

Seismic Wave Attenuation: In Chapter 4, seismic wave attenuation was measured in the Appalachian Province using narrow band pass filtered seismograms and the time rate of decay of coda wave amplitudes. The results indicate that Q_c obeys the relationship $Q_c(f) = 660(f)^{0.40}$. Thus, at 1 Hz, $Q_c = 660$ and at 10 Hz, $Q_c = 1500$. The corresponding relationship for the Grenville Province is $Q_c(f) = 1000(f)^{0.20}$ (Singh and Herrmann, 1983). In the Grenville Province, Q_c at 1 Hz is 1000, and at 10 Hz, Q_c is 1600. Thus at 1 Hz the seismic wave attenuation in the Appalachian Province is 50% greater than in the Grenville

Province. However, at 10 Hz, the seismic wave attenuation is equal in both areas.

Scattering of Seismic Waves: In the Grenville Province, estimates of the scattering of seismic waves based on the frequency dependence of Q_c indicate that the mean free path is on the order of 600 km for 1 Hz waves and 80 km for 10 Hz waves. In the Appalachian Province, the mean free path ranges from 300 km at 1 Hz to 90 km at 10 Hz. Thus, the crust and upper mantle of the Appalachian Province is much more heterogeneous than in the Grenville Province.

5.3 Comparison With Other Eastern US Seismotectonic Environments

In the past ten years there has been a tremendous increase in the study of seismicity earthquake hazards in the eastern US. This has come about because of increased awareness among the public and scientific communities of the hazards posed by earthquakes in the east to critical facilities. These new studies have been conducted in both the geological and geophysical disciplines.

The NEUS-SEC is probably not the most seismically active region of the eastern US. This distinction likely goes to the New Madrid, MO area of the central US. Other areas where destructive earthquakes have occurred include Charleston, SC and Giles County, VA. In this section, we review the recent studies of seismicity in these areas and compare their seismotectonic settings with that of the NEUS-SEC.

5.3.1 *New Madrid, MO*

In the winter of 1811-1812, three earthquakes struck the New Madrid, MO area. The largest earthquake reached intensity XII, and is estimated to have been of magnitude 7.2 (mb) ($M_s \sim 8.0$) (Nuttli, 1973b). Because of the occurrence of this earthquake and the persistent minor seismicity which continues today, this region of the central US was one of the first areas to be intensely studied with a telemetered seismic network (Stauder et al., 1976).

New Madrid seismicity is concentrated in the northern Mississippi Embayment, which is a south-plunging trough of Cenozoic and Upper Cretaceous sedimentary rocks. The seismicity, shown in Figure 5.3, defines three distinct lineations: a northeast striking zone that extends for 100 km from Marked Tree, AR to Caruthersville, MO; a north to northwest striking zone from Ridgely, TN to west of New Madrid; and a northeast trending zone extending from New Madrid to Charleston, MO. Fault plane solutions for earthquakes in this area determined by Herrmann (1979) and Herrmann and Canas (1978) indicate right-lateral movement on the northeast striking zones and reverse motion on the north-northwest zone. This movement is consistent with deformation caused by east-west compression, the present compressive stress regime in the central US (Zoback and Zoback, 1981).

Magnetic surveys in this area indicate the presence of a 70 km wide by 200 km long graben structure which formed during an

episode of continental rifting before the Late Cambrian. The 100 km long seismic trend coincides with the axis of this graben. There are also several mafic plutons near the margins of the graben (Zoback et al., 1981). These plutons were emplaced between the Ordovician and the Late Cretaceous, indicating an episode of renewed activity along the pre-existing zone of weakness. Additional rift activity may have occurred in the Mesozoic as indicated by intrusives of Late Cretaceous age in central Arkansas and by normal faulting of Upper Cretaceous sedimentary rocks (Zartman, 1977). These various stages of rifting along the embayment ended after the Late Cretaceous. Zoback et al., (1980) showed seismic reflection profiles indicating reverse movement after the middle Eocene on a northeast striking fault.

The seismicity of the New Madrid area can be explained in terms of fault movement in response to the present NE-SW compressional stress field. The primary difference between the seismicity of New Madrid and that of New England is that the hypocenters line up on structural features which can be delineated both geologically and in seismic reflection profiles.

5.3.2 *Giles County, VA*

On May 31, 1897 an earthquake in Giles County caused intensity VIII damage in this southwest VA area. Bollinger and Hopper (1971) and Nuttli et al. (1979) estimate that this earthquake was of body wave magnitude 5.8. This is the largest known earthquake to have occurred in VA and thus serves as the

design earthquake for many engineering projects in this part of the Appalachians. Geologically, Giles County consists of northeasterly trending structures of the Valley and Ridge Province. Unmetamorphosed sedimentary rocks are of Cambrian through Pennsylvanian ages, with the upper several kilometers of rocks folded and detached from the basement by thrusting many kilometers to the northwest. The depth of the detachment ranges from 3 km in the north to 6 km in the south. The folding of the Paleozoic rocks in this area was caused by compression from the east during the Appalachian orogeny.

Important new information about the seismicity of Giles County has been recently obtained from dense seismograph network monitoring (Bollinger and Wheeler, 1983). They used velocity models developed specifically in this area to determine accurate hypocentral locations for a number of microearthquakes. The distribution of the foci defines a nearly vertical, tabular zone 40 km long, 10 km wide, and extending from 5 to 25 km in depth (see Figure 5.4). This tabular zone is in the metamorphic and igneous basement beneath the thrust masses. Furthermore, the strike of this tabular zone departs by about 30 degrees from the general trend of the geology in the area, being more closely aligned with the structural trends further north. Bollinger and Wheeler (1983) believe that the 1897 earthquake may have been located in this tabular fault zone.

Such a tabular fault zone in the basement could only have been produced during a few times in the geologic history of the

region. It is unlikely that this fault zone is older than the Late Precambrian, since such a fault would have been healed or deformed during the Grenville orogeny (~ 1.1 B.Y.A.). However, as the Iapetus Ocean opened in the Late Precambrian, extensional faults formed both west and east of Giles County. Bollinger and Wheeler (1983) believe that such a fault, reactivated under the present stress regime, is the likely source of the tabular zone of seismicity.

There is no evidence to date to suggest that the seismic environment in New England is similar to that in Giles County. In New England, the seismicity is shallow and appears to occur in the overthrust masses. However, the seismicity of Giles County may be similar to that of the Charlevoix Seismic Zone where the earthquakes occur at depths down to 20 km and all are in the Precambrian basement.

5.3.3 *Charleston, SC*

Charleston, SC was the site of the second largest (intensity) earthquake to occur in the eastern US. This event, which struck in 1886, reached intensity X and is estimated to have been of magnitude 6.6 to 6.9 (mb) (Nuttli et al., 1979). Charleston is situated in the Atlantic Coastal Plain on a wedge of Cenozoic and Upper Cretaceous sedimentary rocks. Drilling in the area (Gohn et al., 1977) has shown that the coastal plain sediments are underlain by a basaltic layer of Jurassic age which overlies red-bed deposits of Mesozoic age. Seismic refraction, magnetic, and gravity data provide evidence that Mesozoic rifting

occurred in the Charleston area during the opening of the Atlantic.

Seismic network monitoring began in this area in 1977, however the seismicity has been at such a low level that few insights have been provided by the instrumental data. Earthquake focal depths range from 3 to 13 km, which suggests that the 1886 earthquake may have occurred in the upper crust. Fault plane solutions could provide important information on the nature of the faulting. The three available solutions indicate a northwest striking nodal plane and a subhorizontal nodal plane.

Recent COCORP seismic reflection profiling in the southern Appalachians indicates that the platform rocks overlying the Grenville basement can be traced beneath the Blue Ridge and continues at least 150 km to the east (Cook et al., 1979). Because the northern and southern Appalachians show many contrasts in structural style, it may not be possible to extrapolate the findings to the northern Appalachians.

Table 5.1
Seismic Characteristics of the NEUS-SEC
Comparison of Grenville and Appalachian Provinces

	<u>Grenville Province</u>	<u>Appalachian Province</u>
Crustal Structure	Uniform 1 layer Thickness 37 km	2 - 3 layers High vel. lower layer Thickness 40 km
Stress Regime	Uniform horiz. compression ENE-WSW	Horiz. compression Direction highly variable.
Earthquake Mechanisms	Mostly thrust and strike-slip. Uniform over broad areas.	Thrust and strike-slip. Mechanisms change over short distances.
Focal Depths	0 - 20 km	0 - 10 km Most < 5 km
Attenuation	Q(1 Hz) = 1000 Q(10 Hz) = 1600	Q(1 Hz) = 660 Q(10 Hz) = 1500
Scattering	Lmin = 600 km at 1 Hz, 80 km at 10 Hz	Lmin = 300 km at 1 Hz, 90 km at 10 Hz

Figure Captions

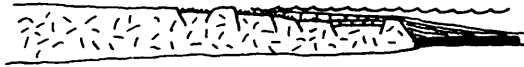
Figure 5.1 Plate tectonic model of the evolution of the northern Appalachians, reproduced from Taylor and Toksöz (1982b).

Figure 5.2 Northeast US crustal models. References are: 1) Chiburis et al. (1980), 2) Taylor and Toksöz (1979), 3) Weston Geophysical Corp. (personal communication), and 4), 5), and 6) Yang and Aggarwal (1981).

Figure 5.3 The seismicity of the New Madrid seismic zone, reproduced from Stauder et al. (1976).

Figure 5.4 Distribution of earthquake hypocenters in the Giles County, VA seismic zone, reproduced from Bollinger and Wheeler (1983).

EOCAMBRIAN - EARLY ORDOVICIAN



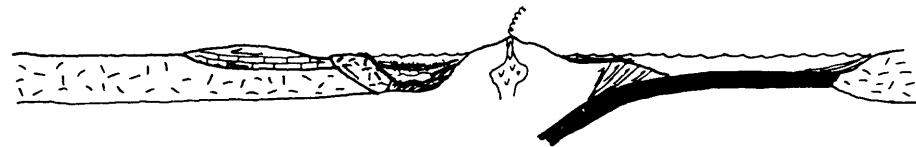
EARLY - MIDDLE ORDOVICIAN



MIDDLE ORDOVICIAN TACONIC OROGENY



SILURIAN - EARLY DEVONIAN



MIDDLE DEVONIAN ACADIAN OROGENY



FIGURE 5.1

NEUS CRUSTAL MODELS

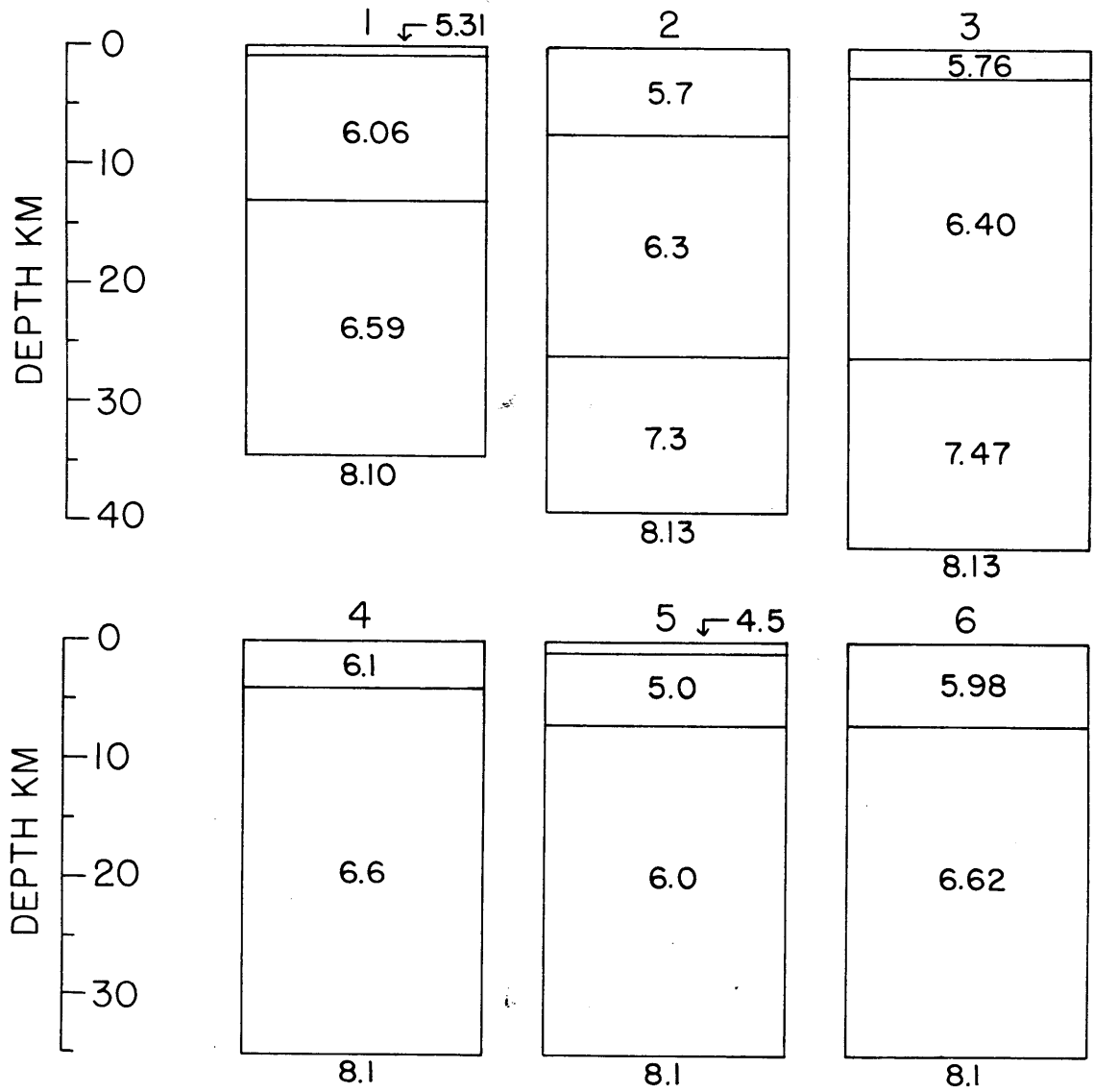


FIGURE 5.2

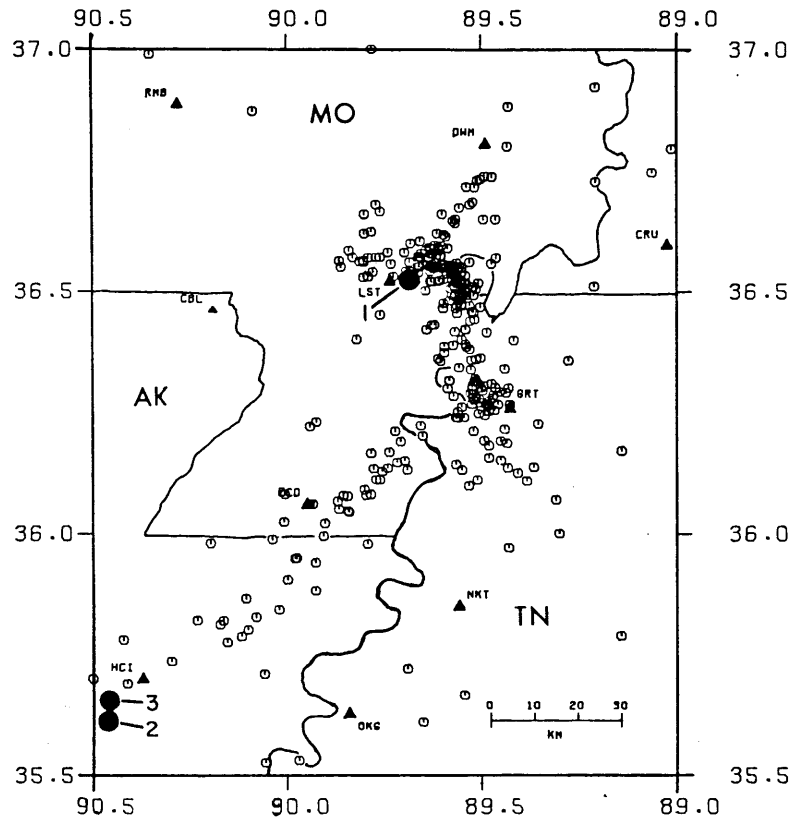


FIGURE 5.3

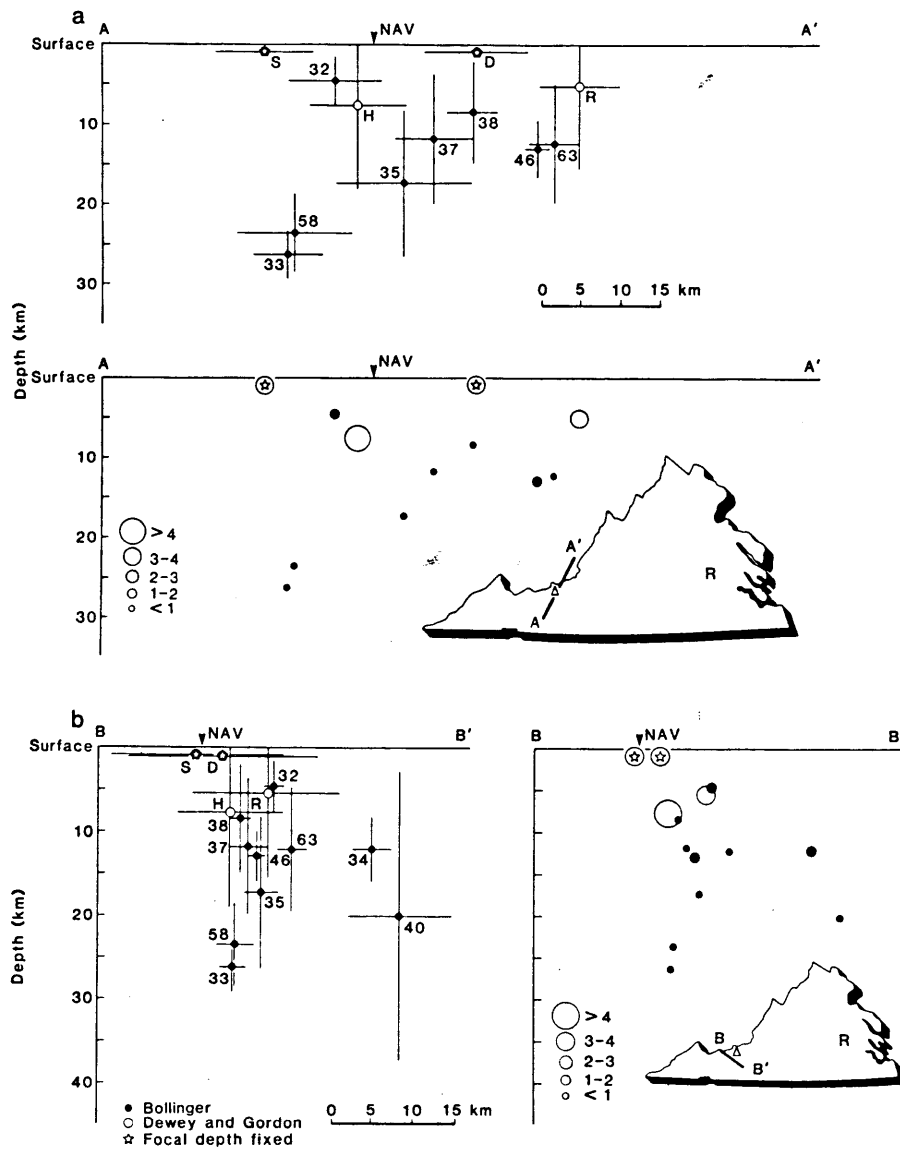


FIGURE 5.4

REFERENCES
(Includes those from the Appendices)

- Acharya, H. (1980a), Possible minimum depths of large historical earthquakes in eastern North America, Geophys. Res. Letters, 7, 619-620
- Acharya, H. (1980b), Spatial correlation of large historical earthquakes and moderate shocks >10 km deep in eastern North America, Geophys. Res. Letters, 7, 1061-1064
- Aggarwal, Y.P. and Sykes, L.R. (1978), Earthquakes, faults, and nuclear power plants in southern New York - northern New Jersey, Science, 200, 425-429
- Aki, K. (1965), Maximum likelihood estimate of b in the formula $\text{Log}(N)=a-bM$ and its confidence limits, Bull. Earthquake Res. Inst. Tokyo Univ., 43, 237-239
- Aki, K. (1969), Analysis of the seismic coda of local earthquakes as scattered waves, J. Geophys. Res., 74, 615-631
- Aki, K. (1980a), Attenuation of shear waves in the lithosphere for frequencies from 0.05 to 25 Hz, Phys. Earth Planet. Inter., 21, 50-60
- Aki, K. (1980b), Scattering and attenuation of shear waves in the lithosphere, J. Geophys. Res., 85, 6496-6504
- Aki, K. and Chouet, B. (1975), Origin of coda waves: source, attenuation, and scattering effects, J. Geophys. Res., 80, 3322-3342
- Albert, R.L., Chiburis, E.F., and Frohlich, R.K. (1976), Intensity and magnitude determination of the Portsmouth, Rhode Island earthquake of March 11, 1976, Earthquake Notes, 47, No. 3, 21-28
- Alexander, S.S. (1981), Use of wide angle reflections and mode converted phases to map lateral variations in crustal structure, (abstract), Earthquake Notes, 52, No. 3, 8
- Andrews, J.T. (1970), Present and postglacial rates of uplift for glaciated northern and eastern North America derived from postglacial uplift curves, Can. J. Earth Sci., 7, 703-715
- Basham, P.W., Weichert, D.H., and Berry, M.J. (1979), Regional assesment of seismic risk in eastern Canada, Bull. Seis. Soc. Amer., 69, 1567-1602

- Bath, M. (1982), Seismic energy mapping applied to Turkey, Tectonophysics, 82, 69-87
- Beauchamp, K.G. (1975), Walsh Functions and Their Applications, Techniques of Physics Series, No. 3, Academic Press, 236 pp.
- Block, J.W., Clement, R.C., Lew, L.R., and de Boer, J. (1979), Recent thrust faulting in southeastern Connecticut, Geology, 7, 79-82
- Bollinger, G.A. and Hopper, M.G. (1971), Virginia's two largest earthquakes - December 22, 1875 and May 31, 1897, Bull. Seis. Soc. Amer., 61, 1033-1039
- Bollinger, G.A. and Wheeler, R.L. (1983), The Giles County, Virginia seismic zone, Science, 219, 1063-1065
- Bouchon, M. (1982), The complete synthesis of seismic crustal phases at regional distances, J. Geophys. Res., 87, 1735-1741
- Brasch, F.E. (1916), An earthquake in New England during the colonial period (1755), Bull. Seis. Soc. Amer., 6, 26-42
- Brigham, W.T. (1871), Volcanic manifestations in New England, Boston Soc. Nat. Hist. Mem., 20, 1-28
- Brooks, J.W. (1960), A study in seismicity and structural geology, part II - earthquakes of the northeastern U.S. and eastern Canada, Bulletin of Geophysics, College Jean - de - Brebeuf, No. 7, 12-40
- Caputo, M. (1974), Analysis of seismic risk, in Engineering Seismology and Earthquake Engineering, NATO Advanced Study Inst. Series E, Applied Sciences, No. 3, 55-86
- Chadwick, G.H. (1920), Large fault in western New York, Geol. Soc. Amer. Bull., 31, 117-120
- Chandra, U. (1979), Attenuation of intensity in the United States, Bull. Seis. Soc. Amer., 69, 2003-2024
- Chang, A.C. and von Seggern, D.H. (1980), A study of amplitude anomaly and mb bias at LASA subarrays, J. Geophys. Res., 85, 4811-4828
- Chaplin, M.P., Taylor, S.R., and Toksöz, M.N. (1980), A coda-length magnitude scale for New England, Earthquake Notes, 51, No. 4, 15-22
- Chiburis, E.F. (1981), Seismicity, recurrence rates, and regionalization of the northeastern United States and

- adjacent southeastern Canada, U.S. Nuclear Regulatory Commission, NUREG/CR-2039
- Chiburis, E.F., Ahner, R.O., and Graham, T., (1980), Northeast U.S. Network Bulletin, No. 17, Weston Observatory, Weston, MA
- Chinnery, M.A. (1979), A comparison of the seismicity of three regions of the eastern U.S., Bull. Seis. Soc. Amer., 69, 757-772
- Chinnery, M.A. and North, R.G. (1975), The frequency of very large earthquakes, Science, 190, 1197-1198
- Chinnery, M.A. and Rogers, D.A. (1973), Earthquake statistics in southern New England, Earthquake Notes, 44, No.'s 3-4, 89-103
- Chung, D.H. and Ingersoll, D.S. (1973), Earthquakes of northeastern United States and eastern Canada 1534-1972, unpublished, Boston College, 162 pgs.
- Coffman, J.L. and von Hake, C.A. (1973), Earthquake History of the United States, U.S. Department of Commerce Publication 41-1
- Collins, M.P. (1937a), Local earthquakes in New England, Bull. Seis. Soc. Amer., 27, 41-48
- Collins, M.P. (1937b), The New Hampshire earthquakes of November 9, 1936 and further data on New England travel times, Bull. Seis. Soc. Amer., 27, 99-107
- Cook, F.A., Albaugh, D.S., Brown, C.D., Kaufman, S., Oliver, J.E., and Hatcher, R.D. Jr. (1979), Thin skinned tectonics in the crystalline southern Appalachians: COCORP seismic reflection profiling of the Blue Ridge and Piedmont, Geology, 7, 563-567
- Crandell, F. (1949), Ground vibration due to blasting and its effects upon structures, J. Boston Soc. Civil Eng., 36, 222-245
- Crosby, I.B. (1923), The earthquake risk in Boston, J. Boston Soc. Civ. Eng., 10, No. 10
- Cushing, H.P., Fairchild, H.L., Ruedemann, R., and Smith, C.H. (1910), Geology of the thousand island region, Bull. NY State Mus. Sci. Ser., 145, 1-185
- Curtin, P.L., Pulli, J.J., and Guenette, M.J. (1983), Crustal structure of central New Hampshire derived from local travel

- time data, Earth Resources Laboratory Technical Report, M.I.T., pp. 21
- Dainty, A. (1981), A scattering model to explain seismic Q observations in the lithosphere between 1 and 30 Hz, Geophys. Res. Letters, 11, 1126-1128
- Dainty, A. and Toksöz, M.N. (1981), Seismic codas on the Earth and the Moon: a comparison, Phys. Earth Planet. Inter., 26, 250-260
- Devane, J.F. and Holt, R.J. (1967), The seismic history of Massachusetts, in Farquhar, O.C., ed., Economic Geology in Massachusetts, Publ. Univ. Mass. Graduate School
- Devlin, J.J., Langguth, L.C., and Arringdale, R.L. (1942), Macroseismic study of the New Hampshire earthquakes of December, 1940, Bull. Seis. Soc. Amer., 32, 67-73
- Dietz, R.S. (1972), Geosynclines, mountains, and continent building, Scientific American, 226
- Dott, R.H. and Batten, R.L. (1976), Evolution of the Earth, McGraw-Hill Book Company, p.p. 504
- Ebel, J.E. (1982), ML measurements for northeastern United States earthquakes, Bull. Seis. Soc. Amer., 72, 1367-1378
- Ewing, W.M., Jardetzky, W.S., and Press, F. (1957), Elastic Waves in Layered Media, McGraw Hill Book Co., N.Y., 380 pp.
- Fletcher, D.B. and Sykes, L.R. (1977), Earthquakes related to hydraulic mining and natural seismic activity in western New York state, J. Geophys. Res., 82, 3767-3780
- Forsyth, D.A. (1981), Characteristics of the western Quebec seismic zone, Can. J. Earth Sci., 18, 103-119
- Fox, F.L. and Spiker, C.T. (1977), Intensity rating of the Attica (N.Y.) earthquake of August 12, 1929: a proposed reclassification, Earthquake Notes, 48, No. 1-2, 37-46
- Gardner, J.K. and Knopoff, L. (1974), Is the sequence of earthquakes in southern California, with aftershocks removed, Poissonian?, Bull. Seis. Soc. Amer., 64, 1363-1367
- Goforth, T. and Herrin, E. (1981), Automatic seismic detection algorithm based on the Walsh transform, Bull. Seis. Soc. Amer., 71, 1351-1360

- Gohn, G.S., Higgins, B.B., Smith, C.C., and Owens, J.P. (1977), Lithostratigraphy of the deep corehole near Charleston, South Carolina, U.S.G.S. Prof. Paper 1028-E, 59-70
- Graham, T. and Chiburis, E.F. (1980), Fault plane solutions and the state of stress in New England, Earthquake Notes, 51, No. 2, 3-12
- Guinn, S. and Long, L.T. (1977), A computer method for the determination of valid focal mechanisms using P-wave first motions, Earthquake Notes, 48, No. 4, 2-33
- Gumbel, E.J. (1954), Statistical theory of extreme values and some practical applications, National Bureau of Standards, Appl. Math Series No. 3355
- Gumbel, E.J. (1958), Statistics of Extremes, Columbia University Press, New York, 375 pp.
- Gutenberg, B. and Richter, C.F. (1942), Earthquake magnitude, intensity, energy, and acceleration, Bull. Seis. Soc. Amer., 32, 163-191
- Hadley, J.B. and Devine, S.F. (1974), Seismotectonic map of the eastern U.S., U.S.G.S. Open File Report, 8 pgs, 2 maps
- Haimson, B.C. (1974), A simple method for estimating in-situ stress at great depths, Field Testing and Instrumentation of Rock, Spec. Tech. Publ., 554, pp. 156-182, Amer. Soc. for Testing Materials, Philadelphia, PA
- Haimson, B.C. and Lee, C.F. (1979), Stress measurements in underground nuclear slant design, in Proceeding of 1979 Rapid Excavation and Tunneling Conference, Atlanta, GA, Soc. Mining Engrs. of AIME, Littleton, CO
- Harmuth, H.F. (1972), Transmission of Information by Orthogonal Functions, 2nd ed., Springer-Verlag, New York, 393 pp.
- Hasegawa, H.S. (1974), Theoretical synthesis and analysis of strong motion spectra of earthquakes, Can. Geotech. J., 11, 278-297
- Hasegawa, H.S. and Wetmiller, R.J. (1980), The Charlevoix earthquake of 19 August 1979 and its seismo-tectonic environment, Earthquake Notes, 51, No. 4, 23-37
- Herrmann, R.B. (1975), The use of duration as a measure of seismic moment and magnitude, Bull. Seis. Soc. Amer., 65, 899-913
- Herrmann, R.B. (1978), A seismological study of two Attica, New York earthquakes, Bull. Seis. Soc. Amer., 68, 641-651

- Herrmann, R.B. (1979), Surface wave focal mechanisms for eastern United States earthquakes with tectonic implications, J. Geophys. Res., 84, 3543-3552
- Herrmann, R.B. (1980), Q estimates using the coda of local earthquakes, Bull. Seis. Soc. Amer., 70, 447-468
- Herrmann, R.B. (1981), Progress in modeling the ground shaking hazard, in Earthquakes and Earthquake Engineering - the Eastern US, Ann Arbor Science Publishers, 337-347
- Herrmann, R.B. and Canas, J. (1978), Focal Mechanism studies in the New Madrid seismic zone, Bull. Seis. Soc. Amer., 68, 1095-1102
- Hill, D.P. (1982), Contemporary block tectonics: California and Nevada, J. Geophys. Res., 87, 5433-5450
- Hodgson, E.A. (1925), The St. Lawrence earthquake of February 28, 1925, Bull. Seis. Soc. Amer., 15, 84-99
- Hooker, V.E. and Johnson, C.F. (1969), Near surface horizontal stresses including the effects of rock anisotropy, U.S.B.M. Report 7224, pp. 29
- Horner, R.B., Stevens, A.E., Hasegawa, H.S., and Leblanc, G. (1978), Focal parameters of the July 12, 1975 Maniwaki, Quebec, earthquake - an example of intraplate seismicity in eastern Canada, Bull. Seis. Soc. Amer., 68, 619-640
- Horner, R.B., Wetmiller, R.J., and Hasegawa, H.S. (1979), The St-Donat, Quebec, earthquake of February 18-23, 1978, Can. J. Earth Sci., 16, 1892-1898
- Isachsen, Y.W. (1975), Possible evidence for contemporary doming of the Adirondack mountains, New York, and suggested implications for regional tectonics and seismicity, Tectonophysics, 29, 169-181
- Johnston, A.C. (1982), A major earthquake zone on the Mississippi, Scientific American, 246, 60-68
- Joyner, W.B. and Boore, D.M. (1981), Peak horizontal acceleration and velocity from strong motion records including records from the 1979 Imperial Valley, California earthquake, Bull. Seis. Soc. Amer., 71, 2011-2038
- King, P.B. (1969), Tectonic Map of North America, U.S.G.S., Washington, D.C., scale 1:5,000,000
- Klein, F.W. (1978), Hypocenter Location Program HYPOINVERSE, U.S.G.S. Open-file Report No. 78-694, 113 pgs.

- Klimkiewicz, G.C. (1980), Ground motion attenuation models for the northeast, (abstract), Earthquake Notes, 51, No. 3, 25-26
- Klimkiewicz, G.C. (1982), Reassessment of ground motion attenuation models for the northeast, (abstract), Earthquake Notes, 53, No. 3, 23-24
- Knopoff, L. and Kagan, Y. (1977), Analysis of the theory of extremes as applied to earthquake problems, J. Geophys. Res., 82, 5647-5657
- Kumarapeli, P.S. (1978), The St. Lawrence paleo-rift system: a comparative study, in Tectonics and Geophysics of Continental Rifts, Ramberg and Neumann eds, 367-384
- Leblanc, G. (1981), A closer look at the September 16, 1732, Montreal earthquake, Can. J. Earth Sci., 18, 539-550
- Leblanc, G., Stevens, A.E., Wetmiller, R.J., and Duberger, R. (1973), A microearthquake survey of the St. Lawrence Valley near La Malbaie, Quebec, Can. J. Earth Sci., 10, 42-53
- Leblanc, G. and Buchbinder, G. (1977), Second microearthquake survey of the St. Lawrence Valley near La Malbaie, Quebec, Can. J. Earth Sci., 14, 2778-2789
- Lee, W.H.K., Bennett, R.G., and Meagher, K.L. (1972), A method of estimating magnitude of local earthquakes from signal duration, U.S. Geol. Surv., Open File Rept. 28
- Lee, W.H.K. and Stewart, S.W. (1981), Principles and Applications of Microearthquake Networks, Academic Press, New York, 293 pgs.
- Leet, L.D. (1938), Earthquakes in northeastern America, July - December, 1937, Bull. Seis. Soc. Amer., 28, 169-176
- Leet, L.D. and Linehan, D. (1942), Instrumental study of the New Hampshire earthquakes of December, 1940, Bull. Seis. Soc. Amer., 32, 75-82
- Linehan, D.L. (1940), The Chelmsford, Massachusetts earthquake of June 23, 1938, Bull. Seis. Soc. Amer., 30, 99-107
- Linehan, D. and Leet, L.D. (1942), Earthquakes of the northeastern United States and eastern Canada, 1938, 1939, 1940, Bull. Seis. Soc. Amer., 32, 11-18
- Lomnitz, C. (1966), Statistical prediction of earthquakes, Rev. Geophys. Space Phys., 4, 377-393

- Mather, K.F. and Godfrey, H. (1927), The earthquake record in New England, paper presented to the Eastern Section of the Seismological Society of America in May 1927
- Mauk, F.J., Christensen, D., and Henry, S. (1982), The Sharpsburg, Kentucky earthquake 27 July 1980: main shock parameters and isoseismal map, Bull. Seis. Soc. Amer., 72, 221-236
- McGuire, R.K. (1977), The use of intensity data in seismic hazard analysis, Proc. 6th World Conf. on Earthquake Engr., New Delhi, vol. 2, 353-358
- McKenzie, D.P. (1969), The relation between fault plane solutions for earthquakes and the directions of the principal stresses, Bull. Seis. Soc. Amer., 59, 591-601
- McTigue, D.F. and Mei, C.C. (1981), Gravity-induced stresses near topography of small scale, J. Geophys. Res., 86, 9268-9278
- Michael, A.J., Gildea, S.P., and Pulli, J.J. (1982), A real-time digital seismic event detection and recording system for network applications, Bull. Seis. Soc. Amer., 72, 2339-2348
- Mitchell, B.J. (1973), Radiation and attenuation of Rayleigh waves from the southeastern Missouri earthquake of October 21, 1965, J. Geophys. Res., 78, 886-899
- Mueller, C.S. and Cranswick, E. (1982), Source parameters of the January, 1982 New Brunswick aftershocks: comparison with Mammoth Lake, (abstract), EOS, 63, 1030
- Nabelek, J., Suarez, G., and Toksöz, M.N. (1982), Source parameters of the New Brunswick earthquake of January 9, 1982 from inversion of teleseismic body and surface waves, (abstract), Earthquake Notes,
- Nottis, G., Mitronovas, W., and Barosh, P. (1981), A new catalog and map of historical and recent tectonic seismicity for northeastern North America, (abstract), Earthquake Notes,
- Nuttli, D.W. (1973a), Seismic wave attenuation and magnitude relations for eastern North America, J. Geophys. Res., 78, 876-885
- Nuttli, D.W. (1973b), The Mississippi Valley earthquakes of 1811 and 1812: intensities, ground motion, and magnitudes, Bull. Seis. Soc. Amer., 63, 73-85

- Nuttli, O.W. (1974), Magnitude recurrence relations for central Mississippi Valley earthquakes, Bull. Seis. Soc. Amer., 64, 1189-1207
- Nuttli, O.W. (1978), A time domain study of the attenuation of 10-Hz waves in the New Madrid seismic zone, Bull. Seis. Soc. Amer., 68, 343-355
- Nuttli, O.W. (1983), Average seismic source parameter relations for midplate earthquakes, Bull. Seis. Soc. Amer., 73, 519-535
- Nuttli, O.W. and Zollweg, J.E. (1974), The relation between felt area and magnitude for central United States earthquakes, Bull. Seis. Soc. Amer., 64, 73-85
- Nuttli, O.W., Bollinger, G.A., and Griffiths, D.W. (1979), On the relation between Modified Mercalli Intensity and body wave magnitude, Bull. Seis. Soc. Amer., 69, 893
- Oliver, J., Johnson, T., and Dorman, J. (1970), Post-glacial faulting and seismicity in New York and Quebec, Can. J. Earth Sci., 7, 579-590
- Overbey, W.K. Jr. and Rough, R.L. (1968), Surface studies predict orientation of induced formation fractures, Prod. Mon., 32, 16-19
- Patton, H.J. (1976), A note on the source mechanism of the southeastern Missouri earthquake of October 21, 1965, J. Geophys. Res., 81, 1483-1486
- Pomeroy, P.W., Simpson, D.W., and Sbar, M.L. (1976), Earthquakes triggered by surface quarrying - the Wappinger Falls, New York sequence of June 1974, Bull. Seis. Soc. Amer., 66, 685-700
- Porter, W.W. (1924), The New England earthquake of January 7, 1925, Bull. Seis. Soc. Amer., 14, 233-239
- Press, F. and Ewing, M. (1952), Two slow surface waves across North America, Bull. Seis. Soc. Amer.,
- Pulli, J.J., Stewart, R.R., Johnston, J.C., Tubman, K.M., and Michael, A. (1980), Field investigation and fault plane solution of the Bath, ME earthquake of April 18, 1979, Earthquake Notes, 51, No. 4, 39-46
- Pulli, J.J. and Aki, K. (1981), Attenuation of seismic waves in the lithosphere: comparison of active and stable areas, in Beavers, ed., Earthquakes and Earthquake Engineering: the eastern U.S., Proceedings of a conference, 129-141

- Pulli, J.J. and Guenette, M.J. (1981a), The Chelmsford-Lowell, MA. earthquakes of 1980 and 1938; Earthquake Notes, 52, No. 2, 3-11
- Pulli, J.J. and Guenette, M.J. (1981b), The Chelmsford-Lowell, MA. earthquake of November 23, 1980: depth control and fault plane solution, Bull. Seis. Soc. Amer., 71, 1369-1372
- Pulli, J.J. and Godkin, C.B. (1981), The Long Island Sound, New York earthquake of October 21, 1981, Earthquake Notes, 52, No. 4, 23-27
- Pulli, J.J. and Toksöz, M.N. (1981), Fault plane solutions for northeastern United States earthquakes, Bull. Seis. Soc. Amer., 71, 1875-1882
- Raleigh, C.B., Healy, J.H., Bredehoeft, J.D. (1972), Faulting and crustal stress at Rangely, Colorado, Geophys. Monogr., Amer. Geophys. Union, 16, 275-284
- Rautian, T.G. and Khalturin, V.I. (1978), The use of the coda for determination of the earthquake source spectrum, Bull. Seis. Soc. Amer., 68, 923-948
- Real, C.R. and Teng, T. (1973), Local Richter magnitude and total signal duration in southern California, Bull. Seis. Soc. Amer., 63, 1809-1827
- Reid, H.F. (1911), The earthquake of southeastern Maine, Bull. Seis. Soc. Amer., 2, 44-47
- Richardson, R.M., Solomon, S.C., and Sleep, N.H. (1979), Tectonic stress in the plates, Rev. Geophys. and Space Phys., 17, 981-1019
- Richter, C.F. (1935), An instrumental earthquake scale, Bull. Seis. Soc. Amer., 25, 1-32
- Roecker, S.W. (1981), Seismicity and Tectonics of the Pamir-Hindu Kush Region of Central Asia, PhD Thesis, Massachusetts Institute of Technology, Cambridge, 298 pp.
- Roecker, S.W., Tucker, B., King, J., and Hatzfeld, D. (1982), Estimates of Q in central Asia as a function of frequency and depth using the coda of locally recorded earthquakes, Bull. Seis. Soc. Amer., 72, 129-149
- Rogers, J. (1970), The tectonics of the Appalachians: New York, Wiley Interscience, p. 271
- Rondot, J. (1971), Impactite of the Charlevoix structure, Quebec, Canada, J. Geophys. Res., 76, 5414-5423

- Rothman, R.L. (1968), A note on the New England earthquake of November 18, 1755, Bull. Seis. Soc. Amer., 58, 1501-1502
- Sato, H. (1977), Energy propagation including scattering effects; single isotropic scattering approximation, J. Phys. Earth, 25, 27-41
- Sbar, M.L., Rynn, J.M.W., Gumper, F.J., and Lahr, J.C. (1970), An earthquake sequence and focal mechanism solution, Lake Hopatcong, northern New Jersey, Bull. Seis. Soc. Amer., 60, 1231-1243
- Sbar, M.L. and Sykes, L.R. (1973), Contemporary compressive stress and seismicity in eastern North America: an example of intraplate tectonics, Geol. Soc. Amer. Bull., 84, 1861-1882
- Sbar, M.L. and Sykes, L.R. (1977), Seismicity and lithospheric stress in New York and adjacent areas, J. Geophys. Res., 82, 5771-5786
- Schafer, K. (1979), Recent thrust faulting in the Appalachians, Nature, 280, 223-226
- Scheimer, J. and Landers, T.E. (1974), Short period coda of a local event at LASA, Seismic Discrimination, Semiannual Tech. Sum., 42, Lincoln Lab, M.I.T., Cambridge, MA
- Schlesinger-Miller, E.A., Barstow, N.L., and Revetta, F.A., (1981), Recent earthquakes near Cornwall, Ontario, Earthquake Notes, (abstract), 53, No. 3, 26
- Seborowski, K.D., Williams, G., Kelleher, J.A., and Statton, T.C., (1982), Tectonic implications of recent earthquakes near Annsville, New York, Bull. Seis. Soc. Amer., 72, 1601-1609
- Shakal, A.F. and Toksöz, M.N. (1977), Earthquake hazard in New England, Science, 195, 171-173
- Shlien, S. and Toksöz, M.N. (1970), A clustering model of earthquake occurrences, Bull. Seis. Soc. Amer., 60, 1765-1787
- Simpson, R.W. and Godson, R.H. (1981), Colored gravity anomaly and terrain maps of the east central United States, U.S.G.S. Open File Report 81-846
- Simpson, R.W., Bothner, W.A., and Godson, R.H. (1981), Colored gravity anomaly and terrain maps of the northeastern United States, U.S.G.S. Open File Report 81-560

- Singh, S. (1981), Regionalization of Crustal Q in the Continental United States, PhD Thesis, Saint Louis University, 183 p.
- Singh, S. and Herrmann, R.B. (1983), Regionalization of crustal coda Q in the continental United States, J. Geophys. Res., 88, 527-538
- Smith, W.E.T. (1962), Earthquakes of eastern Canada and adjacent areas, 1534-1927, Dom. Observ. Publ., 26, 271-301
- Smith, W.E.T. (1966), Earthquakes of eastern Canada and adjacent areas, 1928-1959, Dom. Observ. Publ., 32, 87-121
- Stauder, W., Kramer, M., Fisher, G., Schaefer, S., and Morrissey, S.T. (1976), Seismic characteristics of southeast Missouri as indicated by a regional telemetered microearthquake array, Bull. Seis. Soc. Amer., 66, 1953-1964
- Stevens, A.E. (1980a), Reexamination of some larger La Malbaie, Quebec earthquakes (1924-1977), Bull. Seis. Soc. Amer., 70, 529-557
- Stevens, A.E. (1980b), History of some Canadian and adjacent American seismograph stations, Bull. Seis. Soc. Amer., 70, 1381-1394
- Street, R.L. (1976), Scaling northeastern United States - southeastern Canadian earthquakes by their Lg waves, Bull. Seis. Soc. Amer., 67, 599-614
- Street, R.L. (1982), Ground motion values obtained for the 27 July 1980 Sharpsburg, Kentucky earthquake, Bull. Seis. Soc. Amer., 72, 1295-1307
- Street, R.L. and Herrmann, R.B. (1976), Some problems using magnitude scales for eastern North American earthquakes, Earthquake Notes, 47, 37-45
- Street, R.L. and Lacroix, A. (1979), An empirical study of New England seismicity: 1727-1977, Bull. Seis. Soc. Amer., 69, 159-175
- Street, R.L., Herrmann, R.B., and Nuttli, O.W. (1974), Earthquake mechanics in the central United States, Science, 134, 1285-1287
- Street, R.L., Herrmann, R.B. and Nuttli, O.W. (1975), Spectral characteristics of the Lg wave generated by central United States earthquakes, Geophys. J. Roy. Astro. Soc., 41, 51-63

- Street, R.L. and Turcotte, F.T. (1977), A study of northeastern North American spectral moments, magnitudes, and intensities, Bull. Seis. Soc. Amer., 67, 599-614
- Taylor, S.R. and Toksöz, M.N. (1979), Three-dimensional crust and upper mantle structure of the northeastern United States, J. Geophys. Res., 84, 7627-7644
- Taylor, S.R., Toksöz, M.N., and Chaplin, M.P. (1980), Crustal structure of the northeastern United States: contrasts between Grenville and Appalachian Provinces, Science, 208, 595-597
- Taylor, S.R. and Toksöz, M.N. (1982a), Measurement of interstation phase and group velocity and Q using Weiner filtering, Bull. Seis. Soc. Amer., 72, 73-92
- Taylor, S.R. and Toksöz, M.N. (1982b), Crust and upper mantle velocity structure in the Appalachian orogenic belt: implications for tectonic evolution, Bull. Geol. Soc. Amer., 93, 315-329
- Thurber, C.H. (1981), Earth Structure and Earthquake Locations in the Coyote Lake Area, Central California, PhD Thesis, M.I.T., Cambridge, MA, 332 pp.
- Toksöz, M.N., Johnston, D.H., and Timur, A. (1979) Attenuation of seismic waves in dry and saturated rocks, I, Laboratory measurements, Geophysics, 44, 681-690
- Tsai, Y.B. and Aki, K. (1969), Simultaneous determination of the seismic moment and attenuation of seismic surface waves, Bull. Seis. Soc. Amer., 59, 275-287
- Weichert, D.H. and Milne, W.G. (1979), On Canadian methodologies of probabilistic seismic risk estimation, Bull. Seis. Soc. Amer., 69, 1549-1566
- Weston Geophysical Research, Inc. (1977), The Historical Seismicity of New England, Nuclear Regulatory Commission submittal docket No. So-471 (DE S67601), 641 pgs.
- Wetmiller, R.J. (1975), The Quebec-Maine border earthquake, 15 June 1973, Can. J. Earth Sci., 12, 1917-1928
- Wetmiller, R.J., Adams, J., Stevens, A.E., Anglin, F.M., Hasegawa, H.S., and Berube, J. (1982), Aftershock sequences for the New Brunswick earthquakes of January 9th and 11th, March 31st, and June 16th, 1982, (abstract), Earthquake Notes

- Whitman, R.V. (1983), An engineer's perspective on the Cape Ann, Massachusetts earthquake of 1755, (abstract), Earthquake Notes, 54, No. 1, 8
- Wiggins, J.H. (1964), Construction of strong motion response spectra from magnitude and distance data, Bull. Seis. Soc. Amer., 54, 1257-1269
- Winkler, L. (1979), Catalog of U.S. earthquakes before the year 1850, Bull. Seis. Soc. Amer., 69, 569-602
- Winthrop, J. (1757), An account of the earthquake felt in New England and the neighboring parts of America on the 18th of November, 1755, Phil. trans. Roy. Soc., 50, 1-18
- Wood, H.O. and Neumann, F. (1931), Modified Mercalli intensity scale of 1931, Bull. Seis. Soc. Amer., 21, 277-283
- Woodworth, J.B. (1907), Postglacial faults in eastern New York, Geology, 12, 5-28
- Yang, J.P. and Aggarwal, Y.P. (1981), Seismotectonics of northeastern United States and adjacent Canada, J. Geophys. Res., 86, 4981-4998
- York, J.E. and Oliver, J.E. (1976), Cretaceous and Cenozoic faulting in eastern North America, Geol. Soc. Amer. Bull., 87, 1105-1114
- Zartman, R.E. (1977), Geochronology of some alkalic rock provinces in eastern and central United States, Annual Review of Earth and Planetary Sciences, 5, 257-286
- Zoback, M.D., Hamilton, R.M., Crone, A.J., Russ, D.P., McKeown, F.A., and Brockman, S.R. (1980), Recurrent intraplate tectonism in the New Madrid seismic zone, Science, 209, 971-976
- Zoback, M.D. and Zoback, M.L. (1981), State of stress and intraplate earthquakes in the United States, Science, 213, 96-104

APPENDIX A
SIGNIFICANT EARTHQUAKES OF THE
NORTHEASTERN UNITED STATES AND
SOUTHEASTERN CANADA

A.1 Introduction

In Chapter 2 of this work, the distribution of historical and instrumentally located earthquakes was described in detail, but in-depth examinations of important events were not presented. In this appendix, the effects of three important earthquakes are summarized from published data and writings. These summaries should serve as background material for those readers who are unfamiliar with the effects of moderate-to-large earthquakes in the NEUS-SEC. Then, a catalog and map of significant earthquakes is presented. This catalog includes the results of many re-examinations of intensity and instrumental data by a number of authors.

A.2 Three Important Earthquakes

In order to gain an insight into the effects of NEUS-SEC earthquakes, three important events will now be described in detail: 1755 Cape Ann, MA, 1925 La Malbaie, PQ, and 1940 Ossipee, NH. The Cape Ann, MA earthquake of 1755 is important because of its proximity to the now heavily populated Boston area. This event, more than any other, has served to classify southern New England as an area of moderate earthquake hazard. The La Malbaie, PQ earthquake of 1925 is important because it has

the largest instrumentally determined magnitude and seismic moment of any event in the study area. Finally, the Ossipee, NH earthquakes of 1940 were perhaps the largest and most destructive events to occur within the New England states during this century. Thus, the macroseismic data have been fully documented and are highly reliable. In addition, some instrumental data are available for this earthquake.

Nov. 18, 1755 Cape Ann, MA: The significance of this earthquake lies not simply in its size, because it is probably not the largest event to have occurred in the study area, but in its proximity to metropolitan Boston. If an event of the same intensity as the 1755 earthquake were to occur today, the damage would be considerably greater because of the large population now present. This event is commonly referred to as the "Cape Ann earthquake" although it has never been definitively established that the event occurred in the Cape Ann area, or that the greatest amount of damage was in Cape Ann.

The Cape Ann earthquake of 1755 was studied in considerable detail by Weston Geophysical Corp., (1977). Their isoseismal map is shown in Figure A.1 . The earthquake is generally considered as having occurred offshore, but clearly its epicenter cannot be determined to better than 50 km, and may be as much as 200 km in error. Smith (1966) placed the event farthest from shore at about 300 km east of Boston, while Brooks (1960) placed the event onshore near Boston. Coffman and von Hake (1973) placed the event in Massachusetts Bay, whereas Weston Geophysical Corp.

(1977) placed the event just off Cape Ann (42.7, -70.3). (All of these locations are shown in Figure A.1 .) Aki (personal communication) cites the long duration of shaking reported in the Boston area (2 minutes by Winthrop, 1757) as evidence that the earthquake was farther out to sea than is generally accepted and may be similar in tectonic origin to the Bermuda earthquake of March 24, 1978.

The event was felt over one million square kilometers, from Halifax, NS in the northeast to Annapolis, MD in the southwest, and was reported inland to Fort Crown Point, NY. The earthquake reached intensity VII-VIII in parts of Cape Ann and Boston. However, because the earthquake occurred over 200 years ago, the available information on damage is extremely difficult to assess.

For example, consider the following excerpt from the Boston Gazette (or Country Journal) for Monday, Nov. 24, 1755:

"Having been up and awoke much the greater Part of the Night, I got into a sound sleep betwixt 3 and 4 o'clock in the Morning. About an Hour after which, I was awoked, or rather alarmed, by the shaking of my Bed, and of the House; the cause whereof, I immediately concluded, could be nothing but an EARTHQUAKE, having experienced one before. The Trembling (far as yet it was scarce more) increasing, I soon got out of Bed and went towards the Window on the

other Side of the Chamber, to observe if there were any Thing unusual in the Appearance of the Sky, or Heavens. By the Time I had got half Way across the Room, which might be 6 or 7 seconds from my first awaking; the Shaking was a little abated; so I imagined the Height of the Shock was past. But this thought no sooner came into my Mind, that I found how much I was mistaken: For instantaneously the Shock came on with redoubled Violence and Noise, the Windows, Doors, Chairs, etc. being prodigiously agitated; and indeed, the whole House rocking and cracking (sic) to such a Degree, that I concluded it must soon fell, or be rocked to Pieces; unless perhaps, it should be swallowed up entire..."

"The visible Effects of the Earthquake are very considerable in the Town; to be sure much more considerable than those of other, which has been known in it. Many chimnies, I conjecture from my Observations, not much less than 100, are levell'd with the Roofs of the Houses. Many more, I imagine, not fewer than 12 or

1500, are shattered and thrown down in Part: So that in some Places, especially on the low, loose Ground, made by Encroachments on the Harbour, the Streets are almost covered with the Bricks that have fallen. Some Chimnies tho' not thrown down, are dislocated, or broken several Feet from the Top and partly turned around, as upon a Swivel. Some are shoved on one Side, horizontally; jutting over, and just nodding to their Fall. The Gable Ends of several Brick Buildings, perhaps of 12 to 15, are thrown down; I mean from the Roofs of the Houses to the Eaves: and the Roofs of some houses are quite broken in, by the Fall of the Chimnies. Some Pumps are suddenly dried up; the Convulsion of the Earth having choaked the Springs that supplied them, as altered their Course. Many Clocks were also stopped by being so violently agitated..."

"these are the most considerable Effects of the Earthquake, which have fallen under my Observation: for the shaking of Pewter, etc. from the Shelves, seems hardly worth mentioning after them."

From this and other reports, we find that the greatest intensities occurred on areas of filled land or where the soil layer was thick. However, it is difficult to estimate the condition of the structures prior to the earthquake, as well as the building practices of the time. This would certainly have an effect on the resulting damage and subsequent interpretation of the source size. Whitman and Becker (personal communication) studied many of Boston's old houses to evaluate how buildings were constructed during the 17th and 18th centuries. They found that there were some 3000 to 4000 structures in the area at the time of the earthquake, with approximately one third constructed of masonry or brick at least on the ends. They also estimated that 5 - 10% of the chimneys came down during the 1755 earthquake with 25 - 50% damaged. One or two dozen gable ends of buildings were damaged out of perhaps 1000. Their research also indicated that in the Cape Ann area "it was a non-event", with very little damage documented. This result casts some doubts about the actual location of the earthquake.

Clearly, the 1755 Cape Ann earthquake is of prime importance to the estimation of the earthquake hazard in eastern MA. One problem in the quantification of the hazard is that the intensity distribution has been explained by a wide range of source magnitudes and locations. For example, if the earthquake was shallow and near the coast between Boston and Cape Ann, the magnitude could have been as small as 5.0 (mb). Conversely, if the epicenter was farther offshore than is generally accepted,

the magnitude could have been as high as $6 \frac{3}{4}$ (mb).

Street and Lacroix (1979) attempted to determine the magnitude of the Cape Ann earthquake by correlating the total felt areas at intensity level IV for earthquakes of known magnitude in the NEUS, and then applying the correlation to the 1755 data. Their result was that the Cape Ann event was of magnitude $m_b = 6.0 \pm 0.2$. However, since nearly half of the seismic energy was radiated out to sea, the estimation of the total felt area is subject to considerable error. For example, one of the farthest felt reports for this event was in Halifax, NS. An intensity of IV was assigned at this site; however the original report reads "but just perceivable", which does not correspond to intensity IV. If this datapoint is excluded, the total intensity IV area would be reduced and the magnitude of the earthquake would be closer to $5 \frac{3}{4}$.

We can test these interpretations by comparing the actual isoseismals from Figure A.1 with the theoretical intensity distribution using the equation of Klimkiewicz (1982) (see Section 4.3.2 of this work). First, it must be remembered that the isoseismals in Figure A.1 may be incomplete due to the sparse population in a number of inland areas. Also, the theoretical isoseismals are not unique, since there is some standard error (± 0.85 MMI units) in the Klimkiewicz (1982) relationship. Nevertheless, there are a number of constraining factors in the actual intensity data which make this exercise useful. These include the northern, western, and southern limits of the

intensity IV area, and the intensities of VII to VIII experienced along coastal MA.

Figure A.2 shows four theoretical isoseismal calculations for the 1755 earthquake. In the first case (a), we have used the location from Weston Geophysical Corp. (1977) (i.e., 42.7, -70.3) along with the magnitude estimate of Street and Lacroix (1979) (i.e., $m_b=6.0$). The theoretical map shows that the northern and southern limits of the intensity IV area are much smaller than the actual limits in Figure A.1. If we increase the magnitude to $m_b=6.5$ (b), we obtain a better correspondence to the total felt area. Testing a location farther out to sea (c) (42.7, -69.0) with a magnitude of 6.5 (m_b), we find that the southern limit of the intensity IV area does not extend far enough south, and that the average foundation intensity along coastal MA would be in the low VI range. If we move the event farther south to 41.5, -69.0 and use a magnitude of 6.7 (m_b) (d), we obtain a good fit to both the intensity IV and V areas, but the intensities near Boston are still low. Perhaps the answer to this dilemma lies in the focusing of seismic waves in the Boston Basin, which would give rise to the high intensities experienced in this area. Such an effect was observed during the July 27, 1980 northern Kentucky earthquake, where the greatest intensities occurred in the town of Maysville, 50 km from the epicenter.

Further constraints on the distance from shore of this earthquake can be provided by taking the ground motion estimates in Boston calculated by Whitman (1983), and use the ground motion

attenuation model from Chapter 4 to estimate distance ranges. Whitman (1983) used descriptions of damage in Boston for the 1755 earthquake and mathematical models based on the construction practices of the time to place an upper bound on the level of ground motion. His upper bound estimate was 0.12g, which, using standard response spectra translates to a ground velocity of about 5-7 cm/sec. Referring to Figure 4.12, we find that for a magnitude of 6.0, the corresponding distance for 5-7 cm/sec is 40-70 km. For a magnitude 6.5 event, the corresponding distance is 100-150 km.

Smith (1962), Brigham (1871), and Winthrop (1757) all state that this earthquake produced a tsunami which reached the West Indies. However, Rothman (1968) traced the origin of this report and found that, because of a change in the calendar at that time, the date of this tsunami is likely erroneous. The tsunami in the West Indies was probably caused by the Lisbon earthquake of Nov. 1, 1755.

Mar. 1, 1925 La Malbaie, PQ: The La Malbaie, PQ area is perhaps the most seismically active region of northeastern North America. It has experienced large earthquakes in the past (Basham et al., 1979; Stevens, 1980) and has a well defined rate of microactivity (Leblanc and Buchbinder, 1977). Thus, moderate to large earthquakes can be expected in the area in future years, and the 1925 event provides a good example of the effects of such a large event at this site.

The 1925 earthquake was felt over an area of perhaps 2.5

million square kilometers (Hodgson, 1926; Smith, 1962). The earthquake reached an intensity of IX within a narrow strip of the St. Lawrence River. Hodgson's (1926) isoseismal map for this event is shown in Figure A.3 .

As was seen in the 1755 earthquake, the damage was confined to sites where the soil depth was considerable. In particular, Quebec City, 90 miles from the epicenter, suffered severe damage. Examples of damage, from Coffman and von Hake (1973) include:

"The upper part of the wall of the Canadian Pacific Railway Station was damaged. The large grain receiving sheds and elevators are worthy of mention, because the structure, while very well built, formed a kind of inverted pendulum with the greater part of the mass high above the ground. Cracks were found in the ground parallel to the length of the building, both outside and inside, and the floor pulled apart at these cracks. Columns pulled away from the large bolts holding them to the foundation. In some places, the reinforcing steel worked back and forth so that the concrete fell away and exposed the steel".

There were few structures in the epicentral area at that time. However, churches in the area were badly damaged, and there was considerable rotation of monuments and statues.

In Massachusetts, the earthquake was felt at an intensity level of III to IV. The intensity near Cape Cod was higher at a level of VI, due mostly to soil amplification.

Using some instrumental data, Street and Turcotte (1977) estimated that the magnitude of this earthquake was $m_b = 6.6$ with a seismic moment of $2.3E25$ dyne-cm. This would make it the largest instrumentally determined magnitude and seismic moment for an earthquake in the study area. We can compare the magnitude and moment estimation for this event with that of the New Brunswick earthquake of January 9, 1982. Nabelek *et al.* (1982) determined that the New Brunswick event was of magnitude $m_b=5.7$ with a seismic moment of $1.5E24$. Thus, the 1925 event was considerably larger, and was perhaps one of the largest events to have ever affected the NEUS-SEC.

Dec. 20 and 24, 1940 Ossipee, NH: These events are important for two reasons. First, they are the largest and most damaging earthquakes to have occurred within the New England states during this century, and thus the macroseismic data are highly reliable. And second, some instrumental data are available for the estimation of magnitude, moment, and epicenter.

Because the events occurred only four days apart and were of comparable size, the intensity reports could not be separated and are considered to be a composite of the effects of both

earthquakes. An isoseismal map for this event was published by the US Coast and Geodetic Survey (Neumann, 1940), and is shown in Figure A.4 .

Devlin et al. (1942) conducted a field study of the epicentral area following the events. The greatest amount of damage occurred in the town of Tamworth, NH where

"almost every chimney in the town that was in need of repair was damaged."

Other examples of damage in the area included the cracking of plaster walls, the moving of large cemetery monuments, and some instances of houses thrown out of plumb. It was observed that the greatest damage occurred to those houses built on glacial till, and that

"the chimneys that were damaged were in need of pointing, whereas those which survived without injury were in a state of good repair".

The intensity assigned to the event was VII.

These earthquakes were felt over an area of one million square km. The intensity in Massachusetts was IV. A Danish ship in Portland Harbor, ME reported that both earthquakes were felt aboard ship. Devlin et al. (1942) concluded that

"The damage resulting from the shocks is surprisingly small when one considers the

size of the area over which the earthquakes were felt. This, together with the absence of any surface faulting, would seem to indicate some depth for the source of the disturbances".

Leet and Linehan (1942) presented an examination of the instrumental data for these earthquakes. They placed the epicenter at 43.83 N, 71.28 W,

"about 1 mile west of the village of Whittier, New Hampshire on the northern edge of the Ossipee Mountains."

They also suggested that the hypocenters were deep.

"The distances to which the New Hampshire earthquakes were felt (350 mi) and the computed energy, combined with relatively minor damage to structures in the epicentral zone and the small number of aftershocks, supply independent evidence that the focus was deeper than normal".

Based on travel time data, they suggested a focal depth of

"less than 50 km and leaves the balance of probability favoring the zone at the base of the crustal layers, 35 km deep".

Leet and Linehan (1942) used the Wood-Anderson records at Shawinigan Falls, PQ to estimate the magnitude for these events. Although the records were off scale, they estimated that the magnitudes were

"not less than 6 for the first and slightly greater for the second".

However, they used the distance-amplitude corrections of Richter (1935) which were developed for California and have since been found to be inappropriate for the eastern US (Nuttli, 1973a). This would mean that the magnitudes determined by Leet and Linehan (1942) were too high.

Street and Turcotte (1977) re-examined the instrumental data for the first earthquake (20Dec1940) using Nuttli's (1973) distance-amplitude corrections. Their estimate for the magnitude of the Ossipee earthquake was $m_b = 5.4$ with a seismic moment of $0.9E23$ dyne-cm. Street and Lacroix (1979) used the correlation of the intensity IV felt area with magnitude, mentioned previously, to estimate the magnitude of the Ossipee earthquakes as $m_b = 5.3 \pm 0.2$.

Devlin et al. (1942) and Leet and Linehan (1942) cited four reasons why they believed the hypocenters were deep. These were: 1) the small amount of damage for the event size, which they said was about 6, 2) the large total felt area, 3) the absence of surface faulting, and 4) travel-time information. It is instructive to examine their conclusion in the light of what we

now know about the attenuation of seismic waves and the seismicity of this area.

First, it is now widely accepted that the attenuation of seismic waves is much lower in the eastern US than in the West (see Chapter 4 of this work). Thus, earthquakes in the east are felt much more widely than events in the west of comparable magnitude (Nuttli and Zollweg, 1974). Using this attenuation information to correct the magnitude calculations, the magnitude of the Ossipee, NH earthquakes is now known to be 5.4 rather than 6. Thus, the felt area is not anomalously large and the damage (intensity VII) is typical for an event of this size. This discounts the first two lines of evidence for a deep focus.

Second, the absence of surface faulting for NEUS-SEC earthquakes led many investigators to conclude that the larger earthquakes in this area were deep (on the order of 20 - 40 km). For example, Acharya (1980a,b) developed a geometric model relating fault area to seismic moment and corner frequency, and used the absence of surface faulting as a boundary condition in order to estimate the focal depths of some large earthquakes in this area. Acharya (1980a) concluded that, for a thrust fault dipping 75 degrees, the minimum focal depth for a magnitude 6 (mb) earthquake would be 10 km. This model, as well as earlier interpretations, assumes that the crust deforms in brittle fracture from the focus up to the surface. However, in New England, the bedrock is covered with a thick layer of soil and glacial till. Thus, any vertical deformation which is likely to

reach the surface would be taken up in plastic or viscoelastic deformation by the sedimentary layer. Surface faulting is often observed for very shallow strike-slip faults, but rarely for thrust faults. As we saw in Chapter 3, the predominant earthquake mechanism in this area is thrust faulting, and if the Ossiipee earthquakes were of a similar mechanism, surface faulting would not be expected unless the events were extremely shallow (less than 2 km).

Finally, Leet and Linehan (1942) had at their disposal only limited information on the crust and upper mantle structure of the area (e.g., Leet, 1936; Leet, 1938a). Using updated velocity information, and a joint hypocentral location procedure, Dewey (personal communication) recomputed the locations of these events and found a hypocenter at latitude 43.87, longitude -71.37 at a depth of 10 +/- 10 km. Although the errors are large, these events do not appear to be anomalously deep for this area.

A.3 A Catalog of Significant Earthquakes in the NEUS-SEC

The three events just described are only a small part of the total picture of moderate-to-large earthquake activity in this area. We now present a catalog and map of "significant earthquakes" in the study area. Such a catalog of events is useful to planners and engineers who are interested in earthquake resistant design and disaster relief planning. This new catalog of significant earthquakes is important since many studies have been made to examine historical events in detail, and re-evaluate intensities and locations if necessary. To compile such a

catalog of events, we must first define the term "significant".

The term "significant" in this catalog is defined as any event which has reached at least intensity VII or magnitude 5.2 (mb). Intensity VII was chosen since it is the lowest intensity which accounts for structural damage in some buildings. The original definition of intensity VII includes (Wood and Neumann, 1931),

"... damage slight to moderate in well-built ordinary buildings, considerable in poorly built or badly designed buildings ... cracked chimneys ... shook down loosened brickwork ... broken weak chimneys at the roof line ... fall of cornices from towers ... overturned heavy furniture".

Damage of this nature would certainly have economic significance as well as pose hazards to the population. Magnitude $mb=5.2$ was chosen as a lower limit since it is the smallest event size which is capable of producing such intensities, depending on its distance from structures, its focal depth, and of course the soil conditions in the area (see Section 4.3.2 of this work). Consequently, some of the events in this list may meet the magnitude requirement but did not produce intensities as great as VII. However, we assume that an event of this size is capable of producing some damage, and is thus important to this study.

This catalog of significant earthquakes is given in Table A.1 . The catalog includes 1 event of intensity X, 3 events of intensity IX, 7 events of intensity VIII, and 20 events of intensity VII. A map of the 41 epicenters is shown in Figure A.5. Of the 41 events, 27 earthquakes occurred within Canada, and 14 events occurred within US boundaries. Only 4 significant events have been located within the six New England states.

Table A.1
Significant Earthquakes of the NEUS-SEC
 (Int \geq VII or mb \geq 5.2)

<u>Date</u>	<u>OI</u>	<u>Lat</u>	<u>Long</u>	<u>Int</u>	<u>mb</u>	<u>Area</u>
1534		47.7	-70.1	IX		Les Eboulements, PQ
11Jun1638	1900	47.7	-70.2	IX		La Malbaie, PQ
10Feb1661	1200	45.5	-73.0	VII		S. of Granby, PQ
05Feb1663	2230	47.6	-70.1	X		La Malbaie, PQ
24Feb1665	1645	47.8	-70.0	VIII		La Malbaie, PQ
10Nov1727	0340	42.8	-70.6	VII		Cape Ann, MA
16Sep1732	1600	45.5	-73.6	VIII		Montreal, PQ
19Dec1737	0330	40.8	-74.0	VII		NY City, NY
18Nov1755	0912	42.7	-70.3	VII		Cape Ann, MA
07Dec1791	0100	47.4	-70.5	VIII		Baie-St-Paul, PQ
09Sep1816		45.5	-73.6	VII		Montreal, PQ
08May1831		47.3	-70.5	VII		Ile-Aux-Courdres, PQ
14Ju11831		47.6	-70.1	VII		La Malbaie, PQ
11Nov1840		39.8	-75.2	VII		Woodbury, NJ
17Oct1860	1115	47.5	-70.1	VIII		Riviere Ouelle, PQ
13Ju11861	0200	45.4	-75.4	VII		Ottawa, ON
09Oct1871	1440	39.7	-75.5	VII		Wilmington, DE
10Jan1872	0054	47.5	-70.5	VII		Baie-St-Paul, PQ
10Aug1884	1907	40.6	-74.0	VII		NY City, NY
27Nov1893	1650	45.5	-73.3	VII		Montreal, PQ
23Mar1897	2307	45.5	-73.6	VII		Montreal, PQ
28Mar1897	0314	45.5	-73.6	VII		Montreal, PQ

10Feb1914	1831	46.0	-75.0	V	5.5	NE of Ste. Adele, PQ
30Sep1924	0852	47.6	-69.7	VII	5.5	La Malbaie, PQ
01Mar1925	0219	47.6	-70.1	IX	6.6	La Malbaie, PQ
01Jun1927	1223	40.3	-74.0	VII		Sandy Hook, NJ
12Aug1929	1124	42.9	-78.4	VIII	5.8	Attica, NY
08Jan1931	0013	47.6	-70.2		5.4	La Malbaie, PQ
20Apr1931	1954	43.4	-73.7	VII	5.0	Lake George, NY
01Nov1935	0603	46.8	-79.1	VII	6.2	Timiskaming, PQ
02Nov1935	1431	47.2	-78.2		5.4	NE of Timiskaming, PQ
19Oct1939	1153	47.8	-70.0	VI	5.8	La Malbaie, PQ
20Dec1940	0727	43.8	-71.3	VII	5.4	Ossipee, NH
24Dec1940	1343	43.8	-71.3	VII	5.4	Ossipee, NH
09Apr1944	1244	49.9	-67.4		5.4	Riviere Pentecote, PQ
05Sep1944	0438	45.0	-74.9	VIII	5.9	Massena, NY
24Jan1953	0958	49.1	-66.0		5.3	Marsoui, PQ
14May1958	1741	47.0	-76.4		5.4	Bark Lake, PQ
30Sep1967	2239	49.5	-65.8		5.3	S of Sept-Iles, PQ
09Jan1982	1254	46.9	-66.6	VI	5.7	New Brunswick
11Jan1982	2141	46.9	-66.6		5.5	New Brunswick

Figure Captions

Figure A.1 Isoseismal map for the Nov. 18, 1755 Cape Ann, MA earthquake, reproduced from Weston Geophysical Corp. (1977).

Figure A.2 Theoretical isoseismals for the 1755 earthquake using the intensity attenuation relation of Klimkiewicz (1982) (see Section 4.3.2 of this work.) The epicentral location and body wave magnitude used in each calculation are shown on the individual maps.

Figure A.3 Isoseismal map for the Mar. 1, 1925 La Malbaie, PQ earthquake, reproduced from Hodgson (1926).

Figure A.4 Isoseismal map for the Dec. 20 and 24, 1940 Ossipee, NH earthquakes, from the Coast and Geodetic Survey (1940).

Figure A.5 Map of "significant earthquakes" in the NEUS-SEC for the period 1534 - 1982, from Table A.1. A significant earthquake is defined as an event of intensity at least VII or magnitude at least 5.2 (mb).

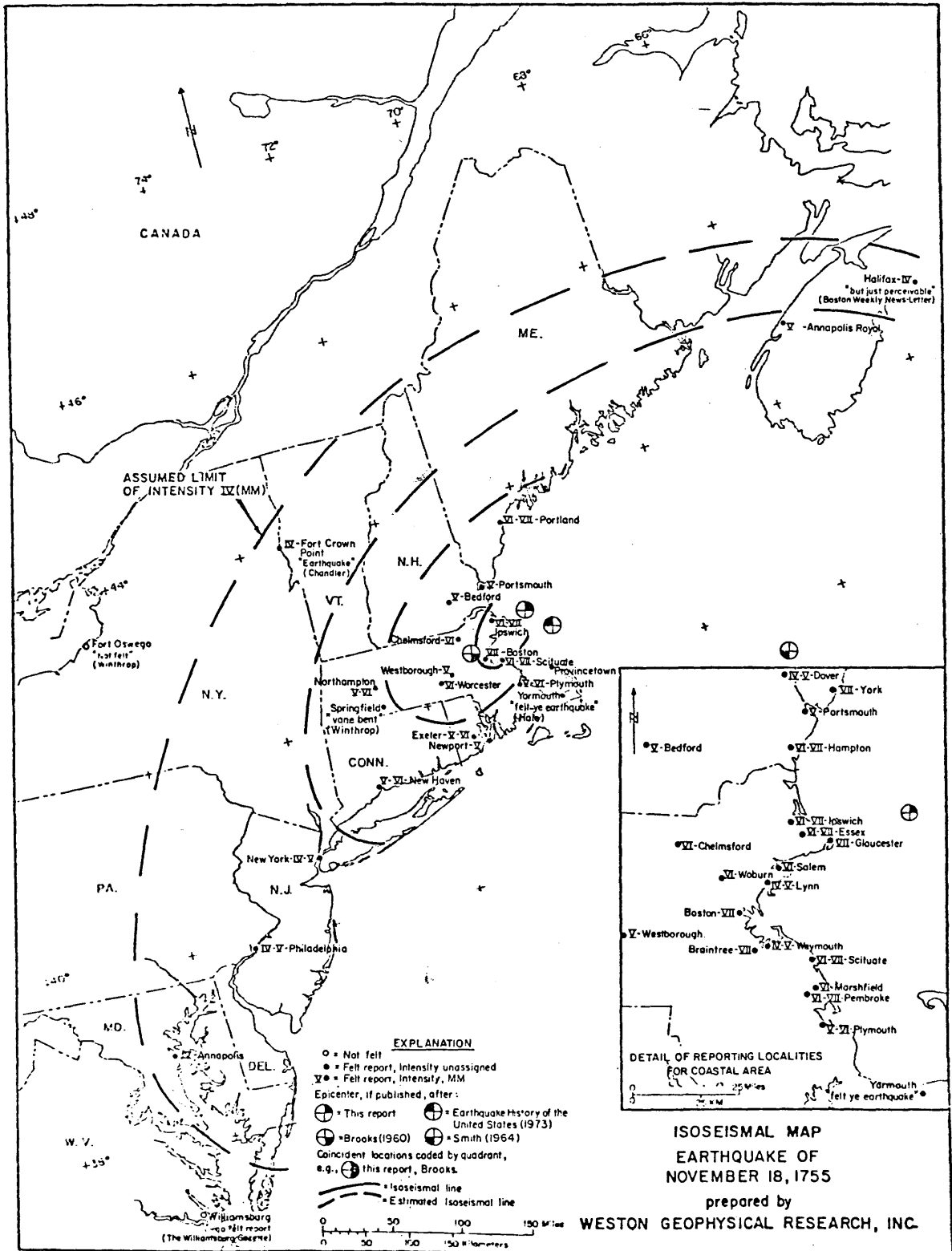


FIGURE A.1

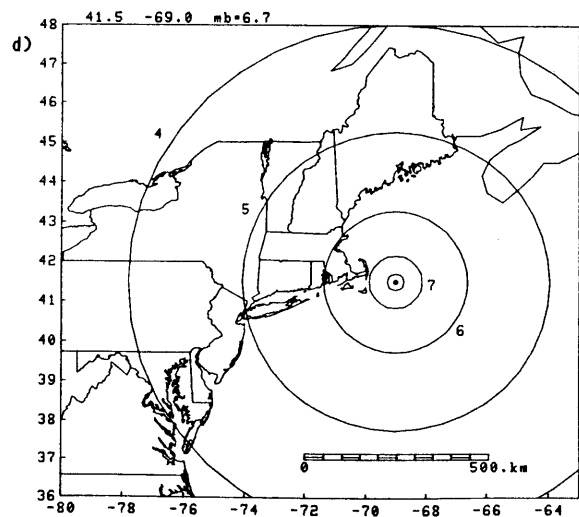
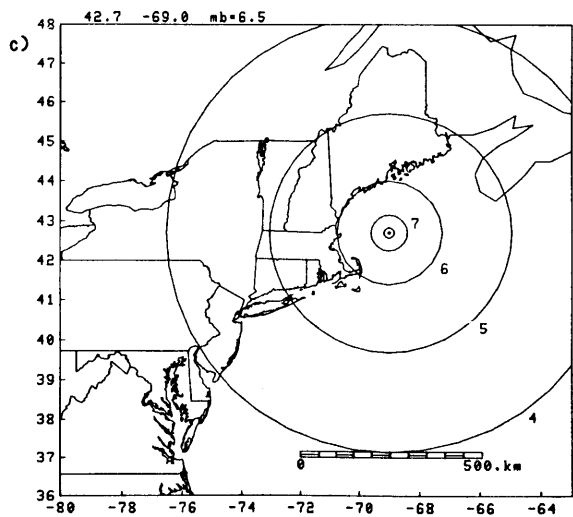
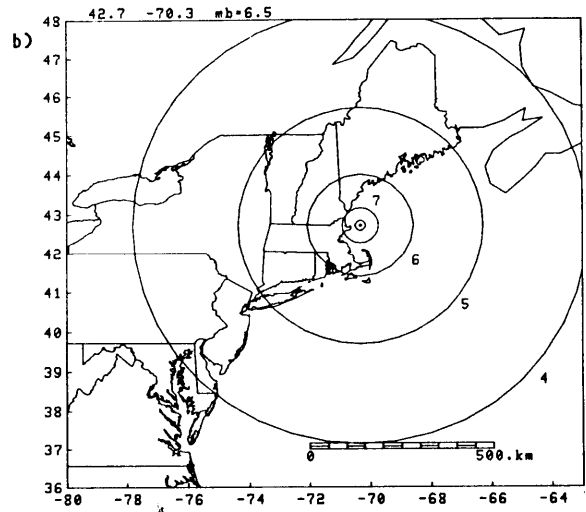
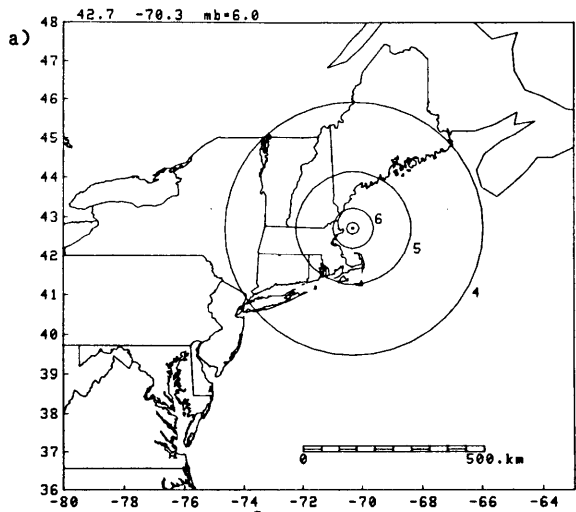


FIGURE A.2

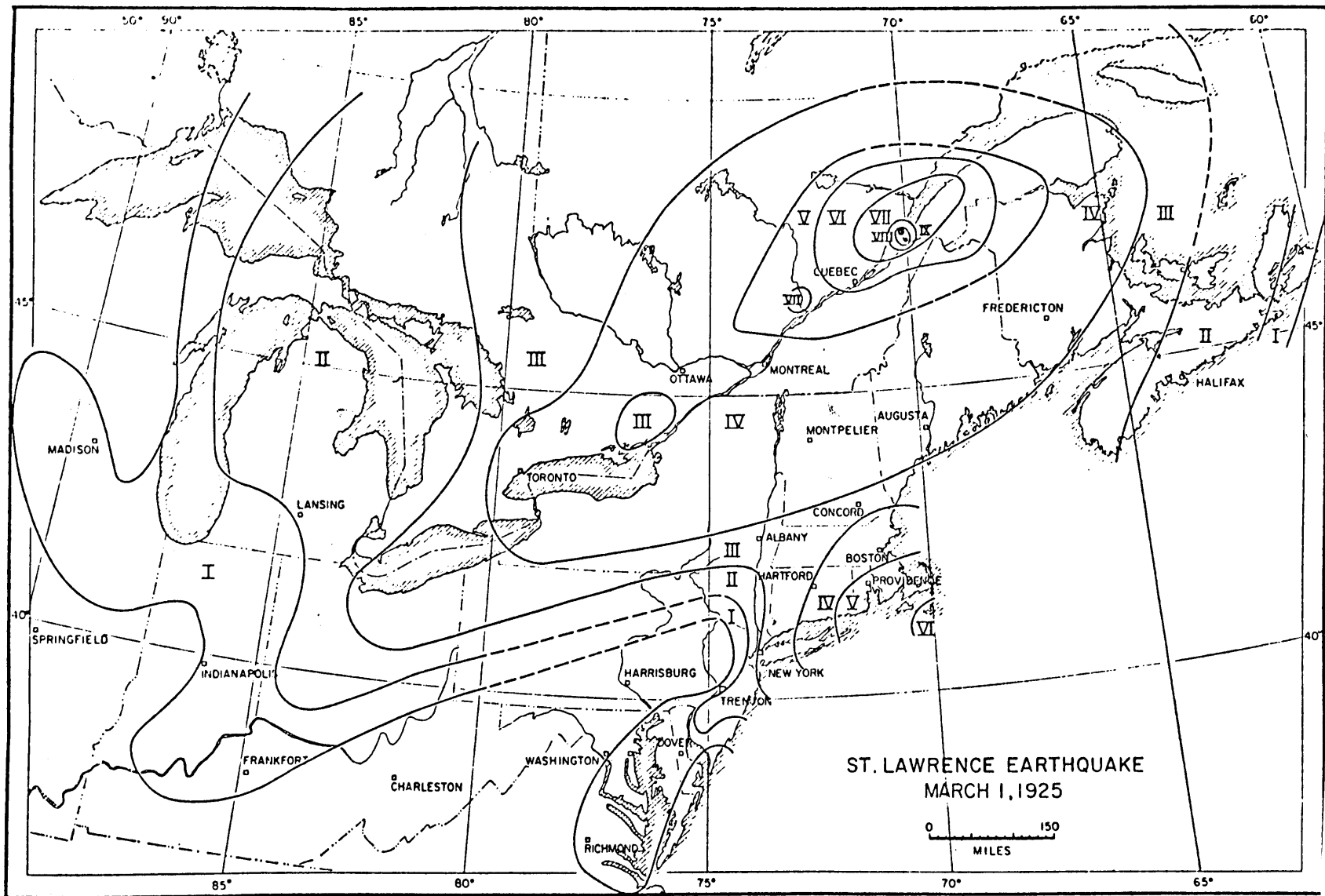


FIGURE A.3

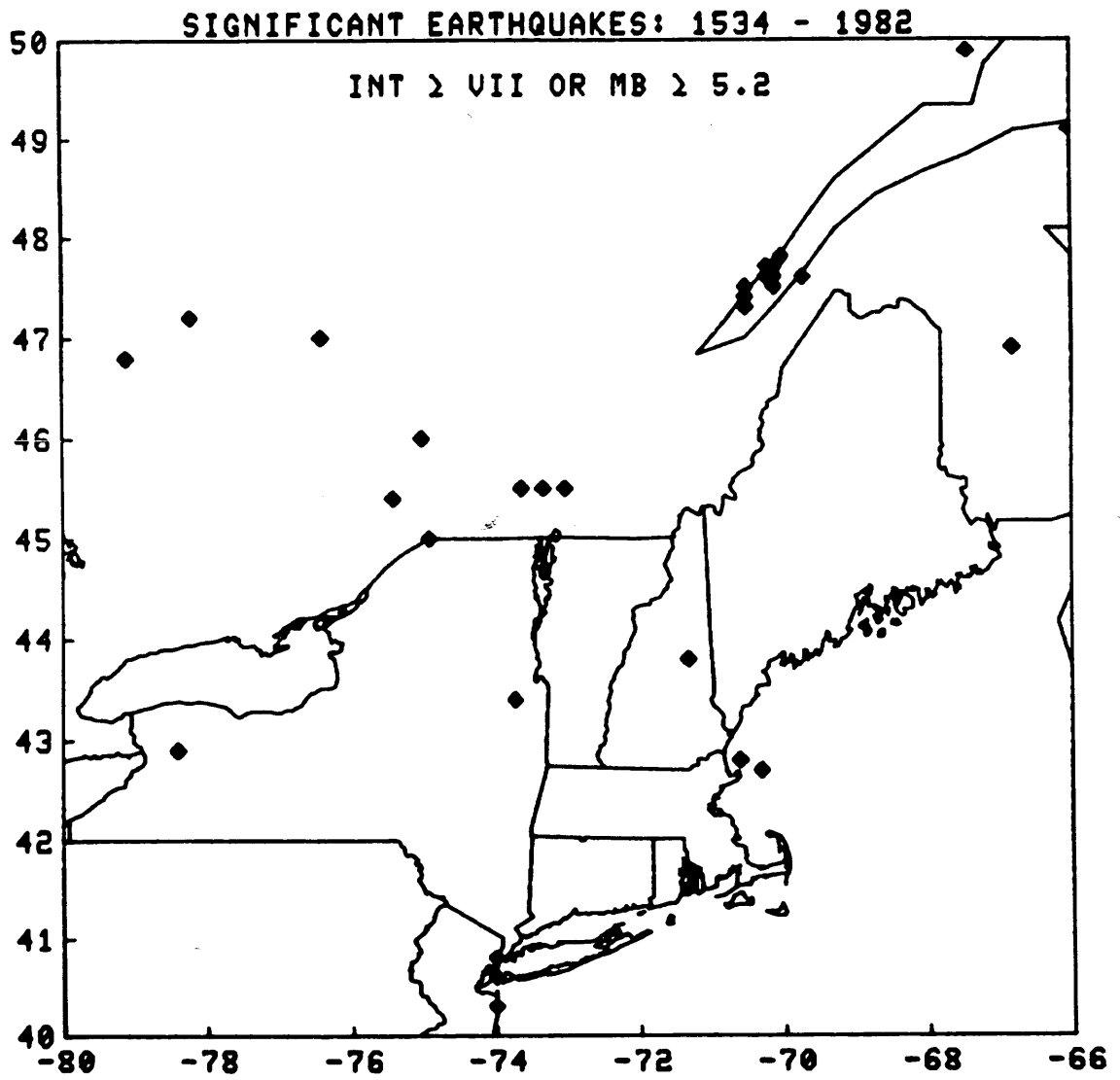


FIGURE A.5

APPENDIX B
APPLICATION OF THE "WINDING-NUMBER ALGORITHM"
TO CATALOGUED EARTHQUAKE DATA

B.1 Introduction

In Chapter 2 of this study, we used a computer regionalization algorithm to delineate seismic zones in the NEUS-SEC, and then computed recurrence relationships in each of these zones. An intermediate step in this process is the selection of events within each seismic zone from the master catalogs of earthquake epicenters. If the zones are rectangular and the boundaries are parallel with latitudes and longitudes, the selection process is simply accomplished using four "if-then" statements which test the epicentral coordinates against these boundaries. However, if the seismic zones are more complicated in shape, another method is required in order to carry out the selection process in a reasonable amount of computer time.

B.2 The Algorithm

A fast and efficient method for determining whether or not a point (earthquake epicenter) lies within an irregularly shaped polygon (seismic zone) is provided by the "Winding-Number Algorithm". This algorithm uses no trigonometric functions, and is thus computationally very fast.

The seismic zone is defined as a polygon by specifying the vertices as a series of points. For an event in question, we first define the origin of a coordinate system at the epicenter,

and then transform the vertices of the polygon into this new coordinate system (requiring only subtractions). Then starting at any vertex, we follow a path describing the polygon's edges and for each segment of the path, we compute the "signed crossing number". This number is an integer which describes a line segment's relationship with the negative x-axis. The signed crossing number has five possible values. It is 0 if the segment does not cross or touch the negative x-axis. If the segment crosses the negative x-axis, its crossing number is +2 or -2 if the crossing direction is from above or below, respectively. If one endpoint of the segment lies on the negative x-axis, the winding number is +/- 1, depending again on the crossing direction.

We proceed with these calculations until we return to the starting point. The sum of the crossing numbers will be either -2, 0, or +2. If the sum is 0, the point lies outside the polygon. Otherwise, the point is inside. The sign simply describes the handedness of the path followed. This algorithm can handle any closed polygon, as long as the segments do not cross over each other. If they do cross, there may be some ambiguity if the distinction between inside and outside is not clear.

To illustrate this algorithm, we will apply the method to the Western Quebec seismic zone, defined in Chapter 2. This zone is shown in Figure B.1. In Figure B.1a, an epicenter has been placed within the defined seismic zone. We start at point A and

proceed clockwise around the zone. The crossing numbers are: A to B, 0; B to C, 0; C to D, 0; and D to A, -2. The sum of the crossing numbers is -2, and the point is inside the zone. In Figure B.1b, an epicenter has been placed outside the seismic zone, and we proceed as before starting at point A. The crossing numbers are: A to B, 0; B to C, +2; C to D, 0; and D to A, -2. The sum is zero and the point lies outside the seismic zone.

Figure Captions

Figure B.1 Illustration of the "Winding Number Algorithm". The test is being conducted for the Western Quebec seismic zone.

a) Example of an epicenter within the seismic zone. The crossing numbers are: A to B, 0; B to C, 0; C to D, 0; and D to A, -2. The sum of the crossing numbers is -2, and the point is inside the seismic zone.

b) Example of an epicenter outside the seismic zone. The crossing numbers are: A to B, 0; B to C, +2; C to D, 0; and D to A, -2. The sum is zero and the point lies outside the seismic zone.

APPENDIX C

SEISMIC STATIONS IN THE NEUS-SEC

<u>Code</u>	<u>Lat.</u>	<u>Long.</u>	<u>Oper.*</u>	<u>Location</u>		
A10	47.246	-70.193	EPB	PQ	Charlevoix	
A16	47.468	-70.010	EPB	PQ	Charlevoix	
A20	47.706	-69.690	EPB	PQ	Charlevoix	
A54	47.457	-70.413	EPB	PQ	Charlevoix	
A56	47.550	-70.327	EPB	PQ	Charlevoix	
A60	47.692	-70.093	EPB	PQ	Charlevoix	
A64	47.827	-69.891	EPB	PQ	Charlevoix	
AGM	47.082	-69.023	WES	ME	Allagash	
ALX	44.322	-75.928	LDO	NY	Alexander Bay	
AMNH	40.781	-73.974	LDO	NY	Manhattan	
ANNS	41.308	-73.913	WCC	NY	Annsville	
APH	43.841	-74.497	LDO	NY	Airport Hangar	
APT	41.316	-72.064	WES	CT	Avery Point	Closed
BBD	39.346	-75.677	DGS	DE	Blackbird	
BCT	41.493	-73.384	WES	CT	Brookfield	
BGR	44.829	-74.374	LDO	NY	Bangor	
BING	42.076	-75.977	LDO	NY	Binghamton	
BLM	41.330	-73.955	CON	NY	Blum	
BNH	44.591	-71.256	WES	NH	Berlin	
BPM	44.632	-68.789	WES	ME	Bucksport	
BPT	41.222	-73.242	WES	CT	Bridgeport	Closed
BUO	43.362	-79.745	EPB	ON	Burlington	
BVR	40.700	-80.333	PSU	PA	Beaver	
BVT	43.349	-72.585	WES	VT	Baltimore	
CANY	42.926	-78.853	LDO	NY	Canisus	
CBM	46.932	-68.121	WES	ME	Caribou	
CHQ	46.890	-71.300	EPB	PQ	Charlesbourg	
CHR	41.208	-74.221	CON	NY	Call Hollow Rd	
CLIN	41.875	-73.849	LDO	NY	Clinton	
CLY	43.851	-74.449	LDO	NY	Crystal Lake	
COD	41.686	-70.135	MIT	MA	S. Dennis, Cape Cod	
COV	44.578	-73.146	LDO	VT	Colchester	
CROG	43.905	-75.412	LDO	NY	Croghan	
CSNH	43.816	-71.462	WGC	NH	Center Sandwich	
CTR	43.874	-74.460	LDO	NY	Castle Rock	
D1A	47.059	-69.099	WES	ME	Dickey	
D2A	47.130	-69.152	WES	ME	Dickey (Kelly Mtn.)	
D3A	47.088	-69.169	WES	ME	Dickey (Carter Brook)	
D4A	47.188	-69.277	WES	ME	Dickey (Rocky Mtn)	
D5A	47.011	-69.265	WES	ME	Dickey (Browns Brook)	
D6A	47.089	-69.496	WES	ME	Dickey (Two Mile Stream)	
DANY	44.758	-73.836	LDO	NY	Dannemora	
DBM	41.294	-73.975	CON	NY	Dunderburg Mtn	
DHN	42.826	-78.193	LDO	NY	Doyle Hill	
DLA	42.858	-81.573	EPB	ON	Delaware	
DNH	43.123	-70.895	MIT	NH	Durham	
DNY	42.836	-78.169	LDO	NY	Dersam	

DPL	41.253	-73.911	CON	NY	Delli Paoli	
DUX	42.069	-70.768	MIT	MA	Duxbury	
DVT	44.962	-72.171	WES	VT	Derby	
ECT	41.835	-73.411	WES	CT	Ellsworth	
EFO	43.092	-79.312	EPB	ON	Effingham	
EGN	43.860	-74.482	LDO	NY	Eagle's Nest	
ELF	43.193	-81.315	EPB	ON	Elginfield	
EMM	44.739	-67.489	WES	ME	East Machias	
ERI	42.133	-79.983	PSU	PA	Erie	
FHO	45.455	-76.217	EPB	ON	Fitzroy Harbour	
FLET	44.723	-72.952	LDO	VT	Fletcher	
FLR	41.717	-71.122	WES	MA	Fall River	
FOR	40.863	-73.885		NY	Fordham	
GAC	45.703	-75.478	EPB	PQ	Glen Almond	
GFN	42.793	-73.415		NY	Grafton	Closed
GHNH	43.870	-71.119	WGC	NH	Gill Hill	Closed
GLO	42.640	-70.727	MIT	MA	Gloucester	
GMTN	40.882	-74.184	LDO	NJ	Garret Mtn	
GNT	46.360	-72.372	EPB	PQ	Gentilly	
GOB	41.329	-73.922	CON	NY	Gobbelet	
GPD	41.018	-74.461	LDO	NJ	Green Pond	
GSC	41.266	-74.004	CON	NY	Girl Scout Camp	
GTD	38.741	-75.414	DGS	DE	Georgetown	
HBVT	44.362	-73.065	LDO	VT	Hinesburg	
HDM	41.486	-72.523	WES	CT	Haddam	
HKM	44.656	-69.641	WES	ME	Hinckley	
HNH	43.705	-72.286	WES	NH	Hanover	
HNME	46.160	-67.987	WES	ME	Houlton	
HNY	42.832	-75.515	LDO	NY	Hamilton	
HRV	42.506	-71.558	MIT	MA	Harvard-Oak Ridge	Closed
IPS	41.267	-73.948	CON	NY	Indian Point Station	
IVT	43.522	-73.053	WES	VT	Ira	
JKM	45.655	-70.243	WES	ME	Jackman	
LAF	41.568	-71.507	WES	RI	Lafayette	Closed
LANH	43.591	-71.490	WGC	NH	Laconia	Closed
LDNY	40.932	-73.468	SBU	NY	Lloyd's Neck	
LDO	41.004	-73.909	LDO	NY	Lamont Doherty	
LMQ	47.548	-70.327	EPB	PQ	La Malbaie	
LND	43.040	-81.183	EPB	ON	London	
LNx	42.339	-73.272	WES	MA	Lenox	
LPQ	47.341	-70.009	EPB	PQ	La Pocatiere	
LVNJ	40.809	-74.752	LDO	NJ	Long Valley	
MARL	42.838	-72.801	LDO	VT	Marlboro	
MASH	41.041	-72.293	SBU	NY	Mashomack	
MBNH	43.727	-71.322	WGC	NH	Moultonborough	Closed
MD1	41.553	-72.467	WES	CT	Moodus (Comstock Bridge)	
MD2	41.531	-72.434	WES	CT	Moodus (Pickere1 Lake)	
MD3	41.507	-72.472	WES	CT	Moodus (Cave Hill)	
MD4	41.502	-72.512	WES	CT	Moodus (Haddam Neck)	
MD5	41.455	-72.495	WES	CT	Moodus (Shailerville)	
MDV	43.999	-73.181	LDO	VT	Middlebury	
MEDY	43.182	-78.390	LDO	NY	Medina	
MGVT	44.914	-72.628	LDO	VT	Montgomery	

MIM	45.244	-69.040	WES	ME	Milo	
MIQ	46.367	-75.967	EPB	PQ	Manawaki	
MNQ	50.530	-68.770	EPB	PQ	Manicougan	
MNT	45.503	-73.623	EPB	PQ	Montreal	
MPVT	44.278	-72.607	LDO	VT	Montpelier	
MSNY	44.998	-74.862	LDO	NY	Massena	
MVL	39.999	-76.351	MSC	PA	Millersville	
NED	39.704	-75.708	DGS	DE	Newark	
NMA	41.295	-70.026	MIT	MA	Nantucket	
NSC	41.481	-71.852	WES	CT	North Stonington	
OCN	43.885	-74.529	LDO	NY	Over Castle Rock	
OGD	41.067	-74.617	LDO	NJ	Ogdensburg	
ONH	43.279	-71.506	MIT	NH	Oak Hill	
OSB	41.360	-73.924	CON	NY	Osborn	
OTT	45.394	-75.716	EPB	PQ	Ottawa	
PAL	41.004	-73.909	LDO	NY	Palisades	
PHI	40.117	-75.133	PSU	PA	Abington	
PNH	43.094	-72.136	MIT	NH	Pitcher Mountain	
PNJ	40.907	-74.154	WCC	NJ	Paterson	
PNY	44.834	-73.555	LDO	NY	Plattsburg	
POC	47.360	-70.040	EPB	PQ	La Pocatiere	
PQO	44.986	-67.467	WES	ME	Cooper Hill	
PQ1	44.904	-67.327	WES	ME	East Ridge	
PQN	41.007	-75.086	LDO	NJ	Pahaquarry	
PRIN	40.367	-74.718	LDO	NJ	Princeton	
PTN	44.572	-74.983	LDO	NY	Potsdam	
QCQ	46.780	-71.280	EPB	PQ	Quebec City	
QUA	42.457	-72.374	WES	MA	Quabbin	
RAMA	41.095	-74.214	LDO	NJ	Ramapo	
SANY	43.174	-78.870	LDO	NY	Sanborn	
SBQ	45.378	-71.926	EPB	PQ	Sherbrook	
SCH	54.816	-66.783	EPB	NF	Schefferville, Labrador	
SCP	40.795	-77.865	PSU	PA	State College	
SFO	41.196	-74.261		NY	Sterling Forest	
SNP	41.241	-73.971	CON	NY	Stoney Point	
SPS	41.302	-73.891	CON	NY	St. Peters School	
SRM	41.228	-74.014	CON	NY	Scherman	
SSL	41.161	-74.916		PA	Sunset Lake	Closed
STL	41.189	-74.004	CON	NY	Stiles	
SUD	46.466	-80.966	EPB	ON	Sudbury	
TBR	41.142	-74.222	LDO	NY	Table Rock	
TMT	41.811	-72.799	WES	CT	Talcott Mountain	Closed
TRM	44.260	-70.255	WES	ME	Turner	
TRQ	46.222	-74.556	EPB			
UCT	41.832	-72.251	WES	CT	UConn (Storrs)	
UNB	45.95	-66.63	EPB	NB	U.N.B., Fredericton	
UWL	43.838	-74.543	LDO	NY	Utowana Lake	
WBNH	43.604	-71.099	WGC	NH	Wolfboro	
WES	42.385	-71.322	WES	MA	Weston	
WFM	42.611	-71.491	MIT	MA	Westford	
WGL	41.359	-73.899	CON	NY	Weigel	
WGMA	42.289	-71.585	WGC	MA	Westboro	
WLI	44.309	-76.010		NY	Wellesley Island	Closed

WND	42.338	-74.153	LDO	NY	Windham
WNH	43.868	-71.400	MIT	NH	Whiteface Mtn
WNY	44.391	-73.859	LDO	NY	Wilmington
WPNY	41.803	-73.971	LDO	NY	West Park
WPR	41.255	-73.586	LDO	NY	Ward Pound Ridge
WVLY	42.471	-78.568	LDO	NY	West Valley

* Operator Code:

- MIT - Massachusetts Institute of Technology
- WES - Weston Observatory (Boston College)
- LDO - Lamont Doherty Geological Observatory
(Columbia University)
- WGC - Weston Geophysical Corp.
- PSU - Pennsylvania State University
- DGS - Delaware Geological Survey
- SBU - State University of New York at
Stony Brook
- EPB - Earth Physics Branch, Division of
Energy, Mines, and Resources,
Ottawa
- WCC - Woodward-Clyde Consultants

Figure Captions

Figure C.1 Seismic stations in southern New England. Station WGMA is operated at the facility of Weston Geophysical Corp., Inc. in Westboro, MA. The Moodus Array is operated by Weston Observatory.

Figure C.2 Seismic stations in central New England. Stations CSNH, GHNH, MBNH, WBNH, and LANH were operated during the late 1970's by Weston Geophysical Corp. as part of a study of the seismicity of the Lake Winnepesaukee, NH area.

Figure C.3 Seismic stations in Maine and southeastern Canada. The Dickey Array is operated by Weston Observatory for the U.S. Army Corp. of Engineers. The Charlevoix Array is operated by the Earth Physics Branch of the Dept. of Energy, Mines, and Resources, Canada.

Figure C.4 Seismic Stations in New York State. Stations in this area are operated primarily by Lamont Doherty Geological Observatory.

Figure C.5 Seismic stations in southeastern NY and northern NJ. The Indian Point Array is operated by Woodward-Clyde Consultants for the Consolidated Edison Co. of NY.

SEISMIC STATIONS IN SOUTHERN NEW ENGLAND

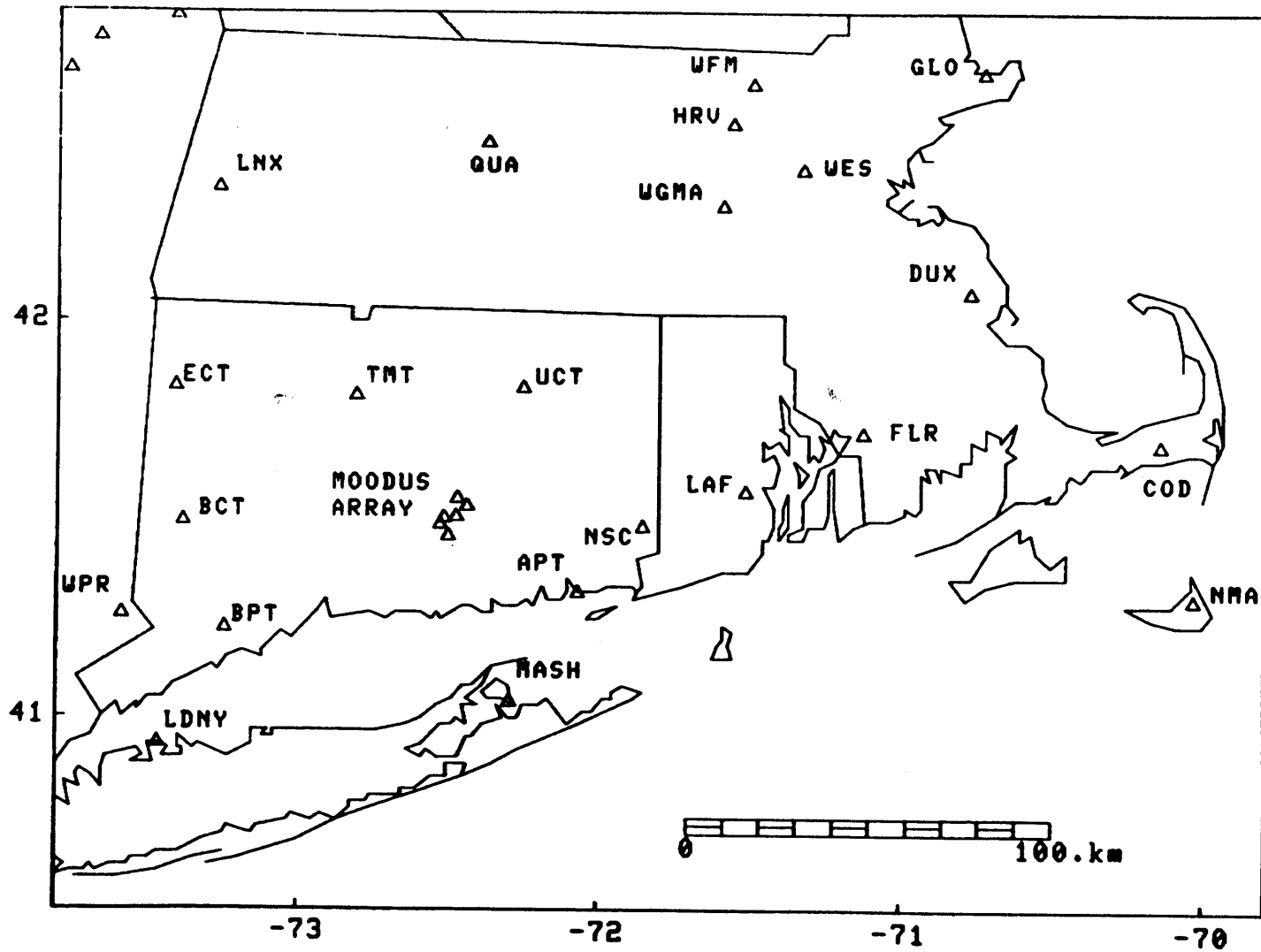


FIGURE C.1

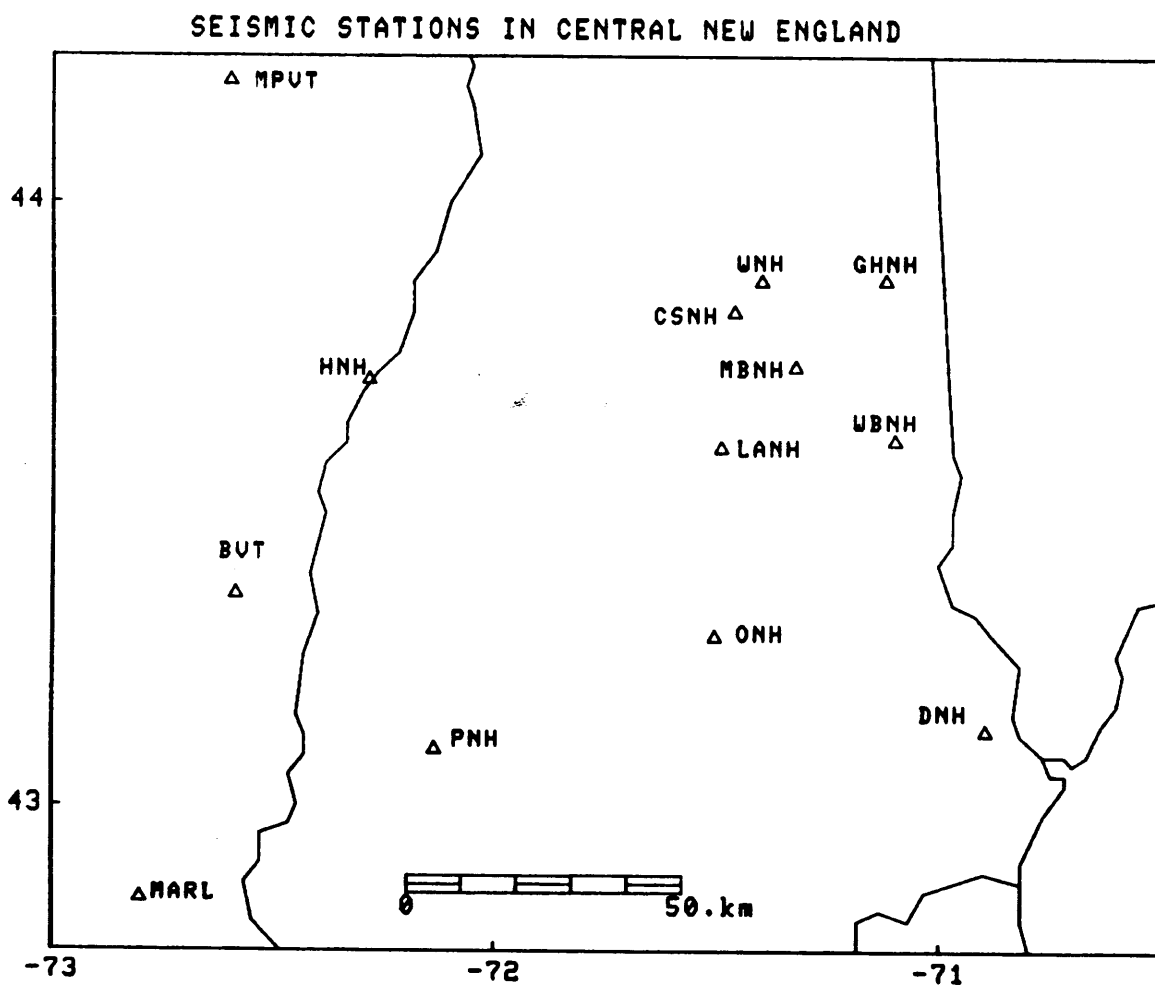


FIGURE C.2

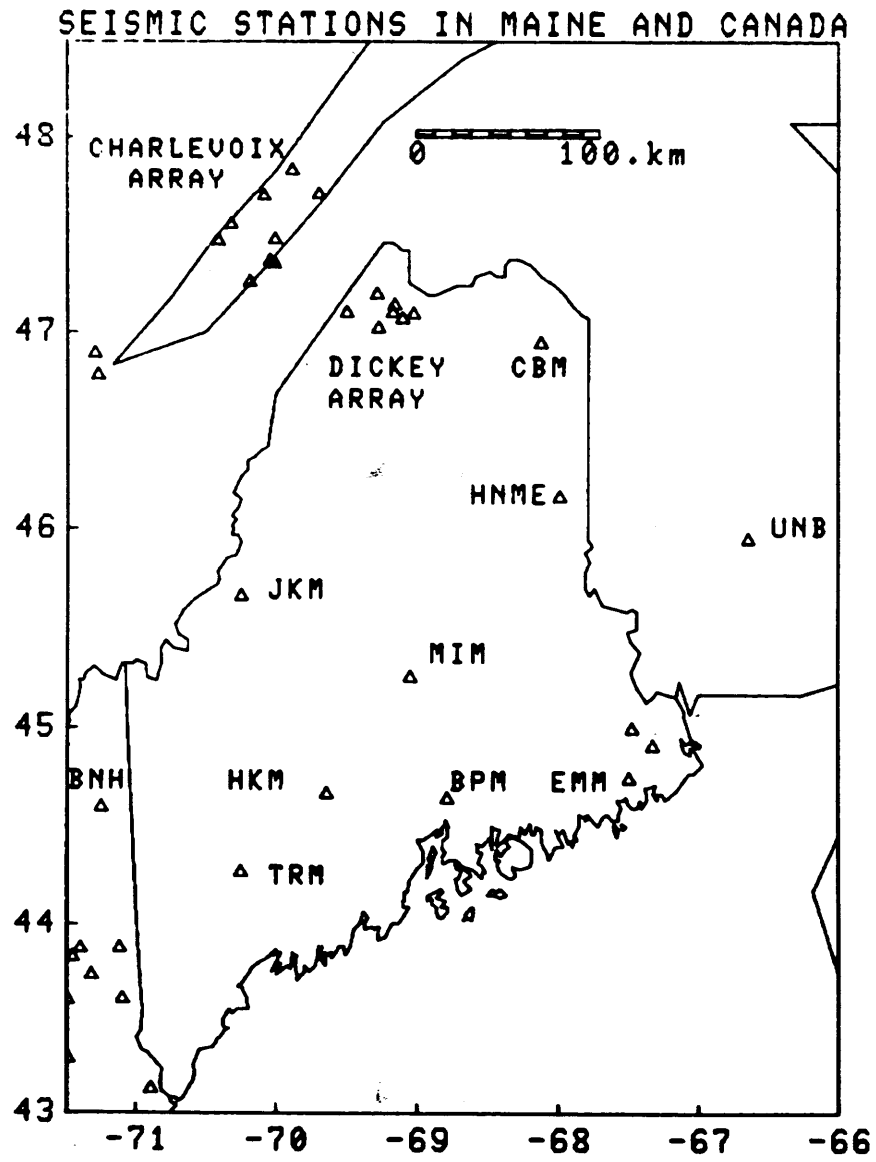


FIGURE C.3

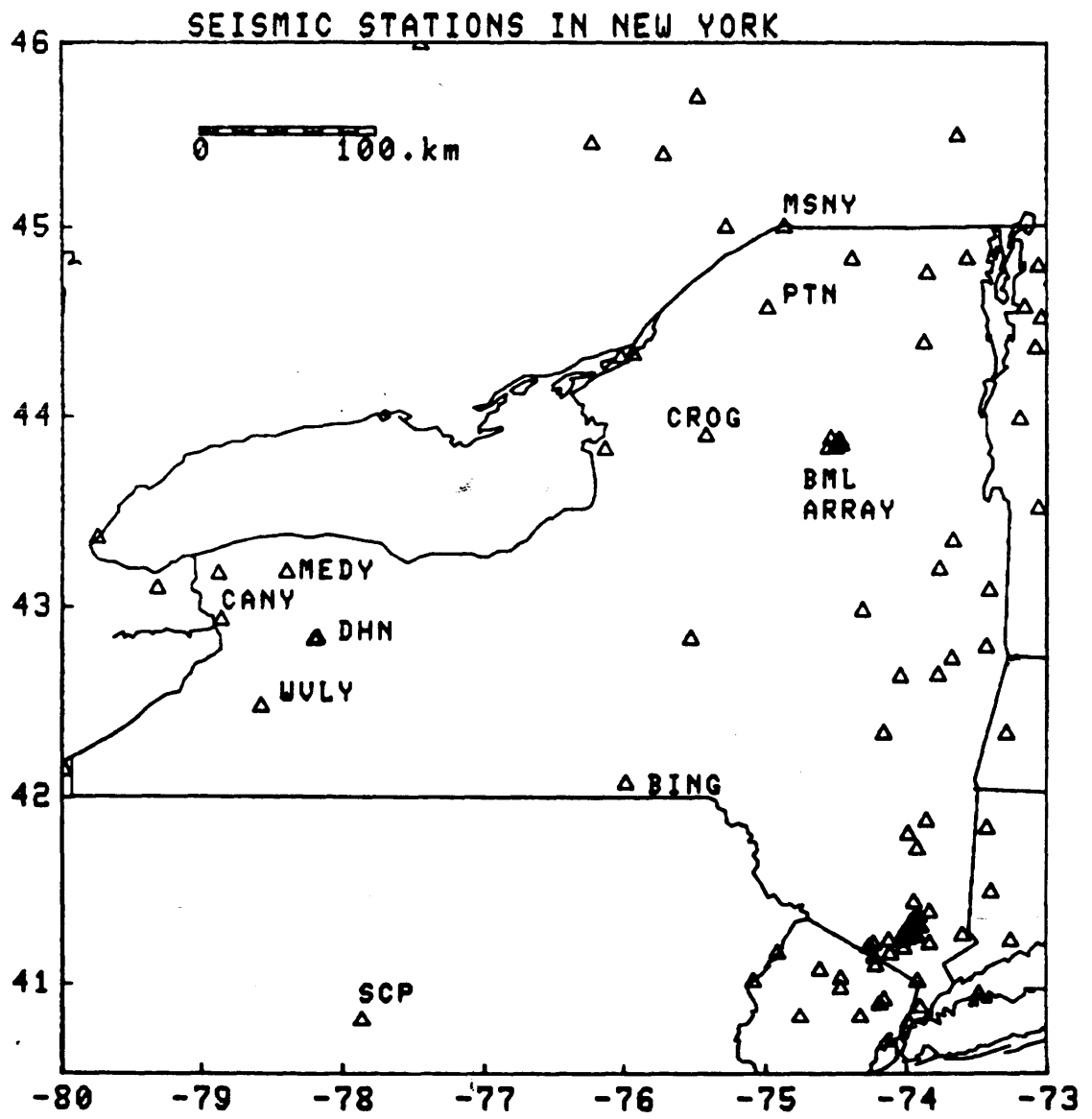


FIGURE C.4

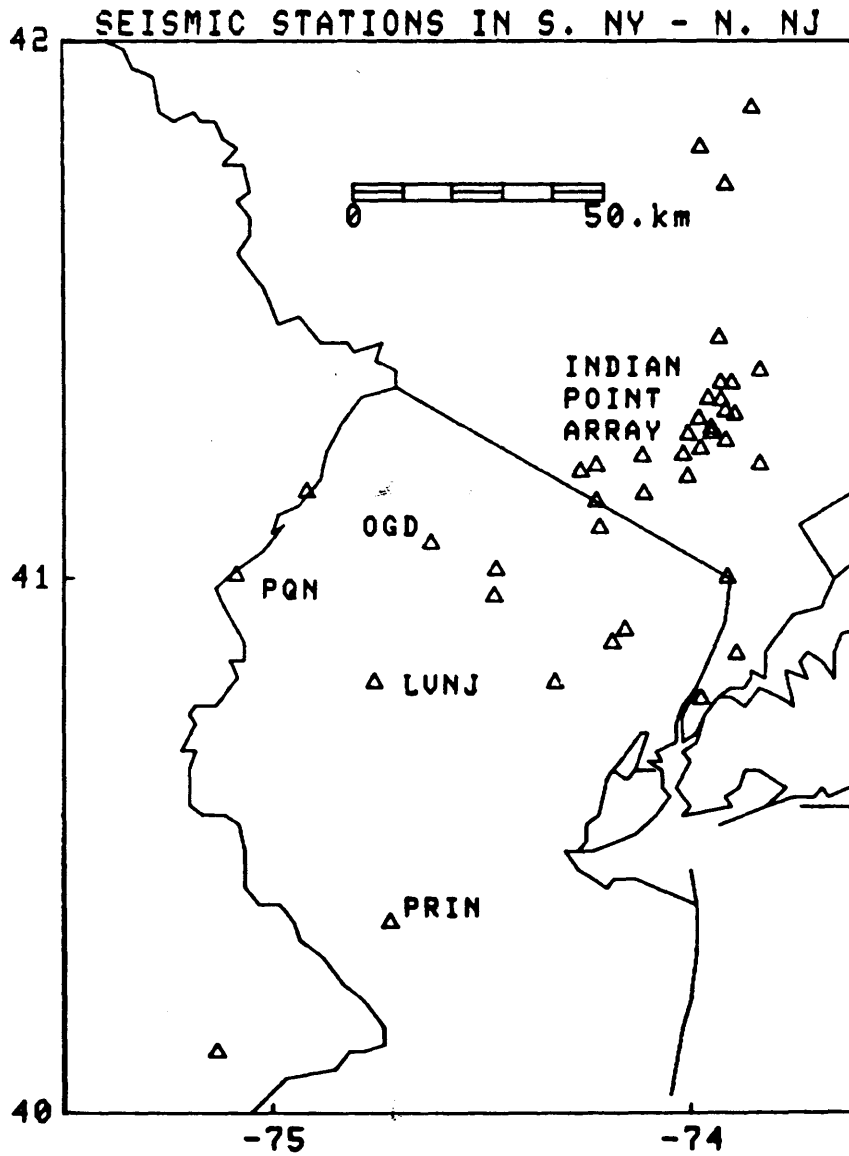


FIGURE C.5

APPENDIX D
THE M.I.T. SEISMIC NETWORK

D.1 Introduction

The M.I.T. Seismic Network, which is part of the N.E.U.S.S.N., began its operation in 1975. The role of this network is to monitor the seismicity of southern New Hampshire and eastern Massachusetts, which is historically one of the most seismically active areas of the NEUS-SEC. In this appendix, we describe the configuration and instrumentation of this network, as well as the digital data acquisition system which has been installed for event detection and automatic data processing.

D.2 Network Configuration and Instrumentation

The M.I.T. Seismic Network presently consists of nine stations in southern New Hampshire and eastern Massachusetts. A map of the network is shown in Figure D.1 with station coordinates given in Table D.1. Not shown in Figure D.1 is station HRV, which was closed in July 1981 as a cost saving measure.

Instrumentation at each site consists of a 1.0 Hz Mark Products L4-C vertical seismometer connected to a preamplifier, amplifier, and voltage controlled oscillator (VCO) of M.I.T. design. The data are then transmitted in analog format across voice-grade telephone lines to the M.I.T. campus in Cambridge, MA. The data are then demodulated and recorded on helicorders, a develocorder equipped with 16 Hz galvanometers, and in digital

format on an HP-1000 computer. The electronic packages are presently being changed to commercial Geotech units without preamplifiers. Stations ONH and WFM also have horizontal seismometers. WFM is the George R. Wallace, Jr. Geophysical Observatory, which in addition to the short period instruments has long period seismometers, tiltmeters, a Lacoste-Romberg tidal gravity meter, and experimental instruments. Station COD is a borehole installation (depth 93 meters) for the purpose of noise reduction. The New Hampshire stations operate at a gain of approximately 100K at 1.0 Hz, while the Massachusetts stations, which are located in noisier environments, operate at about 60K at 1.0 Hz.

D.3 ASAP2 - A Digital Data Acquisition System

The analog recording systems used by the N.E.U.S.S.N. (i.e., helicorders and develocorders) are adequate for routine event detection, arrival time measurement, and some magnitude determinations (especially coda magnitudes). However, many source parameters can only be determined from the spectrum of the seismogram or a full-waveform recording. For this reason, as well as the implementation of automatic data processing schemes, a digital data acquisition and recording system was developed for the M.I.T. Seismic Network. The system, known as ASAP2 (As Soon As Possible Automatic Seismic Analysis Package) is based on direct digital recording with data flagged for archiving by a real-time event detector. (This writeup has been taken in part from the paper by Michael et al., 1982).

ASAP2 was designed with a number of goals in mind. The first was to provide high quality digital records for the analysis of all important events. No FM tapes were to be used. The system was also designed to minimize the number of false triggers by correlating detections among three stations. The ability to access the data while the system is running was an important goal. This allows event location and analysis for an important earthquake without interrupting the detection algorithm or losing recording time. And of course, the system was designed to maximize automation to allow uninterrupted system usage without human interaction.

System Overview: ASAP2 runs on an HP-1000 computer system. The CPU is a 16-bit 21MX E-series processor with 384K bytes of semiconductor memory. A 7905 disc with a capacity of 14.7M bytes is used for temporary data storage, along with a 7920 50M byte disc for interactive users. Permanent storage is on 9-track 1600-bpi magnetic tape.

The computer receives the data through an HP-91000 A/D converter, which places the data in a 12-bit format. The data are transferred directly from the analog transmission system to the computer's digital representation. Timing is provided by the computer's internal crystal clock; however, this clock has an unacceptable drift rate of up to 0.5 seconds per day. To correct this, the computer's clock is periodically set by program GCLOCK to the National Bureau of Standards clock signal which is received via their GEOS satellite. A clock trace from

a Sprengnether crystal clock is also recorded as a short period data channel to allow correction for any drift that does occur.

Figure D.2 traces the data and control flow through ASAP2. Every twenty-fifth of a second (the current short period sampling rate) program DASIN reads the 16 channels on the A/D card. The data are then passed to program DASYS which sorts the data into short and long periods according to the channel list in disk file \$DCHAN. DASYS writes all short period data to disc file #DASSP, the short period temporary storage file. For long period data, only 1 out of every 250 readings is written to disc file #DASLP, the long period temporary storage file. Thus, the short period data are sampled at 25 Hz, while the long period data are sampled at 1 Hz. DASIN and DASYS are separate programs so that DASIN does not have to wait for the disc. This allows DASIN to take samples at exact time intervals.

The event detectors DETSP and DETLP examine the data in #DASP and #DASLP respectively, searching the incoming data for events. #DASSP and #DASLP each contain approximately the past 30 minutes of data. This allows some variation in the speed of the event detectors, but they must average real time operation. It also permits the saving of noise preceding the event.

When an event is detected, DETxP (where x is S or L) starts program SAVxP. SAVxP transfers the event data from #DASxP to the event file #EVExP.

Coordination of all programs is accomplished through the DASTA status tables which are stored in memory.

When files #EVESP or #EVELP are nearly full (determined by running status program SAVTI), program ARCHV is run manually to transfer the data to tape for permanent storage. These tapes are then available for analysis. A library of user programs allows access to all parts of the system.

With the present sampling rate of 25 Hz, ASAP2 uses about one third of the computer's resources: memory, CPU time, and disc space. The remainder is available on a timesharing basis for analysis of the ASAP2 data and general computing.

Event Detection: The purpose of an event detection algorithm is to essentially duplicate human visual event detection. Thus, an algorithm must be devised which simulates the logical steps which a human analyst goes through when deciding if a signal has arrived, and whether that signal is real or is noise.

The most commonly used event detection algorithm employs the ratio of the short-term to the long-term average (STA/LTA) of the incoming signal amplitude. If the amplitude of the signal is $A(\tau)$ at the time sample τ , then the short term average at time t is

$$a(t) = (1/\Phi) \sum_{\tau=t-\Phi}^t |A(\tau)| \delta\tau \quad (D.1)$$

where Φ is the length of the time window for the short-term average, typically 1 second, and $\delta\tau$ is the sampling interval. Similarly, the long-term average at time t is

$$\beta(t) = (1/\Gamma) \sum_{\tau=t-\Gamma}^t |A(\tau)| \delta\tau \quad (D.2)$$

where Γ is the length of the time window for the long term average. The value of Γ depends on the application and may range from a few seconds to tens of minutes. The STA/LTA ratio is then

$$\gamma(t) = a(t)/\beta(t) \quad (D.3)$$

and an event is said to be detected when

$$\gamma(t) > \Psi \quad (D.4)$$

where Ψ is the detection threshold level. If Ψ is set too low, noise bursts will cause many false triggers. If Ψ is set too high, earthquakes of interest may go undetected. Consequently, the STA/LTA algorithm is suited for areas of high seismicity and low noise. In New England, the rate of seismic activity is low and the noise characteristics change both daily and seasonally. Thus, we have chosen to implement a more advanced event detection algorithm.

A human analyst bases his event detection decisions on changes in both signal amplitude and frequency. Thus, by using a machine detector based on a transform of the data into a frequency domain, changes in amplitude and frequency can be automatically sensed and used for the detection process.

The most commonly used transform is the Fast Fourier Transform (FFT). Since the FFT requires many floating point multiplications, it is too slow for real-time application on the HP-1000. In our case, the Walsh Transform is used in the detection algorithm. Walsh functions are a complete orthogonal set of rectangular waveforms that always take the value ± 1 (Beauchamp, 1975; Harmuth, 1972). Thus, the transform is taken by using integer additions and subtractions. Consequently the Walsh Transform is computationally faster than the FFT.

While the FFT transforms a time series into the frequency domain, the Walsh Transform goes into the sequency domain. Sequency is a more general concept of which frequency is a member. The Walsh sequency domain does reflect the frequency domain, but it is important to remember that the Walsh Transform does not yield a true frequency spectrum.

Goforth and Herrin (1981) first applied the Walsh Transform to seismic event detection. The M.I.T. event detector is similar to theirs, but has some improvements and modifications. ASAP2 ignores phase shifts in the data, demands greater continuity of the signal, and uses data from several stations in the decision making process. The last two modifications were necessary due to the noise problems associated with surface stations in populated and coastal areas. A set of criteria for determining the end of an event has also been added.

The explanation of the event detection algorithm will be separated into four parts: taking the transform, computing the

metric, comparing the metric to the past history, and using this comparison to decide when the event begins and ends. Figures D.3a, b show the logical flowcharts of program DETSP. Only the short period detector will be discussed here. The long period detector differs only in the values of several constants.

As data are placed onto the disk by the data acquisition system, the event detector takes 64-sample windows that overlap by 32 samples (or 2.56 second windows that overlap by 1.28 seconds at the present 25 Hz sampling rate). This is indicated in Box 2 of Figure D.3a. This is done for three of the nine stations that are used for short period detection. A subset of the network is used for two reasons. First, it is faster than using the entire network for detection, and second, experience has shown that some stations are better than others for detection due to the properties of their background noise.

These 64-point sections are transformed into the Walsh sequency coefficients 1 to 63 (Box 3, Figure D.3a). Sequency 0 is the DC average and is not computed. Note that this removes DC drift from the data. (DC drift can be significant when the center frequency of the telemetry unit has drifted due to temperature or other changes.) The Walsh functions of sequency 1 and 2 are phase shifts of each other, as are 3 and 4, 5 and 6... Each member of each pair is squared and then each pair is summed. This yields the power sequency spectrum of 32 (1+2, 3+4, ..., 63) coefficients that is unaffected by phase shifts. This last step of moving to the power spectrum was not used by

Goforth and Herrin (1981). It is added here not to work in the power spectrum but to remove the effects of phase shifts. A return to the amplitude sequency spectrum by taking square roots of the coefficients takes too long, so this is not done. Here, $S(k)$ represents the power spectrum.

To form the metric M (Box 4, Figure D.3a) the power spectrum is divided point-by-point by a stored average noise power spectrum $N(k)$ for that station. (Finding the average noise spectrum is the first step in the initialization process of the event detector (Box 1, Figure D.3a). The normalized spectrum is then summed over power coefficients 1 to 25 (sequency 1 to 50) to produce the metric M . It is the division by the noise spectrum that allows the detection of frequency shifts as the following example shows.

Suppose that analysis uses two power coefficients and they have the values 1 and 32 in the noise power spectrum. If the present power spectrum is also 1 and 32, then $M=1/1+3/3=2$. If however the present power spectrum is 3 and 1, then $M=3/1+1/3=3$ (using integer operations). Thus the frequency shift away from the noise spectrum has caused an increase in the metric M .

Once the metric is computed, it is compared against a past history of metrics for that station. This comparison is against a threshold computed as follows (Box 5, Figure D.3a):

$$T = M(50) + [M(75)-M(50)] \quad (D.5)$$

where T is the threshold, $M(50)$ is the median of the M history, $M(75)$ is the 75th percentile value of the M history, and K is a positive constant (presently 25). Note that the quantity $[M(75)-M(50)]$ is similar to the standard deviation of the values in the M history. To compute the threshold we must have an M history; finding this is the second step of the initialization process. At any time, the M history for a station consists of the last 256 values that were below the threshold. For example, let there be 10 values in a station M history (instead of 256) and let them be 2, 3, 5, 7, 8, 8, 10, 11, 11, 12. Then the median value $M(50)$ is 8 and the 75th percentile value $M(75)$ is 10. With $k=25$ we obtain $T=8+25(10-8)=58$.

When the threshold comparison is made, the process splits into two branches. First consider the process for $M \leq T$ (Box 6 goes to Box 7, Figure D.3a). Since M is below or at threshold it replaces the oldest M value in the history (there are 256 M values in the history for each station). Only M values below the threshold are placed into the history, therefore it represents a history of noise metrics.

After this replacement the algorithm proceeds through Box 8 to Box 10 (Figure D.3a) if no event is in progress. That is, it enters the event detection sequence as opposed to the event termination sequence. The criterion for event detection on a station is a continuity of $M > T$ for 5 successive windows for that station. Since the algorithm has reached Box 10, it knows that this station has no continuity of $M > T$.

If an event is in progress then the algorithm enters the event termination stage in Box 11. The event termination criterion is a continuity of $M \leq T$ for 4 windows. The station's continuity of $M \leq T$ is increased by one in Box 11, because $M \leq T$ for one more window.

If $M > T$ then from Box 6 the algorithm proceeds to Box 9. If no event is in progress the algorithm goes from Box 9 to Box 12, the event detection branch for $M > T$. Here the continuity of $M > T$ is incremented for this station. If an event is already in progress then the algorithm goes instead to Box 13. Here in the event termination branch it knows that there is no continuity of $M \leq T$.

Boxes 3-13 of Figure D.3a are within the dotted line because they are carried out independently for each station. Once each station has completed this part of the algorithm it moves to C or D on Figure D.3b, depending on whether or not an event is in progress.

Starting at C or Box 14 on Figure D.3b is the event detection stage that correlates the information from the three stations. Here it finds how many stations have detected an event in the last 20 seconds, the maximum travel time across the array. In Box 15, if two of the three stations have detected an event in the last 20 seconds, then the event saver program is started (Box 16), the algorithm switches to event termination mode (Box 17), and goes to Box 2, Figure D.3a and repeats the process. If fewer than two stations have detected an event,

then the algorithm has not found an event and returns to get a new data window.

Point D or Box 18 of Figure D.3b is the start of the event termination stage. For an event to terminate the two or three stations that detected it must all meet (or continue to meet) the station termination criterion simultaneously. When this occurs the event saver program is stopped and the detection algorithm switches out of event in progress mode before returning to process a new window of data.

If the event termination criterion is not met, one other check is made in Box 19. If an event has been in progress for more than 20 minutes an error is thought to have occurred. Most likely the detector was set off by a change in the noise. When this occurs the saver is stopped (Box 20) and the detector must be reinitialized (Box 20 via A to Box 1, Figure D.3a).

If the event is not terminated by either of these criteria the algorithm returns to process a new window (Box 19 via B to Box 2, Figure D.3a).

Data Processing: The availability of digital data not only makes it possible to implement advanced seismological techniques, but also allows the use of fast and efficient data processing schemes for routine analysis. For example, earthquake locations can be quickly carried out by interfacing the location program with a graphic display terminal for picking arrival times.

Figure D.4 shows a copy of the screen of an HP-2648A

graphics terminal setup for picking arrival times (program WSPEC). The top trace displays every fifth sample and is used to select a time window of interest. Below is a magnified trace showing all samples. This magnified trace is used for picking the arrival times with a moving cursor. The cursor is moved to the appropriate arrival by the analyst, and by touching a key which identifies the phase, the program reads the arrival time and transfers the data, station name, arrival time, and phase identification to a datafile in a format compatible with the location program. When all channels have been examined, the location program is then started from the terminal.

Record sections of various formats (i.e., number of channels, order of channels, gain, time rate, etc.) can also be easily produced. Figure D.5 shows three examples of records produced by program MSAVE. In D.5a, a record section for a small earthquake in Moodus, CT is shown. In D.5b, the propagation of a teleseismic arrival across the array is presented. And in D.5c, the long period recording of an event near Honshu, Japan is shown.

Table D.1
Stations of the M.I.T. Seismic Network

<u>Code</u>	<u>Latitude</u>	<u>Longitude</u>	<u>Elev. (m)</u>	<u>Location</u>
WNH	43.8683	-71.3997	220.0	Whiteface, NH
ONH	43.2792	-71.5056	280.0	Oak Hill, NH
DNH	43.1225	-70.8948	24.0	Durham, NH
PNH	43.0942	-72.1358	659.0	Pitcher Mountain, NH
GLO	42.6403	-70.7272	15.2	Gloucester, MA
WFM	42.6106	-71.4906	87.5	Westford, MA
DUX	42.0686	-70.7678	27.4	Duxbury, MA
COD	41.6858	-70.1350	-85.0	South Dennis, MA
NMA	41.2974	-70.0261	3.1	Nantucket Island, MA

Figure Captions

Figure D.1 Map of the M.I.T. Seismic Network. The locations of the stations are given in Table D.1 .

Figure D.2 System flowchart of ASAP2 showing the relationships between operations and files.

Figure D.3a,b Flowchart of DETSP, the short period event detector.

Figure D.4 Copy of the screen of an HP-2948A graphics terminal used to display seismic traces and pick arrival times.

Figure D.5 Three examples of record sections produced by program MSAVE. D.5a) Short period recording of a local earthquake near Moodus, CT. Note the small foreshock preceding the main event. D.5b) Short period recording of the P-wave propagating across the array from an earthquake in the Kuril Islands. D.5c) Long period recording of an earthquake near Honshu, Japan.

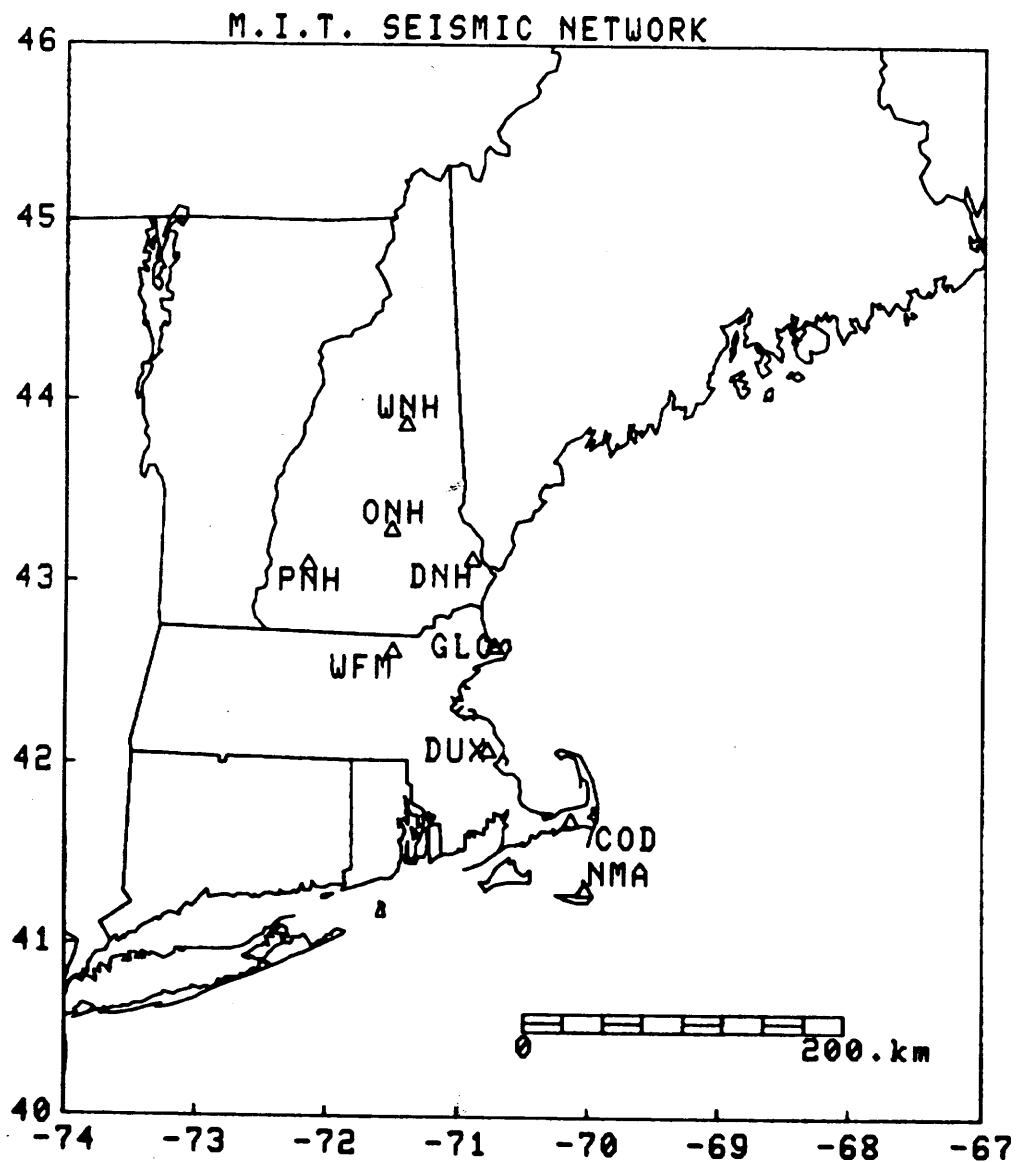


FIGURE D.1

A S A P²

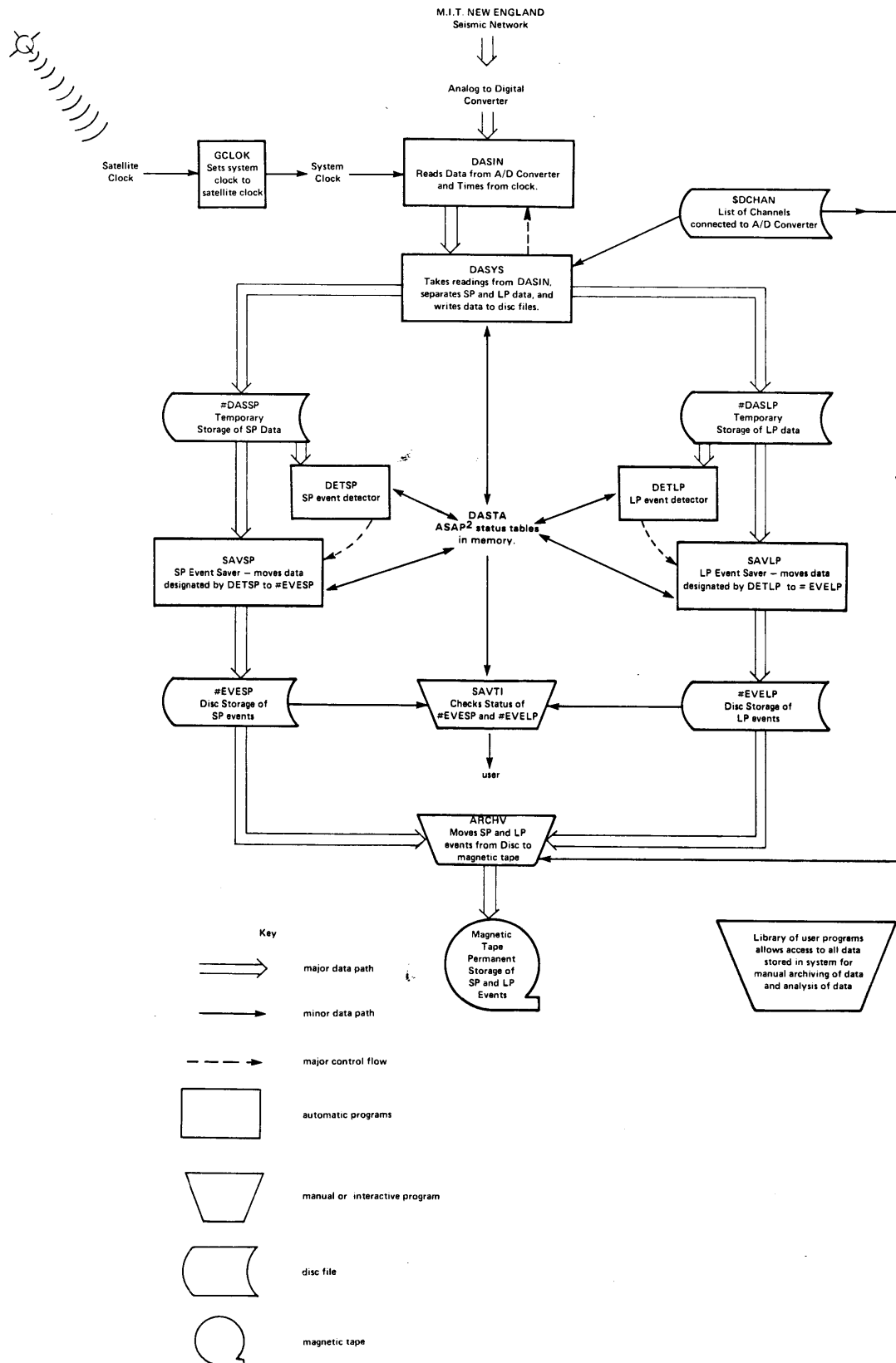


FIGURE D.2

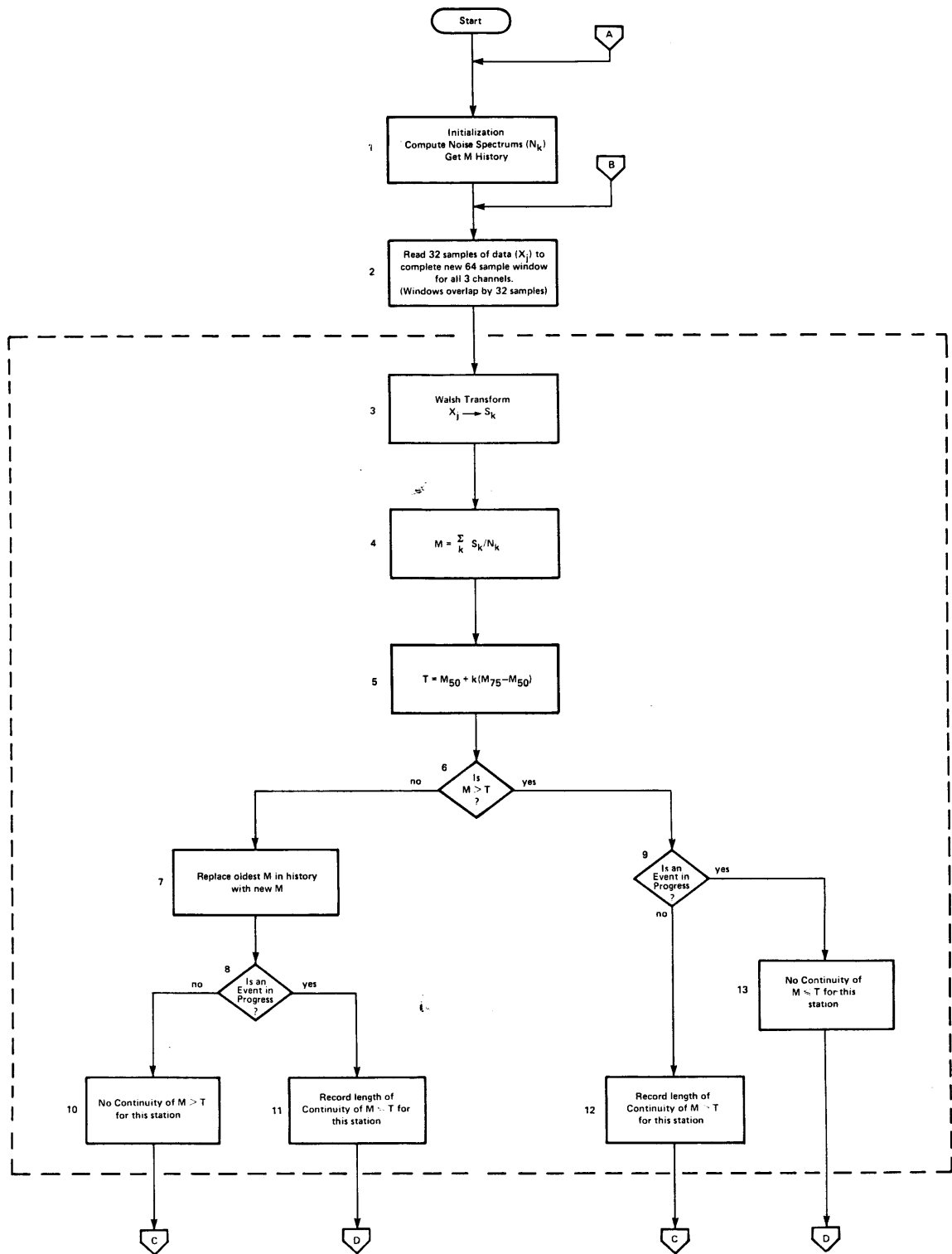


FIGURE D.3a

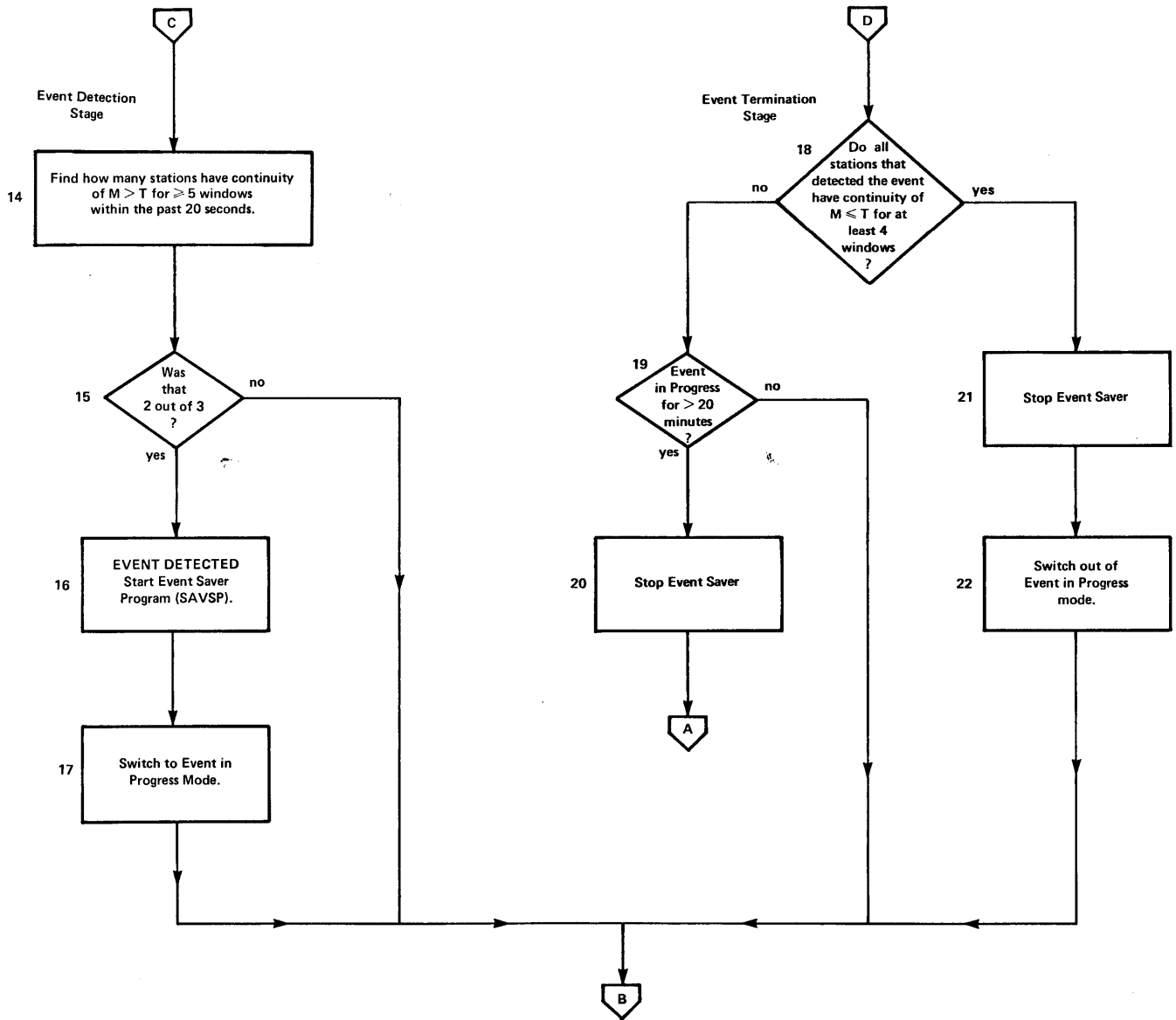
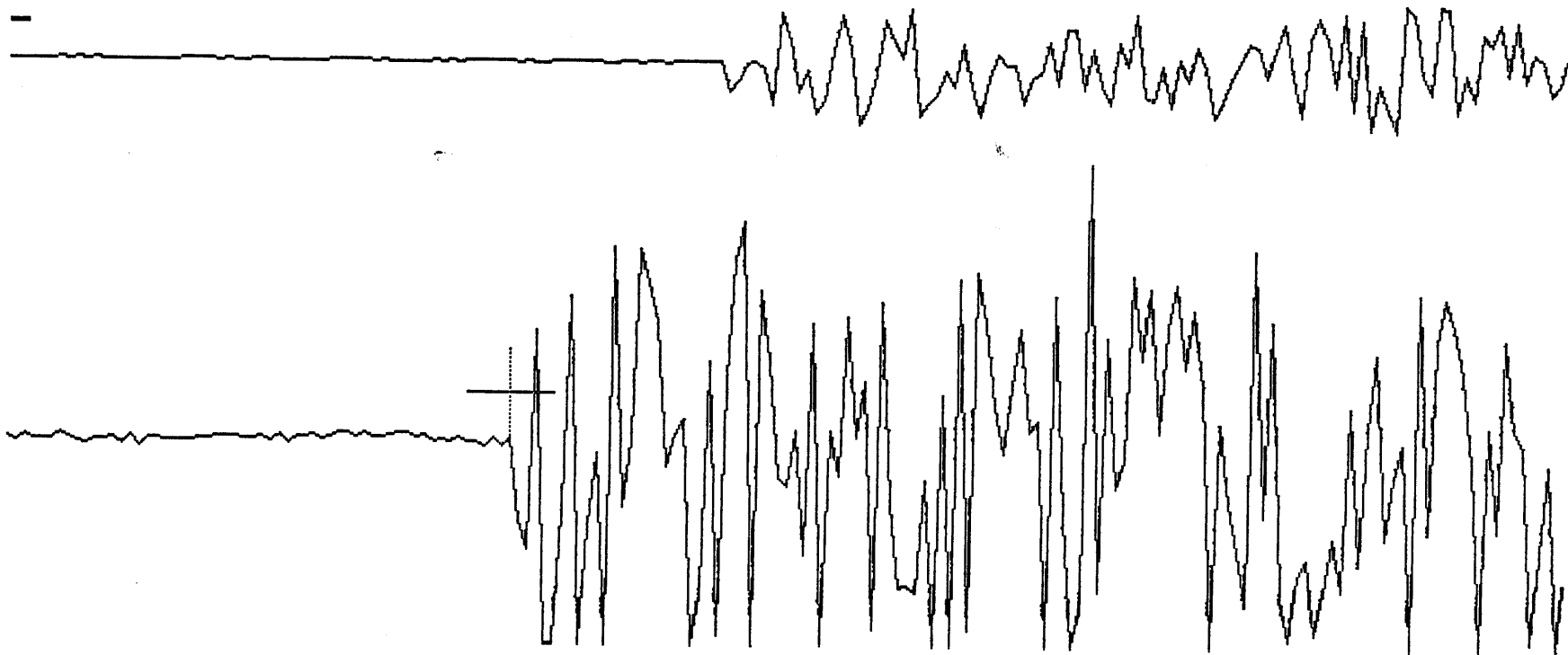


FIGURE D.3b

JUNE 28, 1981
WINNISQUAM, NH

DNH SPZ STARTING AT 1981 179 22:42:24.00
FINE PLOT MODE
1981 179 22:42:40.50 ← time at cursor
DATA= 35



fine plot

FIGURE D.4

P.L.L.T. NEW ENGLAND SEISMIC NETWORK

CHANNEL LIST, NUMBERED LEFT TO RIGHT

CHANNEL 1 18 CYN 802
CHANNEL 2 18 CYN 802
CHANNEL 3 18 CYN 802
CHANNEL 4 18 CYN 802
CHANNEL 5 18 CYN 802
CHANNEL 6 18 CYN 802
CHANNEL 7 18 CYN 802

TIME TICS AS FOLLOWS:
FIRST TICS IN AT
SECOND TICS IN AT
THIRD TICS IN AT
FOURTH TICS IN AT
FIFTH TICS IN AT
SIXTH TICS IN AT
SEVENTH TICS IN AT
EIGHTH TICS IN AT
NINTH TICS IN AT
TENTH TICS IN AT

GAIN/1017.66V/MM

PERIOD TICS IN AT
17 JUNE 1982 14:15

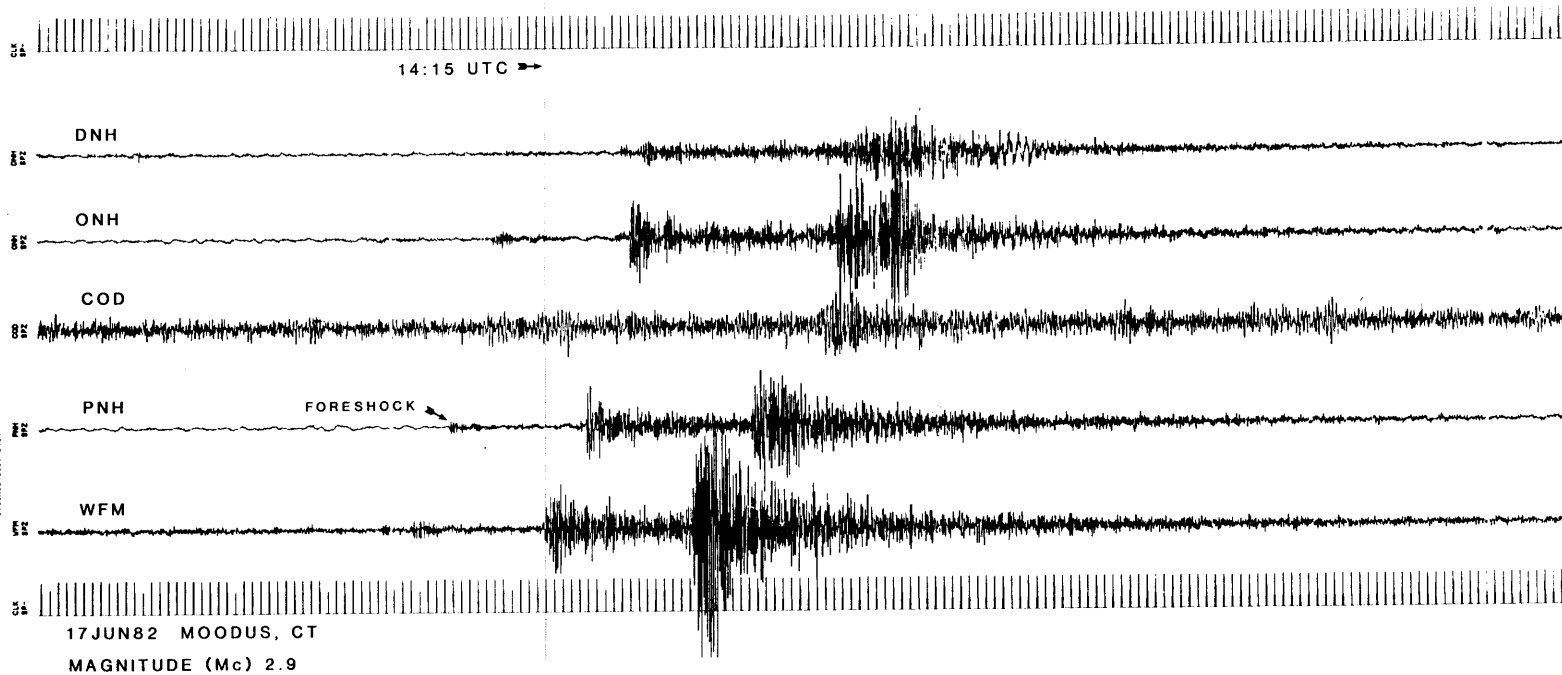


FIGURE D.5a

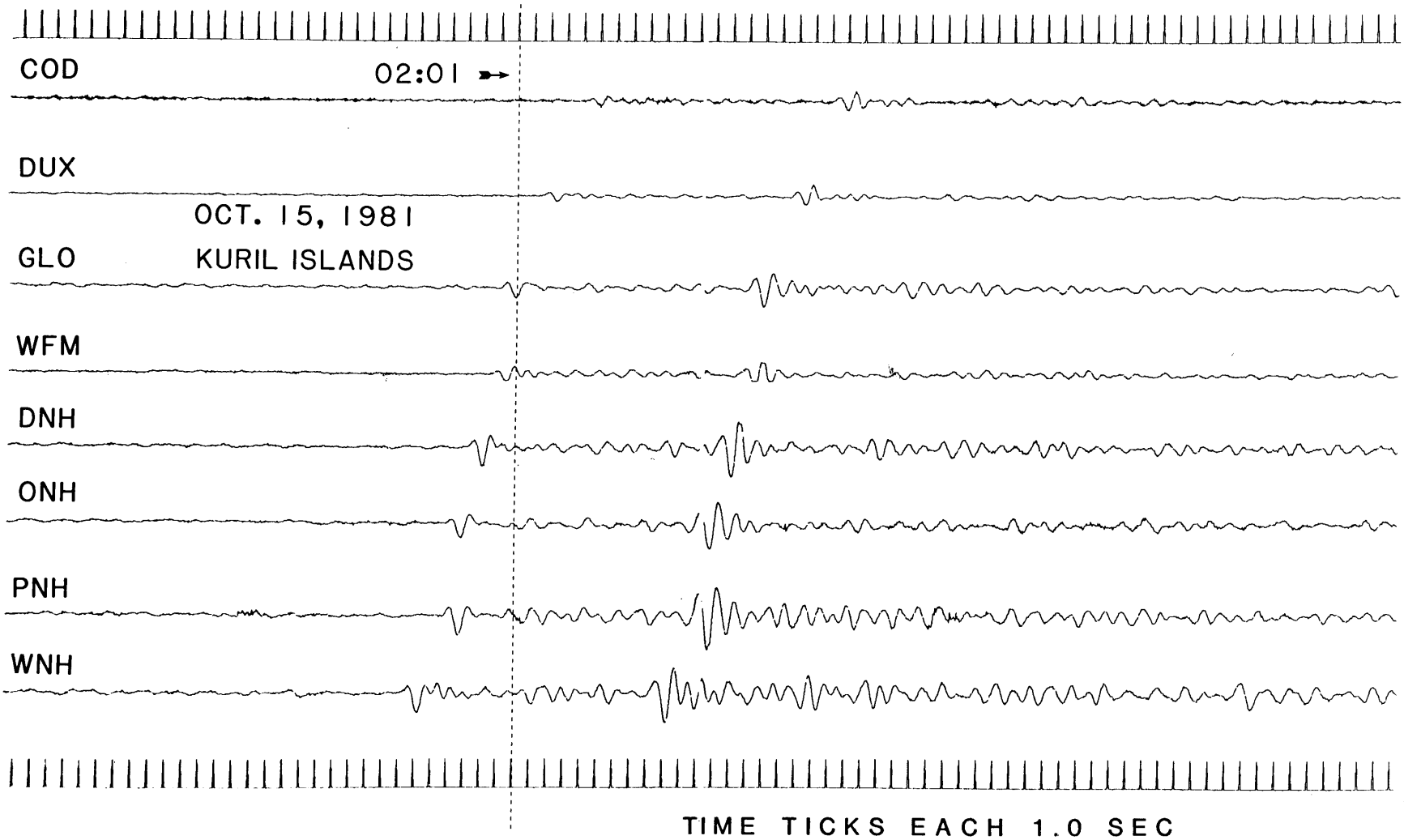


FIGURE D.5b

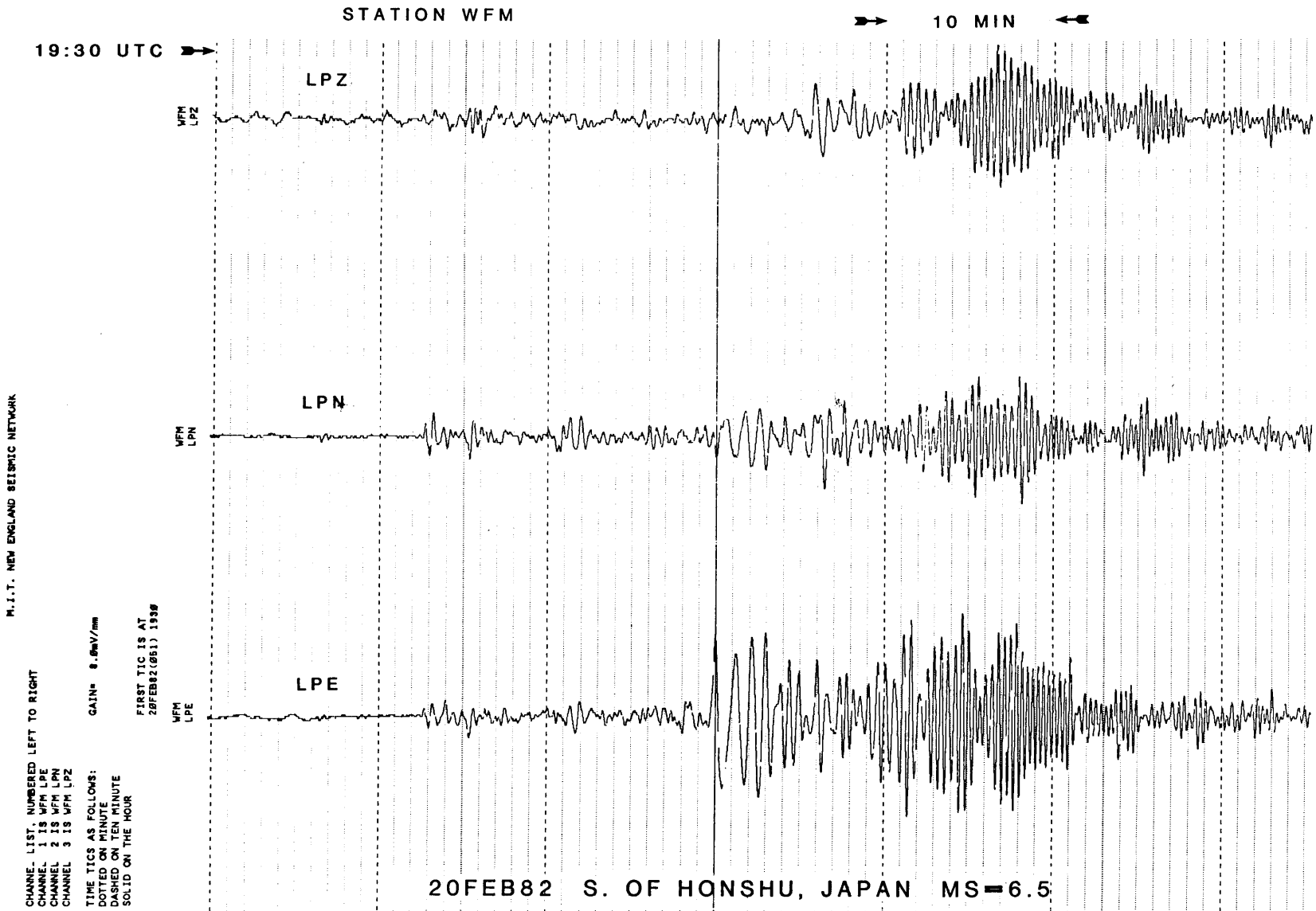


FIGURE D.5c

APPENDIX E
PUBLISHED FAULT PLANE SOLUTIONS IN THE
NORTHEASTERN UNITED STATES AND
SOUTHEASTERN CANADA

In Chapter 3 of this study, we reviewed published fault plane solutions in the NEUS-SEC in order to compile a dataset for interpreting the state of stress in this area. In this Appendix, we show these fault plane solutions, arranged by area. The figures show only the nodal planes and the P- and T-axes, since individual first motions are generally not listed in the publications. Interested readers are referred to the original works for details of these mechanisms. Epicentral data and source parameters for these earthquakes are listed in Table E.1

Table E.1

Fault Plane Solutions for NEUS-SEC Earthquakes

MoDyYr	HrMn	Lat	Long	Dp	Mag	P-Axis		T-Axis		Area	Ref.
						Tr	Pl	Tr	Pl		
010166	1323	42.8	-78.2	2	4.6	62	1	331	28	Attica, NY	1
061367	1908	42.9	-78.2	3	4.4	74	11	336	53	Attica, NY	1
	71	43.81	-74.45	3	3.2	251	18	70	73	Blue Mt Lake, NY	2
061573	0109	45.32	-70.91	6	4.8	47	32	187	51	ME-QUE Border	3
060974	0301	47.43	-70.36	19	-.3	256	7	351	37	La Malbaie, PQ	4
062074	1336	47.41	-70.18	17	1.7	219	58	353	24	La Malbaie, PQ	4
062374	0906	47.51	-70.22	15	0.5	317	1	217	83	La Malbaie, PQ	4
063074	1155	47.72	-69.84	15	2.0	94	5	310	83	La Malbaie, PQ	4
070274	0230	47.56	-70.23	4	0.3	100	3	191	25	La Malbaie, PQ	4
071374	1929	47.49	-69.97	13	0.6	110	17	246	67	La Malbaie, PQ	4
060774	1945	41.63	-73.94	1	3.3	225	10	45	70	Wap. Falls, NY	5
122174	1451	45.04	-74.03	3	2.9	249	6	140	83	Valleyfield, PQ	6
010475	2040	44.89	-74.55	0	2.8	259	16	56	72	Massena, NY	6
060975	1839	44.89	-73.57	13	4.2	253	8	75	84	Altona, NY	6
071275	1237	46.45	-76.21	17	4.2	210	15	5	50	Maniwaki, PQ	7
171975	2059	41.43	-73.79	3	2.3	135	30	333	58	Mahopoc, NY	6
082275	1749	41.14	-73.95	3	2.3	276	18	96	72	Lake de For, NY	6
110375	2054	43.91	-74.64	4	3.9	250	7	65	85	Racquette, NY	6
031176	2107	40.95	-74.35	1	2.6	118	38	303	52	Pomp Lake, NY	6
041376	1539	40.83	-74.05	3	3.0	260	32	133	45	Ridgefield, NJ	6
042476	1022	41.46	-72.49	0	2.2	205	5	30	65	E. Haddam, CT	9
042876	2132	44.58	-74.63	1	2.8	250	15	61	82	Potsdam, NY	6
082076	2208	41.13	-73.76	5	2.5	285	30	158	47	Mt. Pleasant, NY	6
092276	0904	41.29	-73.95	8	1.8	120	15	311	71	Indian Pt, NY	6
112276	0443	40.99	-73.86	5	1.9	294	25	37	64	Yonkers, NY	6
121776	1030	41.47	-72.07	0	2.2	90	45	295	40	Norwich, CT	9
031077	1622	41.18	-74.15	6	2.2	116	23	322	59	Sufferin, NY	6
09 77		41.31	-73.95	0	2.5	220	15	10	65	Annsville, NY	10
092877	1721	44.39	-73.89	3	3.1	64	36	180	34	Wilmington, NY	6
120477	2350	40.80	-74.77	1	2.3	311	7	80	77	Schooley Mt, NJ	6
122077	1744	41.78	-70.66	0	3.1	120	5	300	85	Wareham, MA	9
010478	1928	44.04	-70.51	0	3.2	340	20	150	70	Otisfield, ME	9
021878	1448	46.35	-74.12	7	4.1	255	5	75	85	St. Donat, PQ	11
062178	1831	43.66	-71.38	0	1.8	100	5	10	25	Lake Winn, NH	9
073078	1054	45.64	-74.37	3	3.8	35	8	269	78	Lachutte, PQ	6
082178	0847	44.52	-74.51	1	1.9	53	28	279	62	Bay Pond, NY	6
102978	2359	43.94	-70.40	0	2.5	340	5	160	85	Crescent Lake, ME	9
080979	2249	47.67	-69.90	10	5.0	105	15	355	45	La Malbaie, PQ	12
01 80		41.31	-73.95	0	2.9	260	15	55	75	Annsville, NY	10
070481	2316	45.11	-74.61	16	3.3	45	20	150	45	Cornwall, ONT	13
070581	2147	45.11	-74.61	16	3.3	20	13	140	40	Cornwall, ONT	13
010982	1253	46.98	-66.66	10	5.7	93	0	273	90	New Brunswick	14

References: 1, Herrmann (1978); 2, Sbar et al. (1974); 3, Herrmann (1979); 4, Leblanc and Buchbinder (1977); 5, Pomeroy et al. (1975); 6, Yang and Aggarwal (1981); 7, Horner et al. (1978); 8, Pulli and Toksöz (1981) and this work; 9, Graham and Chiburis (1980); 10, Horner et al. (1979); 11, Hasegawa and Wetmiller (1981); 12, Schlessinger-Miller et al. (1981); 13, Pulli and Godkin (1982) and this work; 14, Nabelek et al. (1982)

Figure Captions

Figure E.1 Focal mechanisms of the Attica, NY earthquakes of 01Jan66 and 12Jun67, from Herrmann (1978). Lower hemisphere projections.

Figure E.2 Focal mechanisms of two earthquakes near Cornwall, ONT from Schlessinger-Miller et al. (1981), and two earthquakes in western Quebec, from Horner et al. (1978) [12Jul75] and Horner et al. (1979) [18Feb78]. Lower hemisphere projections.

Figure E.3 Focal mechanisms of earthquakes in N New York - W Quebec, from Yang and Aggarwal (1981), and a composite fault plane solution for the Blue Mountain Lake earthquakes from Sbar et al., (1972). Lower hemisphere projections.

Figure E.4 Focal mechanisms of earthquakes in the La Malbaie, PQ area, from Hasegawa and Wetmiller (1980) [19Aug79] and Leblanc and Buchbinder (1977) [09Jun74 - 13Jul74]. Lower hemisphere projections.

Figure E.5 Focal mechanism of the 09Jan82 New Brunswick earthquake, from Nabelek et al. (1982)

Figure E.6 Focal mechanisms of earthquakes in New England, from Graham and Chiburis (1980). Lower hemisphere projections.

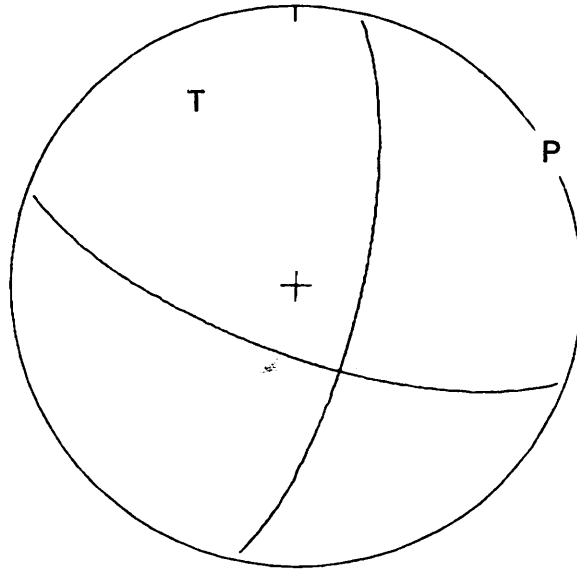
Figure E.7 Three focal mechanisms for the 15Jun73 Maine-Quebec border earthquake, from Wetmiller (1975), Herrmann (1979), and Yang and Aggarwal (1981). Lower hemisphere projections.

Figure E.8 Focal mechanisms of earthquakes in southeastern NY - northern NJ, from Yang and Aggarwal (1981). Lower hemisphere projections.

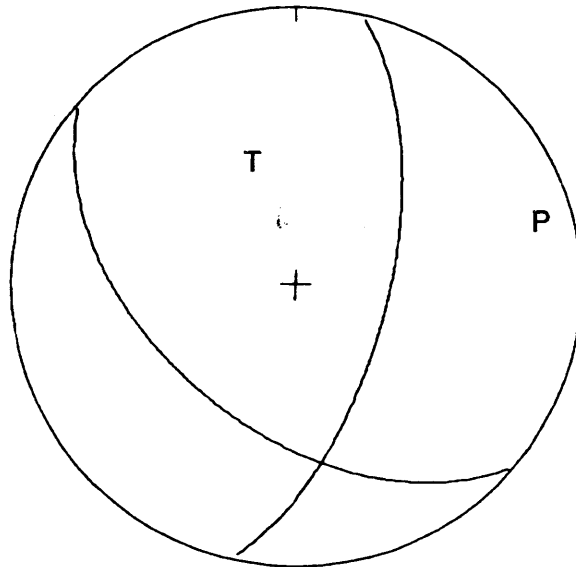
Figure E.9 Two focal mechanisms for the Wappinger Falls, NY earthquake of 04Jun74, from Pomeroy et al. (1974) and Yang and Aggarwal (1981), and two composite focal mechanisms for two earthquakes sequences in Annsville, NY [1977 and 1980] from Seborowski et al. (1982). Lower hemisphere projections.

ATTICA, NY EARTHQUAKES

01 JAN 66



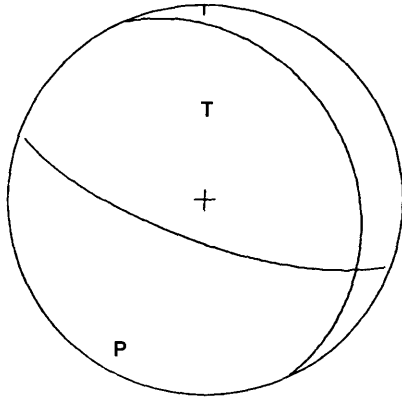
13 JUN 67



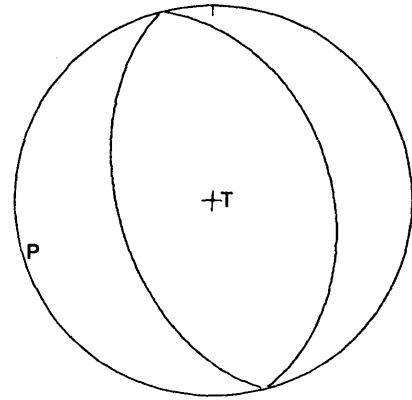
(LHP)

FIGURE E.1

12JUL75 MANIWAKI, PQ

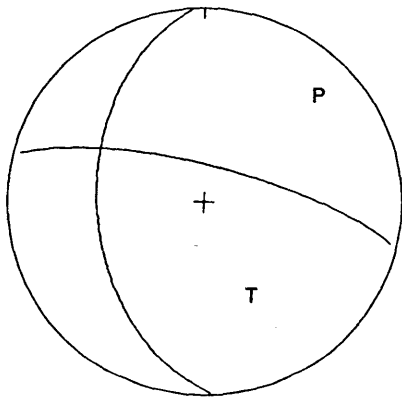


18FEB78 ST-DONAT, PQ

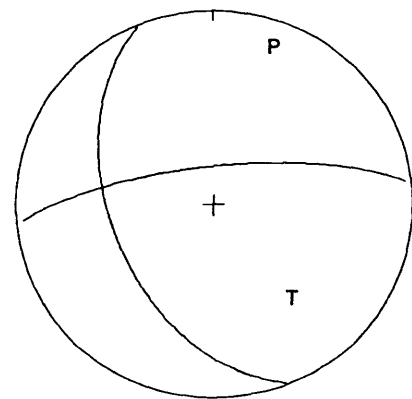


CORNWALL, ONT EARTHQUAKES

04JUL81



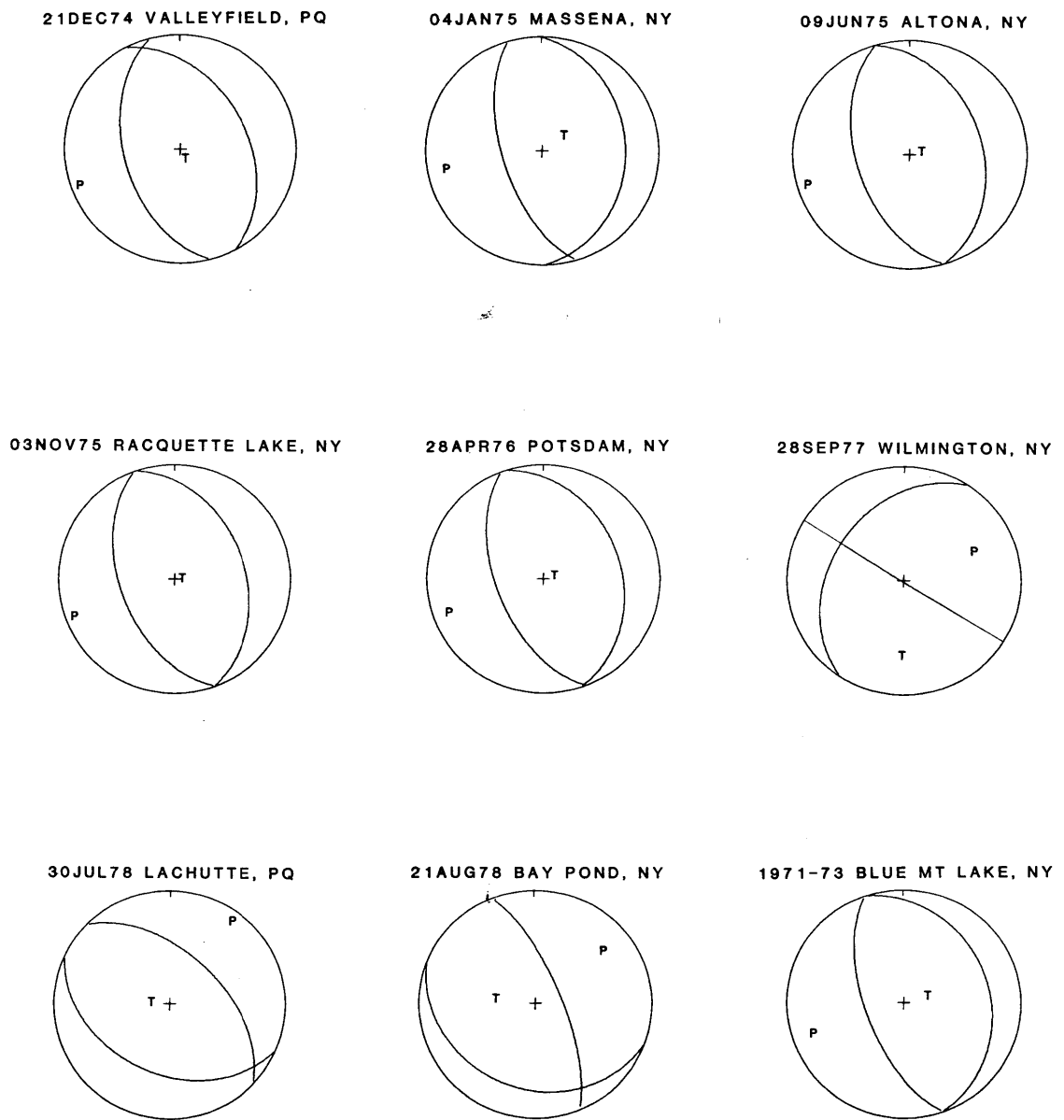
05JUL81



(LHP)

FIGURE E.2

N NEW YORK - W QUEBEC EARTHQUAKES



(LHP)

FIGURE E.3

LAMALBAIE, PQ EARTHQUAKES

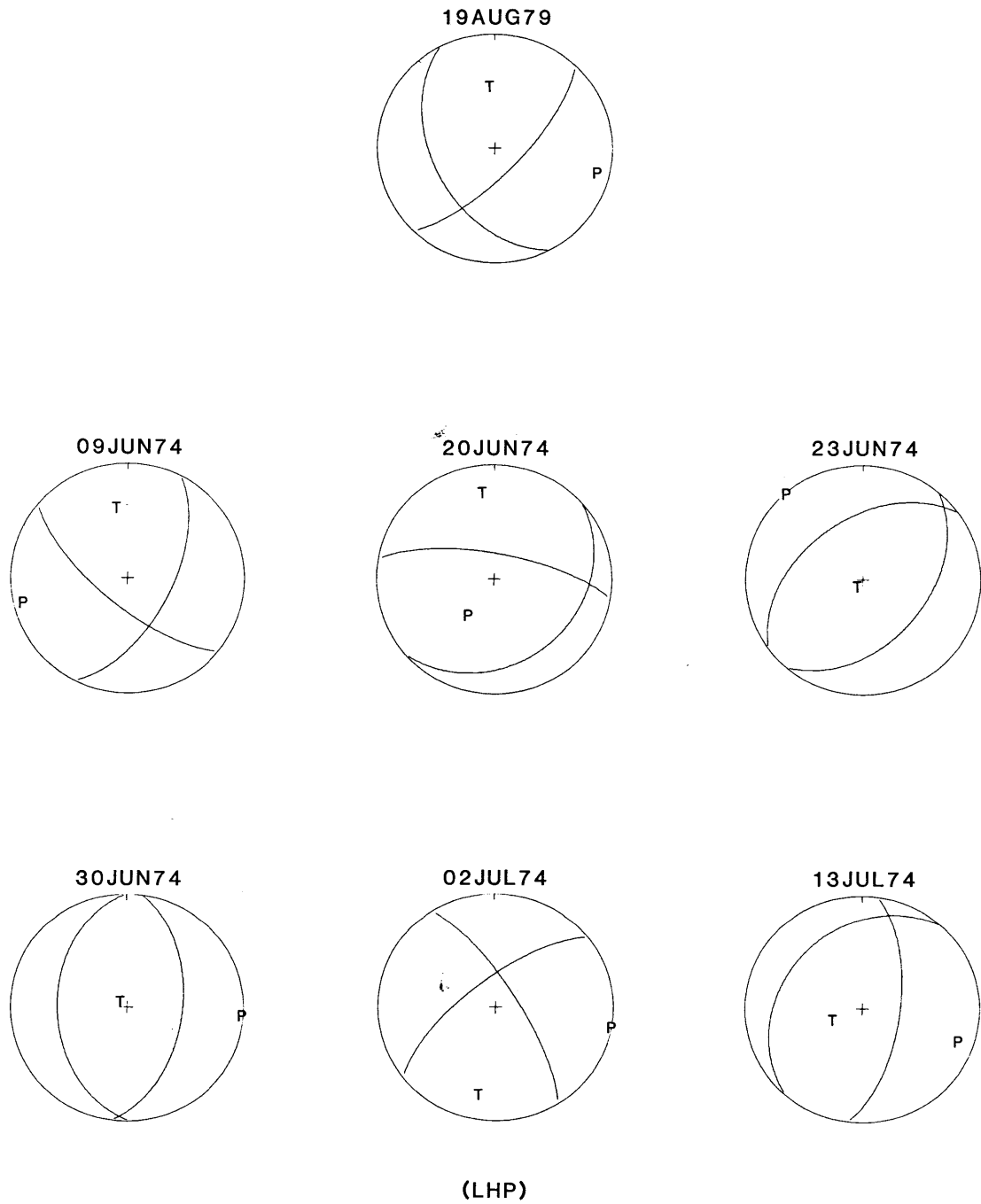
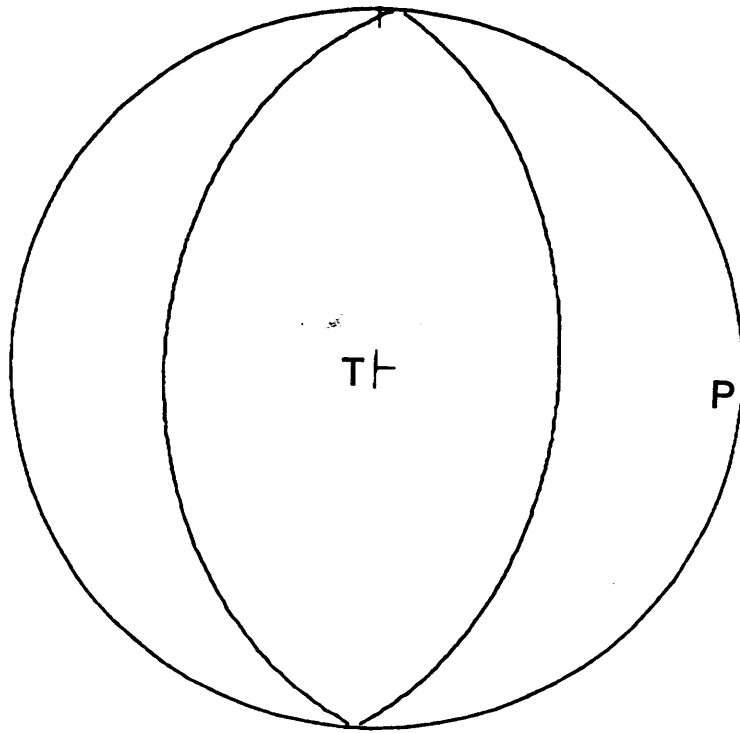


FIGURE E.4

09JAN82 NEW BRUNSWICK

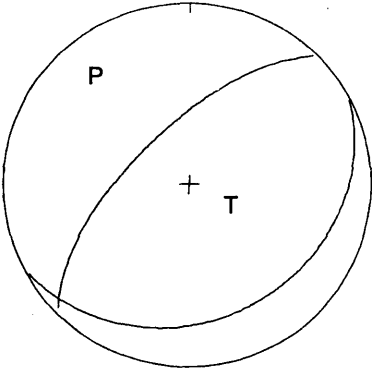


(LHP)

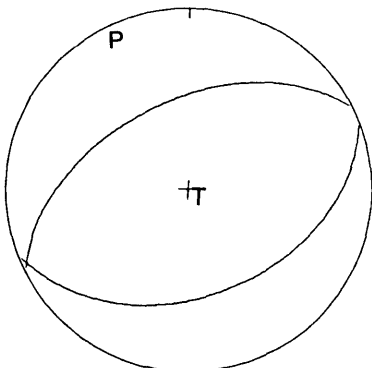
FIGURE E.5

NEW ENGLAND EARTHQUAKES

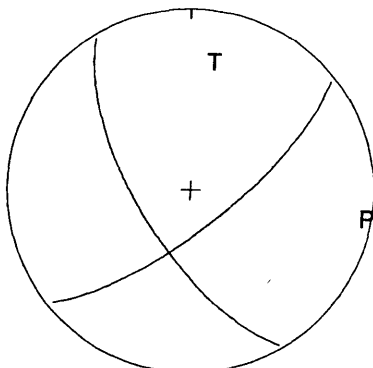
04JAN78 OTISFIELD, ME



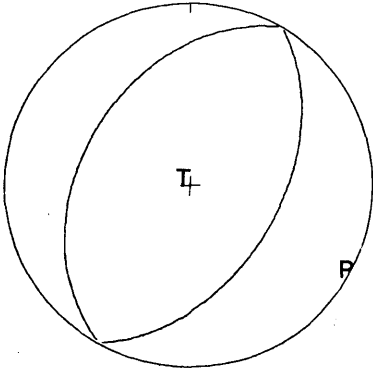
29OCT78 CR LAKE, ME



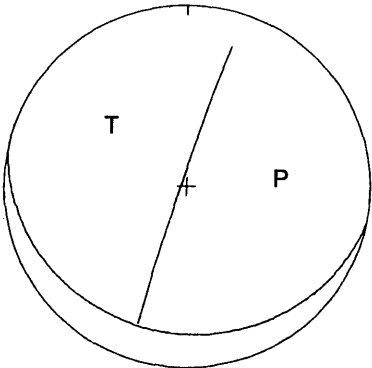
21JUN78 LAKE WINN, NH



20DEC77 WAREHAM, MA



17DEC76 NORWICH, CT



24APR76 E HADDAM, CT

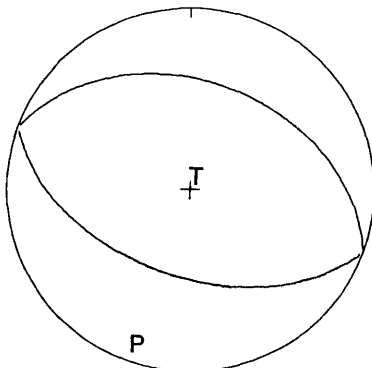
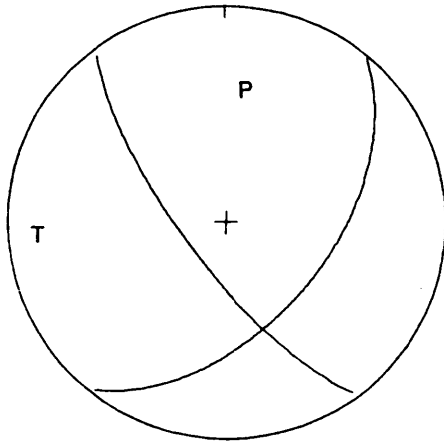


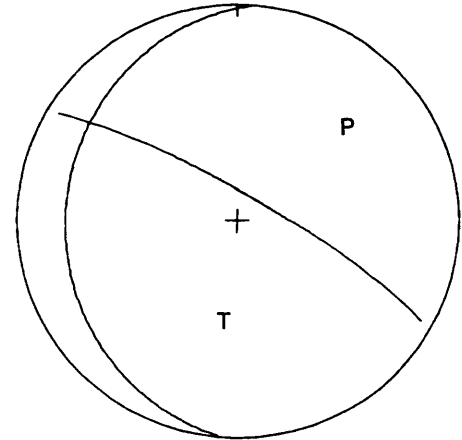
FIGURE E.6

15JUN73 ME-QUE BORDER

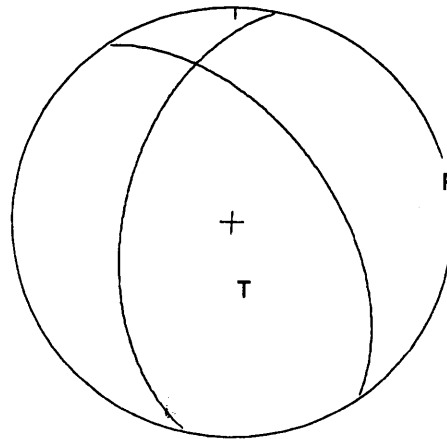
WETMILLER (1975)



HERRMANN (1979)



YANG AND AGGARWAL (1981)

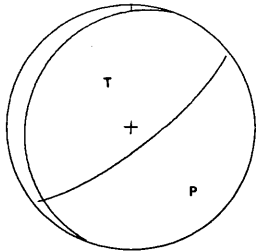


(LHP)

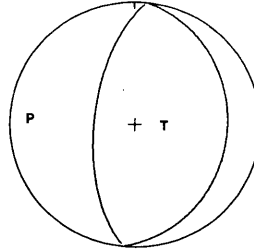
FIGURE E.7

SE NEW YORK - N NEW JERSEY EARTHQUAKES

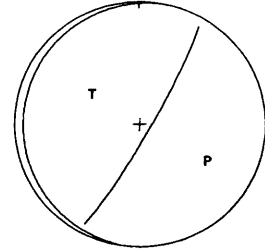
19JUL75 MAHOPOC, NY



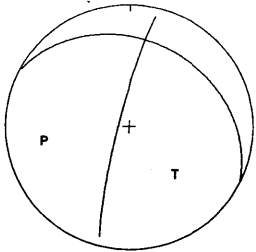
22AUG75 LAKE DE FOREST, NY



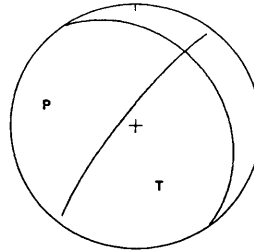
11MAR76 POMPTON LAKE, NJ



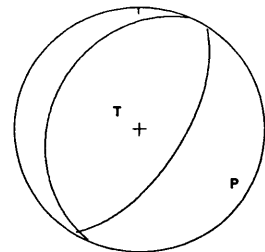
13APR76 RIDGEFIELD, NJ



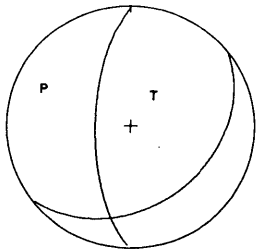
20AUG76 MT PLEASANT, NY



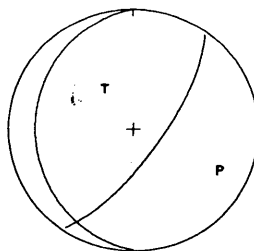
22SEP76 INDIAN PT, NY



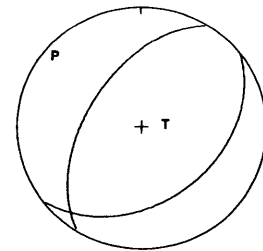
22NOV76 YONKERS, NY



10MAR77 SUFFERN, NY



04DEC77 SCHOOLEY MT, NJ

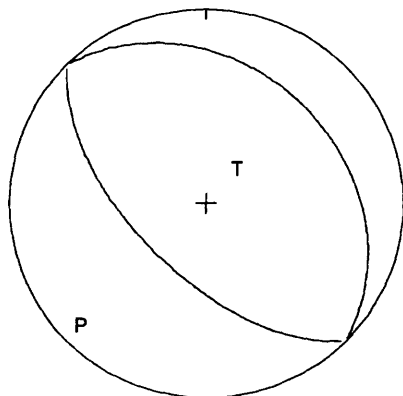


(LHP)

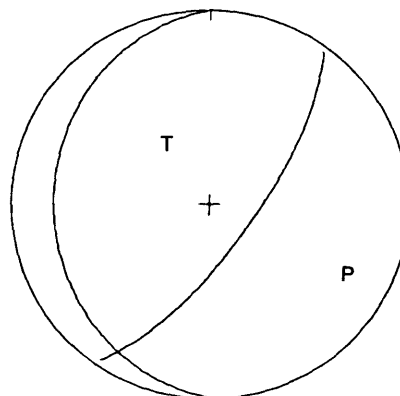
FIGURE E.8

07JUN74 WAPPINGER FALLS, NY

POMEROY ET AL (1976)

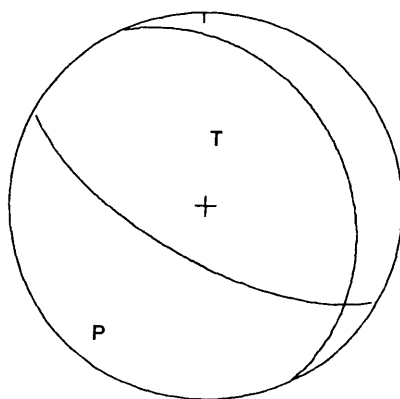


YANG AND AGGARWAL (1981)

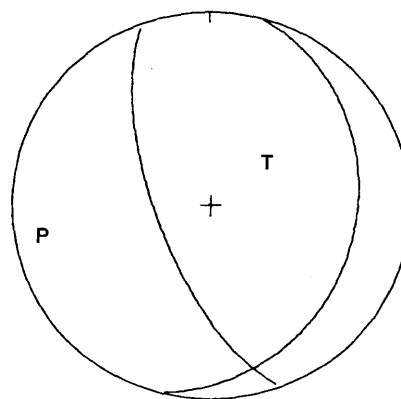


ANNSVILLE, NY EARTHQUAKES

1977



1980



(LHP)

FIGURE E.9

*APPENDIX F**A CLOSER LOOK AT SOME RECENT EARTHQUAKES**F.1 Introduction*

During the course of this study, a number of contemporary NEUS-SEC earthquakes were studied in detail using both network and field data. In this appendix, we present the results of these studies.

F.2 18Apr79 Bath, ME

On April 18, 1979 a moderate earthquake occurred near Bath, ME and was felt over an area of approximately 55,500 square kilometers along the coasts of Maine, New Hampshire, and Massachusetts. This mbLg 4.0 event was the largest earthquake to occur within the New England states since the mbLg 4.8 Maine-Quebec border earthquake on June 15, 1973 (Wetmiller, 1975). This event is important because of its size and its proximity to the Wiscasset Nuclear Power Plant.

A number of moderate earthquakes have occurred in southern Maine according to the historical record. Table F.1 lists some of these events along with condensed comments. The largest intensity experienced in this area has been VII M.M. (e.g. fallen chimneys). Small earthquakes (mbLg < 2.5) have also been located coastal Maine by the N.E.U.S.S.N. over the past six years.

Little crustal refraction work has taken place in this area, and no one crustal model is appropriate for locating the

event. If we use the model from Chiburis et al. (1978) (thickness km, V_p km/sec: 0.88, 5.31; 12.2, 6.06; 21.5, 6.59; halfspace 8.10; $V_p/V_s=1.73$) we obtain latitude 43.979 (43 58.8'), longitude -69.772 (-69 46.3'), depth 0.1 km, at O.T. 02:34:14.5 UTC . The model from Taylor and Toksöz (1979), (thickness km, V_p km/sec: 7.30, 5.70; 18.80, 6.30; 16.10, 7.30; halfspace 8.13; $V_p/V_s=1.73$) produces essentially the same location, but a deeper focal depth. The location using this model is latitude 43.995 (43 59.7'), longitude -69.797 (-69 47.8'), depth 4.0 km, at O.T. 02:34:14.7 UTC . The deeper focal depth with the Taylor and Toksöz model arises from the much thicker low velocity top layer. Since the closest station (TRM) is approximately 50 km from the epicenter, neither depth can be regarded as totally reliable. However, if we use the two models as boundary values on the actual crustal structure (which is realistic considering their differences), we can say that the Bath, ME event occurred at a depth of less than 5 km.

This event was followed by a number of aftershocks (on 09Apr), among the larger were: (O.T., UTC-magnitude, mb) 02:41-3.0; 02:45-2.1; 03:07-2.2; 03:08-2.6; 03:53-1.4; 05:57-1.7; 07:17-2.0 . A month later on May 11 and May 13, two earthquakes of magnitude 2.3 and 2.4, respectively, occurred about 10 km north of the April 18 event. On June 6, two events of magnitude 1.0 were detected on station TRM, with S-P times matching that of the April 18 event. Likewise, on June 18 and 21, two events of magnitude less than one were detected at TRM, presumably from the

Bath area.

A four station temporary network was installed in the epicentral area for three days following the main shock. The participants in this field study included this author, Robert Stewart, Janet Johnston, Kenneth Tubman, and Andrew Michael. Figure The coordinates of these stations are given in Table F.2 . Instrumentation consisted of three Sprengnether MEQ 800 recorders with L4-C vertical seismometers, and one Geotech Portacorder with an S-500 seismometer. Equipment failure prevented the installation of a temporary station southeast of the epicenter which would have improved the accuracy of the aftershock locations. The temporary network was installed to obtain aftershock data which might better constrain the focal depth of the main event, and to obtain P-wave polarities for a composite fault plane solution. Because of the late nite occurrence of this event and its distance from M.I.T., a rapid deployment of equipment was impractical. For a magnitude 4.0 earthquake in New England, most aftershocks occur within a few hours of the main shock. However, we did record two possible aftershocks. The temporary network did not provide enough data for depth computations, but did show that the two aftershocks occurred within three km of the main shock.

During the field recording time, we also conducted intensity interviews with 55 residents of the area. The objective was not to produce a comprehensive isoseismal map (since the U.S.G.S. is better equipped to survey large areas), but to investigate many

of the characteristics found in historical descriptions of New England earthquakes, such as booming sounds. Nearly all of the residents interviewed said that the ground shaking was accompanied by a high frequency booming sound. Some residents who had once lived in southern California noted the distinct difference in the sound of New England earthquakes versus those in California, the latter having low frequency rumbling sounds which generally last much longer. Some residents also reported feeling and hearing the aftershocks, especially if their houses were built on rock or rock ledge. The only exception to the booming sounds were found west of the epicenter near Brunswick, ME where most residents said the shaking was accompanied by a low frequency sound. Possible explanations for the unusual sounds of this earthquake include a shallow focal depth (supported by travel time data), relatively high stress drop - corner frequency, and low crustal attenuation (Nuttli, 1973; Chapter 4 of this work).

Figure F.1 shows the Modified Mercalli intensities determined from the interviews. Damage was minimal in all areas, with the highest intensities found north of the epicenter in Pittston, where we found instances of broken windows (V). These high intensities may be due to the focusing of seismic waves by sediments of the Kennebec River Valley. Most residents reported the moving of small objects on tables and shelves, and some people were awakened from a sound sleep. Our survey indicated that the intensity near the Wiscasset Nuclear Power Plant was IV.

Stover et al. (1980) reported intensities of V near the plant. Their intensity map is reproduced in Figure F.2 . They found intensity V values at the following Maine towns: Auburn, Augusta, Belfast, Buckfield, Damariscotta, Dresden, East Vassalboro, Freedom, Gray, Hallowell, Lebanon, Lisbon Falls, Livermore Falls, Lovell, Mount Vernon, Old Orchard Beach, Scarborough, South Paris, Topsham, Troy, West Bowdoin, West Peru, Wiscasset, and Woolwich.

Approximately half of the pet owners interviewed in our survey reported that their animals showed unusual behavior prior to the earthquakes. The timescales varied from unusual behavior all day to the majority of five minutes before the main shock. Most owners reported their dogs were whining and barking five minutes before the event, with some dogs behaving as they usually do during a thunderstorm. These reports came from residents in all directions surrounding the epicenter. We weigh heavily their information because many of them, when describing the earthquake, volunteered the information about their pets without a specific question from the interviewer. This may be the first reporting of unusual animal behavior before an earthquake in the New England states.

The fault plane solution for this event is discussed in Chapter 3 of this work. The mechanism shows pure thrust faulting on planes oriented nearly N-S.

F.3 23Nov80 and 23Jun38 Chelmsford-Lowell, MA

On November 23, 1980, a small earthquake centered near the

Chelmsford-Lowell, MA border startled many residents of the area, due in part to a favorable time of occurrence (Saturday 7:40 PM EST) and the probable shallow focal depth. This area of Massachusetts has experienced other small earthquakes during this century, most notably the event on June 23, 1938. The occurrence of the November 23, 1980 event prompted a re-examination of the data for the 1938 earthquake, since these events were very similar in location and intensity.

The 1980 earthquake was well recorded by a number of stations of the M.I.T. and Weston Observatory seismic networks. P-wave arrival times from the nine closest stations, along with the two clearest S-wave arrivals, were used to compute the hypocentral location. The crustal model from Taylor and Toksöz (1980) was used to compute the location: (thickness km, V_p km/sec) 7.30, 5.70; 18.80, 6.30; 16.10, 7.30; halfspace 8.13; $V_p/V_s=1.73$. Since the closest station was less than 10 km away, we were able to determine the focal depth within reasonable accuracy, which is generally not the case in New England. The depth free hypocentral solution was latitude 42.63, longitude -71.36, depth 1.2 km at O.T. 00:39:32.0 . To further explore the solution space, we computed RMS errors for source depths from 0 to 15 km at 1 km intervals while allowing the latitude, longitude, and O.T. to vary freely. The RMS error increases with depth down to 7 km, where there is a change in crustal velocity. The epicenter did not move for focal depths in this range. After 7 km, the RMS error abruptly decreases, then

increases for depths down to 15 km. This is accompanied by an epicenter shift to latitude 42.59, longitude -71.37, which is outside the area of maximum intensity. The residual of the closest station is also unrealistically large for this epicenter. Thus, we believe the shallower epicenter to be the most accurate. Next we investigated the depth convergence at this epicenter by constraining the latitude, longitude, and O.T. to the depth free solution and computed RMS errors for source depths from 0 to 15 km. The minimum residual is between 1 and 2 km. Our final solution is latitude 42.63, longitude -71.36, depth 1.5 km at O.T. 00:39:32.0 UTC.

The magnitude of this event was computed using the coda length method for New England, developed by Chaplin et al. (1980). The average coda length was 122 sec and varied by less than 5 sec across the array. Using their equation, $M_c = 2.21[\text{Log}(T)] - 1.70$ where T is the average coda length in seconds, we obtain a magnitude of 2.9 ± 0.3 .

The mechanism of this event was presented in Chapter 3 of this work. It shows either dip slip or strike slip faulting, depending on which fault plane is chosen. The P-axis for this mechanism trends NE-SW. This agrees with overcoring results in a nearby granite quarry.

A telephone intensity survey was conducted for this earthquake during the next day. The earthquake was felt and heard in the cities of Lowell, Dracut, Chelmsford, Billerica, Tyngsborough, Westford, and Nabnasset, MA. Most residents said

the sound was similar to a sonic boom, a boiler explosion, or an empty truck hitting a bump. The earthquake was felt most strongly in Chelmsford and Lowell where residents reported that entire houses shook. On-duty police officers at the newly constructed (of cement) Lowell Police Headquarters also said the entire building shook. However, no instances of minor damage, such as cracked plaster, were found. An intensity of IV (M.M.) has been assigned to this earthquake. The rapid decay of intensity with distance from the epicenter and the large number of "heard" reports support the shallow focus solution. An isoseismal map for this event is shown in Figure F.3 .

The June 23, 1938 earthquake was originally studied by Linehan (1940). Using the graphical distance-arc intersection technique, he determined an epicenter at latitude 42.62, longitude -71.42, at O.T. 03:57:56.5 UTC. His interpretation of the intensity data (IV R.F.) led him to conclude that the hypocenter was "quite shallow". This location coincided with the southernmost tip of the ellipse of greatest intensity, shown in Figure F.7 . No magnitude was given for this event.

We used the P and S wave data given in Linehan (1940) for the stations at Weston , Harvard, and Williams College to relocate the event. With the previously mentioned crustal model, the hypocenter was latitude 42.60, longitude -71.42 at O.T. 03:57:55.9 . The depth was constrained at the surface.

The magnitude of this event was computed using the coda length scale previously mentioned applied to stations WES and HRV.

With an average coda length of 100 seconds, we obtained an $m_b L_g$ of 2.7. The P-wave first motions at the three stations fit the solution of the 1980 earthquake, thus the mechanisms of the 1938 event could have been similar.

Linehan's (1940) intensity survey for this event shows some similarities to that of the 1980 earthquake (Figure F.3). The 1938 earthquake was also heard with the sounds described as an explosion or a truck rumbling down the street. However, there was slight damage to some houses in the area of Nabnasset. In one case, wooden clapboards were pulled away from a wall, and a wall separated from a ceiling to about three inches. Nearby, a three foot square piece of slate was pushed about two inches into a plaster wall. Both locations were on glacial till. In a wooden structure between Tyngsborough and Lowell, small cracks appeared in the bricks of an open fireplace, and some foundation stones were also found to be cracked. Linehan noticed that a three foot diameter glacial boulder had been pushed from its position in a nearby till bank.

Linehan (1940) assigned an intensity of IV (R.F.) to this event and hesitated to raise the intensity because of the relatively small number of damage reports. A IV on the Rossi-Forel scale accounts for the moving of some objects and the cracking of ceilings (de Rossi, 1883). Translation to the Modified Mercalli scale necessitates the upgrading to intensity V (M.M.) which accounts for a few instances of cracked plaster (Wood and Neumann, 1931).

The smaller felt area of the 1938 event compared to that of the 1980 event supports the slightly lower magnitude estimate (2.7 versus 2.9). The higher maximum intensity may have been due to either poorer construction practices at the time, or an even shallower focal depth than that of the 1980 event.

The bedrock formations of northeastern Massachusetts are of late Paleozoic age, consisting mainly of granites, schists, and quartzites. The general structure trends NE-SW. Pleistocene glaciation has produced low, rolling relief, with glacial deposits leaving few outcrops of bedrock visible. The relationship of the geology to the earthquake occurrence in this area is not known at this time. Extensive granite quarrying has taken place during this century. These small, shallow earthquakes may be the result of tectonic stresses in the crust, stresses associated with glacial unloading, or possibly due to quarrying operations.

F.4 21Oct81 Long Island Sound, NY

On October 21, 1981 a small earthquake shook the area surrounding Long Island Sound, NY. Although microearthquakes have been located along the coast of southern New England, no earthquakes have been instrumentally located within the Sound until the present event. Figure F.4 shows the locations of microearthquakes in the region which have been detected by the N.E.U.S.S.N. for the period October 1975 through June 1981. The location of the October 21, 1981 event is indicated by the star. Historical compilations by Smith (1962), Smith (1966) and others

discussed in Chapter 2 also indicate that no earthquakes have occurred in the Sound. However, it is likely that historical events along the coast of Connecticut may have actually occurred within the Sound, or that the present N.E.U.S.S.N. configuration cannot detect microearthquakes of magnitude $m_b < 1.5$ in this area.

A suite of seismograms from M.I.T. Seismic Network stations is shown in Figure F.5. Each channel has been plotted in terms of lapse time. The signals on a number of channels are clipped because preamplifier gain settings have been set too high. These gains have subsequently been lowered to increase the dynamic range of the channels.

This earthquake was large enough to produce clear P-wave arrivals on most N.E.U.S.S.N. stations within 300 km of the epicenter. The following crustal model, from Chiburis et al. (1980) was used to locate this event (thickness km, V_p km/sec): 0.88, 5.31; 12.2, 6.06; 21.5, 6.59; halfspace, 8.10. Using the 35 P-wave arrival times, the following hypocentral solution was obtained: latitude 41.16 (41° 9.4'), longitude -72.57 (-72° 34.1'), depth 6.5 km, at O.T. 16:49:07.3 UTC. The azimuthal coverage for this dataset is shown in Figure F.6a. However, since the crust and upper mantle structure varies considerably in the NEUS (Taylor et al., 1980), two subsets of these stations were used to recompute the hypocenter. The first subset used the eight closest stations which surround the epicenter, with an azimuthal distribution shown in Figure F.6b. The hypocentral

solution obtain using this subset was: latitude 41.14 (41 8.1'), longitude -72.57 (-72 33.9'), depth 5.0 km, at O.T. 16:49:07.1 UTC. Since the closest station was 25 km from the epicenter, the focal depth cannot be regarded as reliable. If we further reduce the number of stations to the four closest stations surrounding the epicenter, with an azimuthal distribution shown in Figure F.6c, we obtain the same solution as with the eight station subset. These two subsets of the 35 stations should provide the most accurate hypocentral solution for this event within the constraints of the crustal model. This location is approximately 40 km southeast of New Haven, CT and 27 km north of Riverhead, Long Island.

Magnitude calculations for this earthquake provide some interesting insights into the problem of scaling NEUS earthquakes. Ebel (personal communication) computed a local magnitude (ML) of 3.4 for this earthquake. He used the standard Wood-Anderson torsion seismometers at Weston, MA with a correction term applied to Richter's (1935) equation to account for the difference in crustal attenuation between California and the NEUS. Ebel also found an mbLg magnitude of 3.7 for this event using the equations of Nuttli (1973). We used the coda length magnitude scale of Chaplin et al. (1980) to compute the mbLg for this earthquake. With an average coda length of 300 seconds across the M.I.T. Seismic Network, their equation ($mbLg = 2.21\log(T) - 1.70$) yields a value of 3.75. However, ML should equal mbLg if the proper values of anelastic attenuation are used

to compute each magnitude (Herrmann and Nuttli, 1982). The discrepancy arises from the fact that Nuttli (1973) calibrated the mBLg scale using 1.0 Hz Lg waves, whereas the predominant frequency of Lg waves in the NEUS is greater than 2 Hz. This leads to an overestimation of the earthquake size in the NEUS. Ebel (1982) found that the mBLg magnitudes reported in the N.E.U.S.S.N. bulletins are greater than the ML magnitudes by an average of 0.4 magnitude units (again, using Richter's formula corrected for the difference in crustal Q). This would make the actual mBLg magnitude for this event 3.3 to 3.4 .

We were able to read 27 P-wave first motions for this event from N.E.U.S.S.N. stations with known polarities. Using the algorithm by Guinn and Long (1977), the mechanism shown in Chapter 3 was obtained. This mechanism shows thrust faulting on NE-SW trending fault planes. Both fault planes may be slightly rotated and still satisfy the data. This mechanism was found to be very stable with respect to changes in focal depth and crustal model.

An intensity survey was conducted for this earthquake by Lamont Doherty Geological Observatory and the State University of New York at Stony Brook. The earthquake was felt throughout Long Island and most of Connecticut, with felt reports also coming from Rhode Island, Massachusetts, and the New York City area. The intensity of this event was IV, however the PDE reports some instances of intensity V in New Haven and New London, CT. An isoseismal map is shown in Figure F.7 .

*Table F.1**Moderate Earthquakes in Southern Maine*

(condensed from Coffman and von Hake, 1973)

<u>Date</u>	<u>Lat.</u>	<u>Long.</u>	<u>Int.</u>	<u>Area and Comments</u>
22May1817	45.2	69.3	V	Dover-Foxcroft, felt widely in ME
20Jan1881	44.0	70.0	V	Bath, felt along southwest coast
21Mar1904	45.0	67.2	VI	southeast ME, felt throughout NE
14Jan1943	45.3	69.6	V	Dover-Foxcroft, felt throughout NE
26Apr1957	43.6	69.8	VI	Portland, fallen chimneys, cracked pl.
01Jul1967	44.4	69.9	V	Kennebec Cty, 14 shocks, cracked pl.

Table F.2
Locations of Stations Setup Around the Epicenter
of the Bath, ME Earthquake

<u>Code</u>	<u>Lat.</u>	<u>Long.</u>	<u>Elev. (m)</u>	<u>Location</u>
WWM	43.975	-69.739	12	Woolwich
BCM	43.908	-69.958	18	Brunswick
BHM	44.031	-69.863	43	Bowdoinham
OBM	43.938	-69.873	18	Bath

Figure Captions

Figure F.1 Modified Mercalli intensities around the Bath, ME earthquake from interviews conducted by the authors.

Figure F.2 Isoseismal map for the Bath, ME earthquake, from Stover et al. (1980).

Figure F.3 Isoseismal map for the 1980 and 1938 Chelmsford-Lowell, MA earthquakes.

Figure F.4 Microearthquakes in the vicinity of the 1981 Long Island Sound, NY earthquake. The epicenters cover the period Oct. 1975 through June 1981.

Figure F.5 Suite of seismograms for the 1981 Long Island Sound, NY earthquake from the M.I.T. seismic network.

Figure F.6 Azimuthal station distributions for the Long Island Sound earthquake.

Figure F.7 Isoseismal map for the 1981 Long Island Sound, NY earthquake, from Schlessinger-Miller (personal communication).

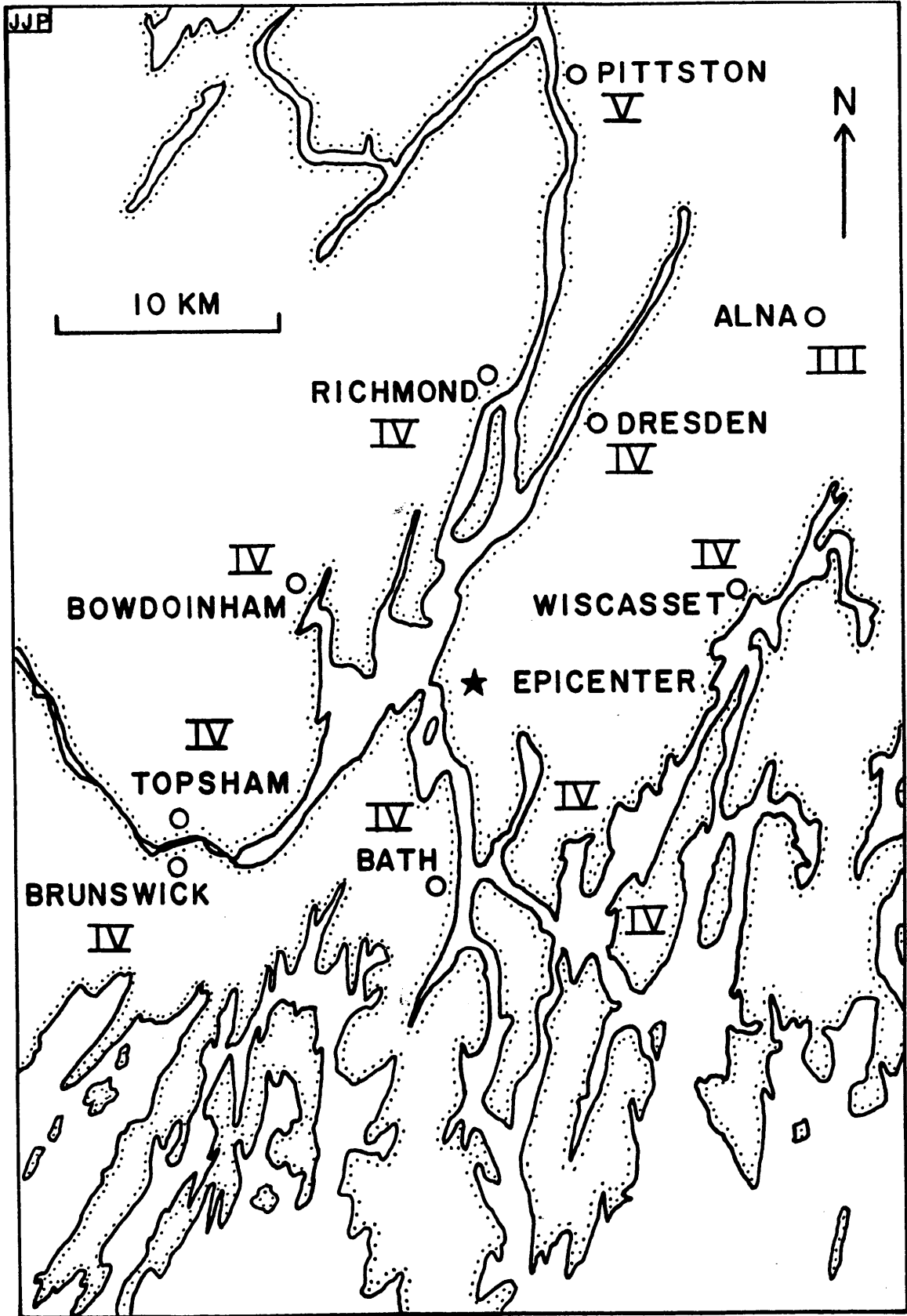


FIGURE F. I

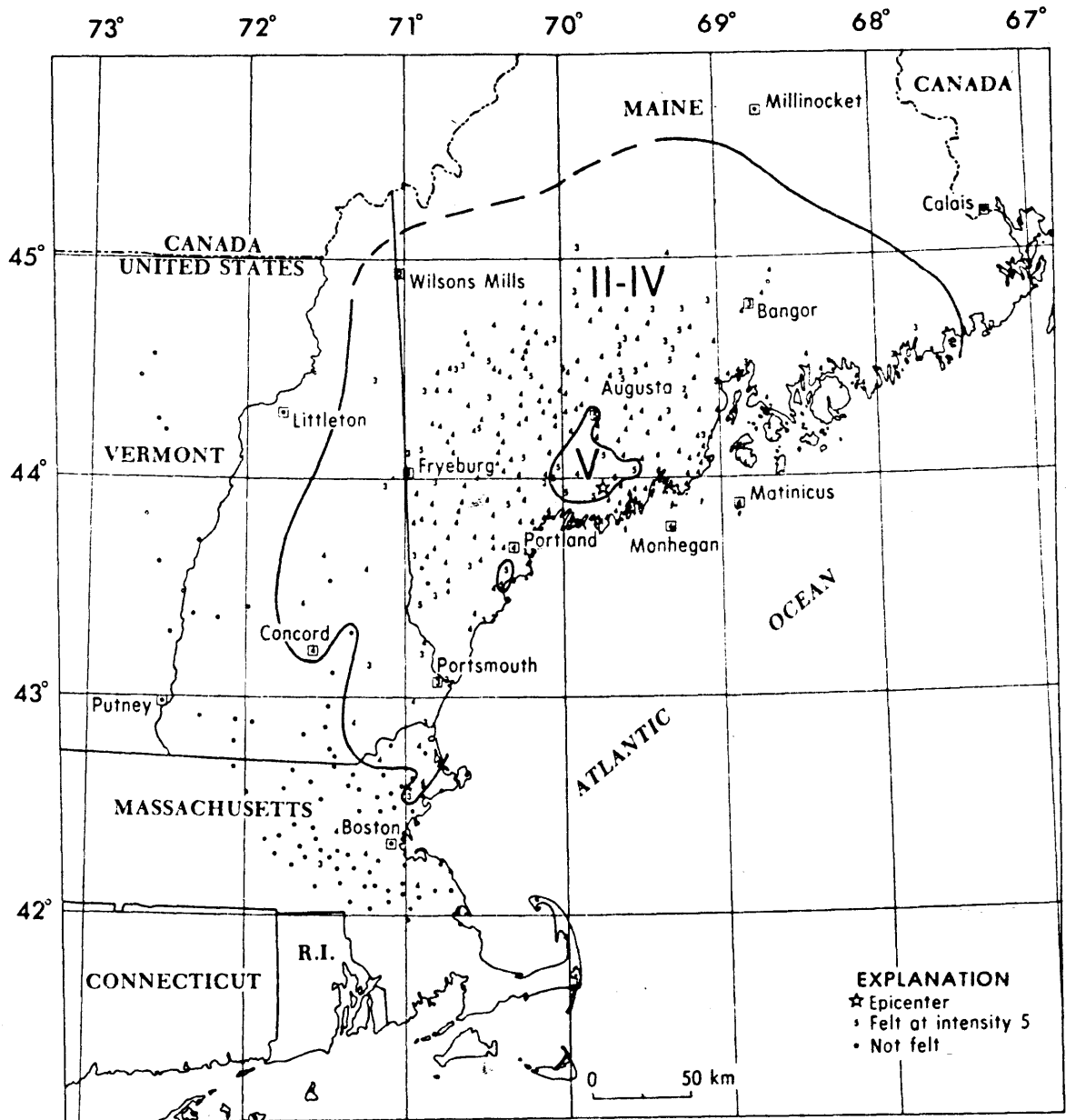
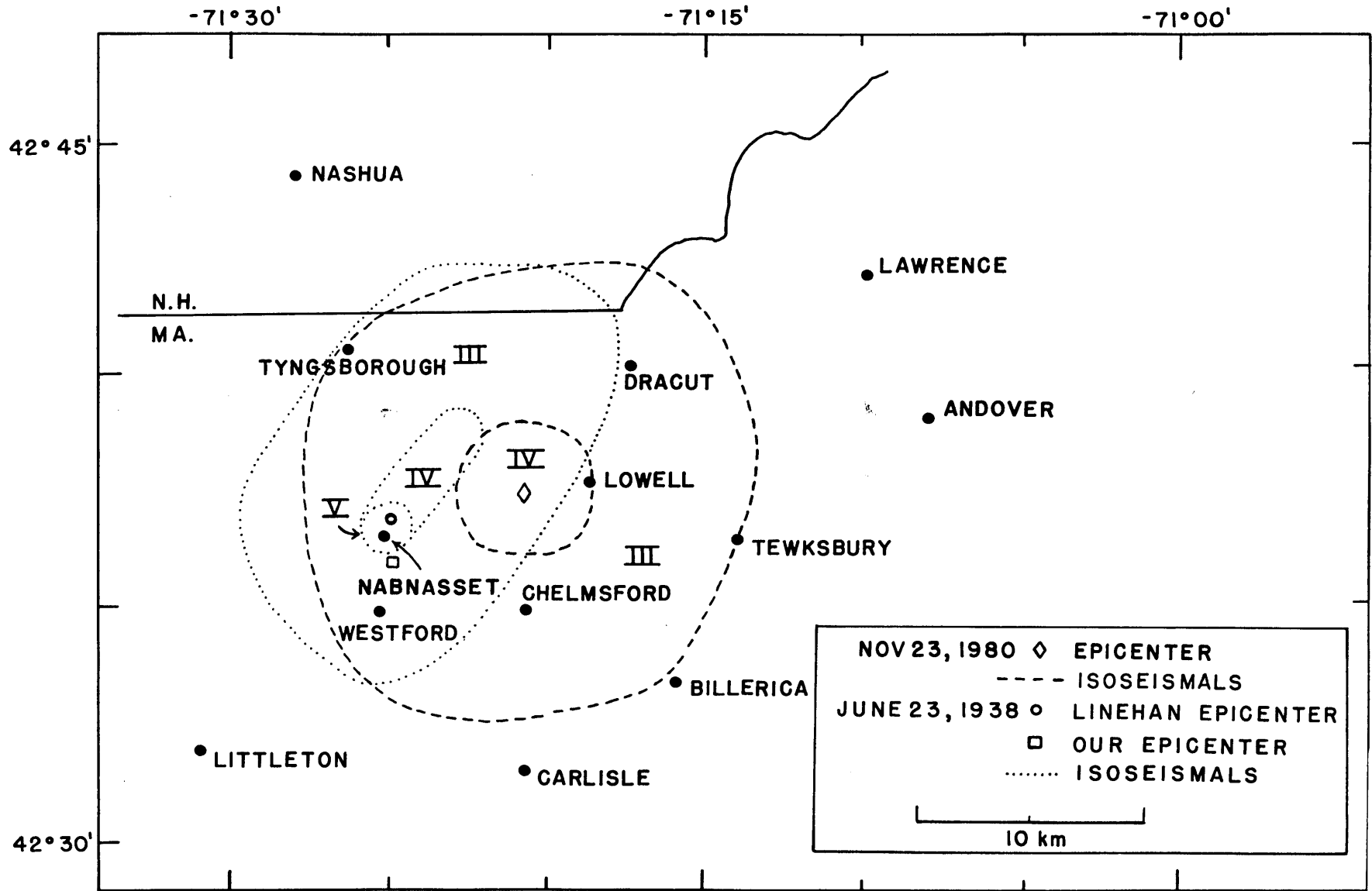


FIGURE F.2

FIGURE F.3



EPICENTERS: OCTOBER 1975 - JUNE 1981

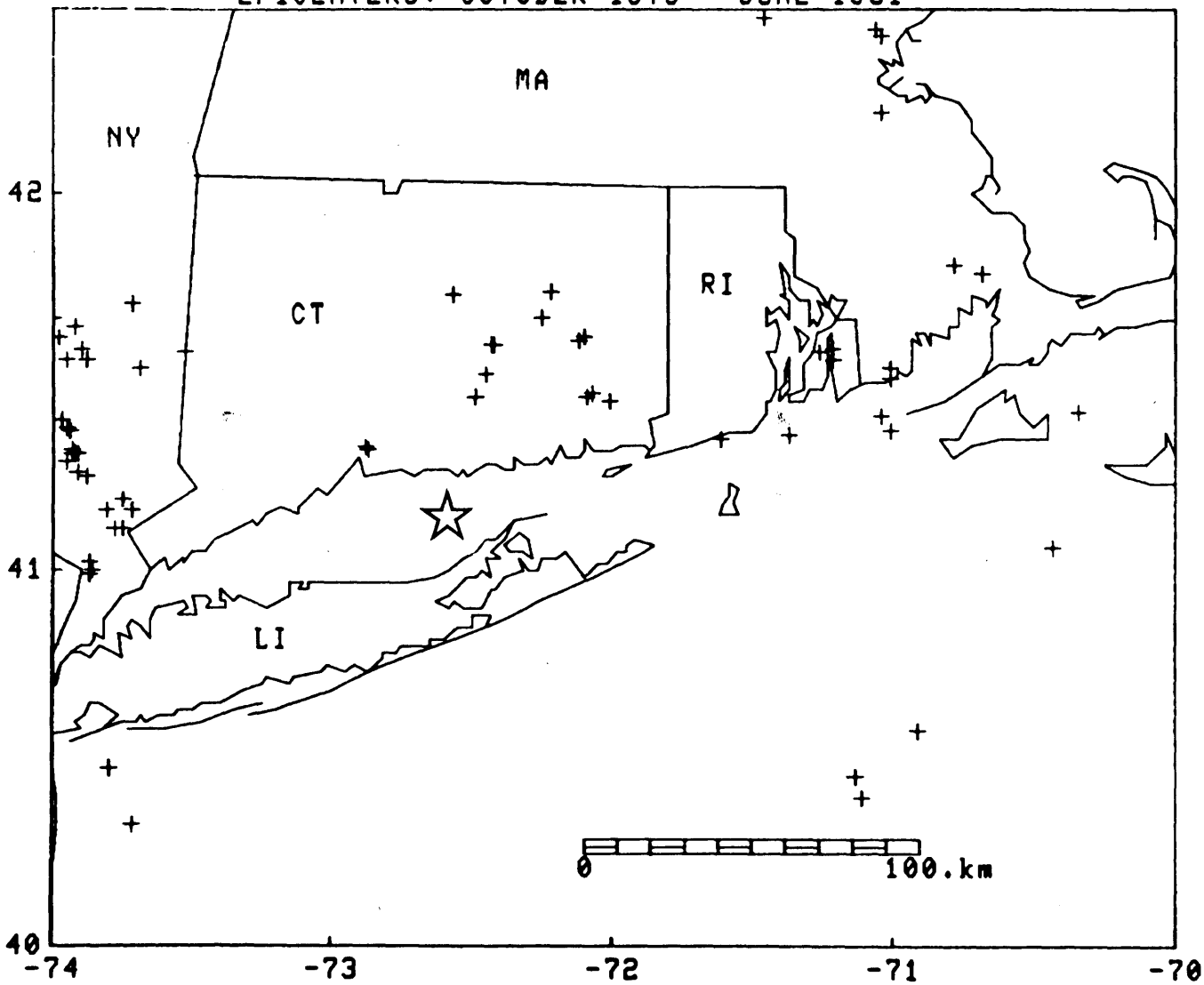


FIGURE F.4

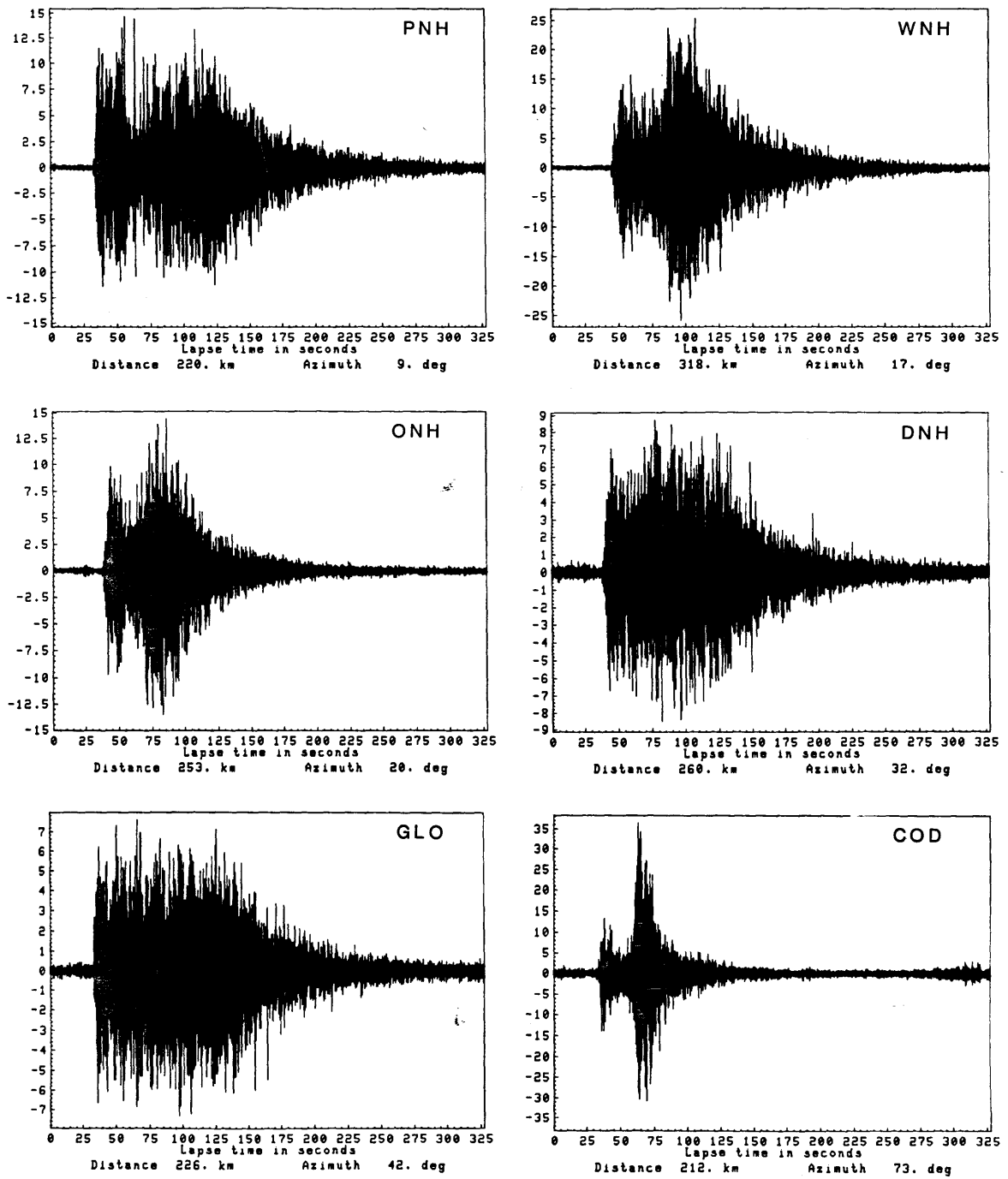


FIGURE F.5

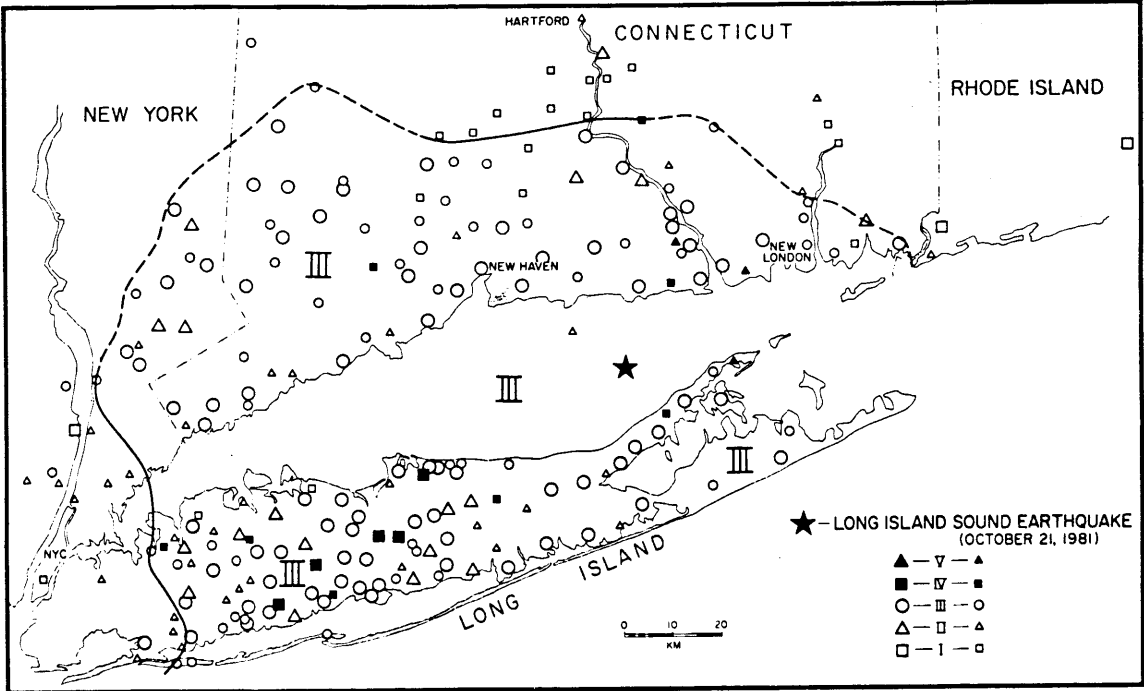


FIGURE F.7

BIOGRAPHICAL NOTE

The author was born on July 8, 1953 in Medford (pronounced Meffa), MA and grew up in the nearby suburb of Somerville. It is unknown when he first picked-up an interest for science and technology, but it may have been when his father taught him how to shift a four speed Mercedes Benz at age nine. In spite of the best efforts of the public education system, his pursuit of knowledge continued to draw him to science, especially with the help of three concerned teachers - Dick Gordineer, Joe Wrobel, and Joe Pignatello. His interest in astronomy then lead him to Worcester Polytechnic Institute in 1971 for a degree in physics. However the long hours spent studying material which had been discovered hundreds of years ago began to wear down his patience. A more practical career was sought. During this time, he engaged in long discussions about seismology and plate tectonics with his good friend and fellow rockhound Msgr. Bill Roche. These fields seemed young and practical enough for the author to make some kind of contribution, so the bug had bitten. From there he went on to Boston College to learn some seismology and bang heads with the Jesuits. Profs. Jeff Johnson and Fr. John Devane succeeded in transforming him from a physicist to a geophysicist. Always the glutton for punishment, he passed up the opportunity to earn real money to come to M.I.T. in 1977 for a PhD in geophysics. The rest is history and the previous 389 pages of this thesis. The author is now a Research Associate at the Earth Resources Laboratory of M.I.T.. One never learns!